

9585

NATIONAL LIBRARY
OTTAWA



BIBLIOTHÈQUE NATIONALE
OTTAWA

NAME OF AUTHOR.....Tze-tang CHUANG.....
TITLE OF THESIS...Infrared...Studies...of...Kinetics
and...Mechanism...of...Reaction...on...
...Some...Secondary...alcohols...on...Several...Aluminos
UNIVERSITY.....~~S~~ U. of A.....
DEGREE FOR WHICH THESIS WAS PRESENTED....Ph. D.....
YEAR THIS DEGREE GRANTED....1971.....

Permission is hereby granted to THE NATIONAL LIBRARY
OF CANADA to microfilm this thesis and to lend or sell copies
of the film.

The author reserves other publication rights, and
neither the thesis nor extensive extracts from it may be
printed or otherwise reproduced without the author's
written permission.

(Signed)....Tze-tang Chuang.....

PERMANENT ADDRESS:

...49 Chung - Hsiang St.
...Kao Hsiung.....
...Taiwan.....

DATED...Sept 14.....1971

NL-91 (10-68)

THE UNIVERSITY OF ALBERTA

**INFRARED STUDIES OF KINETICS AND MECHANISM OF REACTION FOR
SOME SECONDARY ALCOHOLS ON SEVERAL ALUMINAS**

BY

 **TZE-TANG CHIANG**

A THESIS

**SUBMITTED TO THE FACULTY OF GRADUATE STUDIES
IN PARTIAL FULFILMENT OF THE REQUIREMENTS FOR THE DEGREE
OF DOCTOR OF PHILOSOPHY**

DEPARTMENT OF CHEMICAL AND PETROLEUM ENGINEERING

EDMONTON, ALBERTA

FALL, 1971

UNIVERSITY OF ALBERTA
FACULTY OF GRADUATE STUDIES

The undersigned certify that they have read, and recommend to the Faculty of Graduate Studies for acceptance, a thesis entitled "INFRARED STUDIES OF KINETICS AND MECHANISM OF REACTION FOR SOME SECONDARY ALCOHOLS ON SEVERAL ALUMINAS" submitted by TZE-TANG CHUANG in partial fulfilment of the requirements for the degree of Doctor of Philosophy.

J. E. Selby.....

Robert B. Anderson.....

H. W. Helquist.....

Elliot L. Braun.....

Richard Wankel.....

John P. O'Leary.....

Date *August 5, 1971*.....

ABSTRACT

Studies of the adsorption of the secondary alcohols, 2-propanol, 2-butanol and 3-pentanol, on γ -alumina and γ -alumina doped with 2% sodium hydroxide were carried out from room temperature to 300°C using infrared spectroscopy. On γ -alumina four types of surface species were observed: (i) alcohol hydrogen-bonded to surface hydroxyl groups; (ii) an alkoxide-type structure chemisorbed on Lewis acid sites, Al^{+3} ; (iii) a partial double bond type structure which on desorption gives an olefin; and (iv) a carboxylate species which is stable even at high temperatures. The physically adsorbed species are mainly dehydrated, forming a mixture of olefinic isomers. On 2% sodium hydroxide-doped γ -alumina, in addition to the species i, ii, and iv, a ketone-like species was detected which on desorption gave a ketone. Two types of carboxylate species may exist on sodium hydroxide-doped γ -alumina. A mechanism for the formation of carboxylate species, identical for both the catalysts studied, is proposed. The three alcohols follow similar mechanisms for dehydration and dehydrogenation, with 3-pentanol reacting at a lower temperature than encountered with 2-butanol and 2-propanol.

The catalytic activity of the γ -alumina surface has been investigated, using the IR absorption technique, in terms of strong and weak Bronsted-acid sites and Lewis-acid sites. Doping of the γ -alumina

with NaOH was used to eliminate Bronsted-acid sites. The influence of the two types of sites upon catalytic activity and selectivity was shown by the simultaneous dehydration and dehydrogenation of 3-pentanol on γ -alumina or on several doped aluminas of varying NaOH content. The selectivity exhibited towards the two reactions was shifted from dehydration to dehydrogenation by eliminating Bronsted-acid sites.

Finally, simultaneous kinetic and mechanistic studies have been performed by IR spectroscopy to provide both quantitative conversion measurements and spectra for the species adsorbed/reacting on the surface of the solid catalyst. A recycle reactor was designed so that steady-state measurements could be taken of either the recirculating gas concentration or complete spectra scans through the catalyst pellet. On the basis of simultaneous spectral and kinetic data, the kinetics of 2-propanol dehydration on γ -alumina and of 2-propanol dehydrogenation on 8% NaOH-doped γ -alumina were modelled adequately with the appropriate Langmuir-Hinshelwood equations, inferred from the surface mechanism, with a minimum of statistical correlation effort.

ACKNOWLEDGEMENTS

The author wishes to express his sincere appreciation to Dr. I.G. Dalla Lana for his advice and guidance during the course of this investigation and to Dr. D.E. Seborg, who as chairman of his thesis committee, has contributed valuable advice and criticism.

Thanks are due to Mr. H. Singh for his assistance in kinetic model discrimination; to Dr. A.V. Deo for his advice in interpretation of infrared spectra and to Dr. R.G. Moore for his assistance in design of solenoid pump.

The author's greatest personal debt is to his wife, Sueh-Heng, whose encouragement and assistance were so important for the preparation of this dissertation.

The financial support of the National Research Council of Canada and the University of Alberta is gratefully acknowledged.

TABLE OF CONTENTS

	<u>Page</u>
CHAPTER I INTRODUCTION	1
CHAPTER II SURVEY OF RELATED WORK	6
2.1 Dehydration and Dehydrogenation of Alcohols	6
2.2 The Structure of γ -Alumina	8
2.3 The Surface of γ -Alumina	9
2.4 Effect of Sodium Hydroxide on the Structure of Alumina Surface	14
2.5 Infrared Studies of the Adsorption of Alcohols on γ -Alumina Catalysts	17
2.5.1 Physically Adsorbed Alcohols	18
2.5.2 Aluminum Alkoxide Structure	19
2.5.3 Carboxylate Structures	21
2.5.4 Adsorbed Water	23
2.5.5 Adsorbed Ketone	24
2.5.6 Adsorbed Hydrogen	25
2.6 Mechanism of Alcohol Dehydration on γ -Alumina	27
2.7 Kinetics of Alcohol Dehydration on γ -Alumina	31

TABLE OF CONTENTS (continued)

	<u>Page</u>	
CHAPTER II	continued	
2.8	Activation Energy for Alcohol Dehydration on γ -Alumina	33
2.9	Effect of Doping Sodium Ion on γ -Alumina on the Dehydration of Alcohols	35
2.10	Kinetic Model Discrimination Techniques	36
CHAPTER III	REAGENTS AND CATALYSTS	43
3.1	Feed Materials	43
3.2	Alumina Catalysts	44
3.2.1	Preparation of Catalysts	44
3.2.2	Surface Area of Alumina Catalysts	46
3.2.3	Pore Size Distribution for the Alumina Catalyst	47
CHAPTER IV	APPARATUS AND EXPERIMENTAL PROCEDURES	50
4.1	Study of Adsorption of Alcohols	50
4.1.1	Infrared Cell	50
4.1.2	Vacuum System	52
4.1.3	Preparation and Pretreatment of Catalyst Wafer	53
4.1.4	Adsorption, Desorption and Recording of Spectra	54

TABLE OF CONTENTS (continued)

	<u>Page</u>
CHAPTER IV continued	
4.2 Simultaneous Studies of Kinetics and Mechanism	55
4.2.1 Equipment	55
(1) Feed System	56
(2) Vaporization System	58
(3) Recirculation Pump	58
(4) Infrared Cell and Sample Holder	61
(5) Temperature Recording System	65
(6) Product Collection System	66
4.2.2 Operation of Equipment	66
4.2.3 Data Evaluation	69
(1) Quantitative Analysis of Product Mixture	69
(2) Evaluation of Kinetic Data	74
CHAPTER V RESULTS AND DISCUSSION	89
5.1 Adsorption and Surface Reactions of Alcohols	89
5.1.1 2-Propanol on Pure γ -Alumina	89
5.1.2 2-Butanol on γ -Alumina	95
5.1.3 3-Pentanol on γ -Alumina	97
5.1.4 2-Propanol on 2% NaOH-doped γ -Alumina	100

TABLE OF CONTENTS (continued)

	<u>Page</u>
CHAPTER V continued	
5.1.5 2-Butanol on 2% NaOH-doped γ -Alumina	103
5.1.6 3-Pentanol on 2% NaOH-doped γ -Alumina	103
5.2 Catalytic Properties of γ -Alumina Using IR Adsorption Technique	106
5.2.1 Effect of NaOH Concentration on Bronsted-type Acidity on the Alumina Surface	106
5.2.2 Effect of NaOH Concentration on Lewis-type Acidity on the Alumina Surface	110
5.2.3 Effect of NaOH Doping upon Dehydration Catalytic Activity	111
5.2.4 Effect of NaOH Doping on Catalytic Selectivity	113
5.2.5 Surface Structure of γ -Alumina	115
5.2.6 Mechanisms of Dehydration and Dehydrogenation of 3-Pentanol on γ -Al ₂ O ₃ and NaOH-doped γ -Al ₂ O ₃	119
5.3 Simultaneous Kinetics and Mechanism	122
5.3.1 Blank Run	122
5.3.2 Mass Transfer Consideration	122
(1) Gas-film Diffusion	123
(2) Pore Diffusion	124

TABLE OF CONTENTS (continued)

	<u>Page</u>
CHAPTER V	
Continued	
5.3.3 Stability of the Catalysts During the Decomposition of 2-Propanol	125
5.3.4 Consideration of Capillary Con- densation	127
5.3.5 Side Reactions	129
(1) Dehydration	129
(2) Dehydrogenation	130
5.3.6 Kinetics and Mechanism of Dehydra- tion of 2-Propanol	130
(1) Spectra of Adsorbed Species	130
(2) Kinetic Models	133
(3) Model Discrimination	143
5.3.7 Activation Energy for the Dehydration of 2-Propanol	149
5.3.8 Kinetics and Mechanism of Dehydro- genation of 2-Propanol	153
(1) Spectra of Adsorbed Species	153
(2) Kinetic Models	156
(3) Model Discrimination	166
5.3.9 Activation Energy for the Dehydro- genation of 2-Propanol	174

TABLE OF CONTENTS (continued)

	<u>Page</u>
CHAPTER VI CONCLUSIONS	179
CHAPTER VII RECOMMENDATIONS	183
BIBLIOGRAPHY	190
LIST OF NOMENCLATURE	198
APPENDIX A ON-LINE OPERATION OF A PE621-IBM1800 SYSTEM	A-1
A-1 System Components	A-3
A-1.1 PE-621 Infrared Spectrophotometer	A-3
A-1.2 Encoder Readout-Computer Interface	A-3
A-1.3 IBM 1800 System	A-6
A-2 Operation of the System	A-9
A-3 Data Processing	A-14
A-4 Research Applications	A-21
A-4.1 Measurement of Differential Spectra	A-22
on a Single Catalyst	
A-4.2 Infrared Monitoring of a Reaction	A-24
System	
APPENDIX B COMPUTER PROGRAMS FOR MODEL DISCRIMINATION	B-1
APPENDIX C CALIBRATION OF LIQUID SYRINGE FEEDER	C-1
APPENDIX D PORE DIFFUSION LIMITATIONS	D-1
APPENDIX E SAMPLE DERIVATIONS OF RATE EQUATIONS	E-1
E.1 Dehydration, Dual Dissimilar-Site Mechanism	E-1
E.2 Dehydrogenation, Dual Dissimilar-Sites	
Mechanism (Scheme B)	E-2
E.3 Dehydrogenation, Dual Dissimilar-Sites	
Mechanism (Scheme C)	E-6

APPENDIX F THERMODYNAMIC ANALYSIS OF THE DEHYDRATION AND
DEHYDROGENATION OF 2-PROPANOL

APPENDIX G LIST OF IR BANDS ON THE ADSORPTION OF 2-PROPANOL
ON γ -ALUMINA

LIST OF FIGURES

<u>Figure</u>		<u>Page</u>
2-1	Computer Model of a Dehydroxylated Alumina Surface	15
2-2	Spectra of (A) C_2H_5OH on Al_2O_3 at $35^\circ C$, After Evacuating Sample Cell, and (B) $(C_2H_5O)_3Al$	20
3-1	Adsorption Isotherm of γ -Alumina	48
3-2	Pore Size Distribution for the Alumina Catalyst	49
4-1	Infrared Cell for Adsorption Studies	51
4-2	Apparatus for the Simultaneous Studies of Kinetics and Mechanism	57
4-3	Magnetic Solenoid Pump	60
4-4	Schematic Wiring Diagram for the Solenoid Pump	62
4-5	Reactor Cell and Sample Holder	63
4-6	Calibration of 2-Propanol Absorbance Using Beer's Law	75
4-7	Calibration of 2-Propanol Absorbance Using Beer's Law	76
4-8	Calibration of Propylene Absorbance Using Beer's Law	77
4-9	Calibration of Acetone Absorbance Using Beer's Law	78
4-10	Relation of 2-Propanol Feed Rate to Its Partial Pressure Under Non-Reaction Conditions	85
5-1	Spectra on the Adsorption of 2-Propanol on γ -Alumina	90
5-2	Spectra on the Adsorption of 2-Butanol on γ -Alumina	96
5-3	Spectra on the Adsorption of 3-Pentanol on γ -Alumina	98

LIST OF FIGURES (continued)

<u>Figure</u>		<u>Page</u>
5-4	Spectra on the Adsorption of 2-Propanol on 2% NaOH-doped γ -Alumina	101
5-5	Spectra on the Adsorption of 2-Butanol on 2% NaOH-doped γ -Alumina	104
5-6	Spectra on the Adsorption of 3-Pentanol on 2% NaOH-doped γ -Alumina	105
5-7	Variation of Spectrum Above 3500 cm^{-1} of the NaOH-doped γ -Aluminas	107
5-8	Spectra on the Degassing of γ -Alumina at Room Temperature over Varying Time Periods	109
5-9	Spectra on the Adsorption of 3-Pentanol on NaOH-doped γ -Aluminas at 200°C for One Hour	112
5-10	Evaluation of Pore Diffusion	126
5-11	Influence of Time on the Catalyst Activity	128
5-12	IR Spectra of Adsorbed Species on γ -Alumina at Steady-State Reaction Conditions	131
5-13	Temperature Dependency of the Rate of Dehydration of 2-Propanol	152
5-14	IR Spectra of Adsorbed Species on 8% NaOH-doped γ -Alumina at Steady-State Reaction Conditions	154
5-15	Temperature Dependency of the Rate of Dehydrogenation of 2-Propanol	177
7-1	Schematic Diagram for the Use of Long IR Cell in Kinetic Studies	184

LIST OF FIGURES (continued)

<u>Figure</u>		<u>Page</u>
7-2	Online Monitoring and Control of Chemical Reaction Kinetics Studies	185
A-1	Block Diagram of IR-Computer System	A-2
A-2	IBM 1800 Data Acquisition and Control System	A-7
A-3	Flow Diagram of Program Controlled Data Acquisition	
	(a) Start Procedure	A-11
A-4	(b) Data Acquisition	A-11
A-5	(c) Stop Procedure	A-11
A-6	IR On-line Data Acquisition Procedures, MPX System	A-15
A-7	Data Reduction Flow Diagram	A-18
A-8	Comparison Between Raw and Smoothed Data	A-20
A-9	Comparison of IR Spectra "Before and After" the Experiment	A-23

LIST OF TABLES

<u>Table</u>		<u>Page</u>
2-1	IR Spectrum of Hydroxyl Groups on Alumina	16
2-2	Infrared Frequencies of Acetone in Different States	25
2-3	Apparent Activation Energies for the Dehydration of Alcohols	34
3-1	Typical Properties of Alon C	45
3-2	Sodium Hydroxide Content and Surface Area of Doped γ -Alumina	46
3-3	Pore Size Distribution for the Alumina Catalyst	47
4-1	Frequencies Employed for Quantitative Analysis	71
4-2	Least Squares Calibration of 2-Propanol Absorbance at 1148 cm^{-1} Using Beer's Law	79
4-3	Least Squares Calibration of 2-Propanol Absorbance at 1250 cm^{-1} Using Beer's Law	80
4-4	Least Squares Calibration of 2-Propanol Absorbance at 3660 cm^{-1} Using Beer's Law	81
4-5	Least Squares Calibration of Propylene Absorbance at 3102 cm^{-1} Using Beer's Law	82
4-6	Least Squares Calibration of Acetone Absorbance at 1740 cm^{-1} Using Beer's Law	83

LIST OF TABLES (continued)

<u>Table</u>		<u>Page</u>
4-7	Relation of 2-Propanol Feed Rate to Its Partial Pressure under Non-reaction Conditions	86
5-1	Activity and Selectivity of γ -Al ₂ O ₃ or NaOH-doped γ -Al ₂ O ₃ ; Dehydration and Dehydrogenation of 3-Pentanol	114
5-2	Behavior of Various Kinetic Parameters in Each Domain of Control	123
5-3	Possible Kinetic Models for Dehydration of 2-Propanol	140
5-4	Experimental Data for Dehydration Reaction	144
5-5	Expected Entropy Change at Various Partial Pressures of 2-Propanol and Water for Dehydration Reaction	146
5-6	Kinetic Data over Range of Temperatures, for Dehydration of 2-Propanol	150
5-7	Possible Kinetic Models for Dehydrogenation of 2-Propanol	162
5-8	Experimental Data for Dehydrogenation Reaction	167
5-9	Model Performance for Dehydrogenation of 2-Propanol	169
5-10	Expected Entropy Change at Various Partial Pressures of 2-Propanol and Hydrogen for Dehydrogenation Reaction	173

LIST OF TABLES (continued)

<u>Table</u>		<u>Page</u>
5-11	Data for Estimation of the Activation Energy of the Dehydrogenation Reaction	175
A-1	The Usage of the Special Indicators in Data File	A-10
C-1	Calibration of Syringe Feeder by Least Squares Method (Low Speed Range)	C-2
C-2	Calibration of Syringe Feeder by Least Squares Method (High Speed Range)	C-3

CHAPTER I

INTRODUCTION

Classically, the measurement of the kinetics of a homogeneous chemical reaction has been used to deduce the mechanism of the reaction. In heterogeneous catalysis, it is well-established that the solid-catalyzed reaction proceeds by the adsorption of reactants on "active sites" on the surface, reaction of the adsorbed species with either another adsorbed species or a molecule from the surrounding phase, and finally desorption of the products to regenerate the surface active site. Accordingly, from observations of the product distribution and the reaction kinetics, reaction mechanisms have been proposed. One major difficulty that arises in such a procedure is that more than one set of mechanisms can be proposed that fits all of the observed data quite well. The differences in fit may be so slight as to be explainable entirely in terms of experimental error. Therefore, if a number of alternative mechanisms fit the data equally well, the selected rate equation is one of good fit but not necessarily one that represents the true mechanism.

The reason for searching for the "actual" mechanism is that, in reactor design, extrapolation to new or more favorable operating conditions is much more safely done. Since a study of kinetics alone can not always provide a conclusive reaction mechanism, the mechanism problem remains to be solved.

Infrared spectroscopy has proven to be of great value in determining the structure of molecules. In recent years, its application to the study of surface chemistry has provided one of the most direct means of deducing the active sites on the catalyst, the interactions and perturbations that occur on the surface during adsorption, and the structure of the adsorbed species. Such results, would be anticipated to be very useful in inferring mechanisms of solid-catalyzed reactions.

Although it was reported⁽¹⁾ that the adsorbed species observed by infrared analysis may be good candidates for consideration as intermediates of the reaction, it is sometimes difficult to make direct observations on reaction intermediates in the infrared spectrum because they may only exist in small quantities. For a reaction intermediate to be detectable in an infrared spectrum, it must have a relatively high surface concentration. This would be expected to be true only in cases where the slowest reaction step follows the formation of the intermediate. Therefore, the possibility exists that less strongly chemisorbed species, subsequently existing in low surface concentrations, may be the reactive intermediate which may not be detectable in the infrared analysis. A combination of both kinetics and infrared spectral analyses would be thus expected to provide more information for obtaining reaction mechanisms than by either method alone.

In a few cases^(2,3), infrared study of adsorption and surface reactions were used in conjunction with independently obtained kinetic data to suggest kinetic models which were mechanistically sound. How-

ever, this approach has limitations in that different forms of the catalyst, different pretreatments of the catalyst, and different temperatures and reactant pressures may be necessitated by the two different sets of experimental conditions for the kinetic and infrared spectral studies.

To date, spectral analysis has been combined with simultaneous kinetic studies where both infrared spectra and kinetic data are obtained under batch reactions⁽⁴⁻⁸⁾. However, it was shown⁽⁹⁾ that obtaining both infrared spectra of adsorbed species and kinetic data simultaneously under steady-flow conditions facilitates the determination of diffusion limitations and eliminates complications of changing mechanisms which may occur under batch reaction conditions. Goldsmith⁽¹⁰⁾ and Baddour et al⁽⁹⁾ have applied simultaneous kinetic and spectroscopic studies in a flow system to the study of carbon monoxide oxidations on silica-supported palladium. However, their samples of the exit stream were analyzed on a gas chromatograph and steady-state operation was assumed when there was less than 2% variation in the outlet composition over a 30-minute period.

The purpose of this thesis has been to develop and to apply a technique for the simultaneous measurement of the reaction kinetics and the spectra of the adsorbed surface species by using infrared analysis for a solid-catalyzed chemical reaction. This information was then to be used to identify the kinetically important surface species, to determine a realistic mechanism for the reaction, and then

to elucidate the kinetic models for various catalyst modifications. Steady-state operation can be observed directly by setting the infrared spectrophotometer at a single frequency of interest and by recording the changes in the sample beam intensity as a function of time⁽¹¹⁾. This technique appears to be simple, versatile and accurate in obtaining the kinetic data.

The heterogeneous alumina-catalyzed dehydration of alcohols has been known since the end of the eighteenth century. Although the dehydration reaction is generally agreed to involve surface acidic sites, widely different views are still held concerning the mechanism of this reaction. The use of γ -alumina as a catalyst also has been studied intensively for many decades yet, the nature of the sites responsible for their activity remains controversial. Earlier, in a kinetic study of dehydrogenation of 1-propanol over solid catalysts, Vasudeva⁽¹²⁾ reported that the role of the alumina was altered from that of a dehydrating catalyst to one of the dehydrogenating catalyst by doping with sodium hydroxide. The relation of the catalytic activity and selectivity to the supposedly responsible acidic sites on the γ -alumina has not been clearly revealed. For these reasons, the decomposition of secondary alcohols, C_3 to C_5 , on the dual function catalysts made of sodium hydroxide-doped γ -alumina was chosen to study the reaction mechanism using the proposed infrared technique.

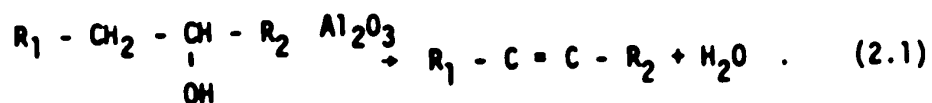
Some of the spectral analysis in this study was obtained with a Perkin-Elmer Model 621 infrared spectrophotometer connected on-line to an IBM 1800 computer. In the study of adsorbed species, elimination

of the background spectra of the catalyst by obtaining infrared data on-line saves a great amount of work and of time. The system components, the operating procedures and data processing methods are described in Appendix A.

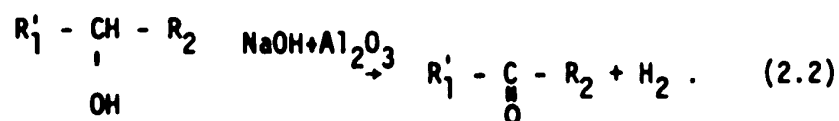
CHAPTER II
SURVEY OF RELATED WORK

2.1 Dehydration and Dehydrogenation of Alcohols

The dehydration of simple alcohols on alumina catalysts leads mainly to the formation of ethers, olefins and water. At lower temperatures, the dehydration of unbranched alcohols (up to 1-hexanol) yields ethers, olefins and water⁽¹³⁾ whereas for secondary alcohols ether has not been detected as a dehydration product. Product distributions for the dehydration of 2-propanol⁽¹⁴⁻¹⁷⁾, 2-butanol^(14,15,18) and 3-pentanol^(2,18) have also been investigated. The dehydration of 2-propanol leads to the formation of propylene, with trace quantities of isopropyl ether at low reaction temperatures. The dehydration of 2-butanol yields 1-butene and, cis- and trans- 2-butenes at all the reaction temperatures studied. The dehydration of 3-pentanol gives predominantly 2-pentenes and traces of 1-pentene according to Pines and Manassen⁽¹⁸⁾. The cis to trans ratio of the 2-pentene found is 2.5 and 1-pentene is thought to be a secondary product by isomerization of 2-pentenes at reaction temperatures above 300°C. Thus the dehydration of secondary alcohols, C₃ to C₅, can be represented as follows:



The dehydrogenation of alcohols on sodium hydroxide-treated alumina catalyst has also been studied^(2,19). In this case the dehydrogenation reaction proceeds as follows.



The catalyst used in their studies was γ -alumina treated with 2N sodium hydroxide aqueous solution. Besides ketone and hydrogen, some dehydration products were found.

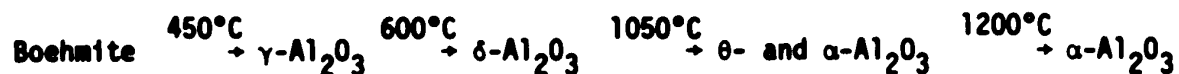
In some studies^(19,20), the dehydration and dehydrogenation of alcohols accompanied by thermal decomposition were also observed. However, the thermal decomposition can be avoided by studying the reactions at lower temperatures (below 450°C) in a glass reactor.

A comprehensive survey of the alcohol dehydration was published by Winfield⁽²¹⁾ for work prior to 1960. The two major issues seem to be the mechanism and the kinetics of the reaction, and the type of active sites of the catalysts. To date, these questions are still the subjects for several investigations.

The catalytic activity of a surface is strongly dependent on its structure and also its properties in addition to the surface compounds of the substrates and reaction products. Henceforth, the structure and properties of the γ -alumina surface, the adsorption structures of both alcohols and their dehydration as well as dehydrogenation products will be reviewed before the kinetic and mechanistic studies are described.

2.2 The Structure of γ -Alumina

The γ -alumina is one of the transition aluminas most commonly used for catalytic purposes. It is formed by controlled thermal decomposition of the hydrate, bayrite, or of the oxyhydrate, boehmite, at 450°C. Above 600°C, however, transformation to the delta phase occurs. The thermal process can be represented by the following sequence:



The crystalline structure of γ -alumina is a defect spinel lattice⁽²²⁾. The unit cell of the crystal consists of 32 oxide ions with 21 1/3 aluminum ions arranged at random in the 16 octahedral and 8 tetrahedral positions of the spinel structure. In a single-crystal electron diffraction study, Lippens and deBoer⁽²³⁾ found that the oxygen lattice of γ -alumina should be fairly well ordered. Consequently, the disorder in the γ -alumina is determined mainly by disorder of the aluminum ions. Saalfeld and Mehrotra⁽²⁴⁾ determined the cation distribution by Fourier synthesis of the electron diffraction patterns and found that the octahedral aluminum sublattice was fully occupied and that the necessary vacant sites were randomly distributed over the tetrahedral interstices. The details of the crystallographic structure determination have been discussed by Lippens⁽²⁵⁾.

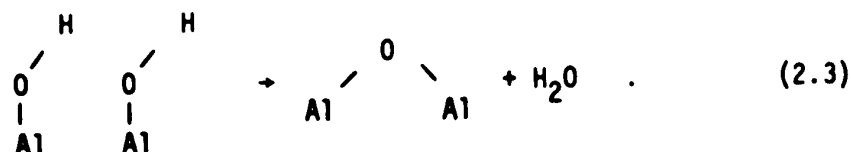
The necessity for maintaining the structural integrity of the

catalyst throughout the investigation is likewise apparent. Often the change in water content of the catalyst is accomplished by treatment at various higher temperatures; care must be taken during this treatment to eliminate possible phase transitions. Pines and Haag⁽²⁶⁾ studied the effect of both the treatment temperature (up to 1000°C) and the water content upon alumina activity towards isomerization of cyclohexene. They found a pronounced decrease in activity between 800 to 900°C, which could be the result of a phase transition of the catalyst⁽²⁷⁾ since delta alumina forms at 600°C. Care must be taken not to alter either the phase or modification of an alumina since by doing so one concurrently changes its surface site configuration and thereby its intrinsic activity.

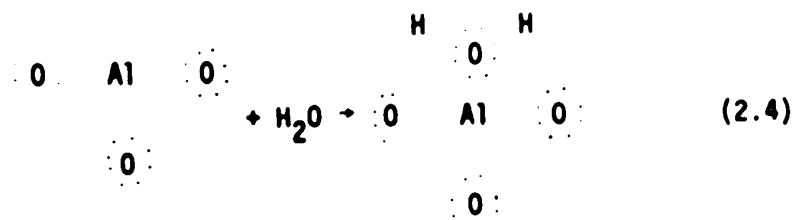
2.3 The Surface of γ -Alumina

Though many authors^(28,29) believe the [111] face of the oxygen sublattice to be energetically favored, Lippens⁽²⁵⁾, based on x-ray and electron diffraction studies, concludes that the [100] plane of γ -alumina is preferentially exposed. Since it is believed⁽³⁰⁾ that the surface is terminated in anions, which are more readily polarizable than cations, the outermost aluminum ions thus lie below the surface plane. These aluminum ions provide the electrophilic centers by which water is dissociatively held on the surface; the electron pair of the OH group being positioned over the aluminum ion while the dissociating proton forms a hydroxyl via binding to lattice oxygen⁽³¹⁾. This reaction proceeds until the surface is completely filled with OH groups.

At higher water vapor pressures more water is bonded in a multilayer physical adsorption process but this water can be removed easily by a drying procedure at about 120°C⁽³²⁾. Upon heating at higher temperatures, the opposite reaction occurs, elimination of water by recombination of the two OH groups, which leaves a lattice oxide ion and an aluminum ion site at the surface in the following manner^(33,34).

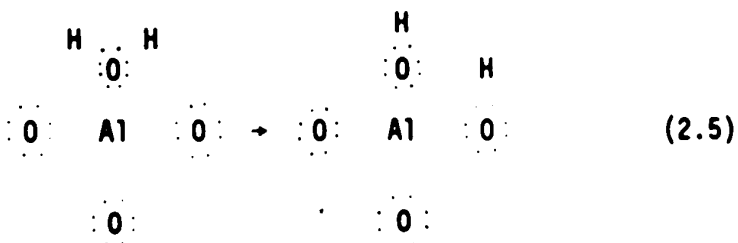


The aluminum ions thus formed may be regarded as acidic centers of the Lewis type^(35,36) which can be selectively poisoned by organic bases^(37,38). However, the OH groups were reported to be very weak acidic Bronsted-acid centers^(37,39,40) which can react with ammonia ($\text{p}K_{\text{B}} = 5$) to form ammonium ions⁽³⁵⁾ but not a strong enough acid to react with pyridine ($\text{p}K_{\text{B}} = 9$) to form pyridium ions⁽³⁷⁾. Tamele⁽²⁷⁾ depicted the attachment of water to the alumina as the completing of the octet of electrons of aluminum and the conversion of a Lewis-acid site to a Bronsted-acid site as shown in reaction (2.4)



An adjacent lattice oxygen provides an electron pair for sharing with

a proton. In this way two hydroxyl groups are created.

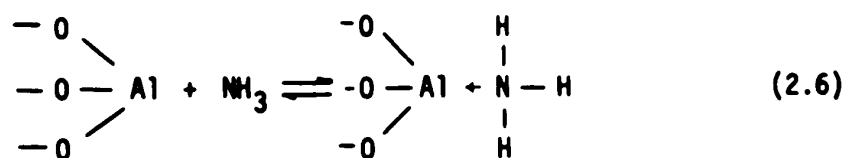


The lattice OH groups thus formed are therefore positionally below the plane of the parent OH groups.

In recent years, the most extensive study of the alumina surface was made by Peri^(35,41,42) using gravimetric and infrared spectroscopic methods. For an undried γ -alumina, infrared bands were observed near 3300 and 1650 cm^{-1} and these bands were assigned to the stretching and bending frequencies, respectively, of molecular water adsorbed on the alumina surface. After evacuation at 720°C, the spectrum has shown three well-defined peaks at 3698, 3737 and 3795 cm^{-1} ⁽⁴¹⁾. These bands are essentially symmetric and are attributed to the stretching vibrations of isolated surface hydroxyl groups. Deuteration causes these bands to disappear and to be replaced by three equivalent bands at 2733, 2759 and 2803 cm^{-1} . All bands are shifted in frequency by a constant factor of 0.738 which is close to the theoretical value (0.73) for the isotope shift. This provides good evidence that the original absorption bands were due to the stretching vibrations of surface hydroxyl groups. Also, it was observed⁽⁴¹⁾ that the 3698 cm^{-1} hydroxyl groups were able to exchange their H for D faster than the other two groups and therefore the groups corresponding to the band at 3698 cm^{-1}

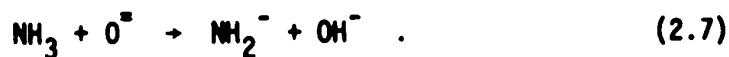
were proposed to be the most acidic of the three hydroxyl groups.

The aluminum ions exposed by vacancies in the oxide lattice were also considered by Peri⁽³⁵⁾ and others⁽⁴³⁾ as Lewis-acid centers which provide the principal sites for the adsorption of ammonia molecules (a Lewis base). Thus, ammonia should react with the alumina surface to give a chemisorbed species as follows:

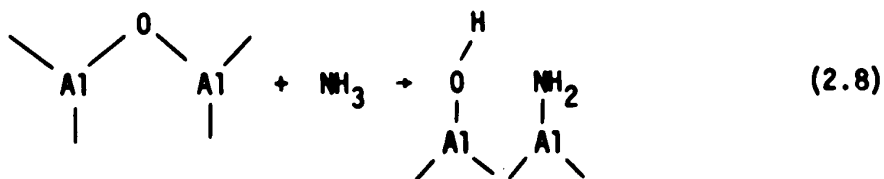


However, ammonia reacts with the alumina via the chemisorption process, reaction (2.6), and other processes as well. The adsorption is complicated by interactions of the ammonia with surface hydroxyl groups and surface oxide ions, and thus does not provide immediate evidence of these Lewis-acid sites. Pyridine was found not to react with hydroxyl groups and oxide ions on the alumina surface. Therefore, the spectrum of adsorbed pyridine can be interpreted as showing the presence of these Lewis-acid centers. The details of the analysis have been given by Parry⁽³⁷⁾ and no further discussion is attempted here.

During the infrared study of the adsorption of ammonia on the alumina surface, Peri⁽³⁵⁾ also reported that a new hydroxyl band appeared at 3725 cm^{-1} . This was considered to indicate the presence of the oxide ions on the alumina surface. The chemisorption reaction can proceed as shown in reaction (2.7).



Peri⁽³⁵⁾ proposed that the above reaction as a completely ionic process. Other workers⁽⁴⁴⁾ have often represented the bonding between atoms in the surface in covalent terms. In this way reaction (2.7) could be written as follows:



The true nature of the bonding in oxides probably lies between the extreme ionic and covalent descriptions⁽⁴⁴⁾.

Several interpretations of the nature of active sites on the γ -alumina surface are available. One view proposed⁽⁴⁵⁾ that the aluminum or oxide ions exposed at the surface act as active sites and that the surface was free of hydroxyl groups. This view is contradictory to that presented by Peri and Hannan⁽⁴¹⁾ who observed that alumina surface is completely hydrated at lower temperatures by investigation of water adsorption and analysis of the infrared spectra of water adsorbed on γ -alumina.

The other view proposed that the alumina surface contains cation defects and strained sites, which result from the dehydration of the original hydrated surface^(46,47). A more detailed model was proposed by Peri⁽⁴²⁾ who obtained the model by a computer simulation from the dehydration of a fully hydrated surface on (100) crystal planes.

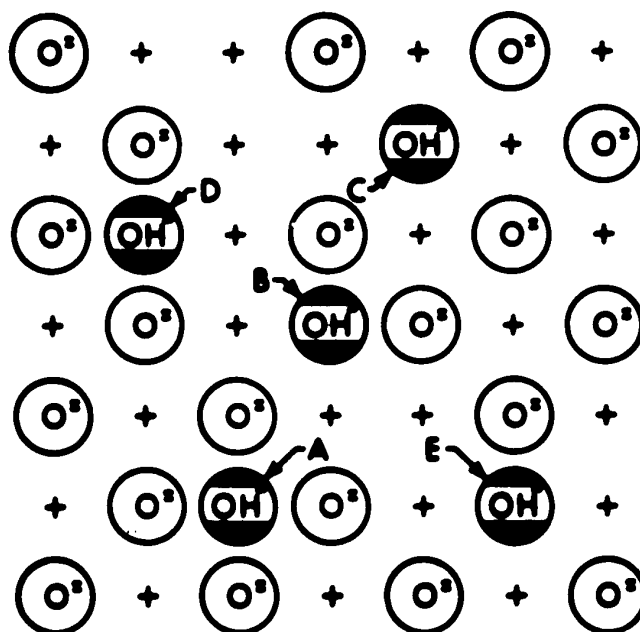
The resultant computer model predicted a surface containing five different types of hydroxyl groups. The various types of hydroxyl site are shown in Figure 2-1 and the corresponding infrared vibrational frequencies are shown in Table 2-1. This model may be considered more or less representative of the dehydration mechanism and the structure of alumina surface. However, the validity of the assumptions proposed by Peri⁽⁴²⁾ have been subjected to criticism by Lippens⁽³³⁾, i.e. for alumina samples heated at temperatures above 600°C, the assumption that a spinel type alumina exposes only (100) planes on the surface is very unlikely energetically.

Although Peri's model could be used to explain some of the experimental observations on the alumina surface, conflicting results were obtained in this study. These will be discussed later in this thesis.

2.4 Effect of Sodium Hydroxide on the Structure of Alumina Surface

In a study of reactions of 1-propanol on solid catalysts, Vasudeva⁽¹²⁾ showed that the activity of alumina towards the dehydration of 1-propanol was completely destroyed when the alumina catalyst was treated with 2N sodium hydroxide solution. It was attributed^(2,19) to the destruction of the "acid centers" on the alumina upon treatment with sodium hydroxide.

Recently, in an infrared study of 1-propanol adsorption on sodium hydroxide doped γ -alumina, Deo and Dalla Lana⁽⁴⁸⁾ reported that a 2% of sodium hydroxide content in γ -alumina was enough to react with the surface hydroxyl groups of 3785 cm^{-1} to form $=\text{Al}-\text{O}-\text{Na}$. Thus,



+ DENOTES Al^{3+} IN LOWER LAYER

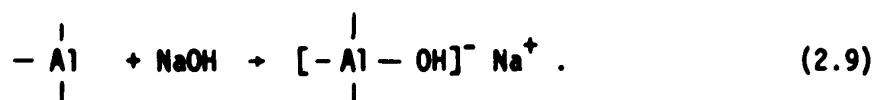
Figure 2-1. Computer Model of a Dehydroxylated Alumina Surface (42). The five types of OH are assigned the frequencies in Table 2-1.

Table 2-1
IR Spectrum of Hydroxyl Groups on Alumina*

Band	Wave number, cm^{-1}	No. of nearest Oxide neighbors
A	3800	4
B	3780	3
C	3744	2
D	3733	1
E	3700	0

*With reference to Figure 2-1

the reaction was considered to be with the Bronsted-acid sites. Unfortunately, no data were presented for the effect of sodium hydroxide on Lewis-acid sites, and the complete reaction mechanism can not be obtained at this stage. However, Pines and Haag⁽²⁶⁾ suggested the possibility that doping with sodium hydroxide could give rise to an acid/base surface complex of the type shown in reaction (2.9)



This reaction is not in agreement with the data reported by Ross and Bennett⁽⁴⁹⁾ who found no evidence for the formation of such a complex in any detectable amount.

2.5 Infrared Studies of the Adsorption of Alcohols on γ -Alumina Catalysts

Infrared spectral studies of the adsorption of alcohols on alumina surface have been previously reported and four different types of surface species were observed:

1. physically adsorbed alcohols via hydrogen bonds^(45,48,50).
2. an aluminum alkoxide type of structure formed by dissociative chemisorption^(45,48,51-56).
3. a carboxylate structure formed by oxidation of the alcohol^(45,48,51-53,57,58).
4. adsorbed water, one of the dehydration products.

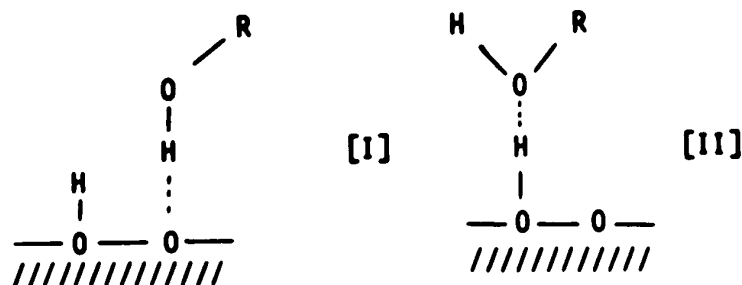
It was reported⁽⁵⁹⁾ that the adsorption of 3-pentanol on the sodium hydroxide doped γ -alumina at higher temperatures yields the corresponding ketone and hydrogen. Therefore, the role of adsorbed ketone

and hydrogen will also be discussed.

2.5.1 Physically Adsorbed Alcohols

The infrared absorption of free hydroxyl groups of alcohols should be expected to appear in the range of 3600 to 3650 cm^{-1} , e.g. spectra of vapor phase alcohols. The OH stretching vibrations shift from ~ 3600 to 3350 cm^{-1} for all the liquid phase alcohols (C_1 to C_5). This frequency shift can be explained by the formation of hydrogen bonds and the extent of the shift is a measure of the strength of the hydrogen bonds. All alcohols adsorbed on alumina give a strong OH stretching bands centered around 3500 cm^{-1} . This can be interpreted to be the formation of weak hydrogen bonds as compared to the 3350 cm^{-1} for liquid alcohols.

Whereas Babushkin et al⁽⁵⁴⁾ and Borekov et al⁽⁵⁶⁾ thought that they could still detect physically adsorbed ethanol even at high desorption temperatures, Greenler et al^(45,51) (methanol and ethanol), Treibmann and Simon⁽⁵³⁾ (ethanol, 1- and 2-propanol), Kage⁽⁴⁵⁾ (1-propanol and 1-butanol), and Deo and Dalla Lana⁽⁴⁸⁾ (1-propanol) found that alcohols are readily desorbed on evacuation even at room temperatures. NMR studies showed that the hydroxyl group of the alcohols interacts directly with the alumina surface⁽⁶⁰⁾; it must therefore be assumed that hydrogen bonds are formed. Kage⁽⁴⁵⁾ proposed, without direct spectroscopic evidence, that the structures, [I] and [II], are present on γ -alumina surface.



Although Knozinger et al⁽⁵⁰⁾ reported the presence of structures [I] and [II], Deo and Dalla Lana⁽⁴⁸⁾ observed very little hydrogen-bonded species when hydrogen atoms of the surface hydroxyl groups were replaced by sodium atoms. This, therefore, indicates that structure [II] is a more probable representation of the hydrogen-bonded alcohols. This is also in agreement with the results obtained by Krylov⁽⁶¹⁾, and Jain and Pillai⁽⁶²⁾.

2.5.2 Aluminum Alkoxide Structure

Ethanol, on adsorption at lower temperatures (20 to 100°C) gives rise to a surface compound whose infrared spectrum is almost identical with that of the corresponding aluminum alcoholate⁽⁵¹⁾. For comparison, both spectra are shown in Figure 2-2. Similar results have been obtained with 1-propanol^(45,53), 2-propanol⁽⁵³⁾, 1-butanol⁽⁴⁵⁾, iso-butanol⁽⁵²⁾, tert-butanol⁽⁵²⁾ and benzyl alcohol⁽⁵²⁾. The differences in the infrared spectra between surface alkoxides and aluminum alcoholates are attributed to the different ratios of -OR radicals to Al atoms.

There are two possible ways for the formation of alkoxide species by dissociative adsorption:

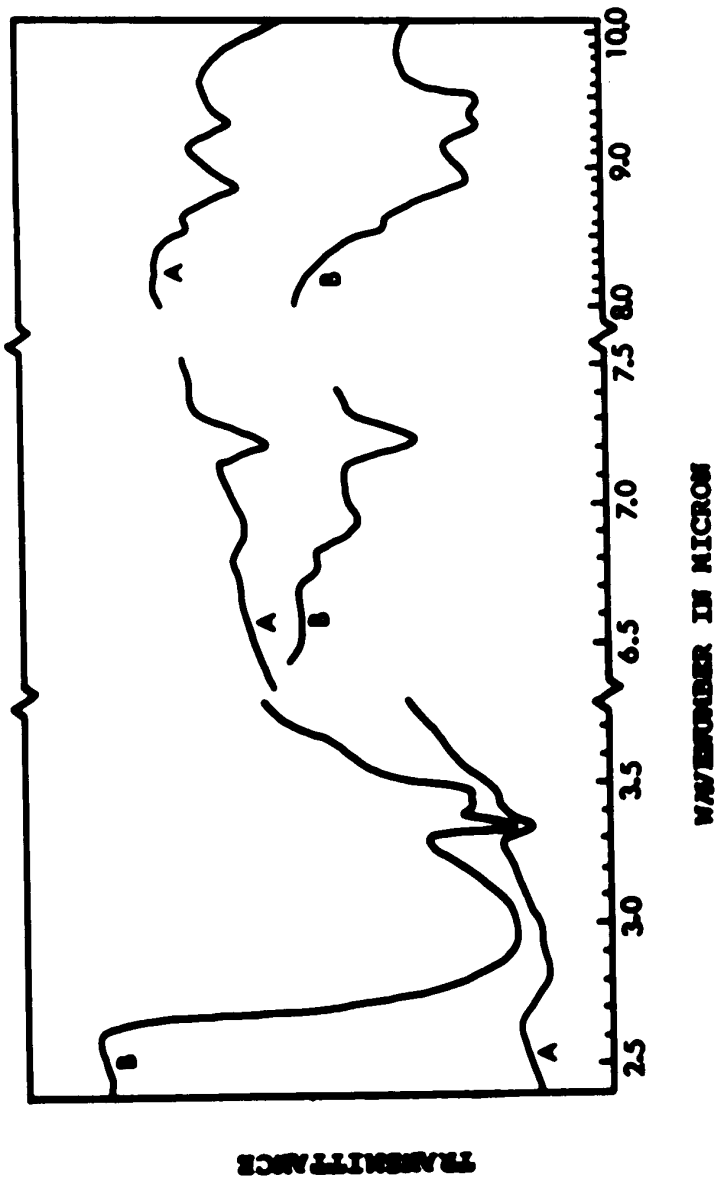
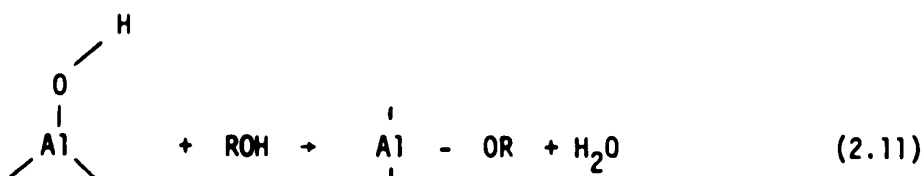
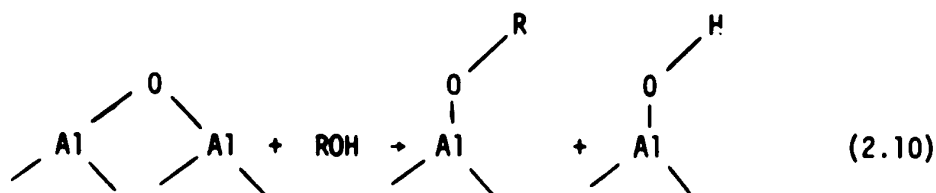


Figure 2-2. Spectra of (A) C_2H_5OH on Al_2O_3 , at $35^\circ C$ after Evacuating Sample Cell, and (B) $(C_2H_5O)_3Al$ (51).



In reaction (2.10) a hydroxyl proton is split off from the alcohol to form an alkoxide structure. The proton then adds to a surface oxide ion to form a hydroxyl group. Reaction (2.11) involves a hydroxyl group from the alcohol and a proton from the surface hydroxyl group. The C - O bond of the alcohol is broken and the resulting hydroxyl group reacts with a surface proton to form water.

Although the somewhat lower energy of rupture of the C - O bond in the alcohol favors the second possibility, reaction (2.11), the lattice energy liberated on incorporation of the alkoxide or hydroxyl group favors the rupture of the O-H bond⁽⁶³⁾. Treibmann and Simon⁽⁵³⁾ concluded from displacement reactions that the alkoxide formation involves incompletely coordinated aluminum ions. Kagel⁽⁴⁵⁾ reached the same conclusion on the basis of mass spectroscopic residual gas analyses after adsorption.

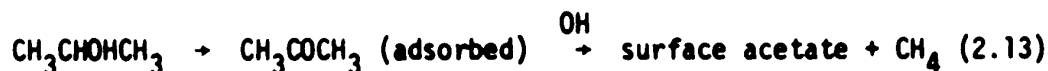
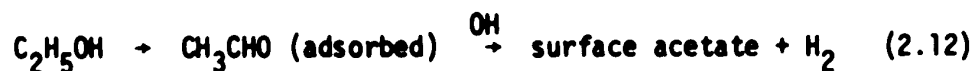
2.5.3 Carboxylate Structures

Oxidation of the alcohols during adsorption on alumina above 170°C to give carboxylate structures has been observed for methanol^(51,58),

ethanol^(51,53,56,58), 1-propanol^(45,48,64), 1-butanol^(45,64) and 2-propanol^(53,58). Also corresponding surface compounds have recently been found on the adsorption of benzyl alcohol and isobutyl alcohol⁽⁶⁵⁾ on alumina above 120°C.

In the study of adsorption of methanol, Greenler⁽⁵¹⁾ observed that on heating the methoxide to higher temperatures the spectrum shows three new infrared absorption bands at 1597, 1394 and 1377 cm^{-1} . By comparison with the published spectra of various metal formates, this indicates that the surface methoxy group has decomposed and produced a surface formate $[\text{H} - \text{C} \begin{array}{l} \nearrow \text{O} \\ \searrow \text{O} \end{array}]^-$. The formate ion may be treated as a simple XYZ_2 molecule that gives rise to a symmetric and an asymmetric C - O stretching vibration. For aluminum formate these are found at 1370 and 1600 cm^{-1} , respectively. Consequently, the bands found at 1377 and 1597 cm^{-1} in the spectrum of the surface species are attributed to these modes. The third absorption band at 1394 cm^{-1} for the surface species and at 1390 cm^{-1} for the aluminum formate are attributed to a C - H bending vibration. Further confirmation of the nature of this species was obtained by isotopic substitution of C^{13} for C^{12} in the reactant alcohol. The resultant spectrum showed that the isotopic shifts were in good agreement with calculated values. Thus, interpretation of the nature of the surface species is considered to be satisfactory.

From an extensive infrared study, Fink⁽⁵⁸⁾ reported mechanisms for the formation of the carboxylate compounds as follows:



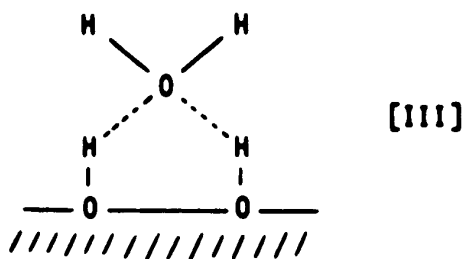
where OH denotes surface hydroxyl group.

All the carboxylate structures are observed at temperatures up to 600°C. In view of its high stability, this structure could hardly be important as an intermediate in surface reactions which occur below 300°C^(57,66). However, it was reported⁽⁶⁷⁾ that, above 300°C, the dehydrogenation of ethanol on alumina could proceed via an acetate structure. This is not in agreement with the experimental results reported by Deo and Dalla Lana⁽⁴⁸⁾.

2.5.4 Adsorbed Water

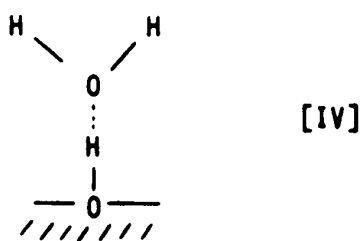
The adsorption of alcohols below the reaction temperature is always accompanied by the appearance of a band at 1600 cm⁻¹ when the infrared spectrum is scanned at room temperature. This band increases in its intensity with increases in the adsorption temperature and it is not believed to be due to the alcohol or any of its surface compounds but due to adsorbed molecules of water⁽⁶⁸⁾.

It is generally assumed that molecules containing oxygen and having two pairs of free electrons are preferentially adsorbed via two passive hydrogen bonds as in structure [III]⁽⁴⁴⁾.



This type of adsorption bonding via two hydrogen bonds requires two adjacent hydroxyl groups on the surface. It is believed⁽⁶⁹⁾ that at 200°C, there are still hydroxyl groups covering 50 to 80% of the alumina surface and thus structure [III] represents the adsorption of water from room temperature to 170°C.

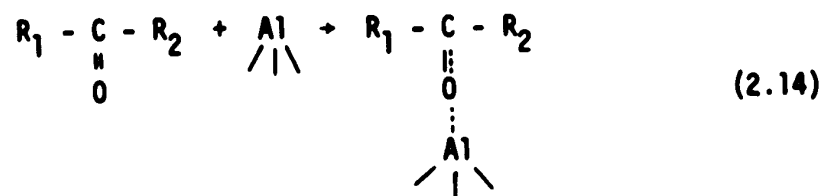
However, adsorption on isolated hydroxyl groups such as structure [IV] should be possible, particularly when two adjacent hydroxyl sites are not available.



It was also proposed⁽⁶³⁾ that structure [IV] is more probable when water is adsorbed in the presence of excess alcohol, e.g. adsorption of alcohols at higher temperatures.

2.5.5 Adsorbed Ketone

It is well established in the literature that ketones will form stable complexes with inorganic Lewis-acid halides such as AlCl_3 and BCl_3 . The complex formation takes place via the oxygen atom of the carbonyl group, and the donation of electrons from the oxygen atom into the vacant orbital of the Lewis acid leads to a delocalization of the electrons in the double bond⁽⁷⁰⁾. In the case of alumina, Lewis-acid sites are believed to be present on the surface and thus a similar reaction should occur:



When acetone is adsorbed on alumina surface, a strong shift in infrared frequency of the free carbonyl group is observed⁽⁵⁸⁾. The type of the chemical bond of the chemisorbed complex is similar to that of electron donor-acceptor complexes. For comparison, infrared absorption peaks of acetone in different states are listed in Table 2-2.

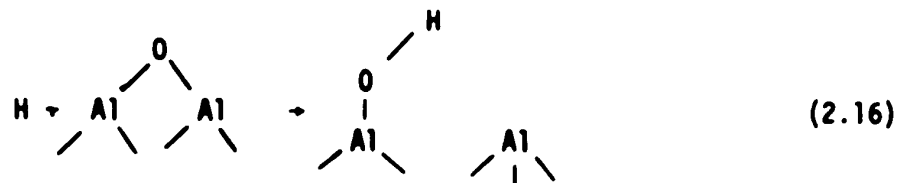
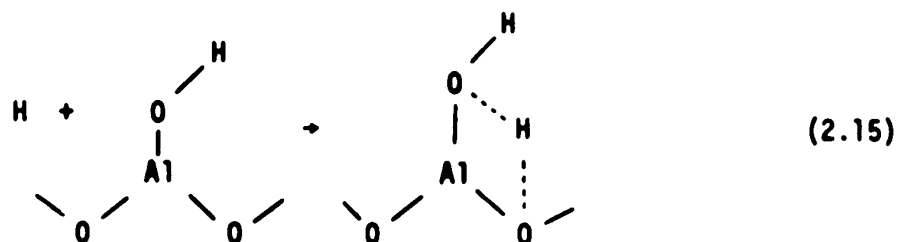
Table 2-2
Infrared Frequencies (cm^{-1}) of Acetone in Different States

Assignment	Acetone liquid	Acetone on BCl_3 Solid ⁽⁷¹⁾	Acetone on $\gamma\text{-Al}_2\text{O}_3$ ⁽⁵⁸⁾
$\nu_{\text{C}=\text{O}}$	1710	1625	1620
$\delta_{\text{s}}\text{CH}_3$	1433	1400	1460
$\delta_{\text{as}}\text{CH}_3$	1358	1362	1380
$\nu_{\text{C}-\text{C}}$	1225	1262	1250

2.5.6 Adsorbed Hydrogen

So far, very little attention has been paid to the study of adsorption of hydrogen on γ -alumina. Russell and Stokes⁽⁷²⁾ reported that hydrogen is adsorbed on alumina surface at temperatures above

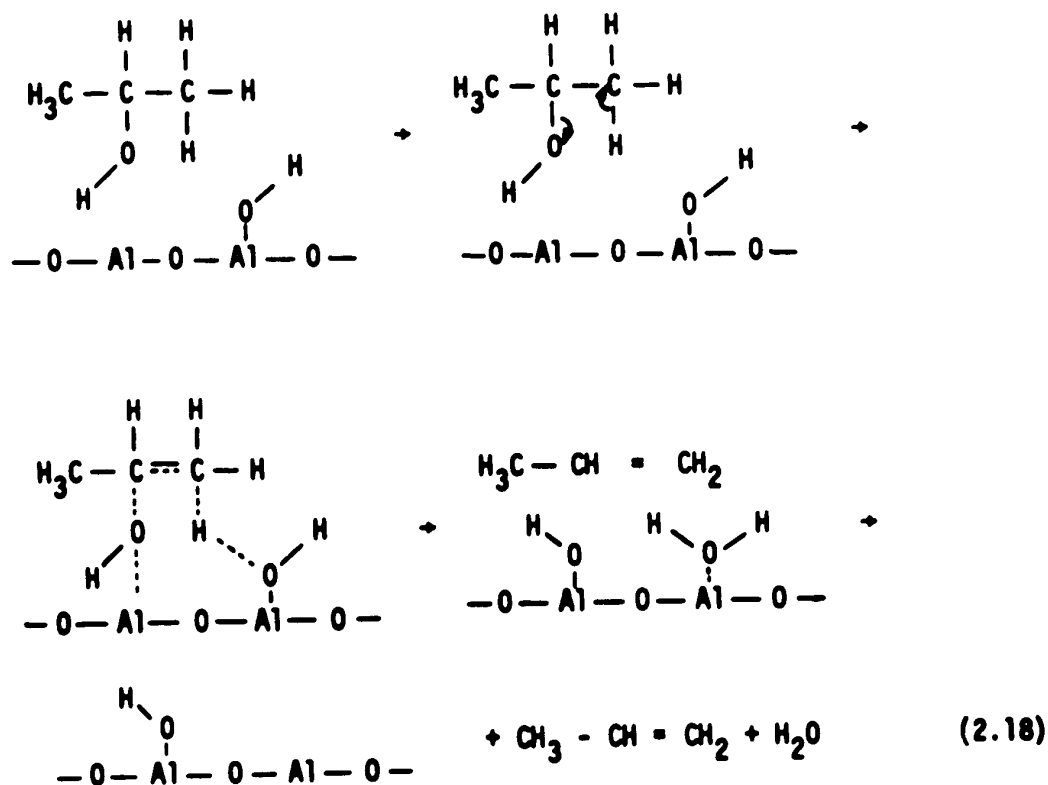
500°C. According to these authors the amount of hydrogen adsorbed is small, comprising less than 0.2 cm³/g (S.T.P.). No adsorption mechanism was given. It is expected that molecular hydrogen can be dissociatively adsorbed on γ -alumina only with difficulty because the free energy change for the dissociation reaction is about 200 K cal/mole⁽⁷²⁾. However, Peri⁽³⁵⁾ and Duken et al⁽⁷³⁾ proposed that ammonia can be dissociatively adsorbed on γ -alumina surface. The proton from ammonia reacts with a surface oxide ion to form a hydroxyl group. More recently, in an infrared study of chemisorption of acetylene on alumina, Bhasin et al⁽³⁴⁾ proposed that protons are accepted in the vicinity of OH groups forming hydrogen bonded groups (Reaction (2.15)), and to some extent by neighboring oxide ions to form isolated hydroxyl groups (Reaction (2.16)).



They claimed that this is evidenced by the rapid appearance of the broad band at 3600 cm⁻¹ due to hydrogen-bonded species and significant increase in the intensity of the infrared bands due to the surface

of the aluminum ions has not been proved.

(b) In an infrared study of the adsorption of ethanol on γ -alumina, Bremer et al⁽⁵⁷⁾ observed an infrared absorption band at 1080 cm^{-1} and attributed this band to the C-O vibration which is due to the alcohol coordinately bound to the Lewis center (aluminum ion). Using the principle of the least structural change, which has been applied in the past to the proton exchange, they proposed a reaction mechanism for the dehydration of 2-propanol on γ -alumina as follows:



The mechanisms (2.17) and (2.18) are similar in that both reactions involve Lewis-acid sites (aluminum ions). However, by poisoning these sites on alumina surface selectively with pyridine, many authors^(63,76,77)

concluded that Lewis-acid sites were not involved in the dehydration reactions.

(c) The formation of olefins by dissociation of surface alkoxide groups has been discussed in literature^(6,31,78,79). In a study of alcohol dehydration on silica-alumina, DeBoer and Visseren⁽⁸⁰⁾ reported that the reaction was not governed by the acid character of the catalyst but by the total number of aluminum atoms present on the catalyst surface. They concluded that the alcoholate formation may be the intermediate process in the dehydration reaction. Surface alkoxide species are indeed formed during the adsorption of certain, but not all, alcohols. For example, tert-butanol which solely forms olefins on dehydration at lower temperatures (85 to 160°C) does not form surface alkoxide structure⁽⁵²⁾. The participation of the surface alkoxide species in the dehydration of secondary alcohols was rejected recently⁽⁸¹⁾.

(d) A carbonium ion mechanism similar to that assumed for liquid phase reaction in acidic media is also proposed by several authors^(82,83) for the dehydration of alcohols on alumina catalyst. A proton from the surface hydroxyl group is assumed to transfer to the adsorbed alcohol molecule. The participation of surface proton (from surface OH groups) is supported by the need of water to be present on the catalyst⁽⁶³⁾. However, Knozinger⁽⁶³⁾ reported that $(CD_3)_3COH$ gives a high primary kinetic isotope effect, contrary to the expectations of a carbonium ion mechanism, in which the rate of C - O heterolytic fission should be rate-determining and should not therefore be in-

in which heavy water is formed on deuterated surface; the rate can not, therefore, be determined by the desorption of water or the cleavage of the R - H bond. On the other hand, a large primary isotope effect is found in the dehydration of $(CD_3)_3COD$, thus the removal of the β -hydrogen in the Reaction (2.19) must be the slowest step in tert-butanol dehydration.

2.7 Kinetics of Alcohol Dehydration on γ -Alumina

In order to understand the mechanism of a heterogeneous reaction, a knowledge of the reaction kinetics is necessary. However, only a few studies have been reported on the kinetics of the dehydration of alcohols on γ -alumina. In the following sections, in light of earlier investigations related to this study, the kinetics of the alcohol dehydration are discussed.

The experimental results of Brey and Krieger⁽⁸²⁾ for the ethanol dehydration on γ -alumina at 350 to 400°C, represent the following rate equation best:

$$22400 \cdot \text{rate} = \frac{kL K_a P_a}{K_a P_a + K_w P_w} \quad (2.20)$$

This equation is derived on the assumptions that surface reaction is the rate determining-step, and that ethanol and water are strongly adsorbed while ethylene is not. This model is essentially a Hougen-Watson type for a single-site mechanism with the assumption that the reaction is irreversible.

More recently, de Mourgues et al⁽¹⁶⁾ have studied the dehydration of 2-propanol on alumina in a flow reactor at low temperatures (100 to 160°C) and low alcohol partial pressures (8 to 23 mmHg). In order to ascertain the inhibiting action of the reaction products, they introduced propylene as well as water into the propanol feed. Their results show that the reaction is zero order with respect to the partial pressure of 2-propanol and that the reaction is inhibited by water, but not by propylene. On the basis of these observations, they claimed that a mechanism with a Hougen-Watson equation and competitive adsorption on the same site does not fit the experimental data well. The following rate equation was proposed

$$\frac{d(C_3H_6)}{dt} = \frac{K_A B_A \theta_A}{1 + K_W B_W \theta_W} \quad (2.21)$$

where B_A and B_W are the total number of sites which can be occupied by alcohol and water, respectively; θ_A and θ_W are the fractional coverages of B_A and B_W , respectively, and K_A and K_W are some constants.

In a study of dehydration of isobutanol, Knozinger⁽⁶³⁾ formulated an empirical kinetic equation in which the reaction rate was proportional to the square root of the partial pressure isobutanol, which is indicative of the dissociative adsorption of the alcohol. The equation is given as follows:

$$r = \frac{r_0 \sqrt{P_A}}{(\sqrt{P_A} + bP_W)} \quad (2.22)$$

where r_0 and r are reaction rates at time zero and time t . P_A and P_W are partial pressures of alcohol and water, and b is a constant. This is in conflict with the reaction mechanism proposed by Knozinger in his earlier investigations.

In later works on the dehydration of alcohols on alumina catalyst, zero and first order kinetic equations were hypothesized in some cases, or else no kinetic equation was given at all.

Several investigations have used the rate equation of Hougen-Watson type to represent the reaction mechanism. From the kinetic data for the dehydration of 2-butanol, Kittrell and Mezaki⁽⁸⁶⁾ proposed a dual-site mechanism with surface reaction as the rate-controlling step. The same conclusion was reached by Carra et al⁽⁸⁷⁾ for the dehydration of cyclohexanol and by Bremer et al⁽⁵⁷⁾ for the dehydration of 2-propanol. On the other hand, Butt et al^(88,89), Krylov⁽⁶¹⁾ and Kasaoka et al⁽⁹⁰⁾ chose a single-site mechanism with surface reaction as the rate-controlling step for the formation of olefins from alcohols.

2.8 Activation Energy for Alcohol Dehydration on γ -Alumina

In the literature, different results on the activation energy of dehydration of alcohols do not agree. The apparent activation energies for the dehydration of alcohols on γ -alumina catalyst are summarized in Table 2-3.

The difference in the two values of Reference (91) was explained to be due to the difference in the heats of desorption of water at the two different temperatures, which is 13 K cal/g-mole.

Table 2-3
Apparent Activation Energies for the Dehydration of Alcohols*

Alcohol	Temperature Range (°C)	Activation energy Kcal/g-mole	References
2-propanol	350	16	(21)
2-propanol	105-145	26	(91)
2-propanol	170-200	39	(91)
2-propanol	100-160	32	(16)
2-butanol	350	14.9	(21)
isobutanol	350	16.4	(21)
isobutanol	160-240	30.0	(52)

*Activation energies are found to be independent of system pressure

The value of 16 K cal/g-mole obtained for the dehydration of 2-propanol at 350°C was explained in a similar way: at 350°C the rate of reaction can be approximated by a first order rate equation with respect to 2-propanol. The apparent activation energy would thus be the difference between the true activation energy (estimated to be 25 K cal/g-mole⁽¹⁶⁾), and the heat of adsorption of 2-propanol (approximated to be equal to the heat of liquification of 2-propanol, which is 10 K cal/g-mole).

2.9 Effect of Doping Sodium Ion on γ -Alumina on the Dehydration of Alcohols

Topchieva et al⁽⁷⁸⁾ showed that the dehydration of ethanol was not affected by the presence of sodium ions whereas other workers^(26,49,57) claimed that the addition of sodium hydroxide suppressed the tendency of γ -alumina to dehydrate alcohols. These investigators did not examine the influence of the sodium ion impregnation upon the catalytic selectivity of γ -alumina. However, on impregnating alumina with KOH, Kuriacose et al⁽⁹²⁾ reported a decrease in the ratio of the rate of dehydration to the rate of dehydrogenation of 2-propanol from 12.20 to 1.75. Písmán et al⁽⁹³⁾ and, Maatman and Vande Griend⁽⁹⁴⁾ also found evidence of 1-butanol dehydrogenation over KOH- and KCl-treated alumina catalyst. Kinetics and mechanism of dehydrogenation of alcohols on the sodium hydroxide-treated γ -alumina are not available in literature at this time.

2.10 Kinetic Model Discrimination Techniques

The model discrimination procedure is often regarded as the process of selecting the best model from the various eligible models, assuming an adequate model is included among the models proposed for the system studied. This problem has been studied extensively and useful techniques have been reviewed by several authors^(95,96). After the preliminary screening of the data to eliminate poor models, model discrimination consists of the following three steps:

1. parameter estimation,
2. computing the model discrimination index - likelihoods of the data, and
3. sequential design of experiments.

The techniques, which cover the above three areas, developed by Singh⁽⁹⁸⁾, were adopted in this work. Details of the methods are summarized as follows:

2.10.1 Model Discrimination Procedure

Several criteria have been used as indices of model performance⁽⁹⁸⁾, the earliest of them being the minimum sum of errors squared. However, one of the most successful criteria is the Bayesian expected likelihood procedure based on a Bayesian interpretation of probability. The Bayesian approach has been used for model discrimination in this thesis and will be described below⁽⁹⁸⁾.

Suppose that after preliminary screening, it is concluded that the true model form is a member of the following set of m models,

which comprises the metamodel:

$$\begin{aligned}
 y &= \phi_1(\underline{x}, \underline{a}_1) + \epsilon_1 \\
 &\vdots \\
 y &= \phi_k(\underline{x}, \underline{a}_k) + \epsilon_k \\
 &\vdots \\
 y &= \phi_m(\underline{x}, \underline{a}_m) + \epsilon_m
 \end{aligned}
 \tag{2.23}$$

where metamodel is defined as the model space containing all the potential mechanisms which are considered simultaneously, and

\underline{x} = vector of independent variables

\underline{a}_k = vector of unknown parameters corresponding to the k^{th} model

y = dependent variable

ϵ_i = error term in the i^{th} model

The models may be in differential, rather than algebraic, form but that will not affect the argument to follow.

Uncertainty about which model form is the true one is expressed quantitatively in the form of a discrete probability distribution, where P_k is the probability that the k^{th} model form is correct. Obviously, the set of P_k 's satisfy the axioms of probability, i.e.

$$0 \leq P_k \leq 1.0 \quad ; \quad \sum_{k=1}^m P_k = 1.0 \quad (2.24)$$

Conceptually, the P_k 's are personal or subjective probabilities in the Bayesian sense and not objective or frequency probabilities in the classical sense. Bayesian probabilities are a measure of our current state of knowledge about an uncertain quantity or hypothesis; they are modified with the acquisition of new information in accordance with Bayes' theorem.

Before any data are taken, probabilities are assigned to the different model forms. In the absence of strong information, it is conventional to make these "prior probabilities" all equal. In a similar way, lacking specific information about the parameters, it is usually assumed that their values are uniformly distributed over the range $- \infty$ to $+\infty$ (called the improper uniform distribution).

Given n sets of observations $\{y_i, \underline{x}_i ; i = 1, 2 \dots n\}$, the posterior probabilities, P_j' , can be calculated in accordance with Bayes' Theorem.

$$P_j' = \frac{P_j' L(\underline{y}|\phi_j)}{\sum_j P_j' L(\underline{y}|\phi_j)} \quad (j = 1, 2 \dots m) \quad (2.25)$$

where P_j' designates the probability prior to observing the data \underline{y} and $L(\underline{y}|\phi_j)$ is the expected likelihood which is used to designate the probability of observing the data, given that the model form ϕ_j is correct.

One disadvantage of the Bayesian discrimination procedure

previously proposed in the literature⁽⁹⁵⁾ is the excessive computations involved in evaluating the expected likelihoods when the number of observations is more than about 20. However, new expressions for the expected likelihood have recently been developed by Singh⁽⁹⁸⁾ which are computationally much simpler for a wide class of problems. For the case where the prior information about the parameters in each model form is so vague that it can be approximated by the improper uniform distribution, the following expression for computing the expected likelihood for the j^{th} model was used⁽⁹⁸⁾.

$$L(\underline{y}|\phi_j) = (2\pi\sigma_j^2)^{-n/2} \left(\frac{1}{2}\right) \exp\left(-\frac{\hat{S}_j^2}{2\sigma_j^2}\right) \quad (2.26)$$

where r = number of parameters involved in the j^{th} model

\hat{S}_j^2 = the minimum sum of errors squared; $\hat{S}_j^2 =$

$$\min_{\underline{a}_j} \sum_{i=1}^n (y_{\text{observed},i} - y_{\text{calcd},i})^2$$

\underline{a}_j = parameter vector that minimize the sum of errors squared

$\sigma_j^2 = \hat{S}_j^2/(n-r)$; the unbiased estimate of error variance

The posterior probabilities of success for the competing models can now be computed from equation (2.25) and the parameters, $a_{j,k}$ with 95% confidence intervals are calculated from equation (2.27)

$$a_{j,k} = \hat{a}_{j,k} \pm 2\sqrt{C_{j,kk}} \quad (2.27)$$

where $\hat{a}_{j,k}$ = k^{th} element of the parameter vector $\hat{\underline{a}}_j$ that minimize the sum of errors squared for the j^{th} model

$C_{j,kk}$ = the diagonal element of the variance covariance matrix of the parameters, \underline{C}_j for the j^{th} model

In order to compute \underline{C}_j , the following equations are required:

$$\underline{x}_{jik} = \left. \frac{\partial \phi_j(\underline{x}_j, \underline{a}_j)}{\partial a_{jk}} \right|_{\underline{a}_j = \hat{\underline{a}}_j} \quad (2.28)$$

$$\underline{x}_j = x_{jik}, \{i = 1, 2 \dots n; k = 1, 2 \dots r\} \quad (2.29)$$

= $n \times r$ design matrix

$$\underline{A}_j = \underline{x}_j^t \underline{x}_j \quad (2.30)$$

The \underline{C}_j can now be obtained by equation (2.31)

$$\underline{C}_j = \sigma_j^2 \underline{A}_j^{-1} \quad (2.31)$$

2.10.2 Design of Experiments

Only in recent years has there been due attention paid to the planning of experiments that would be expected to result in maximum discrimination among the rival models. The idea is to explore the entire operating space to locate a region in which predicted responses

of the various competing models, based on existing information, will provide maximum discrimination. The expected entropy change criterion used for design of experiments in this thesis is due to Singh⁽⁹⁸⁾ and it is both exact and analytically simple unlike the earlier criteria that were only approximately correct⁽⁹⁵⁾. The underlying basis is the concept of entropy as a measure of the uncertainty associated with a situation as outlined by Kulback⁽⁹⁷⁾. For a set of m models after observing n data points, the entropy may be defined as

$$E_n = - \sum_{i=1}^m P_{i,n} \ln P_{i,n} \quad (2.32)$$

where $P_{i,n}$ is the probability of the i^{th} model being true after n observations. A hypothetical $(n+1)^{\text{st}}$ experiment is carried out and the expected posterior probabilities $P_{i,n+1}$ are now used to compute E_{n+1} . It is the difference $-R = E_n - E_{n+1}$ that is a measure of the improvement in our knowledge. The following expression for $-R$ gives the negative of expected entropy change

$$\begin{aligned} -R = 0.5 \sum_{i=1}^m P_{i,n} \left[-\ln \frac{\sigma^2 + \sigma_{i,n+1}^2}{\sigma^2 + \sigma_{n+1}^2} + \frac{(\hat{y}_{i,n+1} - \hat{y}_{n+1})^2}{\sigma^2 + \sigma_{n+1}^2} \right. \\ \left. + \frac{\sigma_{i,n+1}^2 - \sigma_{n+1}^2}{\sigma^2 + \sigma_{n+1}^2} \right] \quad (2.33) \end{aligned}$$

where σ^2 = error variance of a single measurement

$$\sigma_{i,n+1}^2 = \underline{x}_D (\underline{x}_{i,n}^t \underline{x}_{i,n}) \underline{x}_D^t \sigma^2$$

\underline{x}_D = 1 x r design vector for (n+1)st row of the design matrix \underline{x}_{n+1}

$\hat{y}_{i,n+1}$ = prediction from the ith model corresponding to \underline{x}_D

$$\sigma_{n+1}^2 = \sum_{i=1}^m P_{i,n}^2 \hat{y}_{i,n+1}$$

$$\hat{y}_{n+1} = \sum_{i=1}^m P_{i,n} \hat{y}_{i,n+1}$$

The hypothetical (n+1)st experiment is carried out at various experimental conditions and the negative value of the expected entropy change is examined to obtain a region where -R is maximum.

Computer programs used for the above calculations are given in Appendix B.

CHAPTER III
REAGENTS AND CATALYSTS

3.1 Feed Materials

The nitrogen used in the kinetic study was of research grade and was supplied in cylinders by the Union Carbide Chemical Company. The purity specified by the manufacturer was 99.97% nitrogen. Mass spectral analysis on a typical sample showed that this gas contained no water or carbon oxides.

The alcohols, 2-propanol and 2-butanol, were obtained from Fisher Scientific Co. Ltd. and were of spectroscopic grade. The 3-pentanol was obtained from Aldrich Chemical Co. Inc. and is also of research grade. The purity of each alcohol was assessed by gas chromatography using a di-n-decyl phthalate-celite column. No contaminants were detected. Infrared spectra of these alcohols in the vapor phase showed only the characteristic peaks of the alcohols. No further purifications were attempted, except in adsorption studies where these alcohols were purified by repeated freezing and thawing under vacuum.

Acetone, mixed with 2-propanol as feed was used in some of the experimental runs. The acetone, obtained from Fisher Scientific Co. (Catalogue No. A-20) was found to be pure by infrared and gas chromatographic analyses. It was used as received.

3.2 Alumina Catalysts

3.2.1 Preparation of Catalysts

Only one type of alumina, known as Alon C, was used in this work and it was supplied by the Cabot Corporation, Boston, Massachusetts. The typical properties of this alumina, as specified by the manufacturer are listed in Table 3-1. Alon C, a trade-name of Cabot Corporation, is a fumed alumina consisting predominantly of the gamma form. It is made by the hydrolysis of aluminum chloride in a flame process. This process produces a material of extremely small particle diameter, high surface area and high purity. The γ -alumina powder was used to prepare thin infrared-transparent catalyst wafers by pressing in a die under high pressure (2 ton/sq.cm.).

The γ -alumina doped with sodium hydroxide (Fisher Scientific Co. Catalogue No. 5-312) was prepared by adding the required amount of sodium hydroxide to the Alon C with a minimum amount of water to make a thick slurry. The water was removed by heating the slurry at 120°C in air and the resulting cake was crushed into fine powder for preparing catalyst wafers. In this way, catalysts with 1, 2, 3, 5, 8 and 15% by weight of sodium hydroxide in Alon C were obtained. Only one catalyst batch for each level of NaOH content was used in preparation of all catalyst samples examined in this thesis.

Since the catalyst with 5% sodium hydroxide content had approximately 10 Na^+ ions per $100 (\text{Al})_2^0$, and since the maximum possible hydroxyl concentration on the alumina surface was estimated to be 13 OH per $100 (\text{Al})_2^0$ (99), slightly higher than 5% of sodium hydroxide

Table 3-1
Typical Properties of Alon C

Color and Form:	White Powder
X-ray Structure:	90% Gamma form
Alumina Content*:	99% minimum
Ignition Loss:	4.5% maximum
Metallic Oxides**:	0.2% maximum
Avg. Particle Diameter:	0.03 micron
Surface Area:	100 m²/gram
pH (10% Aqueous Suspension):	4.4
Specific Gravity:	3.6
Loose Density:	1.8 - 2 lbs./cu.ft.
Bag Bulk Density:	3 - 4 lbs./cu.ft.
Refractive Index:	1.70

Note: *Excludes physically and chemically combined water

**Other than Al₂O₃

content would correspond roughly to the fully doped level.

3.2.2 Surface Area of Alumina Catalysts

Surface areas of the alumina samples, after pressing into the wafers, were determined by the standard BET method⁽¹⁰⁰⁾. Before each determination, the samples were evacuated for 8 hours at 350°C. Nitrogen was used as the adsorbate at the temperature of liquid nitrogen (- 196°C). Table 3-2 represents these results.

Table 3-2
Sodium Hydroxide Content and
Surface Areas of Doped γ -Alumina

Catalyst Sample	NaOH Content gm/100 gm Al_2O_3	Surface Area (sq.m)/gm Al_2O_3
A	0	91
B	1	75
C	2	74
D	3	55
E	5	45
F	8	39
G	15	26

3.2.3 Pore Size Distribution for the Alumina Catalyst

The pore size distribution was calculated according to the procedure reported by Gregg and Sing⁽¹⁰¹⁾. The adsorption measurements were made with the catalyst wafer of pure γ -alumina as adsorbent and nitrogen gas as adsorbate. The adsorption isotherm is plotted as shown in Figure 3-1, and the pore size distribution is shown in Table 3-3 and is plotted in Figure 3-2.

Table 3-3

Pore Size Distribution for the Alumina Catalyst

p/p_0	v, cm^3 (S.T.P.)	$r_p, \text{\AA}$	Relative Distribution
0.9751	86.50	398	0.00
0.9727	79.62	364	0.22
0.9177	77.46	124	0.00
0.8979	73.18	100	0.22
0.8794	62.77	85	0.90
0.8754	51.92	83	5.39
0.8428	26.42	66	2.03
0.8181	18.68	58	1.11
0.7871	13.03	49	0.82
0.7499	9.52	42	0.48
0.7106	7.40	36	0.26
0.6079	5.66	27	0.13

Notes: p/p_0 = adsorbate gas phase pressure/saturation vapor pressure

v = volume of the adsorbate adsorbed

r_p = pore radius of the adsorbent

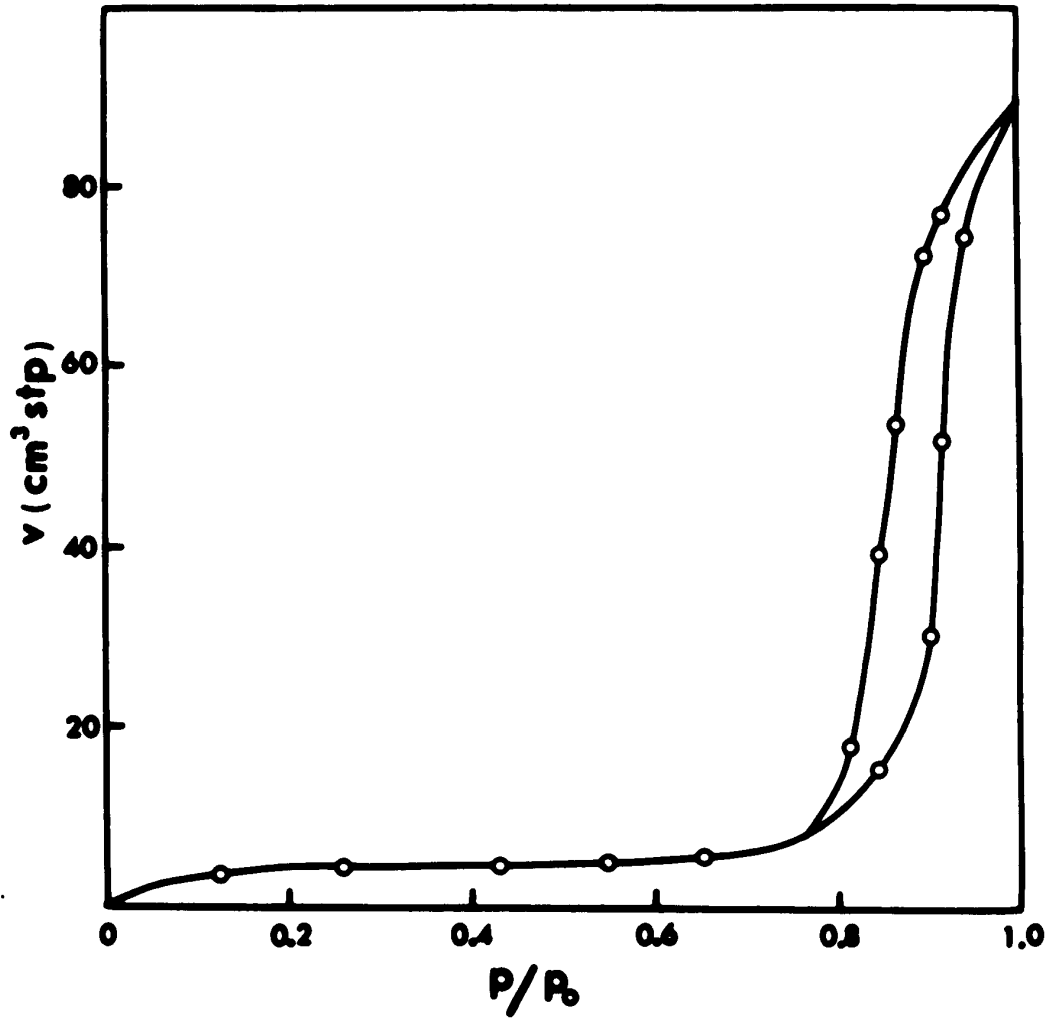


Figure 3-1. Adsorption Isotherm of γ -Alumina

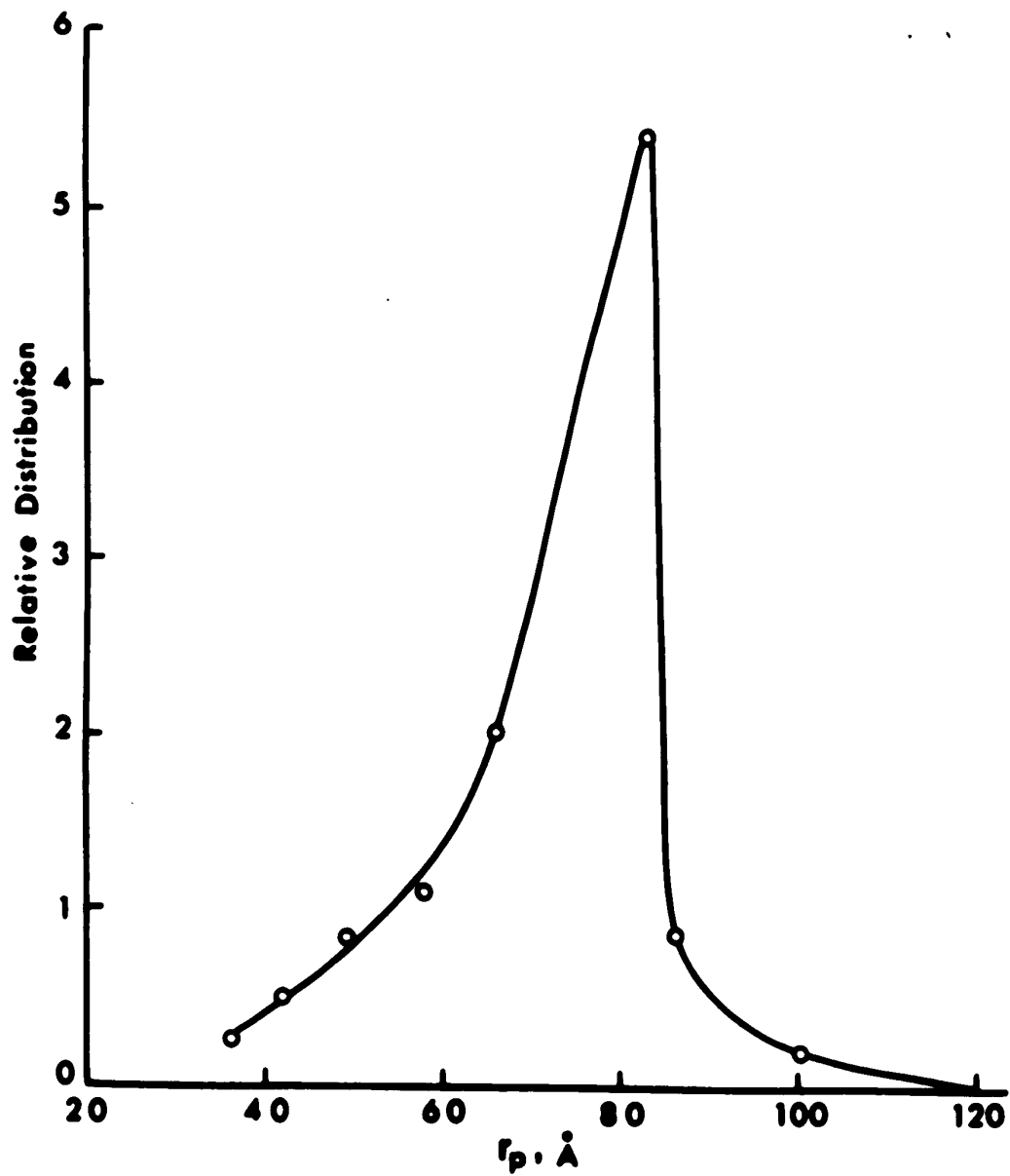


Figure 3-2. Pore Size Distribution for the Alumina Catalyst.

CHAPTER IV
APPARATUS AND EXPERIMENTAL PROCEDURES

4.1 Study of Adsorption of Alcohols

4.1.1 Infrared Cell

A detailed diagram of the quartz reactor-infrared cell for the study of adsorbed alcohols is shown in Figure 4-1. The catalyst wafer was placed between two quartz rings (2.4 cm i.d.) and was moved in and out of the infrared beam by means of an external magnet. Two sodium chloride windows were sealed to both ends of the tube with a silicone rubber potting compound (Fisher Scientific Co., Catalogue No. 4-769-5), which is 100% solid after curing and is stable up to 250°C. The cell can hold a vacuum of 10^{-6} mm Hg and the potting compound is flexible enough to compensate for the different thermal expansion coefficients of quartz and sodium chloride. To remove the NaCl windows for cleaning, if necessary, the cells were heated in an oven at 350°C for 4 hours and allowed to cool to room temperature slowly.

This type of cell enables the catalyst sample to be heated in the heating section and moved to another section of the cell where infrared spectrum can be recorded. The heating section was made of a 25 ohm heating coil whose outside surface was covered with a one inch thick asbestos insulation, so that the cell can be heated up to 650°C.

The cell design did not facilitate a direct measurement of

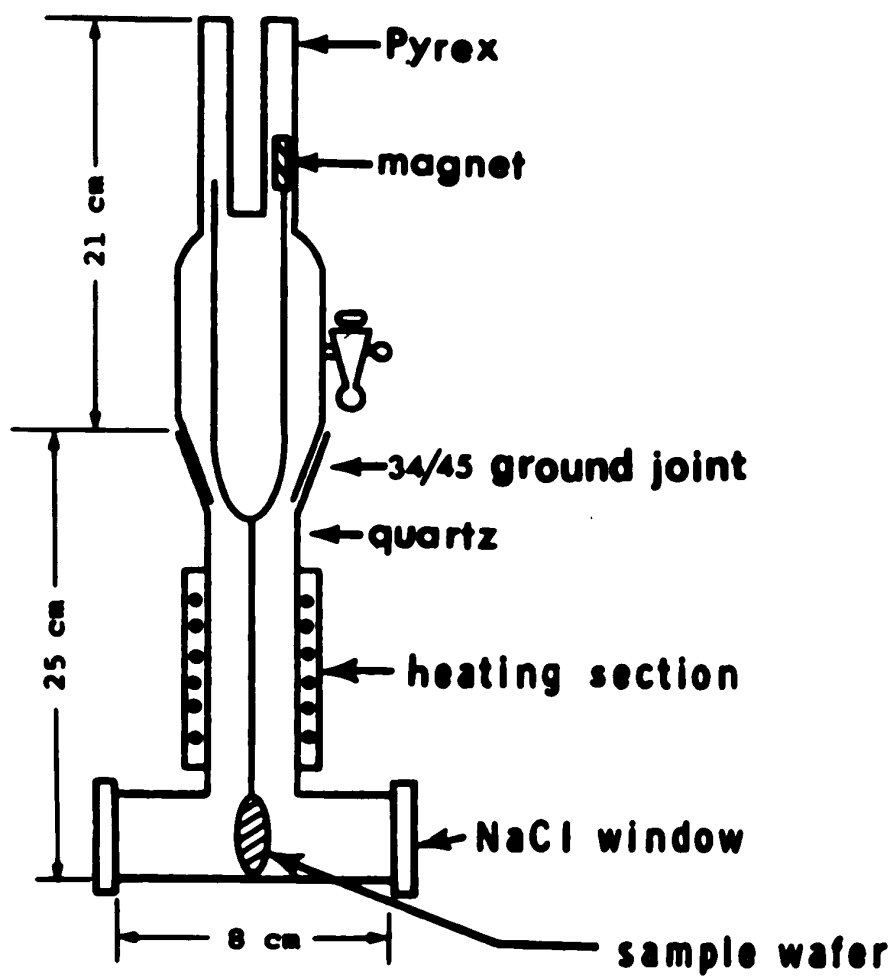


Figure 4-1. Infrared Cell for Adsorption Studies.

the interior temperature. However, a thermocouple was placed between the heater and the exterior quartz surface and the heating temperatures were recorded. A check of these temperatures against other values obtained with a thermocouple placed inside the cell under 10 torr of air indicated that the interior temperature was always substantially lower:

<u>Exterior temperature, °C</u>	<u>Interior temperature, °C</u>
650	465
500	370
400	300
300	220
200	130
150	100
100	80

Thus the catalyst temperature was calculated by the thermocouple placed outside the quartz surface and was then calibrated to the interior temperature by the above table.

4.1.2 Vacuum System

The vacuum system consisted of a mechanical roughing pump (the Welch Scientific Company, Skokie, Illinois, Model No. 1405), a two-stage mercury diffusion pump, and a liquid nitrogen cold trap. The liquid nitrogen trap was installed to prevent oil and mercury particles from diffusing into the infrared cell. The vacuum in the cell was measured with a McLeod vacuum gauge and was about 5×10^{-6} mm Hg under operation conditions.

4.1.3 Preparation and Pretreatment of Catalyst Wafer

For the preparation of a catalyst wafer, about 100 mg. of the catalyst powder was pressed into a thin infrared-transparent wafer. Commercial dies are available and are equipped with facilities for pressing under vacuum. This process does not always lead to best samples. The author has achieved better results by not evacuating during the pressing process and by pressing the powder between two pieces of recording-chart paper (Perkin-Elmer Co., Part No. 221-1613).

The die used in this study was fabricated in the machine shop, Department of Chemical and Petroleum Engineering, University of Alberta and was similar to the commercial dies (2.54 cm. dia.) except no evacuation line was provided.

To prepare the catalyst wafer, the finely divided powder was pressed at two tons/sq. cm. between the two pieces of paper for 10 seconds. On release of the pressure, the sample was easily removed from the paper by a razor blade. The diameter of the wafer was 2.54 cm and the thickness of the wafer was about 0.1 mm (roughly 15 mg/sq. cm.). The catalyst wafer was then placed in situ in the infrared cell.

The pretreatment of the catalyst involved degassing at 400°C for two hours, heating in oxygen at 10 cm Hg pressure for two hours at 400°C, and again degassing at this temperature overnight. After cooling to room temperature, the catalyst was ready for the adsorption study.

4.1.4 Adsorption, Desorption and Recording of Spectra

The catalyst wafer, after pretreatment, was placed in the sample beam of a Perkin-Elmer Model 621 Infrared spectrophotometer installed with a Perkin-Elmer Model 21 presample chopper. The baseline spectrum of the catalyst was recorded using an identical evacuated cell without a catalyst wafer in the reference beam. Because of scattering of the infrared beam by the wafer, especially at the high frequency end of the infrared spectrum (3000 to 4000 cm^{-1}), the transmission may be considerably reduced to anywhere between 5 to 40 percent. In order to obtain a good spectrum, the reference beam had to be attenuated and the slit opened to compensate for the loss in energy. The slit opening was thus set directly proportional to the square root of the reciprocal of the original transmittance. For the required accuracy of the spectrum, slower scanning speeds were also necessary. Detailed operating instructions are available in the Perkin-Elmer Model 621 Manuals (Perkin-Elmer Corporation, Connecticut, U.S.A. Catalogue No. 990-9479).

After purification by repeated freezing and thawing on the vacuum rack, the alcohol was introduced at about one cm Hg absolute pressure into the infrared (sample) cell. To obtain a spectrum due solely to the combination of catalyst and added adsorbate, it is necessary to correct for any spectral adsorption due to the gas phase present in the cell. Often the cell pressures are low enough (0.5 to 2.0 cm Hg) that the gas spectrum is negligible, but, if it is appreciable, its absorption effects must be eliminated. This is most conveniently

done by using an identical cell with no catalyst wafer but containing the alcohol at the same pressure as in the sample cell in the reference beam of the spectrophotometer. The γ -alumina shows strong infrared absorption at frequencies below 1000 cm^{-1} and this forms a lower limit to the useful frequency range for such adsorption studies.

After the spectrum of the adsorbed molecules at room temperature was recorded, the cell was then either pumped off or heated to various temperature levels. Depending on the sequence of experiments being performed, various combinations of heating and/or degassing cycles were used. The infrared spectra were always measured at room temperature during the experimental cycles. To evaluate the extent of reaction, the gas phase was analyzed by infrared and gas chromatographic or mass spectral analyses.

4.2 Simultaneous Studies of Kinetics and Mechanism

4.2.1 Equipment

Simultaneous studies of the reaction rate and the infrared spectra of adsorbed species for the decomposition of an alcohol were performed in an infrared cell which was designed to be operated as a recycle reactor. The main advantages of using a recycle reactor are,

1. near-isothermal conditions exist throughout the catalyst bed and,
2. high recirculation rates eliminate diffusional effects.

The equipment used in the study of dehydration and dehydrogenation of 2-propanol consisted of an alcohol feed system, a recircu-

lation pump, a vaporization system, a reactor (IR cell), the temperature control and recording system, a product collection system and a gas spectral analysis system. A schematic diagram of the apparatus is shown in Figure 4-2. The recirculation line was heated to prevent the condensation of the vapor products in the line. Heating tapes and voltage controllers (Variacs) were used to maintain the line temperature at 170°C. In the following sections, each system will be discussed in detail.

(1) Feed System

Both gas and liquid feeds were introduced into the vaporization system simultaneously (see Figure 4-2). The gas feed used in this work was nitrogen and it was supplied from a pressurized nitrogen cylinder. The pressure of the nitrogen supply at the cylinder was determined by a gas pressure regulator, and the flow-rate of nitrogen was controlled with a needle valve. The flow-rate of nitrogen was measured with a soap bubble meter. A Matheson 601 stainless steel rotameter was connected to ensure a steady nitrogen supply during an experimental run.

A Sage Model 355 syringe pump (Sage Instruments, Inc., White Plains, New York) was employed to inject liquid feed, 2-propanol, into the vaporization system at preset speeds.

The syringe pump was designed to infuse fluids at continuously variable flow rates with a ratio 25,000 to 1 at the maximum and minimum settings with any single syringe. The pump motor drives the gears on top of the pump which engage mating racks on the drive carriage moving

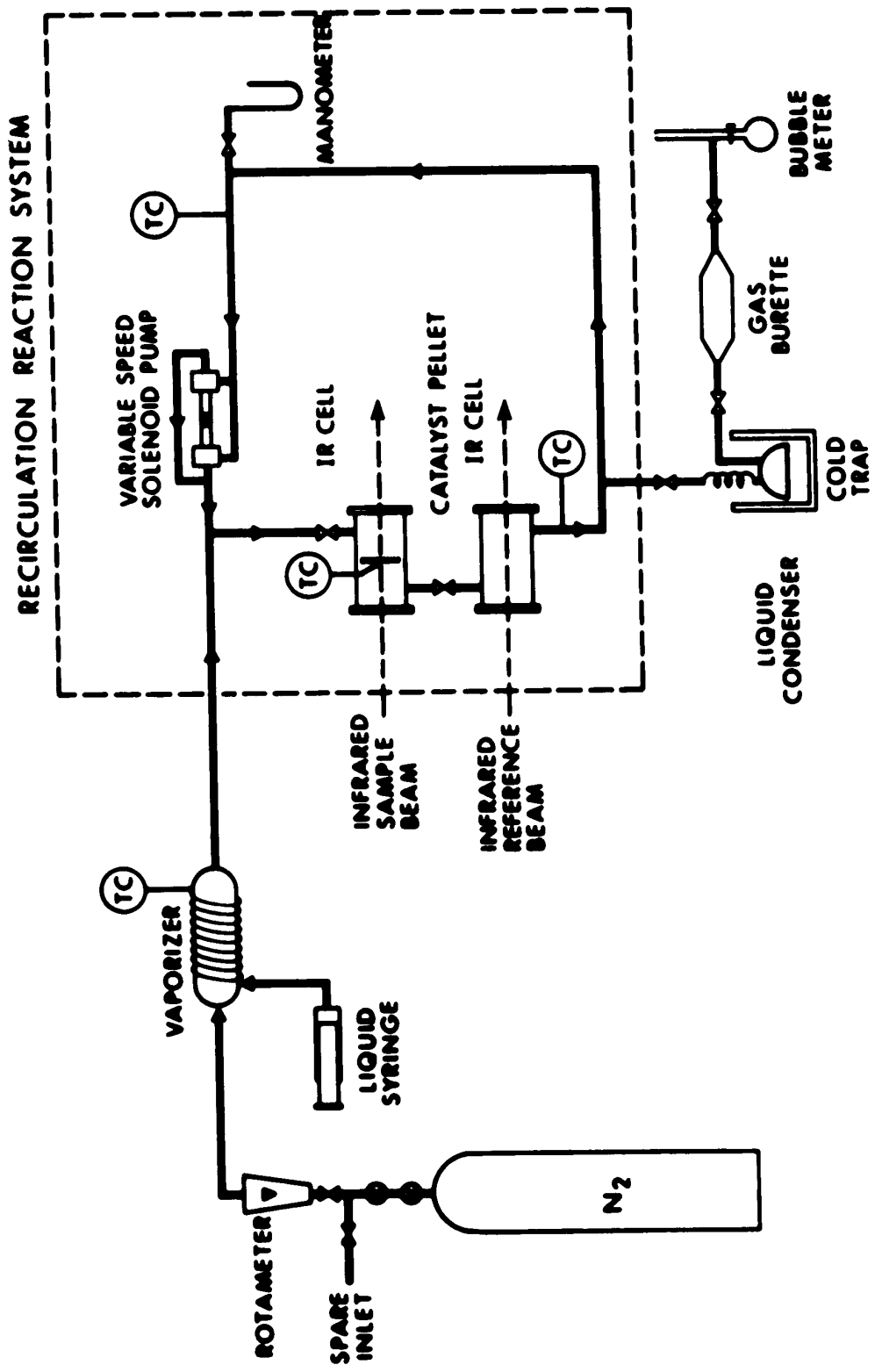


Figure 4-2. Apparatus for the Simultaneous Studies of Kinetics and Mechanism.

it uniformly forward to drive the syringe piston smoothly. An electronic feedback circuit regulates the permanent magnetic DC motor to a reproducibility of $\pm 0.3\%$ full scale, independent of changes in back pressure or $\pm 10\%$ variations in line voltage.

Liquid 2-propanol was fed into the system by a Hamilton 50 cc gas-tight syringe (Catalogue No. 1050) which features a teflon-coated piston in the glass barrel. Very precise and constant feed rates with average variations of less than 0.4% were obtained with this syringe. The calibration of the feeder is given in Appendix C.

(2) Vaporization System

The vaporizer was made from 2 cm O.D. 22 cm. long Pyrex glass tubing. At the inlet, a 1/8 in. Kovar joint was connected to the syringe by 3/32 in. O.D. stainless steel tubing. Another inlet tubing, 1/8 in. O.D., was used to introduce nitrogen gas. The outlet of the vaporizer was a 12/5 female ball joint socket which was coupled to the inlet of the infrared cell (reactor). A 3/32 in. iron-constantan thermocouple was placed inside a 2 mm I.D. glass thermocouple well near the outlet of the vaporizer. This thermocouple was connected to the Honeywell temperature controller (SCR trigger controller, Model R7161J) which controlled the vapor feed temperature at 170°C. The outside of the vaporizer was covered with 1-1/2 cm thickness of asbestos insulation.

(3) Recirculation Pump

A magnetic solenoid pump was incorporated into the recirculation loop. Efficient circulation of the product stream was important

since it would ensure that no concentration gradient existed within the gas phase and that no mass transfer effects influenced the measured reaction rate.

The double acting solenoid pump was of stainless steel construction with teflon-coated piston, valves and O-ring seals. A sectioned sketch of one-half of the pump is shown in Figure 4-3. The two halves of the pump are identical. The O-ring connector on the pump discharge was omitted from the drawing.

Both suction and discharge valves were formed from teflon disks which were back-seated with stainless steel springs. The four external connectors were "Swagelok" 1/4 inch straight-thread connectors. The suction valve disks were seated against the threaded end of the connectors. These connectors had been previously machined to provide the valve seat. The discharge valve seats were machined in the pump heads. The check valves appeared to be the most critical components in the design and operation of the pump.

The pump cylinder was made of one inch I.D. stainless steel tubing. Its total length was 13-3/4 inches.

The pump piston was constructed of mild steel coated with teflon. The clearance between the piston and cylinder wall could be varied by adjusting the thickness of the teflon coating. The overall piston length was four inches.

Three coils, 3-2/3 inches long and separated by 1/4 inch fiber disks, were wrapped on the pump cylinder. Each coil had approximately 2300 turns of No. 20 enameled copper wire. A variable voltage (9 to

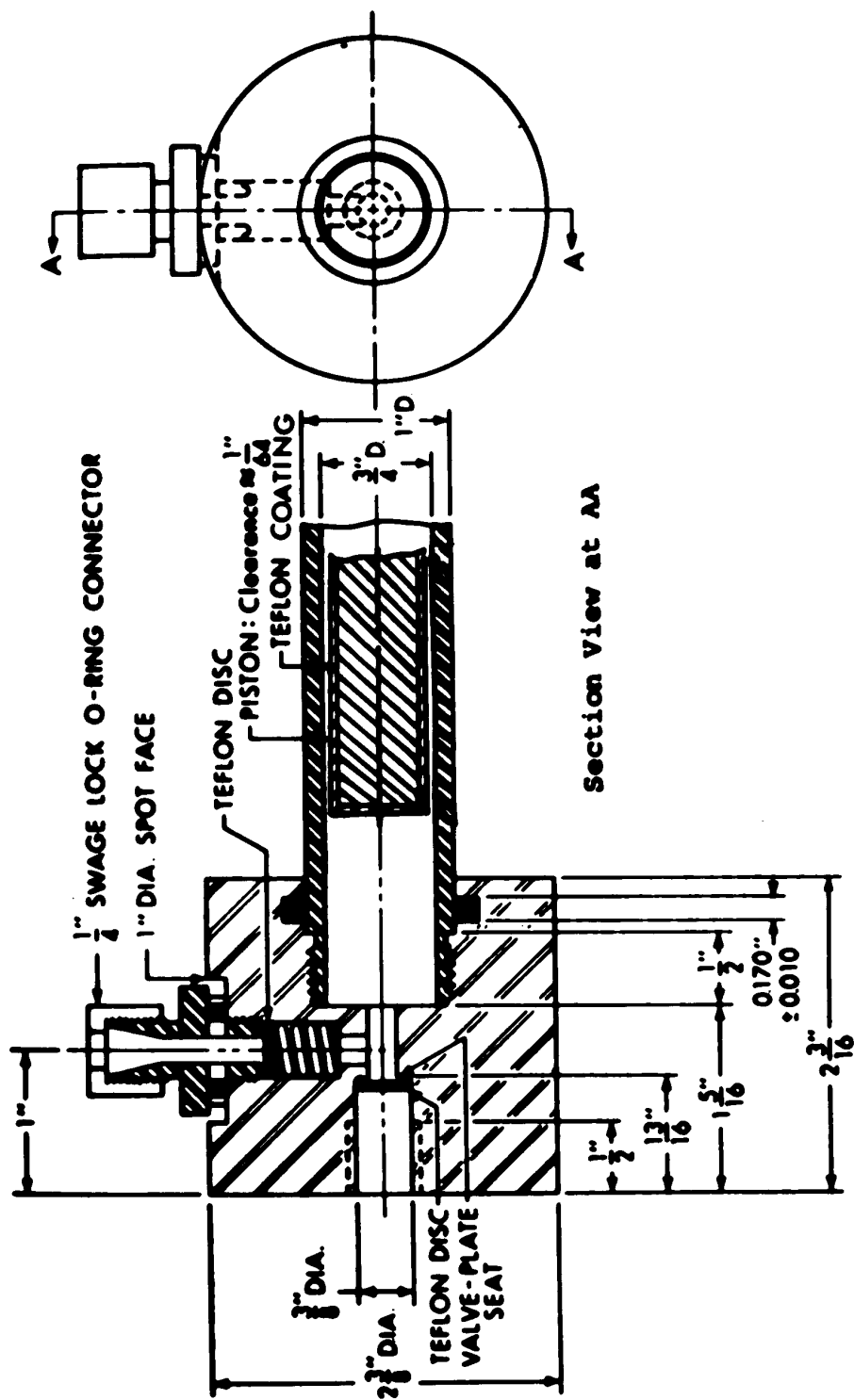


Figure 4-3. Magnetic Solenoid Pump

18 volts D.C.) power supply with a maximum current of three amperes was used to excite the solenoids. At the design condition of 12 volts D.C., each coil carried a current of 1.1 amperes resulting in a rating of 2530 ampere-turns.

The external electronics consisted of the D.C. power supply, a repeat cycle multi-gang timer and three switching relays. The timer was a three gang, single cam assembly driven by a 60 r.p.m. synchronous motor installed with 8-variable speed drives. The three gangs were timed so that they were sequentially offset by 90 degrees. The pump piston would therefore travel one complete cycle for each revolution of the cam. Figure 4-4 shows a wiring diagram of the timer and switching relays.

The designed capacity of the magnetic solenoid pump was ranged from 15.6 to 65.5 liters per minute, but the actual capacity was approximately three quarters of that expected. This reduction was mainly attributed to the efficiency of the check valves.

The pump was insulated with 1/2 inch of asbestos tapes so that the steady-state operation temperature was maintained at 170°C. The pump was mounted horizontally between the two infrared cells. This pump could be operated at a temperature of $170 \pm 35^\circ\text{C}$ without readjusting the thickness of teflon coating on the piston.

(4) Infrared Cells and Sample Holder

The pyrex reactor-infrared cell is sketched in Figure 4-5. The cell length was 11 cm. A 40 mm diameter NaCl window was sealed onto one side of the cell with the silicon rubber potting compound.

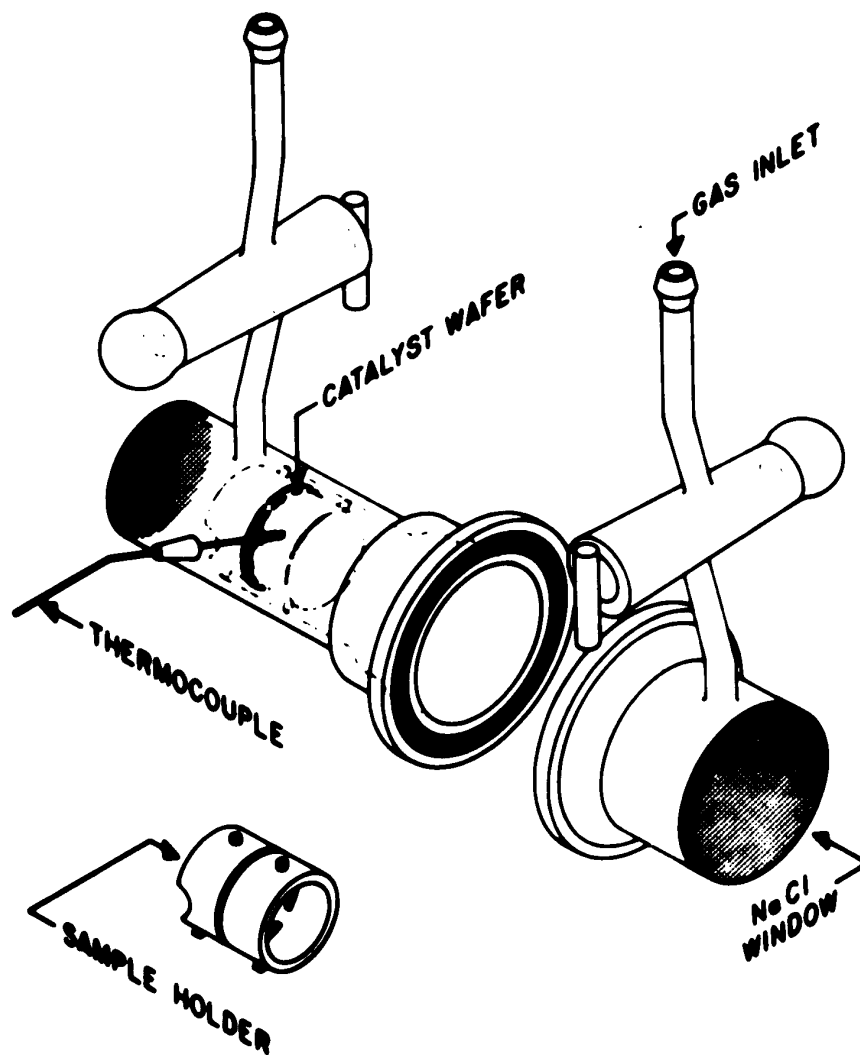


Figure 4-5. Reactor Cell and Sample Holder.

Another side of the cell was sealed by a 50 mm diameter NaCl window. Pyrex vacuum stopcocks were used to isolate the reactor in evacuative treatments of the catalyst. The gas inlet and outlet to the cell are indicated in Figure 4-5. An O-ring (Viton, 40 mm diameter) joint allowed the removal of the front end of the cell for the replacement of the catalyst samples. The catalyst wafer, prepared according to the procedure described in Section 4.1.3, was supported in the cell by the sample holder (see Figure 4-5) and was facing the NaCl windows.

The central part of the cell was heated by a 20-ohm heating coil placed outside the cell while the windows were kept at temperature about 170°C by blowing cold air around the ends of the cell. The outside of the heater was insulated by one inch thickness of asbestos tapes. The temperature in the reactor cell was controlled by a variable voltage transformer (Variac, Fisher Scientific Company). The voltages applied to the heating coil were measured by a voltmeter and were controlled within ± 0.1 volt of the set point. In this way, the reactor temperature was controlled with a variation of less than 0.3°C.

A measure of the sample temperature was provided by a 1/8 inch thermocouple introduced into the cell via a silicon rubber septum; the configuration was such that the junction formed a pressure contact with the catalyst wafer. It can be said that the temperature thus measured was very close to the true wafer temperature based on the following observations:

(a) The measured wafer temperature was found to decrease by less than 0.2°C when the cell was evacuated at 400°C.

(b) Under the evacuated conditions and at a temperature of 400°C, a 1/50 inch thermocouple gave temperature readings which were identical to those measured by the 1/8 inch thermocouple.

One side of the cell was connected to the magnetic solenoid pump using a Kovar joint (1/4 inch) and the other side to the reference cell using glass tubing. The reactor cell can be used up to a temperature of 450°C and a vacuum of 5×10^{-5} mm Hg.

The reference cell was made of pyrex glass tubing, 27 mm I.D. and 11 cm long. Both ends of the cell were sealed with NaCl windows (40 mm diameter). The cell was wrapped with a heating tape and thus the temperature in the cell was maintained at 170°C by applying 34 volts on the heating tape. The cell was insulated with asbesto tapes to prevent excessive heat loss to the surroundings.

The reference cell was used to measure the partial pressures of both the reactant and the products. This provided the information for calculating the material balance as well as the conversion.

(5) Temperature Recording System

The thermocouple (1/8 inch iron-constantan) located in the reactor was connected to a Speedomax Type G temperature recorder (Leeds and Northrup Co.). The thermocouple was calibrated before installation. The temperatures recorded in the calibrated isothermal bath between 273 and 673°K versus the voltages measured from the thermocouple can be represented after applying a least squares fit (see Appendix C for computer programs), by $y = 5.5112 + 18.0013x$

where y = temperature of the bath, °K,

and x = signal measured, mv.

The temperature recorder was checked occasionally by feeding a known voltage from a potentiometer into the recorder. Thus the temperature on the catalyst wafer could be recorded precisely during experimental runs.

(6) Product Collection System

The vapor products leaving the recirculation loop were introduced through a fluid control valve (Hoke, Inc., Catalogue No. 4172G2Y) into the condenser-sampler immersed in an ice-water bath. For better liquid sample collection, a pyrex glass integral condenser-sampler was used (Figure 4-2). The noncondensable gases from the liquid sampler were then passed to a 75 cc gas sampling burette and then to a soap-bubble meter. The samples thus collected were sent for gas-phase chromatographic analysis. The results were used as an additional check of the number of compounds appearing in the reaction product mixture.

4.2.2 Operation of Equipment

The procedure used in preparing the catalyst wafer was identical to that described in Section 4.1.3. The catalyst wafer was placed in the sample holder which was then inserted into the center part of the infrared cell in such a way that the catalyst wafer formed a pressure contact with the thermocouple. This insured that the catalyst wafer remained at the same position for all runs. After the O-ring connection was tightened (see Figure 4-5) the infrared cell was fixed in position to the recirculation loop through the two glass ball joints (12/5). After all joints were sealed with silicone grease and secured, the

equipment was ready for an experimental run.

The vacuum system was similar to that described in Section 4.1.2 except that the McLeod vacuum gauge was replaced by a Pirani vacuum gauge (Edwards High Vacuum Limited, Model G9). The pretreatment of the catalyst was performed by evacuating the sample cell at a catalyst temperature of 350°C for 12 hours. The base line of the catalyst wafer showed an identical spectrum to that obtained in the adsorption study (Section 4.1). However, it was learned later in the research program that heating the catalyst wafer by continuously flushing nitrogen gas through the sample cell for 12 hours gave the same results as pretreating the catalyst in vacuo. Therefore, except for the first catalyst (catalyst (a) in Figure 5-10), all other catalysts were pretreated according to the latter method. It should be mentioned that during the catalyst pretreatment, the magnetic solenoid pump, the recirculation loop heaters and the vaporizer heater were turned on since they took four hours to reach a steady-state operation condition. Thus, except the alcohol feeder, the entire system was under working conditions when the pretreatment of the catalyst was finished.

At this point the nitrogen gas flow rate was measured by the bubble-meter. It was found that the nitrogen flow rate could be maintained constant for all the experimental runs provided the pressure in the nitrogen supply cylinder exceeded 300 psig. Thus no adjustment of the metering valve was necessary.

The base line spectrum of the catalyst was taken by an on-line computer data acquisition system involving coupling of the spectro-

photometer to an IBM 1800 digital computer (see Appendix A).

After obtaining the base line spectrum of the catalyst, the alcohol feeder was turned on and the reactant was passed through the vaporizer into the reaction system. The reactant feed rate was adjusted by the syringe pump control dials (see instruction manual of syringe pump, Sage Instrument, Inc.). The partial pressure of the reactant in the recirculation loop was controlled by the flow rate of the reactant. The reference cell was then inserted into the sample beam of the infrared spectrophotometer. The frequency, at which the desired 2-propanol absorption band occurred, was set and peak intensity was recorded as a function of time. This can be done simply by turning the scan clutch control of the spectrophotometer to the "out" position at the frequency of interest. After the wafer temperature and product mixture composition in the recirculation loop became constant, the on-line computer data acquisition system was activated and steady-state was assumed when the peak intensity became constant for 20 minutes. A data point for the kinetic measurement was then taken. This consisted of

(a) recording the absorption intensity of 2-propanol and propylene in case of dehydration studies, or of 2-propanol and acetone in case of dehydrogenation.

(b) inserting the sample cell in the sample beam and the reference cell in the reference beam and recording the spectrum of the adsorbed species (plus base line),

(c) analyzing the liquid and gas samples collected in the samplers by gas chromatograph. (This provided a check for the presence of any side reactions).

(d) recording the catalyst temperature and alcohol feed rate.

(e) plotting the spectrum, after eliminating base line spectrum with the computer, on the IBM 1627 plotter. (see Appendix A for the plotting program).

About two hours were required per data point. When the temperature was varied, about 30 minutes elapsed before a new steady state condition was obtained. For feed rate changes about 20 minutes were required to reach a new steady state.

4.2.3 Data Evaluation

(1) Quantitative Analysis of Product Mixture

Quantitative infrared analysis is similar to routine colorimetric analysis and makes use of the Beer-Lambert law:

$$A_{\lambda} = \log\left[\frac{I_{0\lambda}}{I_{\lambda}}\right] = \epsilon Cl = \frac{\epsilon l P}{RT} \quad (4.1)$$

where A_{λ} is the absorbance at wavelength λ , $I_{0\lambda}$ and I_{λ} , the intensities of the incident and transmitted beams respectively,

C the concentration

l the length of the cell

ϵ the extinction coefficient

P partial pressure of the gas sample

T absolute temperature and

R the gas constant.

It is important to test the validity of this law in the range of con-

centrations likely to be employed.

In the case of gaseous mixtures, if two or more components of the mixture absorb at the same wavelength, the total absorbance is assumed to be equal to the sum of the absorbances due to each one of the components in the mixture, i.e.

$$A_{\lambda} = \sum_i \epsilon_i C_i l = \sum_i \frac{\epsilon_i P_i l}{(RT)} \quad (4.2)$$

where the subscript, i , refers to the particular species. However, overlapping absorption bands tend to decrease the accuracy of the analysis. Several methods such as the ratio method, etc., have been developed to overcome the difficulties from the overlapping of bands⁽¹⁰²⁾. Fortunately, in this study, it was possible to choose an intense isolated absorption band for each component in the product mixture. Thus, Equation (4.2) reduces to

$$A_{i\lambda} = \epsilon_{i\lambda} C_i l = \frac{\epsilon_i P_i l}{(RT)} \quad (4.3)$$

Thus frequencies chosen for each component in the reaction mixtures are listed in Table 4-1.

Because the vapor phase spectrum of water was found to be inaccurate for the quantitative analysis, and hydrogen gas was found to be infrared-inactive, the partial pressures of water from dehydration and of hydrogen from dehydrogenation were taken to be stoichiometrically equal to that of propylene and acetone, respectively.

Table 4-1
Frequencies Employed for Quantitative Analysis

	Component	Applicable partial pressure range, cm Hg	Frequency, cm^{-1}
(a) Dehydration	2-propanol	< 10	1250
	2-propanol	> 10	3660
	propylene	< 5	3106
(b) Dehydrogenation	2-propanol	< 6	1148
	2-propanol	> 6	3660
	acetone	<2.5	1740

Since no evidence for the occurrence of reactions other than dehydration or dehydrogenation was encountered, this approach was not really questionable.

In infrared quantitative analysis the accuracy in recording the peak intensity is very important. In practice, the peak height or the area of the band is taken as the criterion of band intensity. The former method was chosen in the present study since it was simpler and it gave a good straight line correlation according to Beer's law. The accuracy of the evaluation of I/I_0 was also found to be important in preparing a good calibration curve therefore, the error of the I/I_0 obtained was estimated by the following procedure.

The fractional infrared transmission, I/I_0 , is the ratio of the incident infrared radiation transmitted by the gas to that transmitted in the absence of the absorbing gas. In the present study I_0 was always greater than 80% of the total transmission. The value of "I" decreased, depending on the concentration of the gas in the reference cell, sometimes to values as low as 5% of the total transmission. The deviation in reading the recorder pen was 0.3%. The error in I/I_0 is given by,

$$\text{Error} = \left(\frac{I}{I_0}\right)_{\text{true}} - \left(\frac{I}{I_0}\right)_{\text{measured}}$$

$$E = \left(\frac{I}{I_0}\right) - \left(\frac{I \pm 0.3}{I_0 \pm 0.3}\right)$$

$$E = \left(\frac{I}{I_0}\right) - \left(\frac{I}{I_0 \pm 0.3}\right) \pm \left(\frac{0.3}{I_0 \pm 0.3}\right) \quad (4.4)$$

Since I_0 was always greater than 80%, a value of 80 will be used to determine the maximum error.

$$E_{\text{max}} = \left(\frac{I}{80}\right) - \left(\frac{I}{80 \pm 0.3}\right) \pm \left(\frac{0.3}{80 \pm 0.3}\right)$$

$$E_{\text{max}} = \pm .000047.I \pm 0.00375$$

or $E_{\text{max}} = \pm .0065\%$, for maximum $I = 80\%$.

Thus, the error introduced due to misreading the recording chart is

negligible. This accuracy was improved even further by reading the results with an on-line computer which read the transmission data accurate to 0.1% (see Appendix A).

The calibration curves were prepared by introducing different amounts of vapor into the reference cell. The cell was connected to a quartz precision pressure gage (Texas Instrument Model 141A) and was evacuated to obtain the zero pressure reading of the gage. After introducing the vapor into the cell, the vapor was found to be adsorbed partly on the glass wall. It was shown⁽¹⁰³⁾ that this difficulty could be minimized by prior conditioning of the system with the vapor sample. However, the author found that allowing a thirty-minute stabilization period after introducing the vapor was a more convenient way to eliminate the above difficulty. It was found that for all the absorption frequencies used in determining the concentration no mutual interference of the absorption band was detected, e.g. the band intensity for 2-propanol at 1250 cm^{-1} was not affected by introducing different quantities of propylene or water. The absorbance is plotted against partial pressure to obtain the working curve at 29°C . (After exposing the cell to the infrared beam, the temperature of the cell was recorded to be 29°C which was 5°C above the room temperature). For higher pressures of 2-propanol ($10 < P < 60\text{ cm Hg}$), the calibration was performed by connecting the reference cell to a mercury manometer and the entire system was heated at 100°C to ensure no condensation of 2-propanol vapor. The vapor pressure of 2-propanol as indicated by the manometer was read with a cathetometer. The absorption band at

3660 cm^{-1} was recorded by compressing the band intensity (% transmittance) by a factor of 1/4⁽¹¹⁾. This provides greater accuracy for the band intensity measurements. Figures 4-6 to 4-9 and Tables 4-2 to 4-6 show the calibration results after fitting by least squares.

The pressure-broadening effect was found to be unimportant since the absorbance of the gas samples (2-propanol, acetone, and propylene) was not changed by increasing the cell pressure to one atmosphere by injecting nitrogen gas.

(2) Evaluation of Kinetic Data

In the recirculation loop, the recycle rate was found to be 32.8 liters per minute. The volume of the entire loop was estimated to be 0.72 liter. Consequently, the conversion per pass was low, and the loop was treated mathematically as being equivalent to a well-stirred flow reactor. The reaction rate was thus calculated from the following material balance on component A⁽¹¹²⁾:

$$(-r_A) = \frac{F_{A0} x_A}{w} \quad (4.5)$$

In order to obtain $(-r_A)$, the fractional conversion of the reactant, x_A , should be determined. This was done by determining the partial pressures of the reactant in the feed, p_0 , and in the product stream p_a , and then calculating x_A from

$$x_A = \frac{p_0 - p_a}{p_0} \quad (4.6)$$

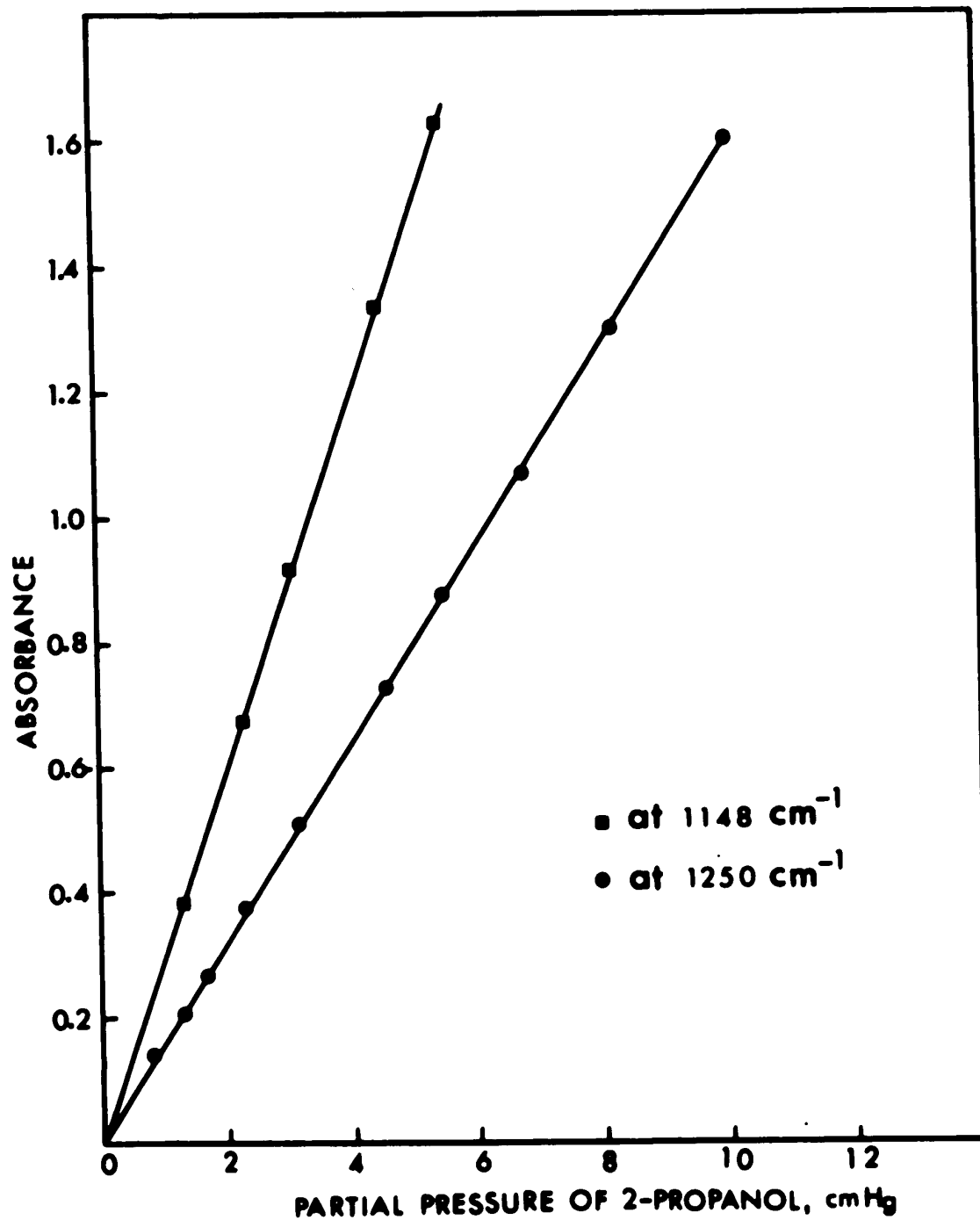


Figure 4-6. Calibration of 2-Propanol Absorbance Using Beer's Law.

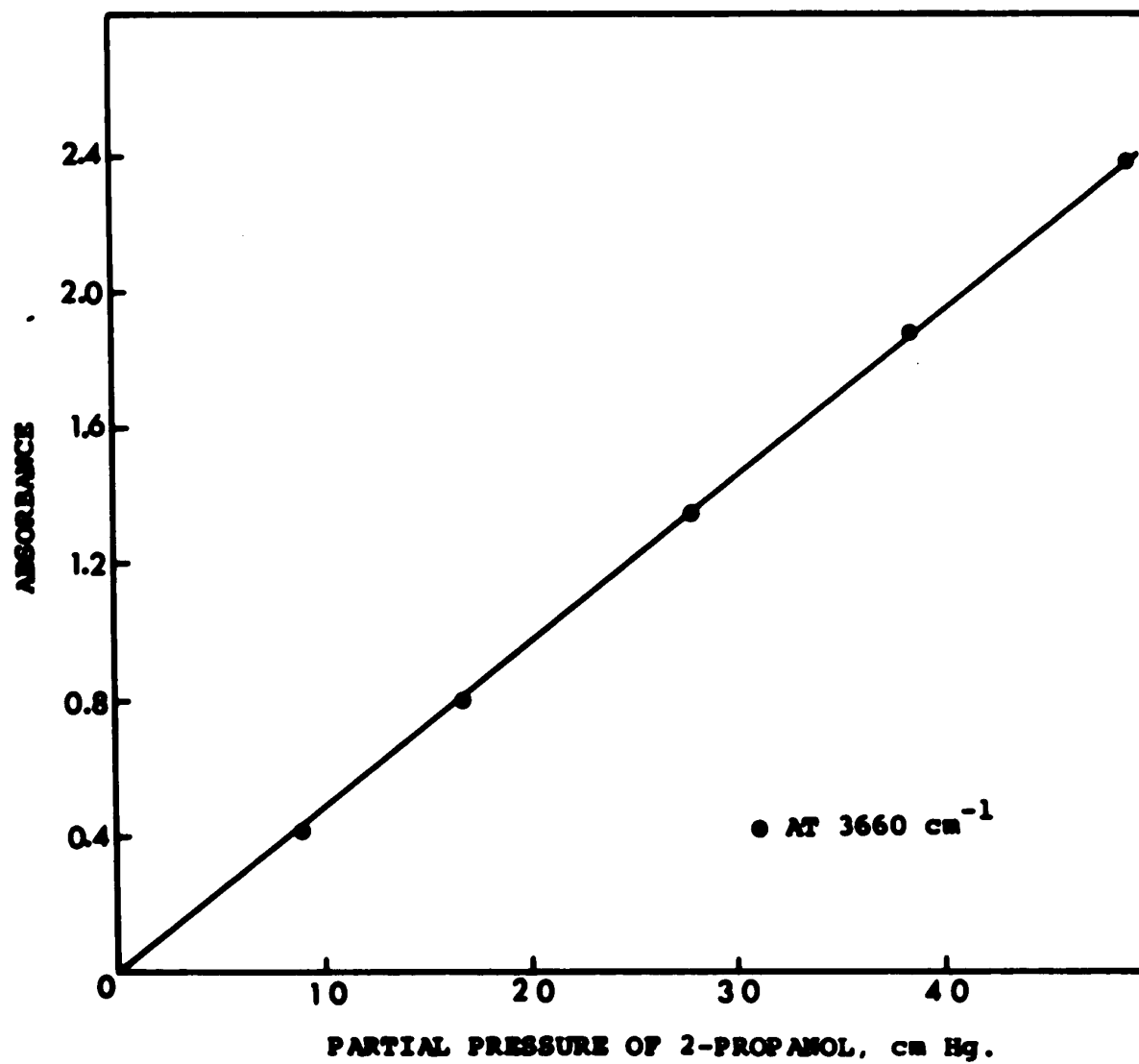


Figure 4-7. Calibration of 2-Propanol Absorbance Using Beer's Law.

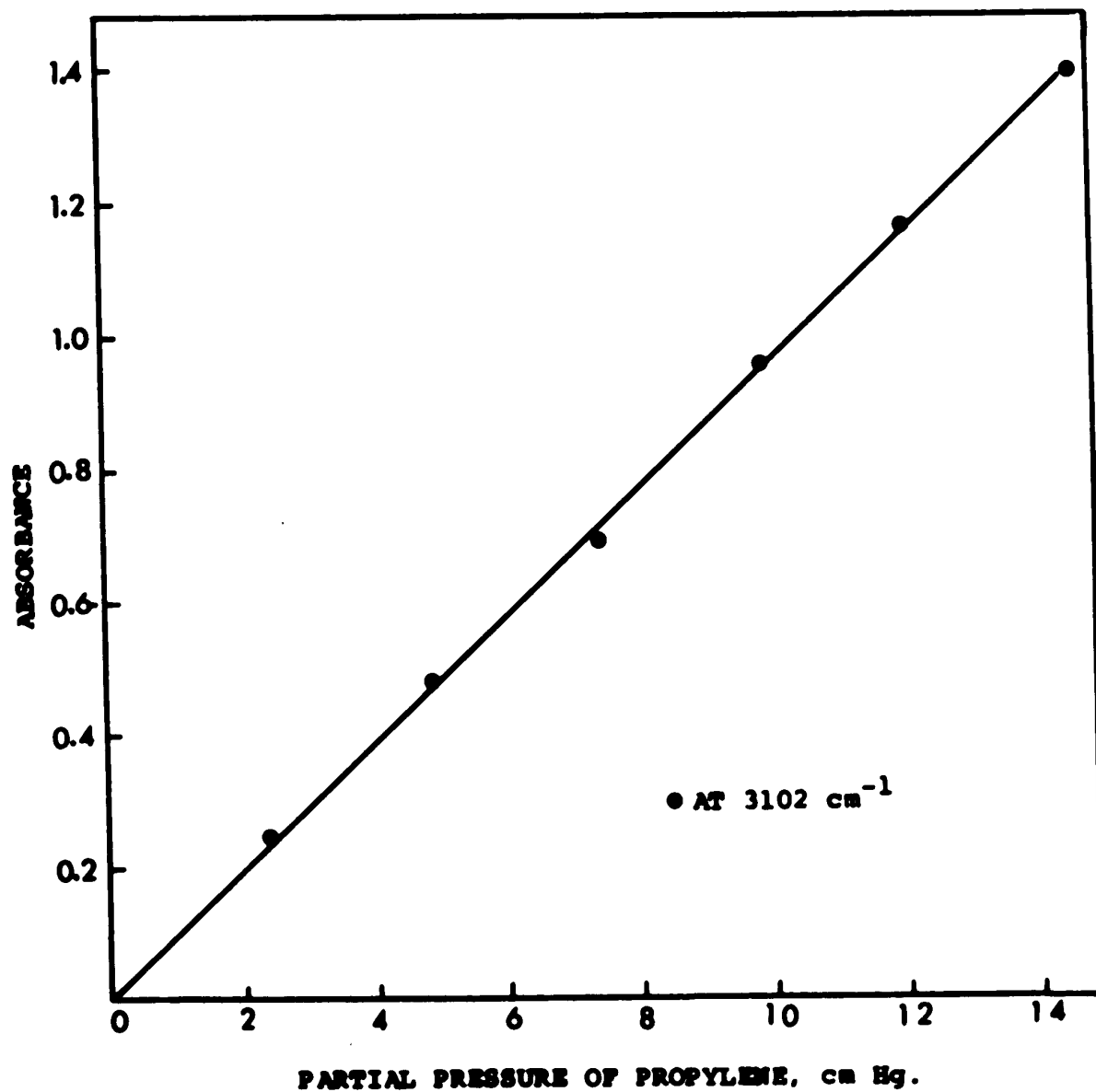


Figure 4-8. Calibration of Propylene Absorbance Using Beer's Law.

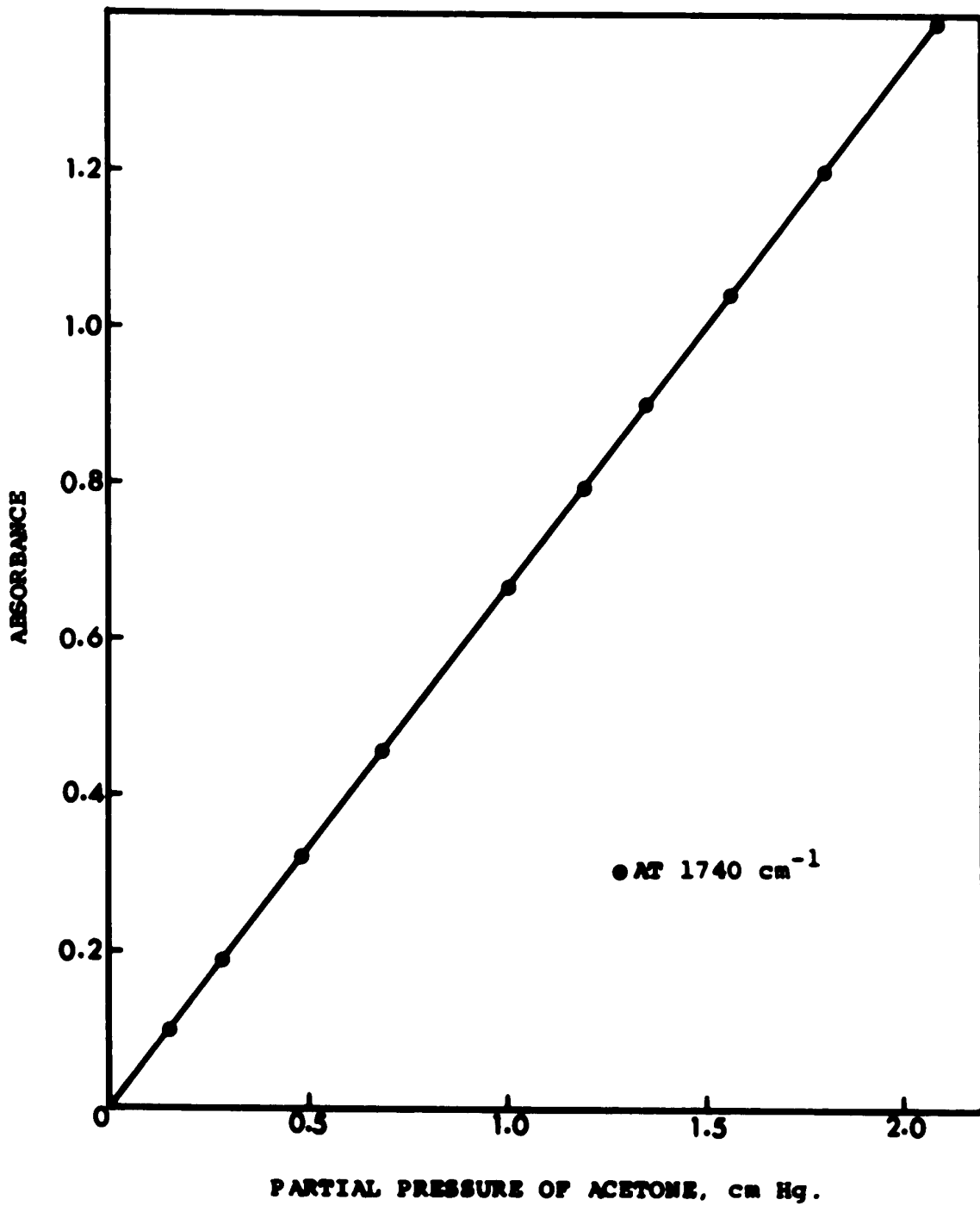


Figure 4-9. Calibration of Acetone Absorbance Using Beer's Law.

**TABLE 4-2. CALIBRATION OF 2-PROPANOL ABSORBANCE
USING BEER'S LAW (1148 CM⁻¹)**

X = PARTIAL PRESSURE OF 2-PROPANOL, CM HG

Y = ABSORBANCE

THE COEFFICIENTS OF THE POLYNOMIAL: $Y = A_0 + A_1 * X$

A₀ = -0.00154

A₁ = 0.29960

REGENERATED DATA			
X MEASURED	Y OBSERVED	Y CALCULATED	PCT ERROR
1.287	0.385	0.384	0.292
2.285	0.680	0.683	0.401
3.053	0.915	0.913	0.206
4.902	1.346	1.347	0.045
5.443	1.629	1.629	0.019

VARIANCE = 0.000003

STANDARD DEVIATION = 0.001787

MAXIMUM PCT ERROR = 0.401405

**TABLE 4-3. CALIBRATION OF 2-PROPANOL ABSORBANCE
USING BEER'S LAW (1250 CM⁻¹)**

**X = PARTIAL PRESSURE OF 2-PROPANOL, CM HG
Y = ABSORBANCE**

THE COEFFICIENTS OF THE POLYNOMIAL, $Y = A_0 + A_1 * X$,

A0 = 0.00270

A1 = 0.15966

REGENERATED DATA

X MEASURED	Y OBSERVED	Y CALCULATED	PCT ERROR
0.824	0.131	0.134	1.793
1.304	0.209	0.210	0.526
1.658	0.265	0.267	0.876
2.300	0.373	0.369	0.930
3.146	0.510	0.505	0.999
4.550	0.730	0.729	0.113
5.474	0.876	0.876	0.068
6.756	1.077	1.081	0.379
8.155	1.305	1.304	0.019
10.031	1.605	1.604	0.051

**VARIANCE = 0.000007
STANDARD DEVIATION = 0.002763
MAXIMUM PCT ERROR = 1.793472**

TABLE 4-4. CALIBRATION OF 2-PROPANOL ABSORBANCE
USING BEER'S LAW (3660 CM⁻¹)

X = PARTIAL PRESSURE OF 2-PROPANOL, CM HG

Y = ABSORBANCE

THE COEFFICIENTS OF THE POLYNOMIAL, $Y = A_0 + A_1 * X$,

A0 = -0.00749

A1 = 0.04846

REGENERATED DATA

X MEASURED	Y OBSERVED	Y CALCULATED	PCT ERROR
5.307	0.252	0.249	0.905
8.894	0.421	0.423	0.514
16.682	0.800	0.801	0.127
27.986	1.350	1.348	0.104
38.823	1.873	1.874	0.048
49.211	2.378	2.377	0.017

VARIANCE = 0.000002

STANDARD DEVIATION = 0.001670

MAXIMUM PCT ERROR = 0.905624

TABLE 4-5. CALIBRATION OF PROPYLENE ABSORBANCE USING
BEER'S LAW (3102 CM⁻¹)

X = PARTIAL PRESSURE OF PROPYLENE CM HG

Y = ABSORBANCE

THE COEFFICIENTS OF THE POLYNOMIAL: $Y = A_0 + A_1 * X$

A0 = 0.02012

A1 = 0.95658

REGENERATED DATA

X MEASURED	Y OBSERVED	Y CALCULATED	PCT ERROR
2.521	2.483	2.431	2.067
4.989	4.835	4.792	0.878
7.514	7.011	7.207	2.808
10.009	9.641	9.594	0.481
12.152	11.707	11.644	0.533
14.725	14.100	14.105	0.041

VARIANCE = 0.009859

STANDARD DEVIATION = 0.099296

MAXIMUM PCT ERROR = 2.808381

TABLE 4-6. CALIBRATION OF ACETONE ABSORBANCE USING BEER'S LAW (1740 CM-1)

X = PARTIAL PRESSURE OF ACETONE CM HG
Y = ABSORBANCE

THE COEFFICIENTS OF THE POLYNOMIAL, $Y = A_0 + A_1 * X$,

A0 = -0.00032
A1 = 0.66321

REGENERATED DATA

X MEASURED	Y OBSERVED	Y CALCULATED	PCT ERROR
0.151	0.099	0.099	0.052
0.283	0.187	0.187	0.140
0.479	0.317	0.317	0.111
0.682	0.453	0.451	0.268
1.001	0.663	0.663	0.067
1.196	0.793	0.792	0.091
1.357	0.898	0.899	0.139
1.568	1.039	1.039	0.008
1.808	1.198	1.198	0.011
2.100	1.392	1.392	0.020

VARIANCE = 0.000000
STANDARD DEVIATION = 0.000672
MAXIMUM PCT ERROR = 0.268247

Before starting an experimental run, a sodium chloride wafer, of the same size as the catalyst wafer, was placed in the sample holder with the equipment operating under steady-state conditions. Since NaCl was found not to catalyze reactions of alcohol, it was used to determine the partial pressure of the reactant in the reference cell when no reaction occurs. The partial pressure thus obtained was assumed to be identical to p_0 .

The partial pressure of 2-propanol was measured according to the procedure outlined in the previous section [4.2.3 - (1)] and was then calculated using equation (4.7):

$$p_0 = p_{\text{calibrated}} \times \frac{T_2}{T_1} = p_{\text{calibrated}} \times \frac{(273 + 170)}{(273 + 29)} \quad (4.7)$$

where $p_{\text{calibrated}}$ is the partial pressure of 2-propanol obtained from the calibration curves (Figures 4-6 and 4-7).

T_2 is the temperature of the reference cell, 170°C, and

T_1 is the calibration temperature, 29°C.

The partial pressure of 2-propanol in the reference cell was found to be proportional to the feed rate by a least squares fit (see Appendix C for computer programs), which can be given by

$$p_0 = 0.09518 + 92.9448 (F_{A0}) \quad (4.8)$$

The results are plotted in Figure 4-10 and are presented in Table 4-7.

The validity of the calibration was checked before and after the experi-

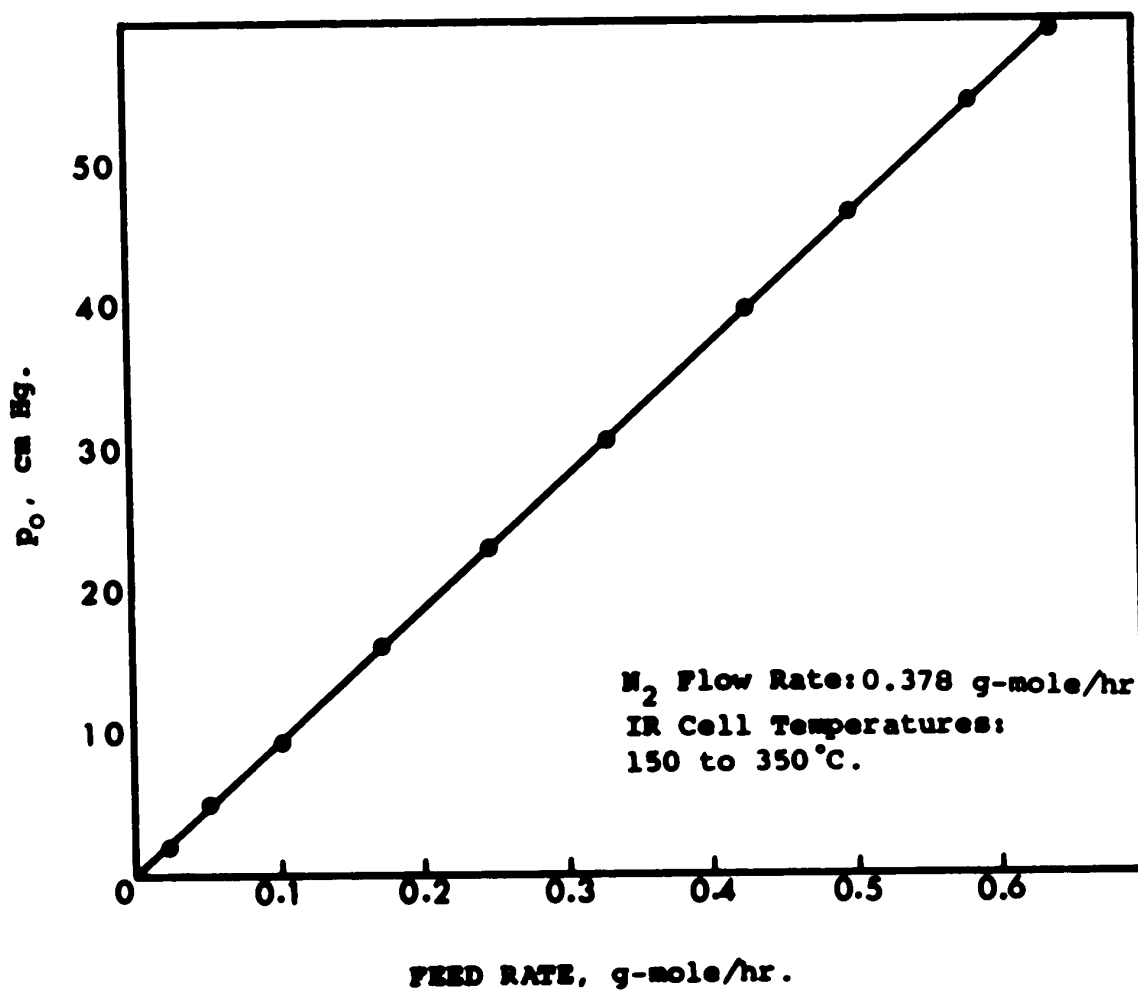


Figure 4-10. Relation of 2-Propanol Feed Rate to Its Partial Pressure Under Non-reaction Conditions.

TABLE 4-7. RELATION OF 2-PROPANOL FEED TO ITS PARTIAL PRESSURE UNDER NON-REACTION CONDITIONS*

X = 2-PROPANOL FEED RATE, GRAM-MOLE PER HOUR
 Y = PARTIAL PRESSURE OF 2-PROPANOL IN REACTOR, CM HG

THE COEFFICIENTS OF THE POLYNOMIAL, $Y = A_0 + A_1 * X$,

A₀ = 0.09518
 A₁ = 92.94480

REGENERATED DATA

X MEASURED	Y OBSERVED	Y CALCULATED	PCT ERROR
0.021	2.051	2.051	0.032
0.052	4.940	4.938	0.029
0.052	9.591	9.594	0.032
0.170	15.927	15.932	0.037
0.245	22.903	22.894	0.036
0.329	30.733	30.748	0.050
0.426	39.723	39.698	0.060
0.496	46.290	46.260	0.062
0.584	54.343	54.412	0.127
0.640	59.611	59.579	0.052

VARIANCE = 0.000836
 STANDARD DEVIATION = 0.028925
 MAXIMUM PCT ERROR = 0.127182

*NITROGEN FLOW RATE = 0.378 G-MOLE/HR.

mental runs and was found to hold quite well.

After obtaining p_0 , the sodium chloride wafer was replaced by a catalyst wafer and the partial pressure of each component in the reaction mixture was collected by measuring the absorbance at the characteristic frequencies for each component after steady-state was reached. Though the reaction mixture was always more than 50% nitrogen and the percentage conversion of the reactant was low, the change in molal flow rate was calculated using the procedure described below.

The partial pressure of each component in the product mixture and fractional conversion of 2-propanol were calculated as follows:

$$p_i = p_{ir} \cdot \frac{(a F_{A0}(1 + x_A) + b)}{(a F_{A0} + b)} \quad (4.9)$$

$$\text{and} \quad 1 - x_A = \frac{p_a}{p_0} = p_{ar} \cdot \frac{(a F_{A0}(1 + x_A) + b)}{(a F_{A0} + b)^2} \quad (4.10)$$

where p_i and p_a are partial pressures of the i^{th} component and of alcohol, respectively, corrected for the volume expansion due to reaction and

p_{ir} and p_{ar} are partial pressures of i^{th} component and of alcohol, respectively measured in the reference cell.

The term, $(a F_{A0}(1 + x_A) + b)/(a F_{A0} + b)$, is the correction factor for the change in molal flow rate due to chemical reaction. Thus by combining equations (4.10) and (4.5), the reaction rate can be calculated.

By changing the feed rate, i.e. the partial pressure of the

reactant, a set of data in the form of $(-r_A) = f(p_i)$ could be obtained for modeling the kinetics.

CHAPTER V
RESULTS AND DISCUSSION

5.1 Adsorption and Surface Reactions of Alcohols

5.1.1 2-Propanol on Pure γ -alumina

Figure 5-1 shows the spectra of 2-propanol adsorbed on pure γ -alumina from room temperature to 300°C. Up to 80°C (Curve 2), one observes that the surface hydroxyl groups are displaced considerably to the lower frequency with the formation of a large broad hydrogen-bonded hydroxyl region. On adsorption, the three bands observed in the gas phase at 2981, 2972 and 2888 cm^{-1} have shifted to the lower frequencies at 2960, 2930 and 2870 cm^{-1} . The C-H bending region shows almost no change in frequencies except that the intensity of the band at 1465 cm^{-1} has increased two-fold over that in the gas phase in contrast to the band at 1373 cm^{-1} . These changes are similar to that observed during the transition from gas to liquid phases⁽⁵²⁾. The three distinct bands at 1245, 1145 and 1065 cm^{-1} in the O-H bending and C-O stretching regions, observed in the gas phase spectrum, on adsorption merge into a single broad band at 1170 cm^{-1} . These observations suggest that 2-propanol is physically adsorbed through the hydrogen-bonding between the -C-OH of the alcohol and the surface hydroxyl groups (as shown in Structure V).

The close similarity between the spectrum of the adsorbed

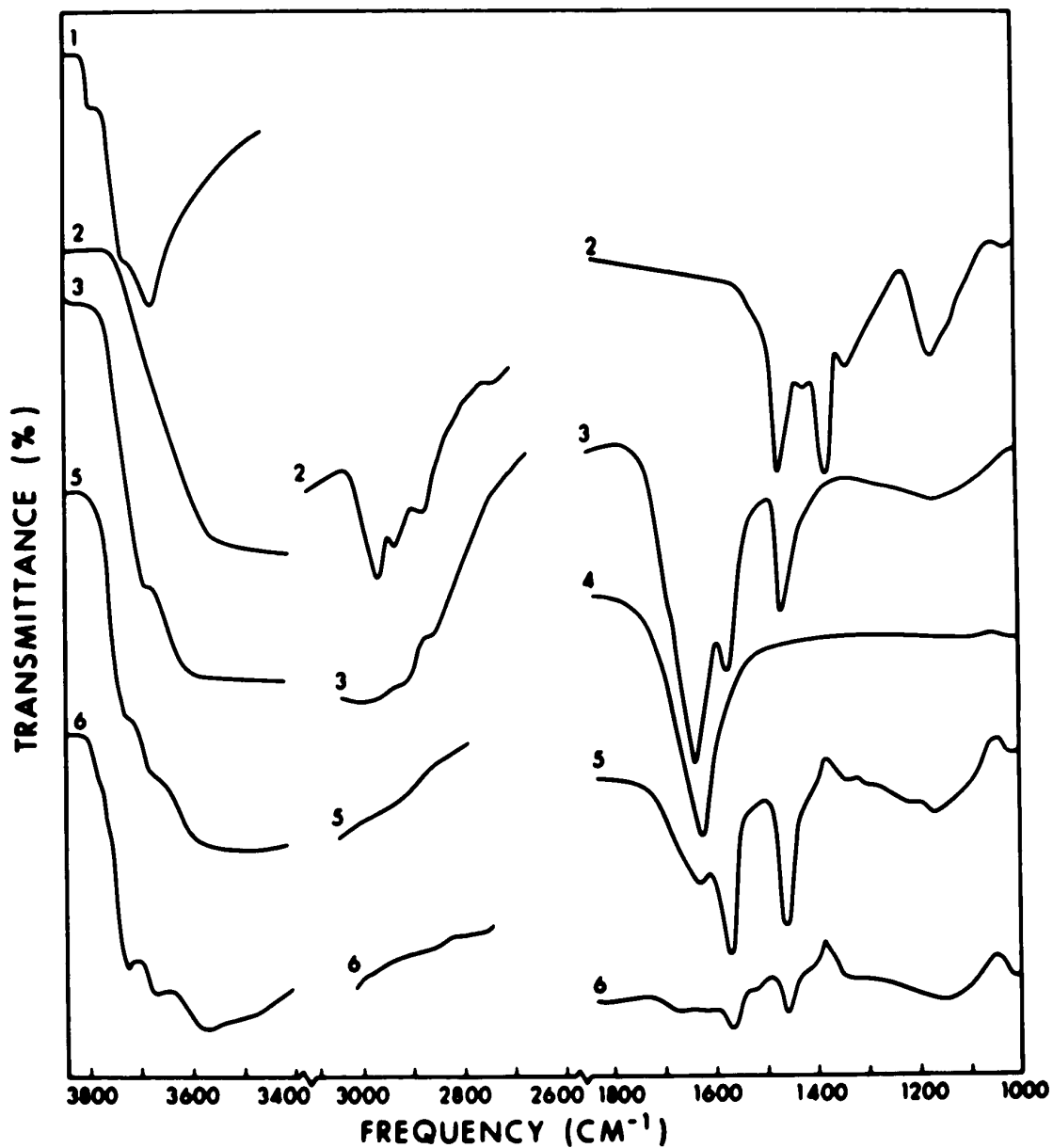
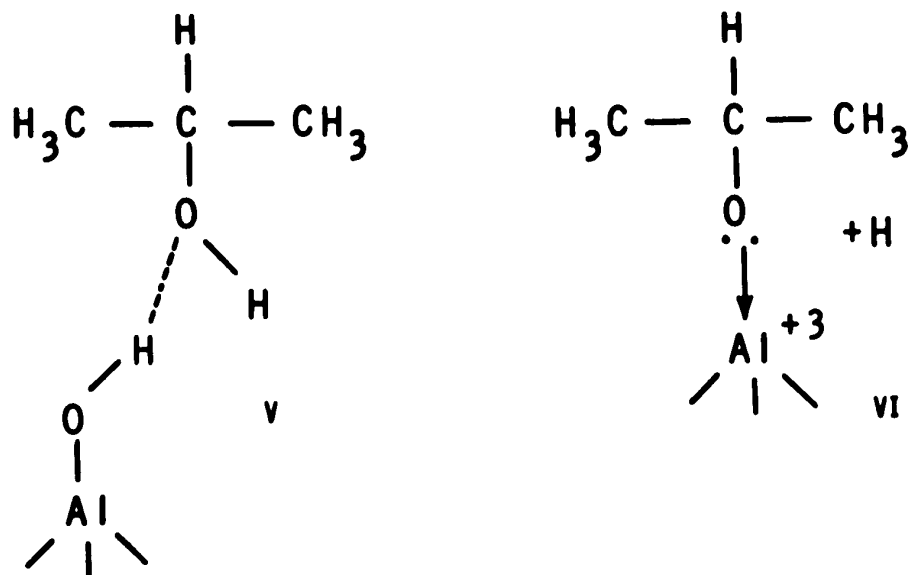


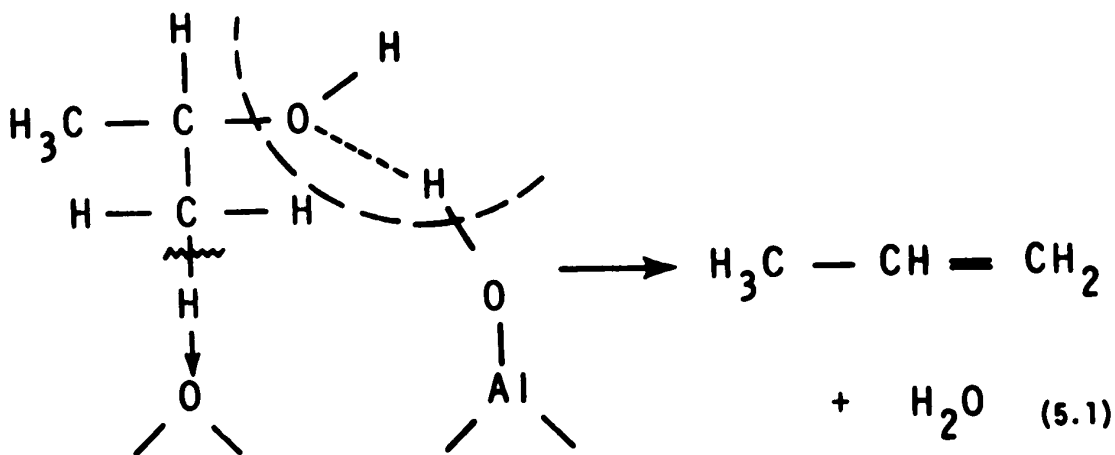
Figure 5-1. Spectra on the Adsorption of 2-Propanol on γ -Alumina. 1. Baseline. 2. Alumina and 2-Propanol at 10 torr and room temperature. 3. Alumina and 2-propanol at 300°C for 1 hr. 4. Alumina and water vapor at 5 torr and room temperature. 5. Degassing of 3. at room temperature for 1 hr. 6. Degassing of 5. at 300°C for one hour.

species and that of aluminum isopropoxide suggests, in addition to the hydrogen-bonded species, the presence of an alkoxide type of structure VI (45,51). Pumping at room temperature and up to 80°C removed most of the physically adsorbed hydrogen-bonded species, leaving the alkoxide type structure on the surface. The formation of such an alkoxide species on the electron-abstracting Lewis-acid site, Al^{+3} , is in agreement with the work reported (45,48,51).

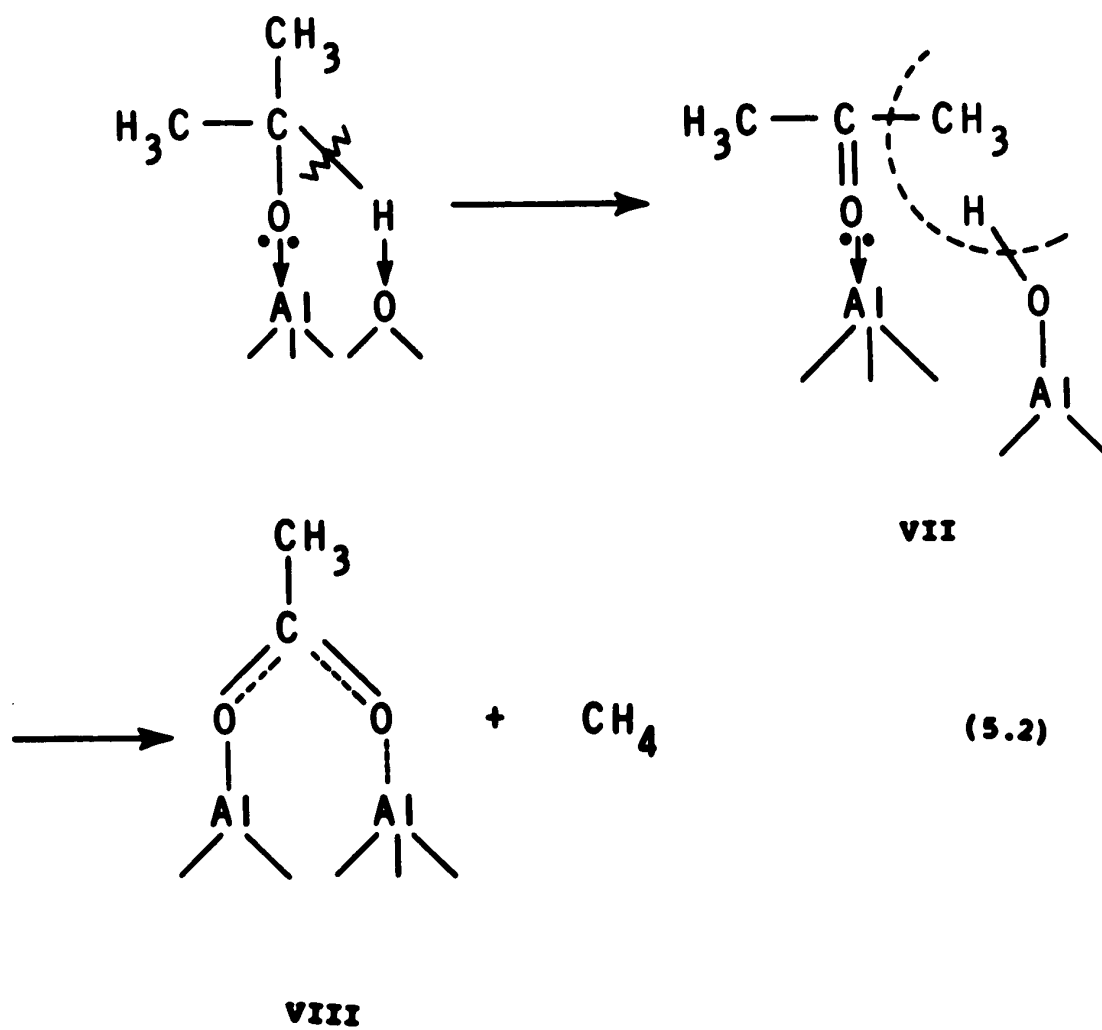
The two species, V and VI, can be represented as follows.



On heating above 100°C and up to 300°C (Curve 3), all of the band structure attributable to these two species disappears, giving propylene in the gas phase and leaving adsorbed water on the alumina surface. This is indicated by the strong band at 1635 cm^{-1} , the O-H bending vibration. For comparison, Curve 4 shows this band when water vapour is adsorbed on γ -alumina. This adsorbed water can be removed by pumping, even at room temperature. The dehydration reaction⁽¹⁸⁾ can proceed as shown in reaction (5.1).



Above 130°C, two new bands appear at 1575 and 1465 cm^{-1} and they increase in intensity with increasing temperature. The observed bands could be assigned to the symmetrical and asymmetrical stretching vibrations of the COO^- groups of an acetate⁽⁵¹⁾. The formation of a carboxylate from the alkoxide species as explained by Greenler⁽⁵¹⁾ and Kage1⁽⁴⁵⁾ has been subject to criticism by Fink⁽⁵⁸⁾, i.e. it seems unlikely that three hydrogen atoms will split from the alkoxide and an adjacent hydroxyl group. However, the adsorption of acetone on γ -alumina at 220°C produced the same infrared characteristics that were observed for the proposed carboxylate species VIII obtained with 2-propanol. Although acetone was not detected as an intermediate product from 2-propanol, the adsorbed acetone may have been present in the form of species VII preceding the formation of the carboxylate structure. Additional evidence supporting this explanation arises from studies with the sodium hydroxide-doped γ -alumina. The doping eliminates or modifies active surface hydroxyl groups. Under these conditions, large amounts of the adsorbed acetone-like species VII can be found by adsorbing 2-propanol at 130°C. Upon further heating above 220°C, large amounts of the carboxylate species were detected. The following reaction scheme seems plausible for the formation of carboxylate:



The presence of methane in the gas products was confirmed by high resolution mass spectral analysis. In addition, the acetate structure VIII could be partially hydrolyzed by water above 220°C to form acetic acid. These observations further support the proposed reaction steps (5.2).

The formation of ether, particularly at low temperatures, as already reported⁽⁶⁾, was not observed in this study. It is possible that the ether is present in undetectable amounts or that it rapidly forms the alkoxide species⁽⁷⁹⁾. Moreover, the formation of ether from secondary alcohols is thermodynamically less favorable than the formation of olefins⁽¹⁴⁾.

5.1.2 2-Butanol on γ -alumina

Figure 5-2 shows the results from the adsorption of 2-butanol on γ -alumina up to 300°C. The spectrum of physically adsorbed 2-butanol (Curve 2) shows changes similar to those observed with 2-propanol. The products from dehydration were observed in the gas phase as a mixture of 1-butene, trans- and cis-2-butene. Consistent with thermodynamics, their distribution appeared in the order,



Little of the carboxylate species was noted even at a temperature of 300°C. Since the carboxylate species is formed from the alkoxide species, the reduced amount of alkoxide present could account for this. Two infrared bands detected at 1561 and 1479 cm^{-1} suggest the presence

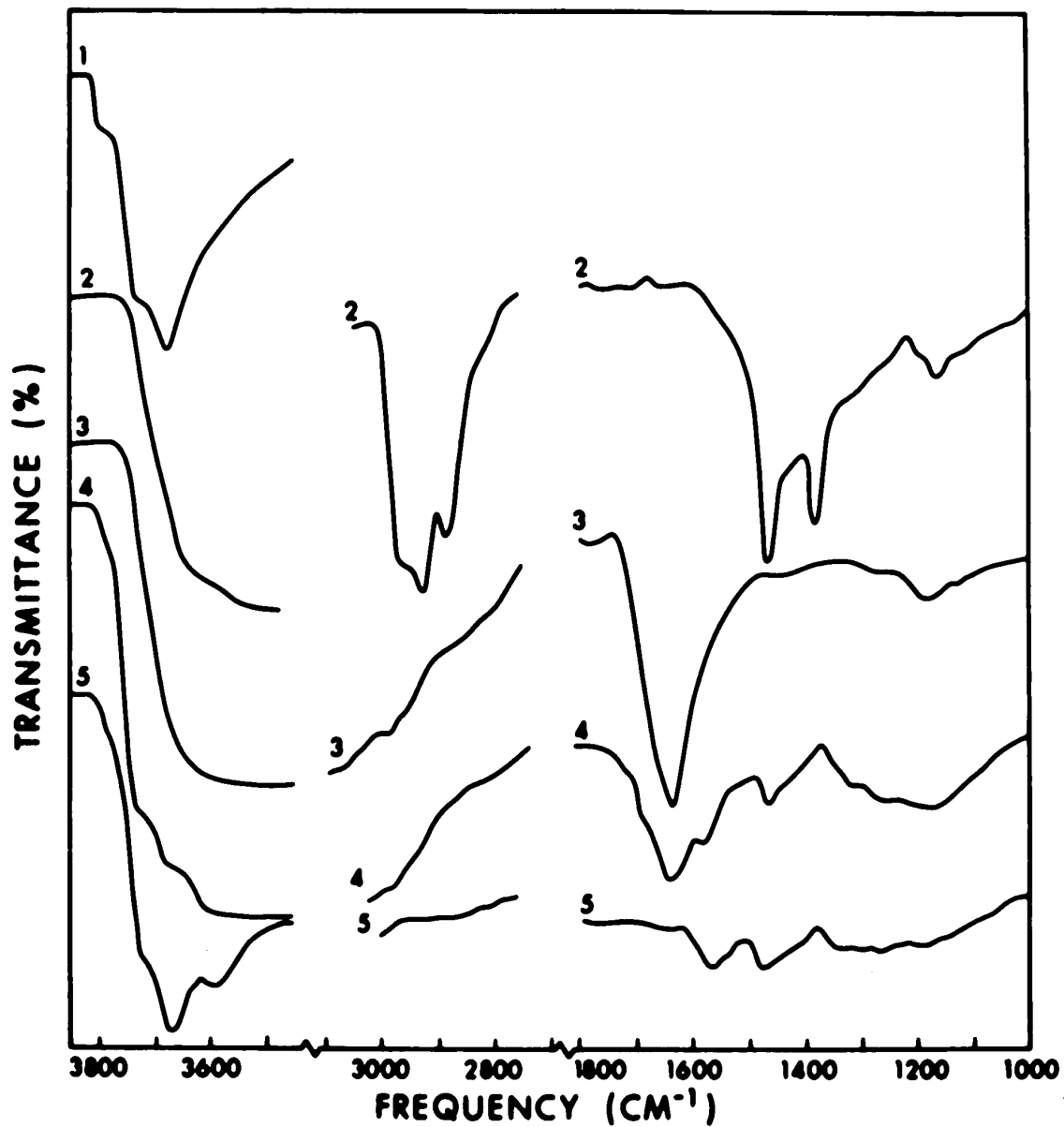


Figure 5-2. Spectra on the Adsorption of 2-Butanol on γ -Alumina. 1. Baseline. 2. Alumina and 2-butanol at 10 torr and room temperature. 3. Alumina and 2-butanol at 130°C for 1 hr. 4. Degassing of 3. at room temperature for one hour. 5. Degassing of 4. at 300°C for one hour.

of a propionate⁽⁴⁸⁾. Analysis of the gas phase confirmed the presence of a propionate structure. Methane accompanied the dehydration products and propionic acid was found upon hydrolysis at 220°C. These observations are consistent with the explanation of the acetate structure formation shown in reaction (5.1). It would thus be anticipated that a secondary alcohol may form some carboxylate and an alkane fragment upon heating in the presence of γ -alumina.

5.1.3 3-Pentanol on γ -alumina

Figure 5.3 shows results of 3-pentanol adsorbed on γ -alumina from room temperature up to 300°C. The spectrum of 3-pentanol adsorbed on γ -alumina at room temperature is similar to those for 2-propanol and 2-butanol, showing the presence of both hydrogen-bonded and alkoxide species.

On heating at 80°C, a new band is observed at 1685 cm^{-1} accompanied by the formation of a trace amount of mixture of cis- and trans-2-pentene. This 1685 cm^{-1} band occurs at a frequency which was considered to be too high to be attributable to the O-H bending band of water formed on dehydration. An alternative explanation suggests that this 1685 cm^{-1} band is due to some partial double bond character, formed as an intermediate just before dehydration occurs at higher temperatures. This species may be represented by structure IX.

A similar band at 1675 cm^{-1} was observed on adsorbing trans-2-pentene on γ -alumina, stable even on prolonged pumping at room temperature. This additional evidence supports the explanation that

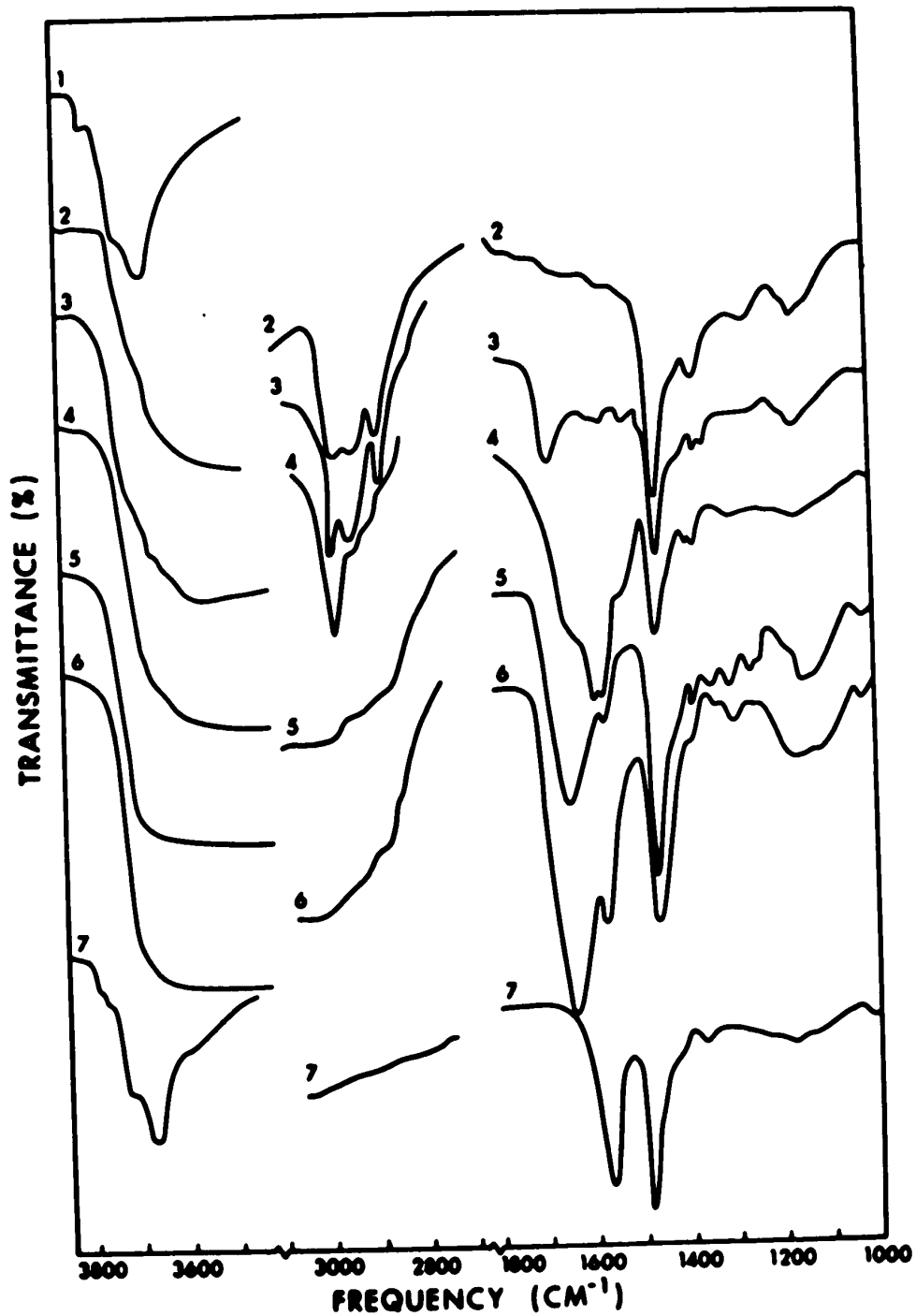
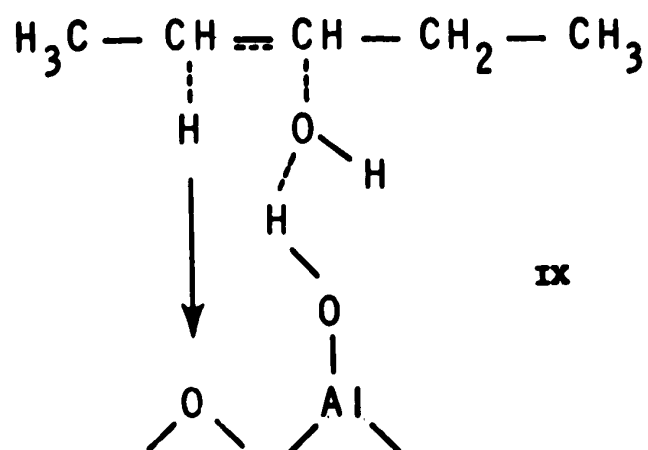


Figure 5-3. Spectra on the Adsorption of 3-Pentanol on γ -Alumina. 1. Baseline. 2. Alumina and 3-pentanol at 10 torr and room temperature. 3. Alumina and 3-pentanol at 80°C for 1 hr. 4., 5. As per 3. but at 130 and 220°C, resp. 6. Alumina and 3-pentanol at 300°C for 1 hr. 7. Degassing of 6. at 300°C for one hour.



a partially double bond form of intermediate is formed before dehydration occurs. Above 80°C, the dehydration proceeds at a faster rate making it more difficult to observe the intermediate, IX. The 1640 cm^{-1} band due to O-H bending of adsorbed water increases with temperature and above 220°C, 1-pentene is formed.

The carboxylate species is formed at 130°C along with parallel formation of the alkoxide species, shown by an increase in the intensity of the broad band at 1150 cm^{-1} . The carboxylate structure (in this case, propionate) remains stable even when pumping at 300°C. The formation of the carboxylate would, in this case, be expected to produce ethane analogous to the methane formed in reaction (5.2).

5.1.4 2-Propanol on 2% NaOH-doped γ -alumina

Figure 5.4 shows the spectra obtained from adsorption of 2-propanol on 2% sodium hydroxide-doped γ -alumina from room temperature to 300°C. At temperatures up to 130°C (Curve 2), the hydrogen-bonded species V is formed to a much lesser degree than was observed on the γ -alumina. The elimination of many surface hydroxyl groups by reaction to form $=Al-O-Na$ would account for this reduced physical adsorption. The presence of the alkoxide species VI was shown by the deep band at 1165 cm^{-1} .

Above 130°C, the dehydrogenation reaction occurs forming acetone as the product along with minor dehydration indicated by a trace of propylene. The bands at 1705, 1640, 1440, 1360, 1330 and 1227 cm^{-1} (Curve 3) originate with the acetone adsorbed on Al^{+3} sites. The band at 1640 cm^{-1} results from the adsorbed acetone as well as from some adsorbed water formed during dehydration. In addition to this band structure, four more bands are observed at 1572, 1456, 1330 and 1170 cm^{-1} (Curve 3). The pair of bands at 1572 and 1456 cm^{-1} are attributed to the carboxylate species, similar to those found on γ -alumina. The remaining two bands at 1330 and 1170 cm^{-1} , which also always appear as a pair and occur in the carboxylate frequency range, were tentatively assigned to a second type of carboxylate structure. On pumping from room temperature (Curve 5) to 300°C (Curve 6), the band structure due to acetone completely disappears, leaving only the four carboxylate bands. Adsorption of acetone on the doped alumina at 150°C showed the presence of both the adsorbed acetone and carboxylate species.

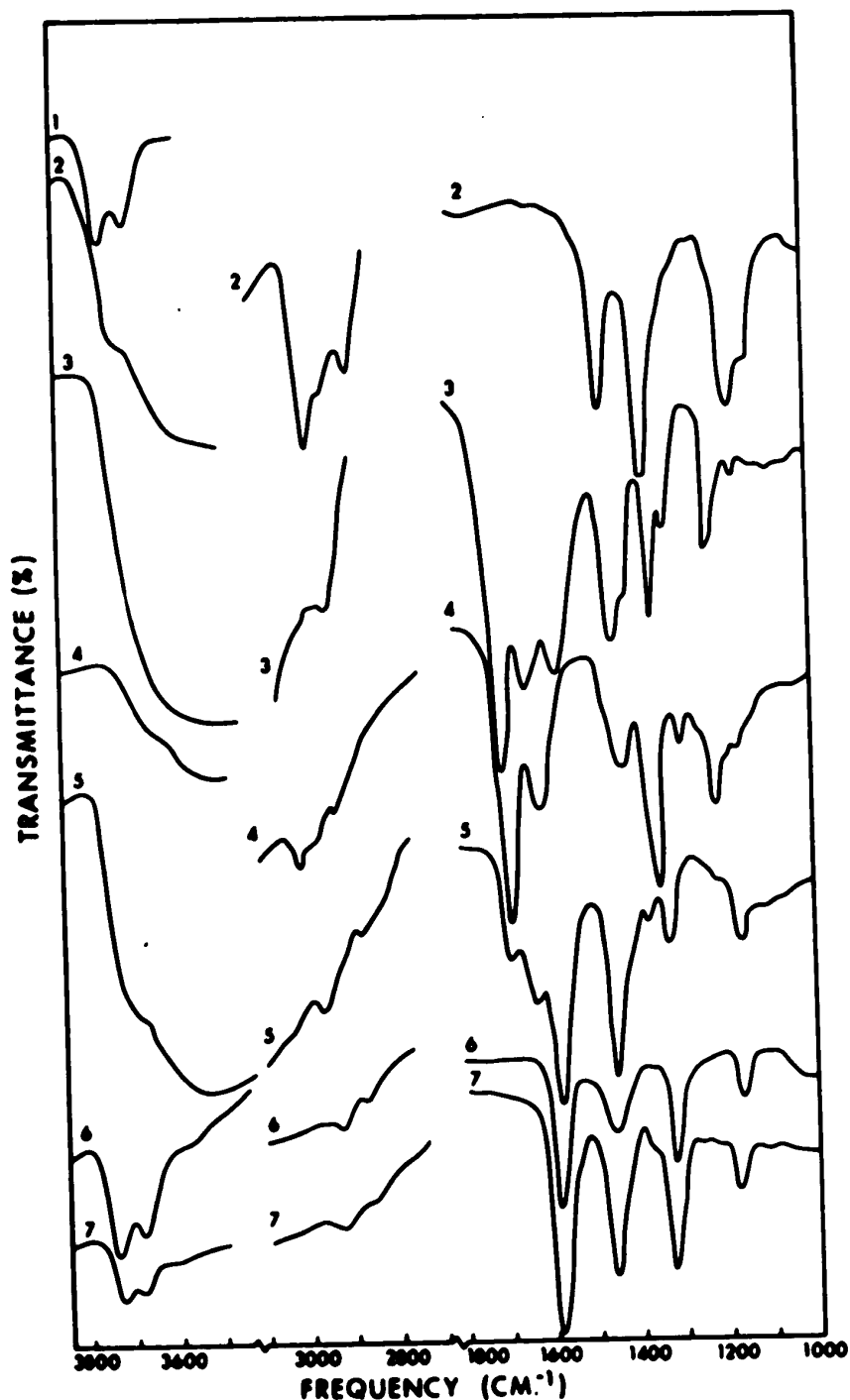


Figure 5-4. Spectra on the Adsorption of 2-Propanol on 2% NaOH-doped γ -Alumina. 1. Baseline. 2. Doped alumina and propanol at 10 torr and room temperature. 3. Doped alumina and propanol at 300°C for one hour. 4. Doped alumina and acetone at 10 torr and room temp. 5. Degassing of 3. at room temperature for one hour. 6. Degassing of 5. at 300°C for one hour. 7. Degassing of 4. at 300°C for one hour.

Upon heating the ketone bands diminished in intensity along with an increase in intensity of both pairs of carboxylate bonds. Further, mass spectral analysis of the degassed phase showed only methane to be formed, in substantial agreement with the proposed mechanism shown in reaction (5.2). On this basis, the assignment of the additional band pair at 1330 and 1170 cm^{-1} to a second carboxylate structure seemed logical.

The presence of these two pairs of bands may be the result of differences in charge distributions and in symmetry considerations for oxygen atoms and their energy of bonding to the surface⁽¹⁰⁴⁾. By doping γ -alumina with sodium hydroxide, it was observed that the high frequency hydroxyl groups disappeared. This may change the charge distribution of oxygen atoms which are responsible for the carboxylate formation.

Acetone was adsorbed on fresh sodium hydroxide-doped γ -alumina catalyst and the system was then heated to 130°C (Curve 4) to compare adsorbed acetone and its behavior, with the intermediate which led to the formation of acetone. This spectrum is very similar to that observed on heating the catalyst in the presence of 2-propanol (Curve 3). Upon degassing the catalyst exposed to pure acetone at 300°C, only the carboxylate structure remained (Curve 7). This confirms the formation of an adsorbed acetone-like species, VII, like that obtained from 2-propanol which on desorption gives acetone.

5.1.5 2-Butanol on 2% NaOH-doped γ -alumina

Figure 5.5 shows the spectra of 2-butanol adsorbed on 2% sodium hydroxide-doped γ -alumina from room temperature to 300°C. At temperatures up to 80°C, the alkoxide species is formed with very little hydrogen-bonded species appearing (Curve 2). Near 130°C, the dehydrogenation reaction starts to form species VII as shown by the increased bond intensity at 1730 cm^{-1} attributed to the C=O stretching frequency (Curve 3). After heating at 300°C (Curve 4), the carboxylate structure spectrum became dominant. Heating of adsorbed 2-butanone on a newly prepared catalyst wafer gave spectra similar to those from 2-butanol (Curve 5). Both 2-butanol and 2-butanone produced carboxylates with bands identical to those observed with 1-propanol⁽⁴⁸⁾ on the doped γ -alumina.

5.1.6 3-Pentanol on 2% NaOH-doped γ -alumina

Figure 5-6 shows the various spectra of 3-pentanol adsorbed on 2% sodium hydroxide-doped γ -alumina from room temperature to 300°C. At room temperature (Curve 2), the main species is again the alkoxide type. The dehydrogenation reaction occurs at a still lower temperature, 80°C, and continues up to 300°C with the formation of the stable carboxylate species (Curves 3,4,5,7). Adsorption of 3-pentanone (Curve 6) formed by heating shows spectral characteristics comparable to those expected from reaction (5.2).

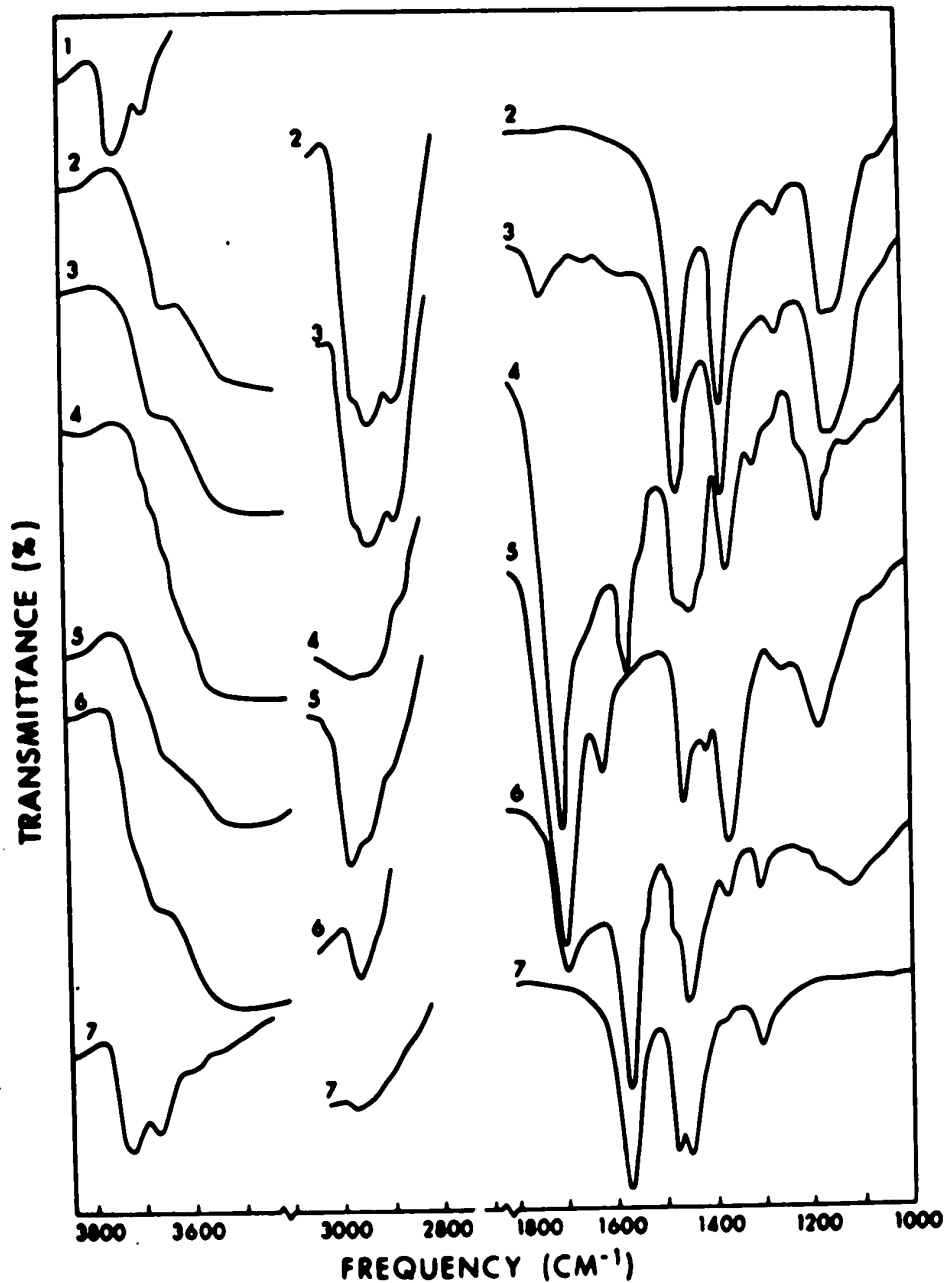


Figure 5-5. Spectra on the Adsorption of 2-Butanol on 2% NaOH-doped γ -Alumina. 1. Baseline. 2. Doped alumina and butanol at 10 torr and room temperature. 3. Heating 2. at 130°C for one hour. 4. Heating 3. at 300°C for one hour. 5. Doped alumina and 2-butanone at 10 torr and room temperature. 6. Degassing of 4. at room temp. for one hour. 7. Degassing of 6. at 300°C for one hour.

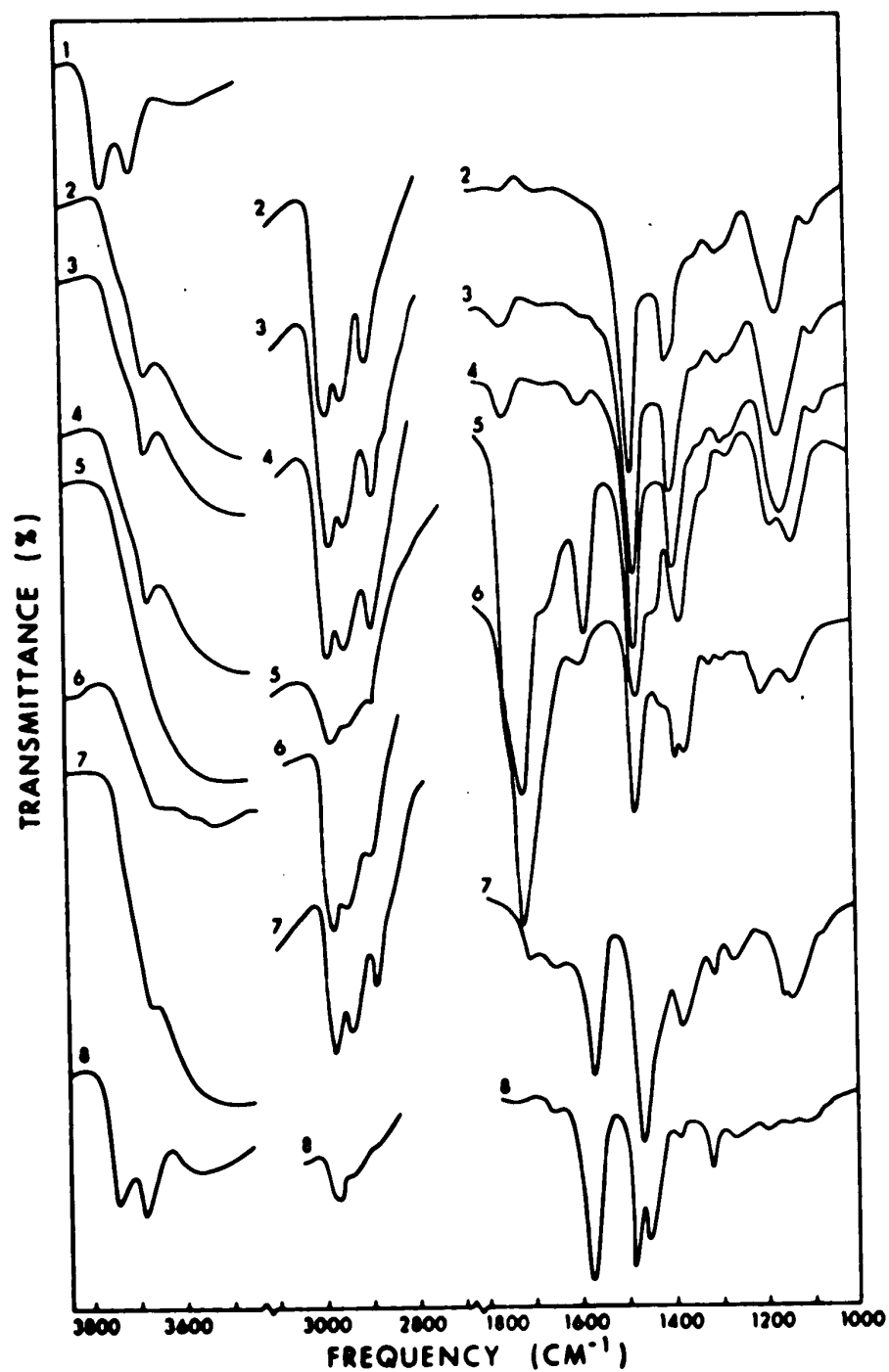


Figure 5-6. Spectra on the Adsorption of 3-Pentanol on 2% NaOH-doped γ -Alumina. 1. Baseline. 2. Doped alumina and pentanol at 10 torr and room temperature. 3. Heating 2. at 80°C for one hour. 4., 5. As per 3. but at 130 and 300°C, respectively. 6. Doped alumina and 3-pentanone at 10 torr and room temperature. 7. Degassing of 5. at room temp. for 1 hour. 8. Degassing of 7. at 300°C for one hour.

5.2 Catalytic Properties of γ -alumina Using IR Adsorption Technique

5.2.1 Effect of NaOH Concentration on Brønsted-type Acidity on the Alumina Surface

Figure 5-7 shows the spectra of sodium hydroxide-doped γ -aluminas in the OH stretching region ($3500\text{-}3850\text{ cm}^{-1}$). Figure 5-7A shows the spectrum of the pure γ -alumina. The related spectra for varying levels of NaOH doping are shown in Figures 5-7B to 5-7G. Three characteristic bands are observed for pure γ -alumina at 3785 , 3720 and 3680 cm^{-1} . Increased doping results in the disappearance first of the 3785 and then the 3680 cm^{-1} bands, the 3720 cm^{-1} band remaining largely unaffected. Doping at the 1% NaOH level, eliminated the 3785 cm^{-1} band, but the intensities of the 3732 and 3680 cm^{-1} corresponded almost identically to those for their counterpart frequencies, 3720 and 3680 cm^{-1} , on pure γ -alumina. Elimination of the 3785 cm^{-1} band also resulted in a slight shift from 3720 to 3732 cm^{-1} for the middle hydroxyl band, implying increased freedom for its stretching frequency. The presence of excess NaOH could be observed in the spectrum of the 15% NaOH sample (Figure 5-7G) in the form of bands characteristic of NaHCO_3 . The high frequency 3785 cm^{-1} band decreased in intensity very rapidly with doping. Since the doping was carried out in the "liquid-phase", the acidity of the hydroxyl groups, commonly associated with these three bands can be inferred to be stable at normal conditions, and may be considered in terms of the groups' relative reactivity with the NaOH. The evidence suggests that the 3785 cm^{-1} hydroxyl group is the most acidic, followed by the 3680 cm^{-1} band. The continued presence

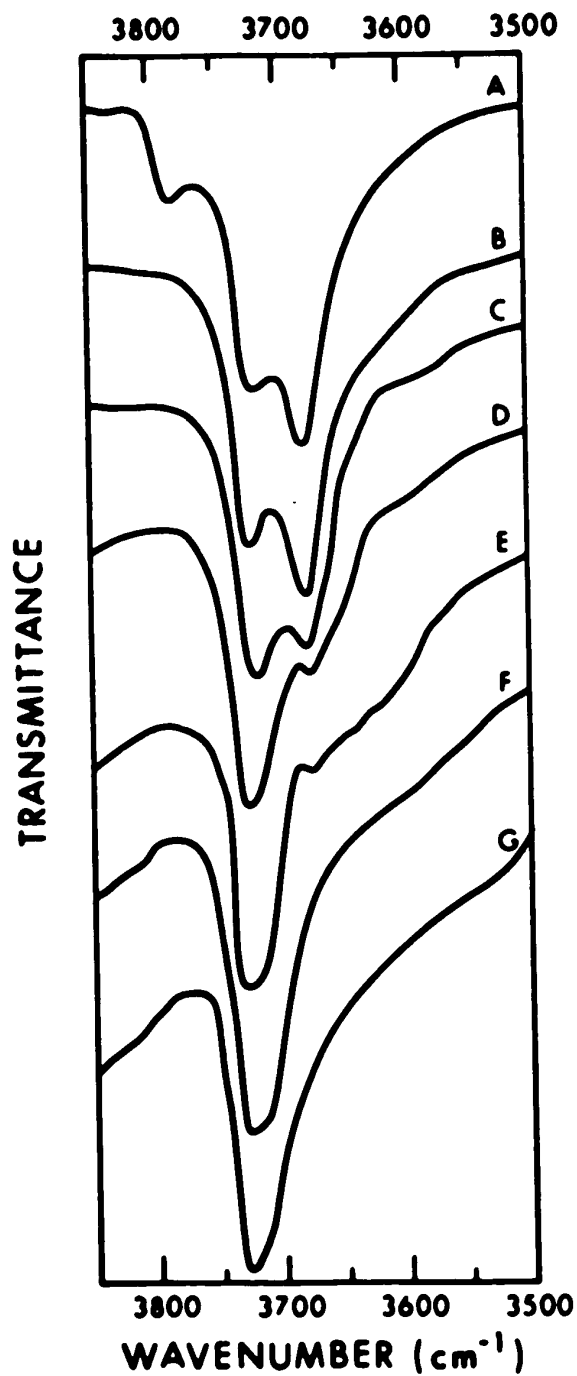


Figure 5-7. Variation of spectrum above 3500 cm^{-1} of the NaOH doped γ -aluminas. NaOH content (w/w, %) A, 0; B, 1; C, 2; D, 3; E, 5; F, 8; G, 15.

of the 3720 cm^{-1} band irrespective of the level of doping implies that it exhibits little, if any, acidity or else, that its acidic behavior, thus defined, is suppressed by steric factors or low reactivity.

Additional insight into the acidic behavior may be inferred by studying the catalytic selectivity of γ -alumina towards dehydration or isomerization reactions. Pines and Haag⁽²⁶⁾ suggested that alumina exhibited either strong or weak types of acidic character. Their work suggested that the total number of hydroxyl-type acid sites in γ -alumina can be measured by dehydrating 1-butanol, and that the fraction of these which are strong acid sites can be determined by cyclohexene isomerization. Heating in 5 torr of cyclohexene at 200°C for one hour, sample A (pure Al_2O_3) was found to catalyze the cyclohexene isomerization but sample B (1% NaOH) was found to be catalytically inactive for this reaction; thus the strong acid sites at 3785 cm^{-1} were eliminated by doping. Proceeding further, both samples A and B catalyzed the dehydration of 1-butanol under identical reaction conditions, B to a lesser extent, hence the weak acid sites alone would be expected to remain on the series of doped catalyst, and probably decrease with increased doping. This point-of-view is consistent with the observation that the 3785 and 3680 cm^{-1} hydroxyl bands correspond, respectively, to strong and weak Bronsted-acid behavior of the surface hydroxyl groups.

Additional infrared spectra were obtained for the hydrated surface of γ -alumina by slowly drying a wafer of pure γ -alumina at room temperature and under vacuum over a 48-hour period as shown in Figure 5-8. Starting with a hydrated surface whose IR spectrum exhibited no



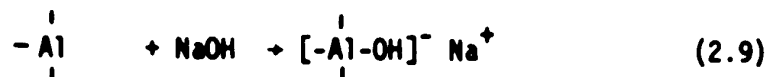
Figure 5-8. Spectra on the Degassing of γ -Alumina at Room Temperature over Varying Time Periods: A, 0.5 hr.; B, 4 hr.; C, 24 hr.

bands characteristic of free hydroxyl groups, pumping led first to the appearance of the 3720 cm^{-1} band and then to the 3680 cm^{-1} band; additional pumping having no further visible effect. Since the degree of hydrogen-bonding between surface hydroxyl groups and water molecules on the surface is somewhat proportional to the "acidity" of the hydroxyl groups, this also supports the view that the 3720 cm^{-1} band exhibited weaker acidic character than the 3680 cm^{-1} band. The high frequency 3785 cm^{-1} band was not observed at room temperature pumping indicating that its strongly acidic character resulted in stable hydrogen-bonding of surface water molecules.

As a result of the NaOH-doping, the hydroxyl groups likely formed structures of the type, $=\text{Al-O-Na}$, since the various IR spectra did not reveal bands attributable to other types of bonding.

5.2.2 Effect of NaOH Concentration on Lewis-type Acidity on the Alumina Surface

Lewis-acid sites are believed to be abundant on the dehydrated alumina surface⁽³⁷⁾, probably as incompletely coordinated aluminum ions. On this basis, Pines and Haag⁽²⁶⁾ also suggested the possibility that doping with NaOH could give rise to an acid/base surface complex of the type shown in reaction (2.9).



To determine whether reaction (2.9) had occurred upon doping, it is necessary to measure whether the number of aluminum ion sites decreases

with increased NaOH doping. The aluminum ion sites are generally regarded as being Lewis-acid sites. In the presence of pyridine, Parry⁽³⁷⁾ reported that the infrared spectra of the coordinately bonded species (on Lewis-acid sites) should differ from those of the pyridinium (on Bronsted-acid sites). In this work, neither pure alumina nor the doped aluminas exhibited IR spectra of pyridinium ions on their surfaces hence their Bronsted-acid sites are too weakly acidic to react with pyridine. On the other hand, the spectral intensities suggested that the amount of pyridine bonded on the Lewis-acid sites remained constant with increased NaOH doping. This evidence verifies that only the Bronsted-acid sites (two types of hydroxyl group sites) reacted with the NaOH to form = Al-O-Na and thus reaction (2.9) does not occur.

5.2.3 Effect of NaOH Doping upon Dehydration Catalytic Activity

Since the mechanisms for dehydration or dehydrogenating of different lower secondary alcohols were found to be virtually identical for each alcohol (see Section 5.1), 3-pentanol was chosen as the model reactant to study the catalytic activity and selectivity of NaOH-doped γ -aluminas. Figure 5.9 shows the results obtained from adsorbing 3-pentanol on the various NaOH-doped γ -aluminas after heating at 200°C for one hour. The catalytic reactions which occur are either the dehydration,



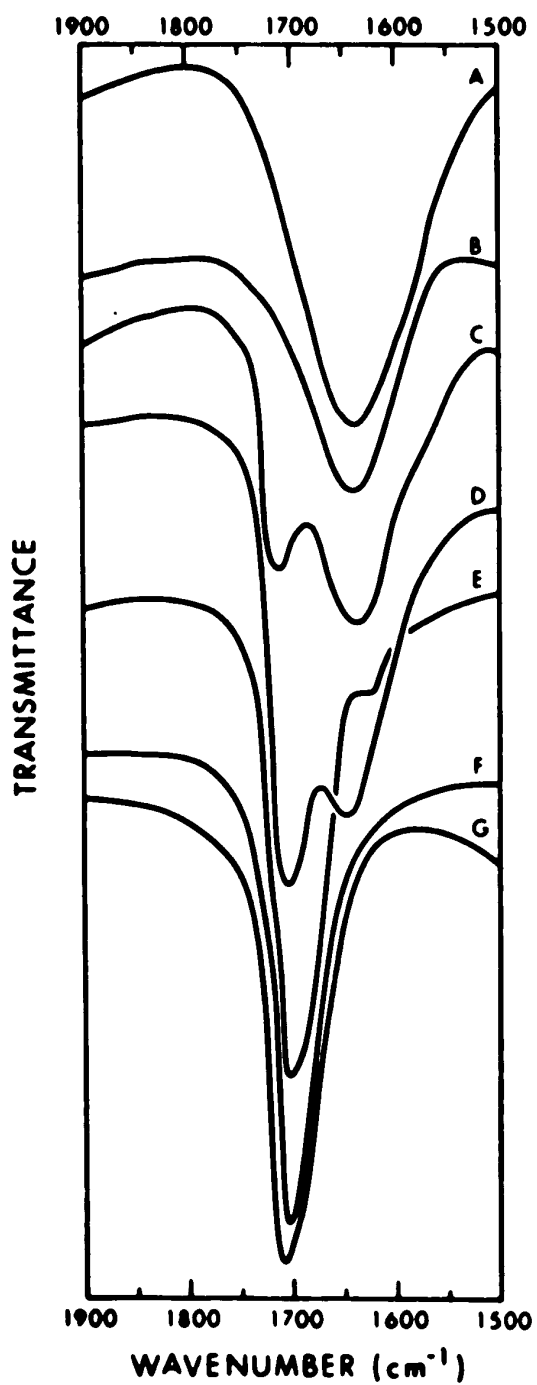
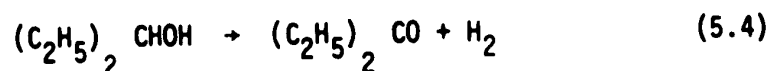


Figure 5-9. Spectra on the adsorption of 3-pentanol on NaOH doped γ -aluminas at 200°C for one hour. Sample numbers correspond to those given in Figure 5-7.

or the dehydrogenation,



and the relative amounts of reactions (5.3) and (5.4) which have proceeded may be estimated by comparing the 1715 cm^{-1} band, from the carbonyl group of the adsorbed 3-pentanone, or by the 1635 cm^{-1} band for adsorbed water. The spectra for pure γ -alumina (Figure 5.9A) shows that only dehydration is catalyzed. The spectra for 8% and higher doping levels (Figures 5.9F and 5.9G) show that only dehydrogenation has occurred. Increasing doping levels of NaOH content, to between 5 and 8%, catalyzed varying amounts of both reactions (Figures 5.9B to 5.9E). The selectivity of the catalyst towards dehydrogenation increased with increasing NaOH content. The influence of excessive NaOH doping was also checked by contacting 3-pentanol vapor with a wafer of pure NaOH at 200°C . The results showed that neither NaOH nor NaHCO_3 exhibited catalytic activity and hence the role of NaOH in reactions (5.3) and (5.4) is essentially that of a "doping" agent.

5.2.4 Effect of NaOH Doping on Catalytic Selectivity

The distribution of chemical products 3-pentanone and water for series of tests to evaluate the influence of NaOH doping on catalytic selectivity in reactions (5.3) or (5.4) was determined by gas chromatographic analysis, using an eight-foot "Porapak T" (80-100 mesh) column at 160°C and a thermal conductivity detector. The relative activity of each catalyst sample (100 mg Al_2O_3) was studied by introducing 5 mm Hg of 3-pentanol vapor into the infrared cell at 200°C with a contact

time of one hour. Consistent and reproducible spectra and GC analyses were obtained in this manner. The experimental results are shown in Table 5-1, expressing activities in terms of mole % of 3-pentanol reacted per 10 m^2 of the catalyst surface (see Table 3-2 for surface area of each catalyst sample). This activity criterion provided a means of correcting for loss in catalyst specific surface area attributable to increases in NaOH content.

Table 5-1
Activity and Selectivity of $\gamma\text{-Al}_2\text{O}_3$ or NaOH-doped Al_2O_3 ;
Dehydration or Dehydrogenation of 3-pentanol at 200°C

Catalyst Sample	NaOH Content %	% of 3-pentanol converted per 10 m^2 catalyst surface	% of 3-pentanone formed per unit total conversion
A	0	87	0
B	1	78	0
C	2	61	38
D	3	47	51
E	5	16	96
F	8	13	100
G	15	11	100

The product distributions show that the % of 3-pentanol which has chemically reacted decreases with increasing NaOH doping. In addi-

tion, the % of 3-pentanone formed per unit total conversion (via combined dehydration and dehydrogenation) increased from zero between one and two percent NaOH content to 100% between 5 and 8% NaOH content. These results quantitatively demonstrate the shift in catalytic selectivity from dehydration to dehydrogenation, and the decline in catalytic activity per unit surface area with level of NaOH doping.

Assuming that the surface hydroxyl groups act as the catalytic sites for dehydration (see Section 5.1), comparing the spectra of Figure 5-9 with the product distributions in Table 5-1 suggests that the hydroxyl groups with the 3680 cm^{-1} band (samples B to E) and possibly, those with the 3785 cm^{-1} band (sample A) catalyze dehydration. When these two bands vanished upon doping (Samples F and G), only dehydrogenation catalytic activity appeared. Although the 3785 cm^{-1} hydroxyl groups could not be isolated from the 3680 cm^{-1} groups, their greater acidity suggests that they should be more active towards dehydration than the 3680 cm^{-1} groups.

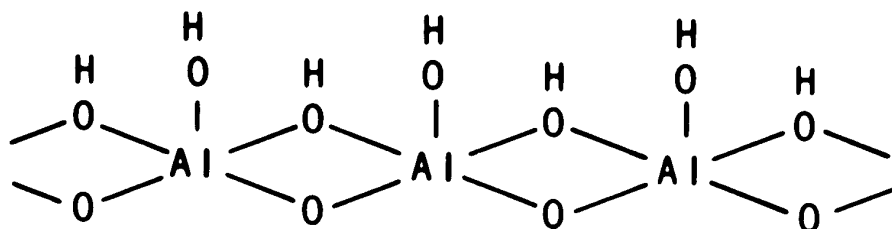
Figures 5-9C to 5-9F show that the selectivity for dehydration decreases with the decreasing intensities of the 3680 cm^{-1} hydroxyl band. The 3720 cm^{-1} hydroxyl sites are either not accessible to NaOH doping or are catalytically inactive towards dehydration since their band intensities did not change with increased doping.

5.2.5 Surface Structure of γ -alumina

Several interpretations of the nature of active sites on the alumina surface are available. One view proposed⁽⁴⁵⁾ is that the aluminum or oxide ions exposed at the surface act as active sites and that the surface was completely free of hydroxyl groups. This view

is contradictory to a conclusion of this study based upon the infrared spectra of alumina being characteristic of surface hydroxyl groups in the region, $3600 - 3800 \text{ cm}^{-1}$. The current widely accepted model, proposed by Peri⁽⁴²⁾, assumes a random configuration of hydroxyl groups after dehydration, leaving adjoining residual oxide ions and oxide vacancies, and exposed aluminum ions. The variations in the number of oxide ions surrounding the hydroxyl groups differentiate them into several types and imparts varying Bronsted-type acidity to each of the three groups. The three hydroxyl bands at 3680 , 3720 , and 3785 cm^{-1} are thus interpreted.

The general view of the structure of γ -alumina surface, based upon crystal chemistry proposed by Verwey⁽²²⁾, suggests that the unit cell of γ -alumina, a tetragonally formed spinel, consists of 32 oxide ions with $21\frac{1}{3}$ aluminum ions arranged at random in the 16 octahedral and 8 tetrahedral positions of the spinel structure. It is believed⁽³⁰⁾ that the surface is terminated in anions and the outermost aluminum ions lie below the surface plane. These aluminum ions provide the electrophilic centers by which water is dissociatively held on the surface; the electron pair of the OH being positioned over the aluminum ion while the dissociating proton forms a hydroxyl via binding to lattice oxygens⁽³¹⁾. The structure of the hydrated aluminum surface can be represented by the following,



The lattice OH is positioned on the surface below the plane of the OH adsorbed over the aluminum ion. It seems reasonable to assume that there are differences in the energies of interaction of surface hydroxyl groups with octahedrally and tetrahedrally coordinated aluminum ions, and that these differences result in the appearance of different isolated infrared bands, characteristic of hydroxyl groups, between 3680 and 3785 cm^{-1} .

Peri and Hannan^(41,105) used the exchange reaction between deuterium gas and surface aluminol groups to determine the number of such groups on their sample. They determined from the IR spectra obtained during exchange with deuterium that the average infrared absorptivity of the hydroxyl groups was of the order of $8 (10^4) \text{ cm}^2/\text{mole}$. They also suggested that Beer's law could probably be used to compare relative amounts of hydroxyl groups at coverages below 15%, where no hydrogen bonding appears to exist. Applying this suggestion to the catalysts used in this investigation, the highest frequency OH groups were calculated to number about 15% of the lowest frequency groups (Figure 5-7A); in reasonable agreement with Pines and Haag⁽²⁶⁾ who reported the fraction of strong acid sites numbered roughly 10% of the total acidic sites. Although the absorptivity calculations agree with Peri and Hannan's view, their interpretation that the higher acidity is associated with the lower frequency hydroxyl groups is not consistent with our findings based upon the chemical reaction of Bronsted-acid sites with NaOH solutions.

Lewis-acid sites, such as the incompletely coordinated aluminum ion, are believed to be abundant on the dehydrated alumina surface⁽³⁷⁾.

Assuming their presence as well as that of the Bronsted-acid sites, their relative numbers and corresponding relative catalytic activities can be estimated. Using $2 (10^{13}) \text{ site/cm}^2 (106)$ and $10 (10^{13}) \text{ site/cm}^2 (26)$ for Lewis-acid and Bronsted-acid sites, respectively, a dehydrogenation to dehydration selectivity ratio of 1 to 5 would be anticipated for both types of site which are equally active. Comparing sample A (total Bronsted-acid) and sample B (weak Bronsted-acid) to sample E (total Lewis-acid) in Table 5-1, it can be estimated that a value of 15 for the % of 3-pentanol converted per 10 m^2 surface would be approximately equal to the value for the complete dehydrogenation of 3-pentanol on the fully doped alumina. Thus,

$$\frac{\text{Number of total Bronsted-acid sites}}{\text{Number of total Lewis-acid sites}} \propto \frac{\text{Fractional conversion of 3-pentanol on pure Al}_2\text{O}_3}{\text{Fractional conversion of 3-pentanol on fully doped Al}_2\text{O}_3} = \frac{87}{15} \approx \frac{5.8}{1}$$

and

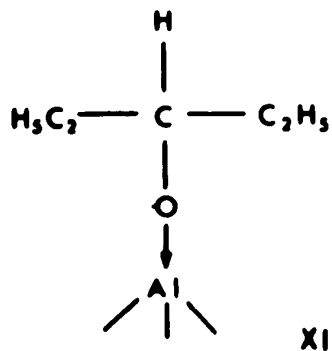
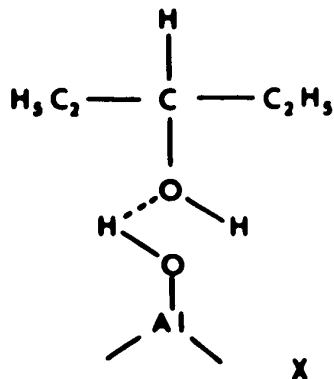
$$\frac{\text{Number of weak Bronsted-acid sites}}{\text{Number of total Lewis-acid sites}} \propto \frac{\text{Fractional conversion of 3-pentanol on 1\% NaOH-doped Al}_2\text{O}_3}{\text{Fractional conversion of 3-pentanol on fully doped Al}_2\text{O}_3} = \frac{78}{15} \approx \frac{5.2}{1}$$

Since these ratios are of the order of magnitude to be expected, the activities per site do indeed appear to be roughly equivalent, and differences in catalyst selectivity appear to be the result of relative site accessibilities. Furthermore, the roughly 1% NaOH content of sample B eliminated the strong Bronsted-acid type of sites (3785 cm^{-1}

hydroxyl band). The relative selectivities can thus be used to estimate the strong Bronsted-acid sites; they number roughly 10% of the total Bronsted-acid sites, $(\frac{5.8-5.2}{5.8}) = 10.3$, the figure reported by Pines and Haag. The saturation level for doping of Bronsted-acid sites corresponded to a NaOH content slightly in excess of 5%. The amount of NaOH used in samples B to E did not correlate with the estimate of numbers of Bronsted-acid sites eliminated by doping and calculated using Beer's Law. This may be due to the non-uniform dispersion of NaOH on alumina surface during the drying process.

5.2.6 Mechanisms of Dehydration and Dehydrogenation of 3-pentanol on γ -Al₂O₃ and NaOH-doped γ -Al₂O₃

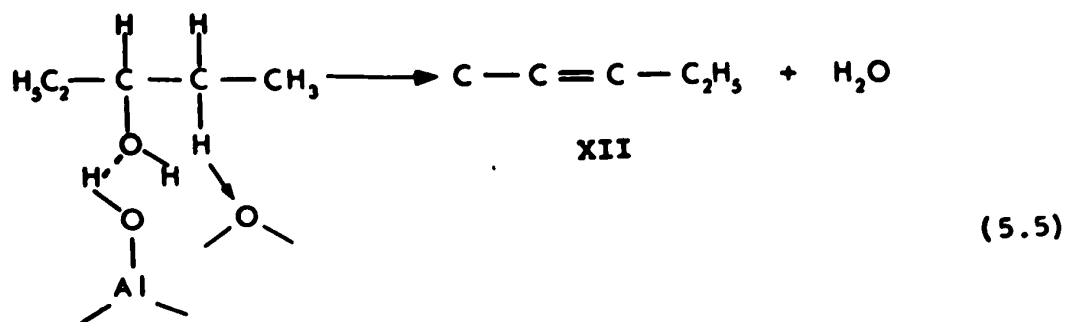
Adsorption of 3-pentanol on pure γ -Al₂O₃ at temperatures up to 150°C resulted in the formation of two types of surface species: (X) 3-pentanol strongly hydrogen-bonded to the surface hydroxyl groups and, (XI), an aluminum pentyl oxide type of structure chemisorbed on Lewis-acid sites. These structures can be represented by the following,



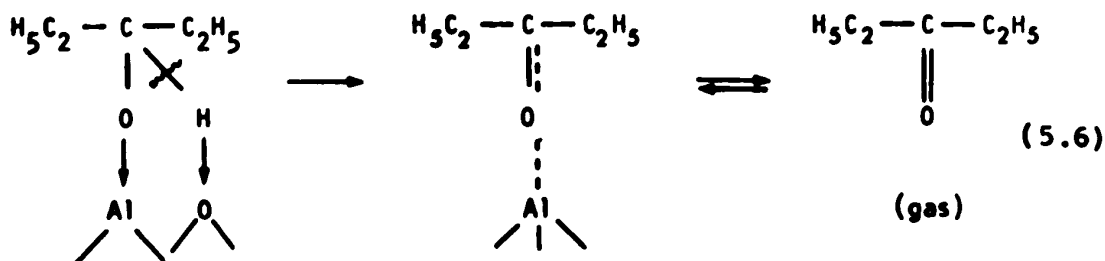
The structure (X) was proposed in Section 5.1 based upon its infrared spectrum. When the NaOH doping level was increased with the resulting elimination of hydroxyl groups, the peak intensity of the 3500 cm^{-1} band decreased, suggesting a reduction in hydrogen-bonding of type (X). These results suggest that the H atom of the hydroxyl group in the alcohol is free and that the alcohol molecules are hydrogen-bonded to the surface hydroxyl group through the oxygen in the alcohol.

The interpretation of structure XI has also been discussed (Section 5.1) in terms of the alkoxide species, characterized by the deep band at 1165 cm^{-1} . Since the intensity of this band and thus the amounts of the surface alkoxide species were found to be identical for all of the catalyst samples investigated, the view is re-enforced that the Lewis-acid sites, which are responsible for the formation of species XI, are not affected by NaOH doping of the alumina. Thus, it is unlikely that the alkoxide species, XI, appears as an intermediate in the dehydration step. The participation of the surface alkoxide species in the dehydration of alcohols was also rejected recently⁽⁵²⁾ on independent grounds. Thus, a hydrogen-bonded alcohol molecule seems to be the most probable adsorption state from which the elimination of water is initiated.

Several different views of the mechanism of the dehydration of alcohols on alumina surfaces exist⁽⁸⁵⁾ but this work supports the previous reaction schemes (Section 5.1) for dehydration and dehydrogenation reaction mechanisms:



XII is a mixture of cis- and trans-2-pentenes



Reaction (5.6), involving dehydrogenation requires that an alkoxide reaction intermediate be formed. The observed hydrogen-bonded species (X) and the alkoxide species, (XI), thus are involved in the dehydration and dehydrogenation mechanisms, respectively. They, in turn, involve Bronsted-acid or Lewis-acid surface sites, respectively, and their activity and selectivity on various NaOH-doped aluminas conform to the preceding discussions.

5.3 Simultaneous Kinetics and Mechanisms

In this study 2-propanol was chosen to be the reactant because it gives only two reaction products, propylene and water, in the dehydration step, and acetone and hydrogen in the dehydrogenation step. According to the results in Section 5.2, pure γ -alumina, or 8% NaOH-doped γ -alumina could be used to catalyze either dehydration alone or dehydrogenation alone, respectively.

5.3.1 Blank Run

To determine the threshold temperature at which the catalytic effects of the reactor surfaces became significant, the temperature of the reactor (without a catalyst wafer) was raised in a stepwise manner over a period of 10 hours; during this time 2-propanol was continuously passed through the reaction system. At a reactor temperature of 400°C and a reactant pressure of 0.9 cm Hg, conditions at which appreciable reaction occurred in the presence of a compressed catalyst wafer, no reaction was detected in the empty reactor by IR and GC analyses. Since the maximum temperature employed in this work was always less than 400°C, the catalytic effects, if any, of the reactor surfaces may be neglected. It is concluded that in the kinetic studies all of the observed reaction occurred on the catalyst surface.

5.3.2 Mass Transfer Considerations

Interpretation of experimental results become difficult when mass transfer resistances are significant in comparison with chemical resistances. Recently, Carberry⁽¹⁰⁷⁾ reported an extensive survey of

the effect of mass transfer upon observed reaction kinetics. Since catalytic activity is usually exhibited as a function of some key experimental variables, the effect of these key variables in each rate-controlling domain is summarized in Table 5.2.

Table 5-2
Behavior of Various Kinetic Parameters
in Each Domain of Control⁽¹⁰⁷⁾

Domain	Activation Energy	Order	Pellet Size*	Fluid Velocity
Chemical reaction	E	n	independent	independent
Pore diffusion - reaction	$\frac{E}{2}$	$\frac{(n+1)}{2}$	$(-r_A) = f\left(\frac{1}{L}\right)$	independent
Bulk mass transfer	≈ 0	first	$(-r_A) = f\left(\frac{1}{L}\right)^{3/2}$	$\approx (\text{velocity})^{1/2}$

*1/L = external surface area-to-volume ratio for the wafer.

Prior to considering the reaction kinetics for the dehydration of 2-propanol, the influence of mass transfer on the rates of reaction must be evaluated. In this regard, two possible contributions to diffusional retardation of the reaction rate exist, namely bulk gas-film diffusion and pore diffusion:

(1) Gas-film Diffusion

To establish the absence of concentration gradients between

the bulk gas phase and the catalyst external surface, it was necessary to determine the relationship between the bulk flow rate of the reactant in the reactor and the conversion to products. In this study, since the rates of reaction of 2-propanol were obtained directly, the experimental determination of the mass transfer effect was greatly simplified. If the rates of reaction were unaffected by film diffusion, an increase in bulk flow rate in the recirculation loop (keeping the reactant feed rate constant) would have no effect on the conversion of the reactant (Table 5-1). Accordingly, the speed of the recirculation pump was varied to change the recycle flow from 13.2 to 21.7 liters per minute and finally to 32.8 liters per minute. The conversion was found to be unaffected by the volumetric flow rate in the recycle loop at the reactant partial pressure of 0.479 cm Hg and a reaction temperature of 261.7°C. Since these values represented the highest reaction temperature and lowest reactant partial pressure employed in this study, the bulk diffusion limitation was assumed to be negligible in all of the experimental runs.

(2) Pore Diffusion

The effects of pore diffusion can be determined by measuring reaction rates for different sizes of catalyst particles under otherwise identical conditions⁽¹¹²⁾. The catalyst effectiveness factor approaches unity (absence of pore diffusion effect), when no increase in reaction rate per unit quantity of catalyst occurs on further subdivision of the catalyst pellet. Accordingly, three different weights

of wafers, and correspondingly, three different catalyst wafer thicknesses were investigated. The results, plotted in Figure 5-10, show that the reaction rates (see equation 4.5) were identical for both catalysts of 0.1325 and 0.3024 gram weight. It was concluded that no mass transfer limitations were present for a catalyst wafer of less than 300 mg weight.

For the series of runs at 252.7°C, if any of the dehydration rates were limited by diffusion of the reactant into the wafer, the diffusional limitation would be expected to be most severe for large values of the Thiele diffusion modulus $\phi_L = \frac{RT}{D(1/L)^2} \cdot \frac{(-r_A)}{p_A}$ and hence for experimental runs at the largest ratio of reaction rate $(-r_A)$ to partial pressure (p_A) ⁽¹⁰⁸⁾. Calculations, based on equations given by Satterfield⁽¹⁰⁸⁾, showed that the effectiveness factor for pore diffusion was close to unity, and thus the intra-particle concentration gradient was negligible, for all the rate data obtained in this study. The detailed calculations are given in Appendix D.

For dehydrogenation reaction, similar results were obtained. It is thus concluded that pore diffusion limitations were negligible for both catalysts (pure γ -alumina and 8% NaOH-doped γ -alumina) when weights were less than 300 mg.

5.3.3 Stability of the Catalyst Activity During the Decomposition of 2-Propanol

Successful kinetic measurements require reproducible catalytic activity during the various experiments. The activity of the 2N NaOH-treated alumina catalyst on both dehydration and dehydrogenation at

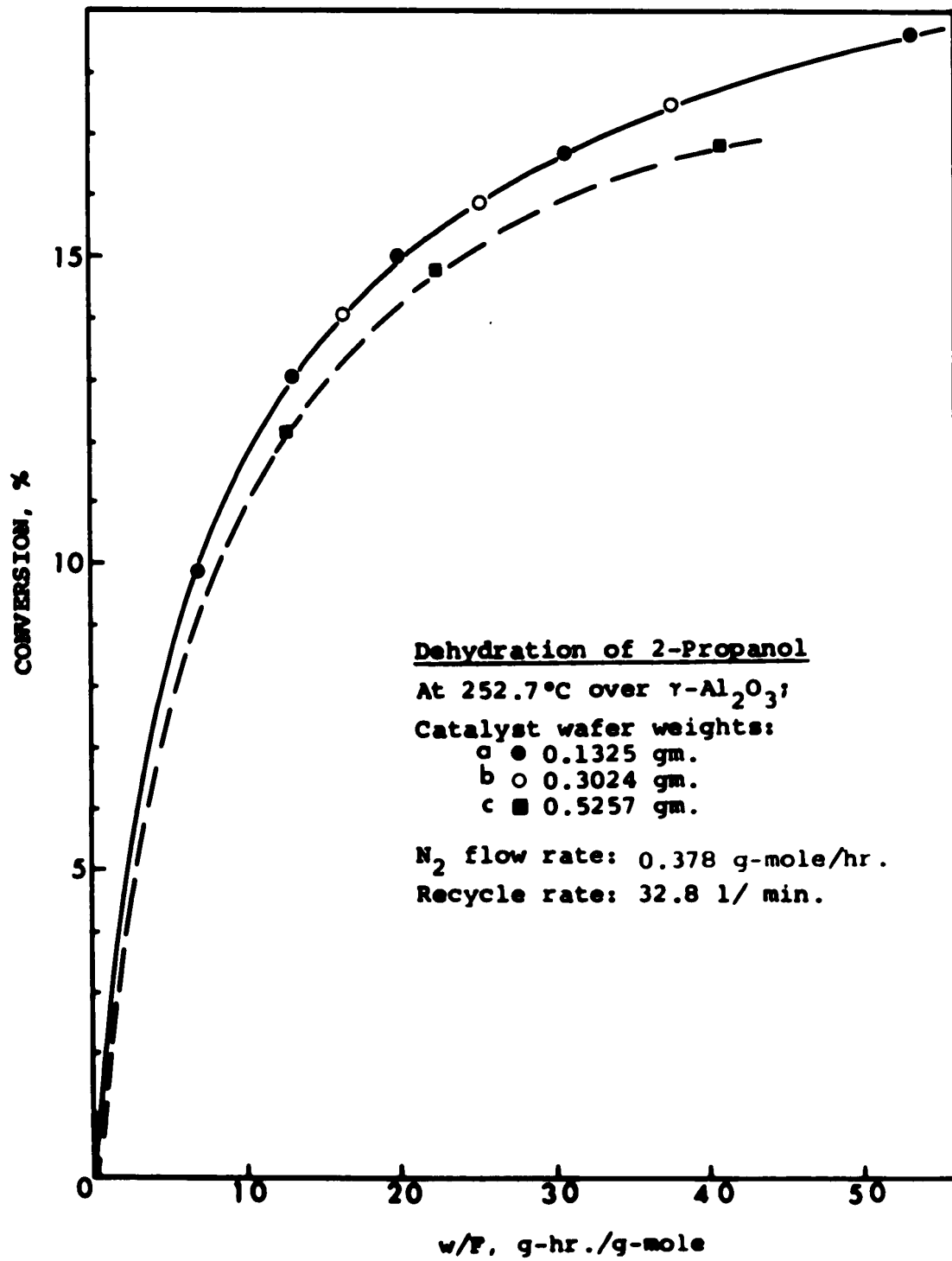
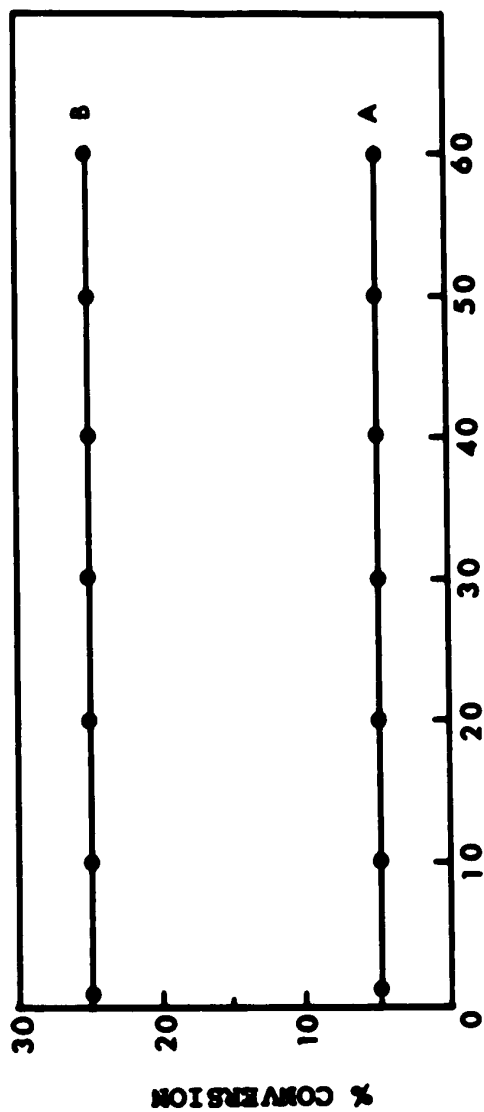


Figure 5-10. Evaluation of Pore Diffusion.

465°C was previously reported⁽¹⁹⁾ to decrease with process time. This was explained by the deposition of elemental carbon on the catalyst surface and deactivation by water absorption in the catalyst. However, in this study the catalyst activity was found to remain constant during 0.5 to 60 hours of use. Since the time of use for any charge of catalyst in the various runs never exceeded 48 hours, the deactivation of the catalyst during the experimental runs was believed to be negligible. For illustration, the dependence of activity, in terms of fractional conversion of 2-propanol, on time for both dehydration and dehydrogenation is shown in Figure 5-11. Surface spectra were also recorded at both one and sixty hours of the reaction time. The spectra of 2-propanol adsorbed on pure γ -alumina show the presence of hydrogen-bonded 2-propanol as well as the carboxylate surface structure. The intensity of the peaks associated with these two species remained identical after 60 hours of reaction time. Hence at reaction temperatures below 400°C it is safe to assume that the catalyst activity will remain unchanged for at least 60 hours. For the case of dehydrogenation on NaOH-doped γ -alumina, the surface spectra show the presence of carboxylate species which again gave identical spectra at one and 60 hours of reaction time.

5.3.4 Consideration of Capillary Condensation

In essence, capillary condensation occurs when the vapor pressure of the reactant and/or products over a liquid-phase concave meniscus in a catalyst pore is lower than that of the bulk liquid-phase. If this difference is sufficient to lower the vapor pressure to the



REACTION TIME, hr.

Figure 5-11. Influence of Time on the Activity of the Catalysts during the Dehydration and Dehydrogenation of 2-Propanol.

(A) Dehydrogenation on alumina,
w/F=2.3; T=252.7°C.

(B) Dehydrogenation on 8% NaOH-doped alumina,
w/F=67.2; T=343.2°C.

total pressure of the system, the small pores will be filled at total pressures lower than the saturation pressure of the bulk liquid. As the pressure increases, larger pores will also be filled. At the vapor pressure of the bulk liquid, of course, the pore volume will be completely filled.

Johnson⁽¹⁰⁹⁾, while studying the dehydration of alcohols at lower temperatures, listed several points of difficulty which should be considered in obtaining kinetic data. He has shown that some of his data were complicated by the influences of both pore diffusion and capillary condensation effects. However, in this study, the lowest temperatures employed for the dehydration and dehydrogenation were 220°C and 283°C, respectively. For dehydrogenation, the reaction temperatures were above the critical temperatures of 2-propanol (235°C) and acetone (235.5°C). For dehydration, the reaction temperatures were near the critical temperature of water (374°C) and above that of 2-propanol. Moreover, infrared spectra of the catalyst surface under reaction conditions show no liquified propanol, acetone and water. The capillary condensation effects on the reaction rates are thus believed to be negligible.

5.3.5 Side Reactions

(1) Dehydration

During the study of catalyst stability (Section 5.3.3), no side reactions were evident from the infrared and gas chromatographic analyses. One side reaction which is thermodynamically possible is the dehydration step to form ether. The absence of this side reaction

is in agreement with the observations of deMourgues et al⁽¹⁶⁾ for the same reaction system.

(2) Dehydrogenation

In the case of dehydrogenation, the dehydration reaction would be the potential side reaction. No evidence was observed for the presence of water and propylene (dehydration products) by both IR and GC analyses. It is thus assumed that only dehydrogenation reaction occurred on the 8% NaOH-doped γ -alumina.

5.3.6 Kinetics and Mechanism of Dehydration of 2-Propanol

Infrared spectra of the adsorbed species were obtained under reaction conditions. In light of the infrared observations, various chemically and mechanistically plausible kinetic models were proposed and the kinetic data were used to establish by statistical discrimination methods which kinetic model was the most satisfactory one. In principle, this would appear to be the usual approach of modern kineticists, however, the mechanistic data largely eliminated the majority of the kinetic models usually considered on a priori basis. The following sections enumerate the details of this approach.

(1) Spectra of Adsorbed Species

Infrared spectra of the species adsorbed on γ -alumina surface under the reaction conditions were recorded for each kinetic run. Figure 5-12 shows the typical spectra of the adsorbed species after eliminating the base-line spectrum due to Al_2O_3 . The close similarity of each set of spectra, as shown in Figure 5-12, suggest that the reaction mechanisms are identical for all runs.

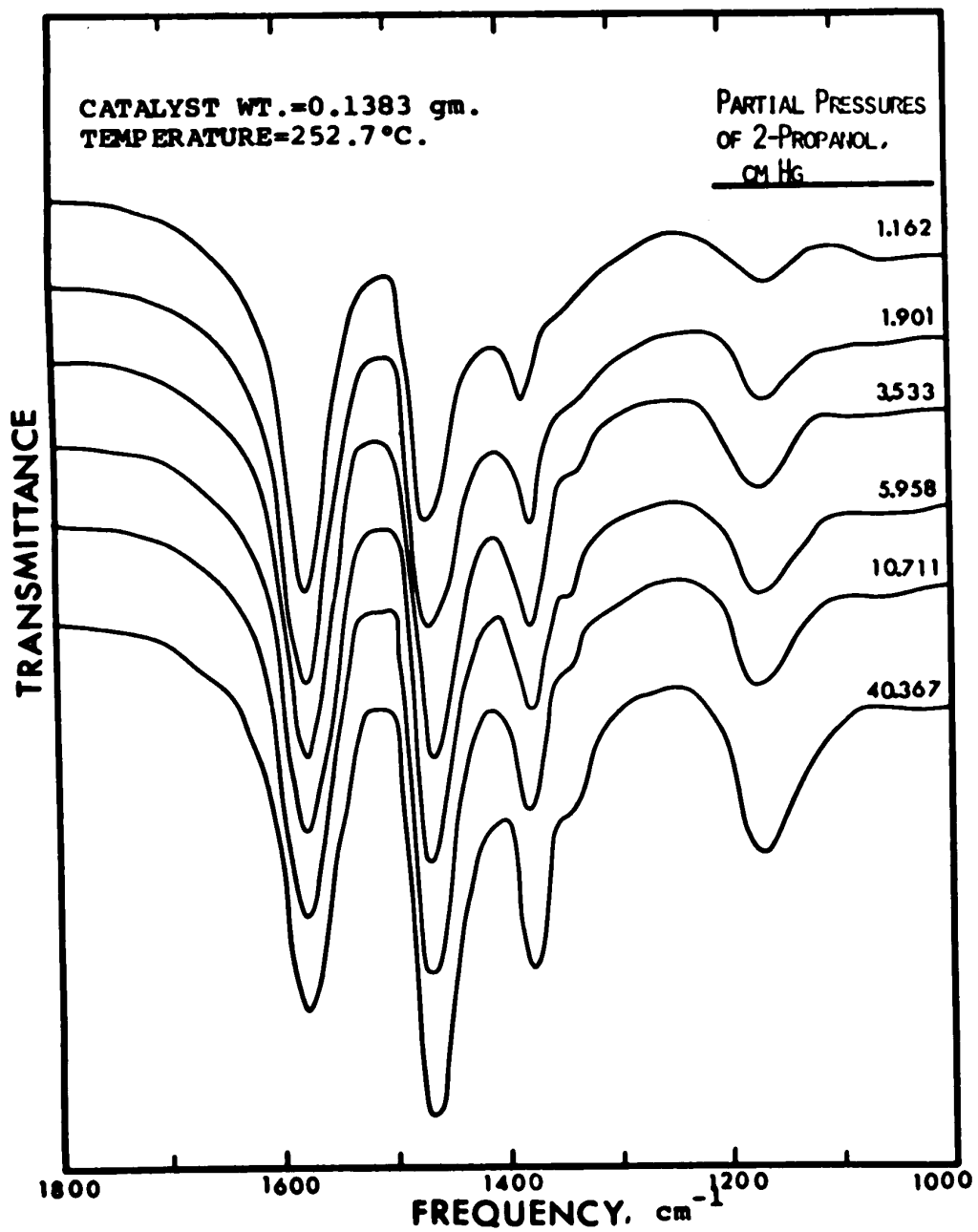


Figure 5-12. IR Spectra of Adsorbed Species on γ -Alumina at Steady-state Reaction Conditions.

In the study of dehydrogenation of ethanol on copper catalyst, Bradshaw and Davidson reported⁽¹¹⁰⁾ that the rate-controlling step of the reaction changes from surface reaction at lower temperatures to adsorption of ethanol at higher temperatures. Thaller and Thodos⁽¹¹¹⁾ obtained the rate data for the catalytic dehydrogenation of 2-butanol to 2-butanone and concluded that the rate-controlling step of the reaction at 600°F shifts between surface reaction-controlling and desorption of hydrogen-controlling steps, depending upon the experimental pressures. In this study, if the reaction mechanism changes as a function of either reactant pressure or the reaction temperature the infrared spectra of the adsorbed species should also change accordingly. However, no evidence for such shift in mechanism was observed for the dehydration of 2-propanol on γ -alumina.

Spectra obtained at the reaction temperature of 252.7°C show the presence of hydrogen-bonded 2-propanol at 1465, 1373 and 1170 cm^{-1} and carboxylate structure at 1575 and 1465 cm^{-1} . At this temperature, the infrared absorption bands due to the hydrogen-bonded 2-propanol increase in intensity with increasing partial pressure of 2-propanol (Figure 5-12). However, the intensity of the bands due to carboxylate species remains constant throughout the period of investigation, i.e. between one and sixty hours of reaction time. This is also an indication that the carboxylate species, although very stable on the alumina surface even at high temperatures, do not poison the catalyst surface. No bands at 1635 cm^{-1} (due to water) and between 3000 and 3200 cm^{-1}

(due to olefins) are observed in the surface spectra. This suggests that under the reaction conditions, water and propylene were not adsorbed on the catalyst surface to any significant degree.

(2) Kinetic Models

For any given reaction system, it is generally assumed that there exists a rate model by which one can describe adequately all of the phenomena actually occurring in the system. In the case of heterogeneous catalysis, it is a common practice to postulate not one, but a number of plausible models which are in agreement with the overall chemistry and, then, to discriminate between these rival models with the aid of experimental data. Thus, the success in rate modeling a given system is vitally affected by the degree of postulation involved in the models to be screened and, of course, is directly affected by the effectiveness of the model discrimination technique. If an adequate model is not included among those models proposed for the system under study, any sophisticated model discrimination method will generate a meaningless correlation. In fact, all statistical discrimination techniques are developed on the basic assumption that one adequate model must be contained among the rival models to be discriminated.

Basically, two model-postulation methods are most commonly employed in the correlation of kinetic rate data for solid-catalyzed gaseous reactions:

- (a) The over-all reaction rate is correlated empirically as a function of the operating conditions (e.g. power-function models).

(b) Rate equations are developed which describe a rational mechanism by which the reactions may occur, and the best-fitting relationship is assumed to describe the reaction mechanism.

The first method has a limited scope of application since it is not safe to extrapolate beyond the range of the experimental data⁽¹¹²⁾. The usefulness of this type of analysis is also reduced by the fact that little insight into the steps occurring during the reaction process is obtained. As a result, this approach will not be considered in the study of dehydration of 2-propanol.

In the second method, the rate data are fitted by a model describing a plausible reaction mechanism. The most widely employed models to describe the mechanism of gaseous reactions on solid surfaces are Hougen-Watson type⁽¹¹³⁾ models. This class of models assumes that the reactants are adsorbed on one type of active site on the catalyst surface where they react, either with themselves, with other adsorbed species on neighboring sites, or with components in the gas phase adjacent to the catalyst surface. Further assumptions in formulating Hougen-Watson rate models include the existence of a single rate-controlling step, such as adsorption, surface reaction, or desorption, within a mechanism involving a series of reaction steps, and the absence of interactions between adsorbed molecules.

Although the assumption of a single rate-controlling step greatly simplifies the derivation of the rate expression, rate equations that involve more than one rate-controlling step should be considered for some reaction systems to obtain a more adequate representation of

the experimental data^(110,114). For example, Bischoff and Froment⁽¹¹⁵⁾ reanalyzed the rate data obtained by Thaller and Thodos⁽¹¹¹⁾ and proposed a rate model of Langmuir-Hinshelwood type in which two consecutive steps, surface reaction and desorption of ketone, are both rate-controlling. Despite the lack of experimental justification to indicate that these two steps are comparatively slow, the proposed model appeared to be adequate.

The assumptions applied in the formulation of Hougen-Watson rate equations⁽¹¹³⁾ can be modified in various ways. An obvious extension of the assumptions is a heterogeneous surface with different types of adsorption sites which produce non-interacting chemisorbed gases. For the reaction system studied by Thaller and Thodos⁽¹¹¹⁾, Kolboe^(116,117) proposed a rate model that involves two chemically different chemisorption sites and showed that the goodness-of-fit of rate data is improved noticeably compared to models based upon a non-interacting, uniform surface.

Although the approach followed in developing rate equations of the Hougen-Watson type is straight forward, the task involved in determining the best rate expression for a complex reaction system is immense. If all possible reaction models are listed within the assumptions of the Hougen-Watson scheme, a relatively large number of models is obtained. For example, 84 models have been postulated⁽¹¹⁸⁾ for methane oxidation and 47 models for ethanol dehydration⁽¹¹⁹⁾. The presently available model discrimination techniques can not be easily applied to a group of rival models, as large as 47 or more,

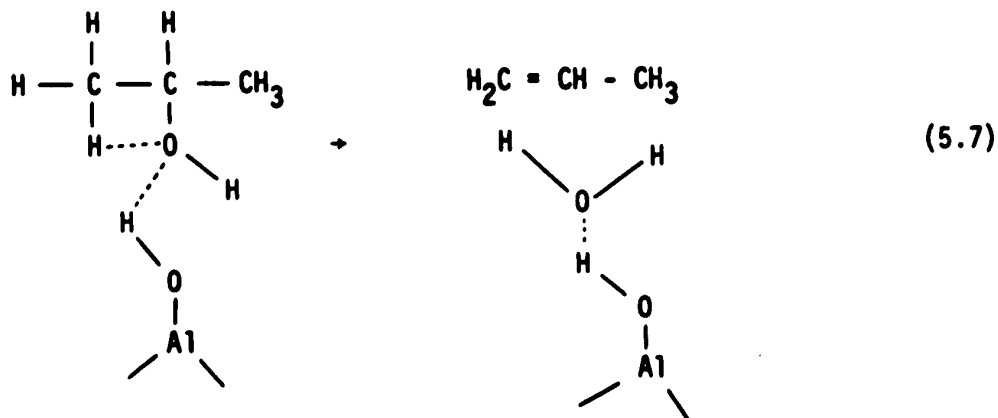
due to the prohibitive amount of computer time that would be required. Consequently, it is desirable if not necessary, to eliminate obviously inadequate models before utilizing the better model discrimination procedures. Not infrequently, the results of the discrimination procedure turn out to be ambiguous in that no one model is shown to be clearly superior. However, a generally effective screening technique is not yet available in the literature.

The infrared spectroscopic technique has provided considerable insight into the identity of chemisorbed species which may act as intermediates in catalytic reactions, and also the nature of the interaction between an active site and an adsorbed molecule. This information, obtained at the molecular rather than the macroscopic level, should serve as a good screening method because the mechanisms proposed according to infrared data would incorporate more detailed knowledge of the mechanism taking place on the catalyst surface.

The infrared study of adsorption of 2-propanol on γ -alumina surface at temperatures varying from room temperature to 300°C, has been discussed in Section 5.1 and a reaction mechanism has been proposed based on the observed adsorbed species at the different temperatures. According to the proposed mechanism, two types of active sites are involved in the reaction sequence, surface hydroxyl groups and surface oxide ions. This is also in good agreement with other evidence from the literature (see Section 2.6). Both single-site and dual-site mechanisms of the Hougen-Watson type rate equation have been proposed

in different studies (see Section 2.7) for the dehydration of alcohols, however, in formulating the dual-site Hougen-Watson model there seems to be no justification for treating the two types of active sites as being identical (reaction 5.1). A dual dissimilar-site mechanism was therefore used in extending the Langmuir-Hinshelwood assumptions. The assumptions are generally valid if the reactant is adsorbed on highly selective sites so that the surface coverage is rather low. The model thus derived may provide an appropriate approximation of the true mechanism. The low surface coverage of 2-propanol under reaction conditions is supported by the infrared spectra of the adsorbed species. The absorbance of the IR band at 1373 cm^{-1} due to adsorbed 2-propanol increased from 0.057 to 0.65 when the temperature of the cell was lowered from 252° to 150°C for a 2-propanol partial pressure of 1.9 cm Hg. The monolayer coverage would be expected to give an absorbance for the band at 1373 cm^{-1} much higher than 0.65. Since the maximum absorbance observed in this study was 0.33 at 1373 cm^{-1} , the surface coverage for all the kinetic runs was believed to be quite low.

The plausibility of involving only surface hydroxyl groups as active sites is also proposed according to the following representation of chemical steps,



The generalized mechanisms for single-site and dual dissimilar-sites mechanisms are given below:

(a) Single-site mechanism



where A, P, W and ℓ_1 represent 2-propanol, propylene, water and surface hydroxyl groups, respectively, and propylene is assumed not to be adsorbed. The latter assumption is based upon the failure to detect adsorbed propylene even at room temperature by the infrared technique. Equations (5.8) to (5.10) imply a reversible reaction mechanism but a feed consisting of a mixture of propylene and water

does not yield any detectable alcohol. Consequently, one of the above three steps of the single-site mechanism must be irreversible. Since adsorption and desorption of gaseous reactants or products are inherently reversible steps, the surface reaction (step (5.9)) is therefore the most likely step to be irreversible. The irreversible form of step (5.9) of the generalized single-site mechanism becomes,



The rate expressions derived for the single-site mechanism are listed in Table 5-3 for all of the possible combinations of the rate-controlling steps.

It can be seen from Table 5-3 that the assumption of a single rate-controlling step, as proposed by Hougen and Watson, is not necessary for this dehydration reaction if one of the reaction step is irreversible. This may be the reason why Hougen-Watson models generally express the experimental data well, even if the reaction may involve more than one step rate-controlling.

(b) Dual dissimilar-sites mechanism

From the representation of the chemical reaction steps, reaction (5.1), the generalized mechanism can be written in the form,

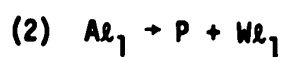
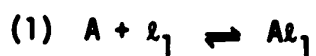


Table 5-3

Possible Kinetic Models for Dehydration of 2-Propanol, $A \rightarrow P + W$

A = 2-Propanol; P = Propylene; W = Water

(a) Single-site mechanism



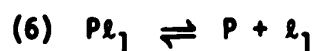
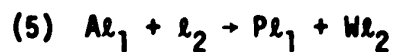
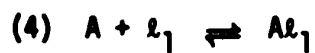
Controlling Step(s)	Rate Expression ($-r_A$)	Assigned Model No.
(1)	$\frac{b_1 P_A}{(1+b_2 P_W)}$	M1
(2)	$\frac{b_1 P_A}{(1+b_2 P_A+b_3 P_W)}$	M2
(3)	Same form* as M2	
(1) & (2)	Same form as M2	
(2) & (3)	Same form as M2	
(1) & (2) & (3)	Same form as M2	

*"Same form" implies different constant terms but an identical functional form

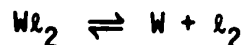
...continued

Table 5-3 (continued)

(b) Dual dissimilar-sites mechanism



Controlling Step(s)	Rate Expression ($-r_A$)	Assigned Model No.
(4)	Same form as M1	
(5)	$\frac{b_1 P_A}{(1+b_2 P_A)(1+b_3 P_W)}$	M3
(6)	$\frac{b_1 P_A}{(1+b_2 P_A)(1+b_3 P_W)+b_4 P_W}$	M4
(7)	Same form as M4	
(4) & (5)	$\frac{b_1 P_A}{(1+b_2 P_A)(1+b_3 P_W)+b_4 P_A}$	M5
(5) & (6)	Same form as M4	
(5) & (7)	Same form as M4	



where ℓ_1 's represent surface-active sites with ℓ_1 = surface hydroxyl group, ℓ_2 = surface oxide. The step (5.13) is again assumed to be irreversible as per the arguments employed for the single-site mechanism. The desorption constant of propylene for step (5.14) is assumed to be very large since no detectable amount of propylene was adsorbed on the catalyst surface and, also, introducing propylene into the feed had no effect on the observed reaction rate. The possible rate expressions for this mechanism are also given in Table 5-3. The combination of three or more rate-controlling steps is rejected for the following reasons:

- (a) The rate expressions become exceptionally complex and the available model discrimination methods cannot be employed effectively;
- (b) Water and propylene were not observed in the surface spectra under reaction conditions and thus desorption of water or propylene is unlikely to be the rate-controlling step.

The derivation of rate equations for the single-site mechanism is similar to that given by Hougen and Watson⁽¹¹³⁾. In the case of the dual dissimilar-sites mechanism, a sample derivation of the rate equation, assuming step (5.13) to be rate-controlling, is given in Appendix E.

(3) Model Discrimination

The literature available on model discrimination procedures is extensive. Bard and Lapidus⁽⁹⁵⁾ give an excellent review of the methods available at the present time. In this study, a Bayesian approach suggested by Quon and developed by Singh⁽⁹⁸⁾ at the University of Alberta has been adopted to discriminate among the proposed rival kinetic models.

A set of ten dehydration experiments was conducted in order to obtain the best model from the proposed five rate equations, M1 to M5. The kinetic data are presented in Table 5-4. From the IR calibration curves (Tables 4-2 and 4-4), it was found that the measurements of the propylene partial pressure were less accurate than those of 2-propanol. Since no side reactions were detected, the partial pressures of water and propylene in the reactor were computed from the difference of the partial pressures of 2-propanol in the feed and in the exit stream. This resulted in a substantially better fit than if the partial pressures of water were obtained from the propylene calibration.

It was assumed, initially, that each of the five models was equally likely. A 20% prior probability was thus assigned to each model. The following criteria were used for model rejection:

- (a) lack of fit of the model to the data, as indicated, by an extremely small posterior probability of the examined model, and
- (b) unacceptable characteristics of the estimated parameters.

Table 5-4
Experimental Data for Dehydration Reaction

Catalyst weight = 0.1383 gm

Feed composition = 2 propanol with N₂ at .378 g-mole/hr

Reactor temperature = 252.7°C

Run No.	Reaction Rate $\frac{\text{g-mole}}{\text{hr-g-catalyst}}$	P _{AO} cm Hg	P _A cm Hg	P _W =P _P cm Hg	Material* balance, %
1	0.03947	1.044	0.479	0.570	100.5
2	0.06355	1.677	0.812	0.859	99.6
3	0.08569	2.311	1.162	1.158	100.4
4	0.12663	3.578	1.907	1.759	102.5
5	0.16365	4.845	2.700	2.193	101.0
6	0.19739	6.113	3.533	2.491	98.5
7	0.27938	9.597	5.958	3.510	98.7
8	0.40000	15.934	10.771	5.131	99.8
9	0.8851	60.110	52.016	11.434	95.0
10	1.0105	51.090	40.367	10.416	100.5
11**	0.2901		47.951	40.124	

*Material balance = $(P_A + P_W)/P_{AO} \times 100$

**with 45% of H₂O in the feed

In case (b), for instance, estimates of adsorption/desorption constants are generally required to be positive and to possess negative temperature coefficients. If several models have acceptable parameter estimates, the model with the highest posterior probability, say larger than 0.95, was selected.

Incorporating all of the ten data points in Table 5-4 by the Bayesian expected likelihood method, the following posterior probabilities were obtained for the five different models:

$$P_{2,10} = 0.476 ; P_{3,10} = 0.524 ; P_{1,10} = P_{4,10} = P_{5,10} = 0$$

where the first subscript refers to the model number assigned in Table 5-3 and the second subscript to the number of data points incorporated. Thus, model M3 is regarded to be the most likely candidate but by no means conclusively; actually, both M2 and M3 can be considered equally favored by the ten data points employed. The need for further experiments in order to obtain a better discrimination between M2 and M3 is apparent.

It was decided to design the future experiments on a rational basis. The criterion of Singh⁽⁹⁸⁾ as given in Section 2.10.2 was employed and the region yielding the maximum value for the expected change in entropy was chosen in obtaining additional data points. Table 5-5 gives some of the results of this exploration by assuming the variance of experimental measurements to be 0.001. The maximum entropy change occurs in the region of $p_A = 50$ cm Hg and $p_W = 30$ to 50 cm Hg. Since

Table 5-5
Expected Entropy Change at Various Partial Pressures
of 2-Propanol (A) and Water (W) for Dehydration Reaction

P_A , cm Hg	P_W , cr. Hg	Expected Entropy Change - R
10	5	5.8×10^{-6}
20	5	0.264
30	5	0.43
40	5	0.40
50	5	0.37
10	20	0.094
20	20	0.154
30	20	0.209
40	20	0.285
50	20	0.396
10	30	0.09
20	30	0.18
30	30	0.26
40	30	0.35
50	30	0.46
10	40	0.08
20	40	0.18
30	40	0.27
40	40	0.37
50	40	0.476
50	50	0.476

the partial pressure of water with a feed of $P_A = 50$ units would be expected to be somewhere between 10 and 15 cm Hg, it was decided to inject additional water into the feed. Data point 11 in Table 5.4 was thus obtained at $P_A = 47.951$, $P_W = 40.124$ and $(-r_A) = 0.2901$, at a temperature of 252.7°C , with 45% water in the feed. The results obtained after including this additional data point strongly favored the dual dissimilar-site mechanism, M3. The results are given below:

(a) Single-site mechanism, M2

Parameters	$b_1 = 0.124$	$b_2 = 0.0234$	$b_3 = 0.4292$
95% limits	± 0.025	± 0.0130	± 0.1360
Variance (σ^2)	$= 2.59 \times 10^{-4}$		
Model likelihood	$\propto 1.42 \times 10^{13}$		

(b) Dual dissimilar-site mechanism, M3

Parameters	$b_1 = 0.09544$	$b_2 = 0.007856$	$b_3 = 0.25747$
95% limits	± 0.00800	± 0.0020	± 0.04830
Variance (σ^2)	$= 4.126 \times 10^{-5}$		
Model likelihood	$\propto 3.436 \times 10^{17}$		

Variance - covariance matrix:

1.595×10^{-5}	-2.858×10^{-6}	9.13×10^{-5}
-2.86×10^{-6}	9.81×10^{-7}	-2.15×10^{-5}
9.13×10^{-5}	-2.15×10^{-5}	5.83×10^{-4}

The posterior probabilities for M2 and M3 are respectively equal to 0.00004

and 0.99996. Since the posterior probability of M2 was extremely low, the single-site model was rejected. The rest of the models were also examined with this additional data point. The results showed that the posterior probability of each model is much less than 0.001% and therefore, they were also rejected.

From Table 5-3, it can be seen that M2 also represents the combined steps, surface reaction and desorption of water, to be rate-controlling. However, it was found that water was not present on the catalyst surface at any detectable level under the reaction conditions. Thus, it is clearly shown that the dehydration of 2-propanol proceeds via a dual dissimilar-site mechanism in which the surface reaction is the rate-controlling step.

It is interesting to make a comparison between the conventional dual similar-site Hougen-Watson model and the dual dissimilar-site rate equation developed in this thesis. The results are given as follows:

(a) Dual-site Hougen-Watson model, surface reaction-controlling

$$-r_A = \frac{b_1 P_A}{(1+b_2 P_A + b_3 P_W)^2} \quad \sigma^2 = 1.387 \times 10^{-4}$$

Posterior probability < 0.0001%

(b) Dual dissimilar-site mechanism, surface reaction-controlling

$$-r_A = \frac{b_1 P_A}{(1+b_2 P_A)(1+b_3 P_W)} \quad \sigma^2 = 4.126 \times 10^{-5}$$

Posterior probability > 99%

Thus, it may be concluded that assuming a dual-site mechanism without a priori knowledge about the nature of active sites could lead to poor formulation of kinetic models.

5.3.7 Activation Energy for the Dehydration of 2-Propanol

The kinetic data obtained at different reaction temperatures, Runs 12 to 18, are presented in Table 5-6. After having finalized the reaction mechanism for the dehydration of 2-propanol from isothermal rate data at 252.7°C, an estimation of the activation energy was attempted by applying the same reaction mechanism to other temperatures. This assumption was based upon the observation that infrared spectra of the adsorbed species exhibited the same spectral band characteristics as those obtained for the 252.7°C runs. Therefore, the mechanism was believed to be applicable in the range of temperatures, 120°C to 171°C, studied. By the usual Arrhenius rate expression, the following kinetic equation can then be used⁽¹¹²⁾ for the temperature range studied:

$$(-r_A) = \frac{b_{1,0} \exp(-E_1/RT) P_A}{[1+b_{2,0} \exp(-\frac{H_A}{RT})P_A][1+b_{3,0} \exp(-\frac{H_W}{RT})P_W]} \quad (5.16)$$

The statistical analysis can not be expected to give a good estimation for the six parameters in equation (5.16) without a very large number of data points over a wide range of reaction temperatures. Since it was found that the dehydration reaction was extremely slow at temperatures below 110°C and that the side-reactions were significant at temperatures above 350°C⁽⁹⁴⁾, kinetic runs could be performed

Table 5-6
Kinetic Data over Range of Temperatures,
for Dehydration of 2-Propanol

Catalyst weight = 0.1489 g

Feed rate = 0.02386 g-mole of 2-propanol per hour*

Run No.	Reactor temp. °K	Reaction Rate ($\times 10^3$) ($\frac{\text{g-mole}}{\text{hr-g-catalyst}}$)	P_A , cm Hg	P_W , cm Hg
12	393	1.904	2.286	0.025
13	409	3.917	2.256	0.055
14	413	5.091	2.240	0.071
15	418	5.830	2.230	0.081
16	427	8.271	2.196	0.115
17	439	13.091	2.129	0.182
18	444	15.204	2.100	0.211

*With N_2 flow rate = 0.378 g-mole/hr

only in the range of 110°C - 300°C. This resulted in a restriction for obtaining a large number of data points for parameter estimation. It was decided to keep P_A and P_W deliberately low to ensure the denominator terms, $b_2 P_A$ and $b_3 P_W$, in model M3 were small compared to unity. Therefore, $(1+b_2 P_A)$ and $(1+b_3 P_W)$ in model M3 would be expected to be much less sensitive to temperature than the specific rate constant, b_1 . The low values of P_A and P_W will also give a uniform temperature over the catalyst surface. As an approximation, b_2 and b_3 were treated as constants, $b_2 = 0.007856$ and $b_3 = 0.25747$. Equation (5.16) is now rewritten as equation (5.17) by assuming that the Arrhenius form of temperature-dependency for the rate constant was applicable to this reaction system,

$$-r_A = \frac{b_{1,0} \exp\left(-\frac{E_1}{RT}\right) P_A}{(1+b_2 P_A)(1+b_3 P_W)} \quad (5.17)$$

The parameters, $b_{1,0}$, the so-called frequency factor and E_1 , the apparent activation energy, were estimated by the same methods used in the previous section. The results with 95% confidence limits are

$$b_{1,0} = (1.276 \pm 0.001) \times 10^5 ; \quad E_1 = (1.46 \pm 0.05) \times 10^4 \frac{\text{cal}}{\text{g-mole}} .$$

For illustration, the log of the specific reaction rate constant ($\log_{10} b_1$) is plotted against the reciprocal of the absolute temperature ($1/T$) as shown in Figure 5-13⁽¹¹²⁾ and a fairly linear plot is obtained. From this plot, the apparent activation energy is calculated to be

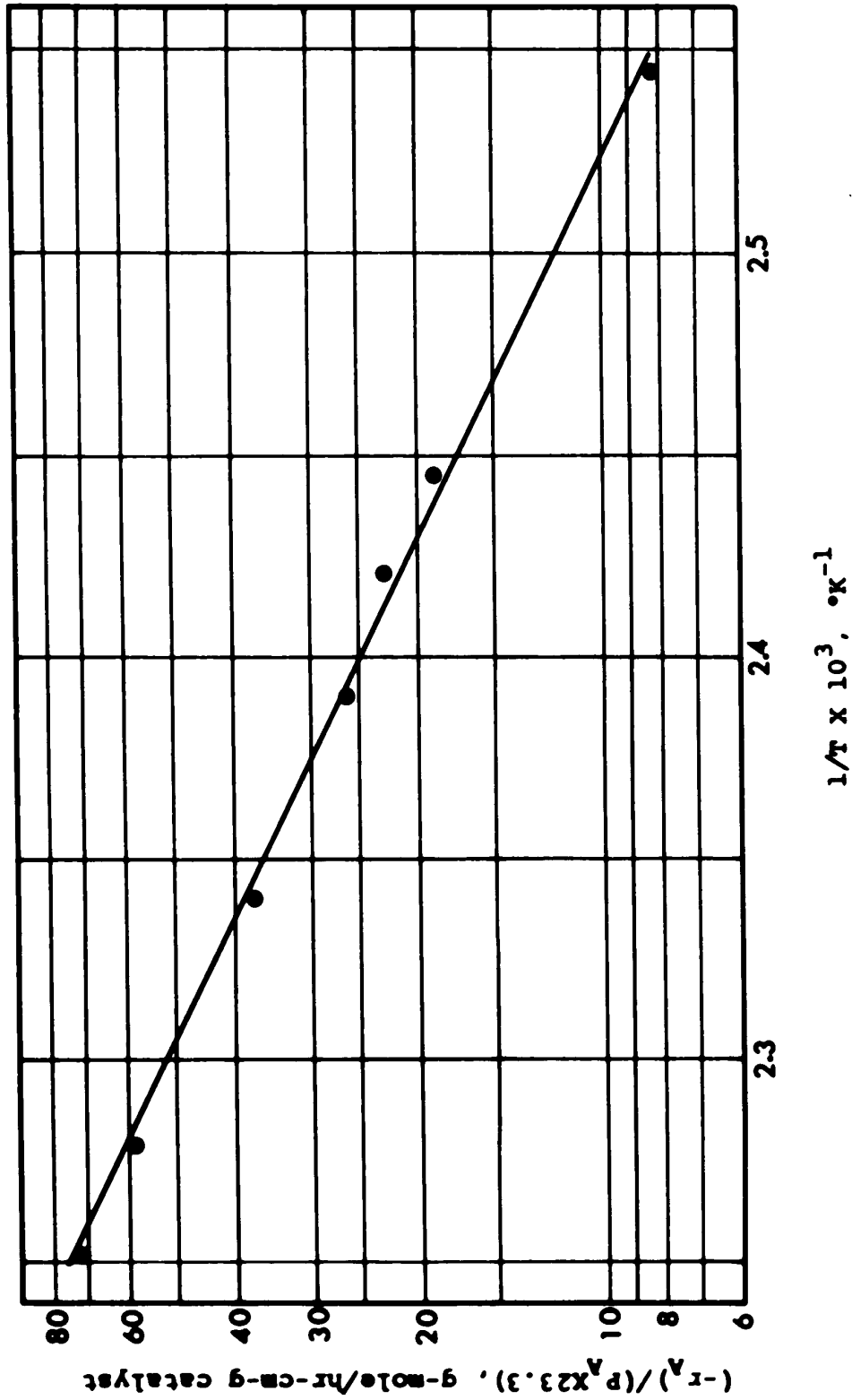


Figure 5-13. Temperature Dependency of the Rate of Dehydration of 2-Propanol.

15 K cal/g-mole which is very close to the value of 14.6 obtained by Singh's parameter estimation method⁽⁹⁸⁾.

It can be seen from the derivation of model M3 in Appendix E that $b_1 = L_1 L_2 K_A k_3$ or, in terms of Arrhenius relationship over a range of temperature, $b_1 = L_1 L_2 K_{A,0} k_{3,0} \exp[-(H_A + E_T)/RT]$. Therefore the true activation energy, E_T , for the dehydration should be the sum of apparent activation energy, E_1 , and the enthalpy change for adsorption of A, $-H_A$. Since $-H_A$ is approximately equal to 10 K cal/g-mole⁽¹⁶⁾, E_T is thus estimated to be $14.6 + 10 = 24.6$ which is in good agreement with the value of 25 reported in the literature⁽¹⁶⁾.

5.3.8 Kinetics and Mechanism of the Dehydrogenation of 2-Propanol

Suitable kinetic and mechanistic studies with which to compare quantitatively the rate expression for the dehydrogenation of 2-propanol on 8% NaOH-doped γ -alumina do not exist. Nevertheless, the methods for treating the kinetic data are similar to those discussed in the case of dehydration.

(1) Spectra of Adsorbed Species

Infrared spectra of the adsorbed species on 8% sodium hydroxide-treated γ -alumina under steady-state reaction conditions are shown in Figure 5-14. The alkoxide structure and carboxylate species were again observed on the catalyst surface. The infrared bands at 1560, 1445, 1360 and 1155 cm^{-1} were attributed to the carboxylate species and the bands at 1545, 1360, 1155 and 1125 cm^{-1} were attributed to the alkoxide species, as was found in the room temperature spectra obtained in the adsorption study (Section 5.1). Since the IR band at 1705 cm^{-1} ,

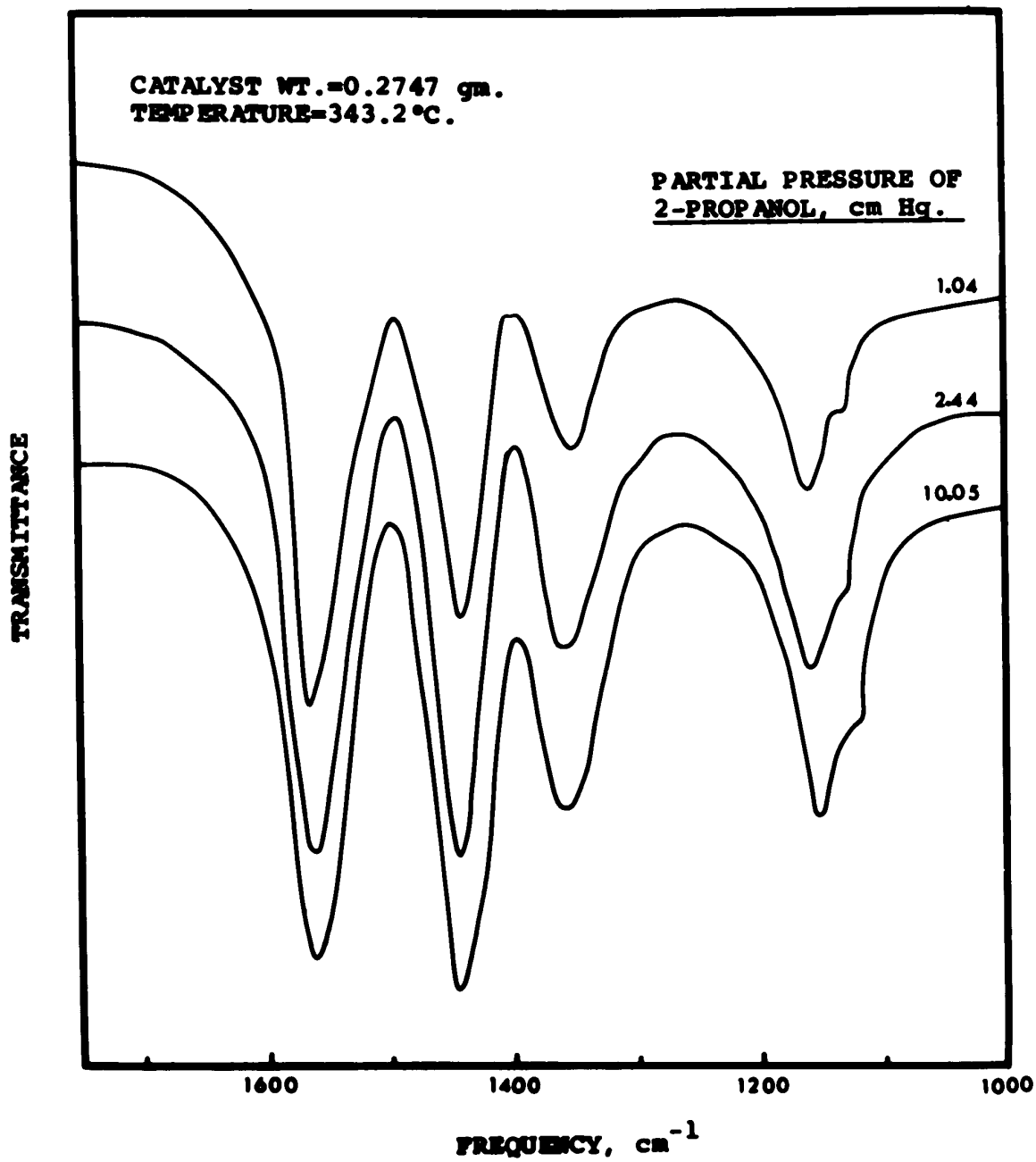
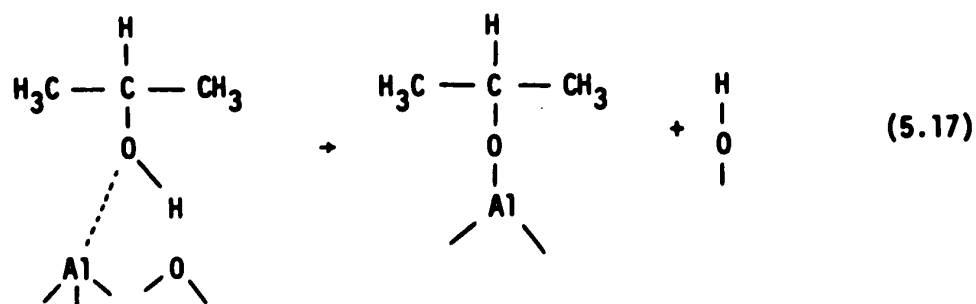


Figure 5-14. IR Spectra of Adsorbed Species on 8% NaOH-doped γ -Alumina at Steady-state Conditions.

which corresponds to the stretching vibration of C = O, was not observed in the surface spectra, it was concluded that acetone, one of the dehydrogenation products, was not adsorbed on the catalyst under the reaction conditions. Hydrogen, in the form of H which splits off from 2-propanol was proposed⁽⁴⁵⁾ to be adsorbed on the surface oxide ion to form a surface OH group. The parent alcohol thus formed an adsorbed alkoxide. The reaction can be represented as follows:



The presence of the newly formed OH groups due to the reaction (5.17) may be evident from the increase in peak intensity of the surface spectra in the region of 3600 to 3800 cm^{-1} which are attributed to OH stretching vibrations⁽³⁴⁾. However, a strong, broad hydrogen-bonding peak centered at 3550 cm^{-1} developed when alkoxide and carboxylate species were present on the catalyst surface; thus, the change in peak intensity in the OH stretching region cannot be effectively measured.

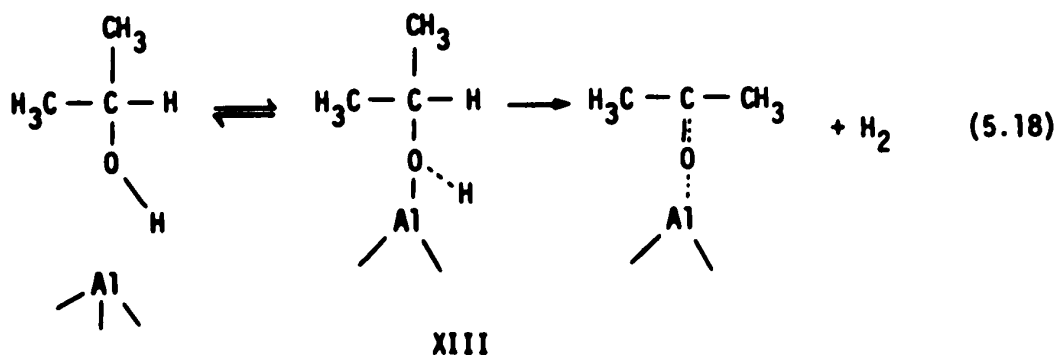
Again, as in the case of dehydration, the spectra of the alkoxide species showed an increase in intensity, with increasing partial pressure of 2-propanol although to a lesser extent than the

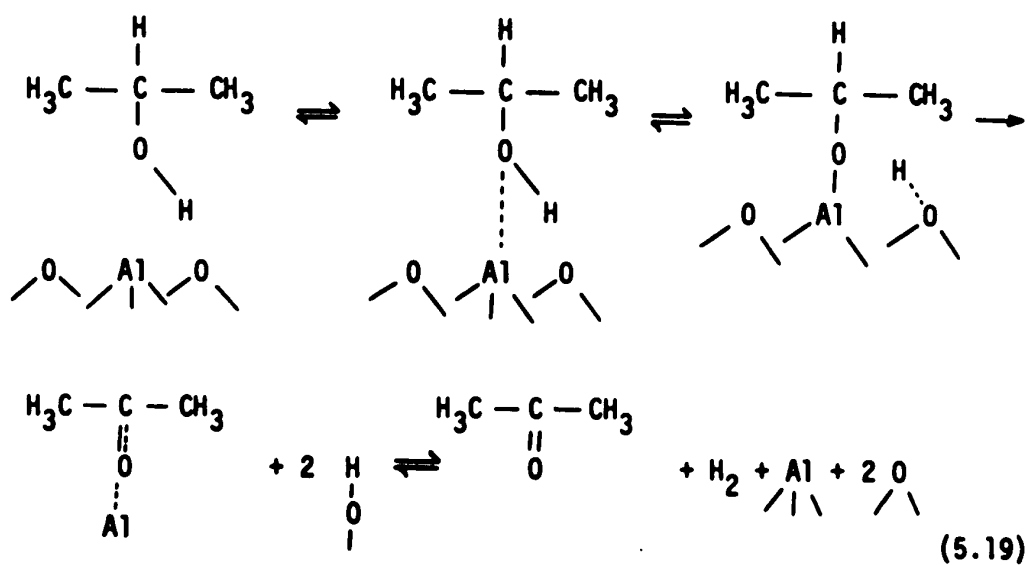
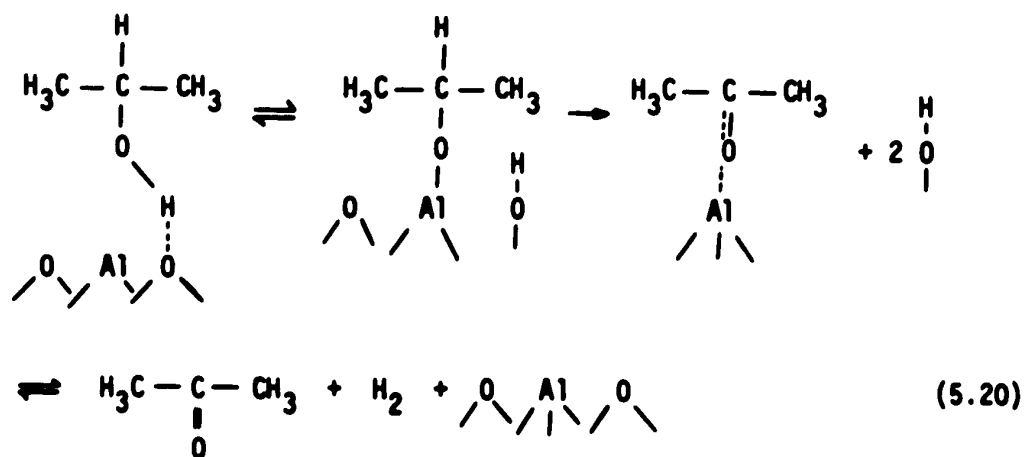
intensity increase of the hydrogen-bonded alcohol in the case of dehydration. The bands at 1560, 1445, 1360 and 1155 cm^{-1} are attributed to the surface carboxylate species, and are observed to remain unchanged for reaction times of one to sixty hours. These results suggest that the carboxylate species had very little effect, if any, on the catalyst activity. Since the alkoxide structure, and the carboxylate species, were the only components observed on the catalyst surface for all of the kinetic runs, it was believed that the reaction mechanism remained unchanged for those runs. The mechanism proposed for the dehydrogenation from the adsorption study (Section 5.1) seems applicable to the high temperature kinetic runs.

(2) Kinetic Models

From the study of infrared spectra of the adsorbed species, the possible reaction mechanisms for the dehydrogenation reaction can be represented as follows:

Scheme A, Single-site mechanism



Scheme B, Dual dissimilar-sites mechanism**Scheme C, Alternate dual dissimilar-sites mechanism**

Scheme D, Dual dissimilar-sites mechanism, reduced from Scheme B, by assuming 2-propanol to be dissociatively adsorbed simultaneously on the oxide and the aluminum ion.

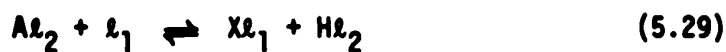
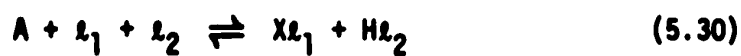


where A, K and ℓ_1 represent alcohol, ketone and surface aluminum ion, respectively.

The participation of surface aluminum and oxide ions in the dual-site mechanism resulted in several possible reaction mechanisms and this has been already discussed partly in Section 5.1. Schemes B to D show these possibilities. In order to develop rate equations for all possible combinations of rate-controlling step(s) for each mechanism, it is more convenient to rewrite these mechanisms in the generalized form with the additional notations, ℓ_2 = surface oxide ions, and $X\ell_1$ = surface alkoxy species.

Scheme B



Scheme CScheme D

Since acetone was found not to adsorb on the surface under reaction conditions and since the addition of acetone to the liquid

feed stream does not inhibit the reaction rate, it is assumed that the desorption constant for step (5.24) is very large. Using this assumption, the possible rate expressions derived for the dehydrogenation in a similar way to those of dehydration are summarized in Table 5-7. A sample derivation is given in Appendix E. It should be noted that in the case of Scheme C, the derived rate expressions are highly nonlinear and complex, except when the surface reaction (step 5.26) alone is assumed to be the rate-controlling step. A sample derivation, showing the complexity of this kind of rate equation, is again given in Appendix E. It is thus expected to be very difficult to perform a reasonable parameter estimation and model discrimination with existing statistical methods. However, the surface spectrum of 2-propanol on 8% NaOH-doped γ -alumina shows the presence of alkoxide species but not of hydrogen-bonded 2-propanol. This is supported by the spectra of adsorption of 2-propanol at room temperature and then evacuation at the same temperature. In both cases the IR spectra showed the same characteristic bands. Since hydrogen-bonded alcohol, but not the alkoxide-species, was found to be removed upon evacuation at room temperature, these results suggest that only the alkoxide species, not the hydrogen-bonded 2-propanol, was formed as a reaction intermediate on this catalyst. This is also in agreement with the results of Knozinger⁽⁸⁵⁾ who showed that decomposition of hydrogen-bonded alcohol leads only to the formation of olefin. Therefore no attempt was made to analyze the rate equations for the Scheme C mechanism which involved hydrogen-bonded alcohol as one of the reaction intermediates.

Table 5-7

Possible Kinetic Models for Dehydrogenation of 2-Propanol, $A \rightarrow K + H_2$

A = 2-Propanol ; K = Acetone ; H_2 = Hydrogen

Mechanism	Controlling Step(s)	Rate Expression, $(-r_A)$	Assigned Model No.
(a) Scheme A			
(1) $A + L_1 \rightleftharpoons AL_1$	(1)	$b_1 P_A$	N1
(2) $AL_1 \rightarrow K L_1 + H_2$	(2)	$\frac{b_1 P_A}{1 + b_2 P_A}$	N2
(3) $K L_1 \rightleftharpoons K + L_1$	(3)	Same as N2	
	(1) + (2)	Same as N2	
	(2) + (3)	Same as N2	
	(1) + (2) + (3)	Same as N2	
(b) Scheme B			
(1) $A + L_1 \rightleftharpoons AL_1$	(1)	$\frac{b_1 (P_A / \sqrt{P_{H_2}})}{(1 + b_2 P_A + b_3 \sqrt{P_{H_2}} + b_4 \sqrt{P_{H_2}})}$	N3

Table 5-7 (continued)

Mechanism	Controlling Step(s)	Rate Expression, $(-r_A)$	Assigned Model No.
(b) Scheme B - continued			
(4) $A_{L_1} + L_2 \rightleftharpoons X_{L_1} + H_{L_2}$	(4)	$\frac{b_1 P_A}{(1+b_2/P_{H_2})(1+b_3 P_A)+b_4 P_A}$	N4
(5) $X_{L_1} + L_2 \rightarrow K_{L_1} + H_{L_2}$	(5)	$\frac{b_1 (P_A/\sqrt{PH_2})}{(1+b_2/P_{H_2})(1+b_3 P_A+b_4 \frac{P_A}{\sqrt{PH_2}})}$	N5
(6) $2H_{L_2} \rightleftharpoons H_2 + 2L_2$	(6)	Cannot develop a reasonable form of equation*	
(3) $K_{L_1} \rightleftharpoons K + L_1$	(3)	Same as N5	
	(1) + (5)	Same as N3	
	(4) + (5)	Same as N4	
	(5) + (6)	Cannot develop a reasonable form of equation*	
	(5) + (7)	Same as N5	

Table 5-7 (continued)

Mechanism	Controlling Step(s)	Rate Expression, $(-r_A)$	Assigned Model No.
(c) <u>Scheme C</u>			
(7) $A + L_2 \rightleftharpoons AL_2$	(7)	Cannot develop a reasonable form of equation*	
(8) $AL_2 + L_1 \rightleftharpoons XL_1 + HL_2$	(8)	Cannot develop a reasonable form of equation*	
(5) $XL_1 + L_2 \rightarrow KL_1 + HL_2$	(5)	$\frac{b_1 P_A / P_{H_2}}{P \frac{A}{\sqrt{P_{H_2}}} (1 + b_3 P_A + b_4 \sqrt{P_{H_2}})}$	N6
(6) $2HL_2 \rightleftharpoons H_2 + 2L_2$	(6)	Cannot develop a reasonable form of equation*	
(3) $KL_1 \rightleftharpoons K + L_1$	(3)	Cannot develop a reasonable form of equation*	
(d) <u>Scheme D</u>			
(9) $A + L_1 + L_2 \rightleftharpoons XL_1 + HL_2$	(9)	$\frac{b_1}{(1 + b_2 \sqrt{P_{H_2}})^2}$	N7

Table 5-7 (continued)

Mechanism	Controlling Step(s)	Rate Expression, $(-r_A)$	Assigned Model No.
(d) Scheme D - continued			
(5) $X_{L_1} + L_2 \rightarrow K_{L_1} + H_{L_2}$	(5)	$\frac{b_1 P_A / P_{H_2}}{(1 + b_2 \sqrt{P_{H_2}})(1 + b_3 \sqrt{P_{H_2}})}$	N8
(6) $2H_{L_2} \rightleftharpoons H_2 + 2L_2$	(6)	Cannot develop a reasonable form of equation*	
(3) $K_{L_1} \rightleftharpoons K + L_1$	(3)	Same as N3	
	(9) + (5)	$\frac{b_1 P_A}{(1 + b_2 \sqrt{P_{H_2}})(1 + b_3 \sqrt{P_{H_2}} + b_4 P_A)}$	N9
	(5) + (6)	Cannot develop a reasonable form of equation*	
	(5) + (3)	Same as N3	

*See Appendix E.2 and E.3 for the explanation

In the case of Schemes B and D, the rate expressions obtained are also very complex whenever the combination of two hydrogen atoms (step (5.27)) is assumed to be involved in the rate-controlling step. (See Appendix E for a sample derivation). Since some earlier studies^(72,120) have indicated that hydrogen is dissociatively adsorbed on alumina surface only to an extremely small extent, it is presumed that the amount of adsorbed hydrogen in atomic form is so small that it is not a rate-controlling consideration.

(3) Model Discrimination

Model discrimination for the dehydrogenation reaction was also achieved by the Bayesian approach as was used in the case of dehydration. The prior probabilities of the nine proposed kinetic models, N1 to N9, were taken to be 1/9 for each, showing no initial preference for any specific model. Twenty-four kinetic data points were obtained at the conditions as shown in Table 5-8. These data were examined to determine which of the reaction mechanisms was best fitting. The results are listed in Table 5-9. Models N1 and N2 were rejected because these two equations indicate that the reaction rate is independent of hydrogen pressure and therefore give a very poor fit compared with the other models. Among all of the other models examined, N3, N5, and N8 were found to represent the experimental data quite well (see Table 5-9 for model probabilities).

The parameters estimated for N3 gave a value for the coefficient of P_A , b_2 , equal to zero. In terms of adsorption-desorption coefficients for the mechanism of Scheme B, derived with the adsorption

Table 5-8

Experimental Data for Dehydrogenation Reaction

Catalyst weight = 0.2747 gm

Feed composition - 2-propanol except when specified[†]

Reactor temperature - 343.2°C

Run No.	Reaction rate ($\times 10^3$) g-mole hr-g-catalyst	P_A , cm Hg	P_{H_2} , cm Hg	P_K , cm Hg
19	3.49	0.362	0.111	0.111
20	4.52	0.529	0.134	0.134
21	5.42	0.698	0.156	0.156
22	6.22	0.870	0.174	0.174
23	6.98	1.040	0.194	0.194
24	7.67	1.215	0.209	0.209
25	8.34	1.386	0.228	0.228
26	8.94	1.564	0.244	0.244
27	9.58	1.737	0.257	0.257
28	10.65	2.091	0.283	0.283
29	11.71	2.440	0.315	0.315
30	12.71	2.799	0.336	0.336
31	13.66	3.156	0.359	0.359
32	14.56	3.514	0.381	0.381
33	15.40	3.873	0.402	0.402
34	16.25	4.231	0.424	0.424
35	20.26	6.222	0.524	0.524
36	26.61	10.052	0.686	0.686
37	38.97	20.001	1.000	1.000
38	47.89	29.280	1.227	1.227
39	58.28	42.322	1.492	1.492

Table 5-8 (continued)

Run No.	Reaction Rate (x 1000)	P_A , cm Hg	P_{H_2} , cm Hg	P_K , cm Hg
40*	34.85	16.306	0.895	1.615
41*	64.72	51.662	1.656	6.998
42*	30.22	12.622	0.777	2.117
43**	72.59	19.972	0.397	0.397

* (1) feed composition: 10% acetone in 2-propanol

(2) P_{H_2} is computed from $P_{A0} - P_A$

** Catalyst weight = 0.0586 gm

+ N_2 flow rate = 0.378 g-mole/hr

Table 5-9

Model Performance for Dehydrogenation of 2-Propanol

Model No.	Variance (σ^2)	Posterior Probability
N3	1.59×10^{-9}	81%
N4	2.7×10^{-9}	1%
N5	Reducible to N8	
N6	3.45×10^{-9}	≈ 0
N7	2.48×10^{-8}	≈ 0
N8	1.75×10^{-9}	18%
N9	3.36×10^{-9}	≈ 0

of alcohol and surface decomposition of alkoxide assumed to be rate-controlling, the constant b_2 is equivalent to,

$$b_2 = \frac{K_{22}(1 + K_{25})}{1 + aK_{25} \sqrt{K_{27}}}$$

where the subscripts of K's refer to the reaction step number, and a is an arbitrary constant. The value, $b_2 = 0$, is possible if either $K_{22} \approx 0$ or $K_{27} \approx \infty$. For the reaction to proceed in the forward direction to a significant extent, K_{22} cannot be equal to zero. If $K_{27} \approx \infty$, then the equilibrium of step 5.27 is highly in favor of the formation of hydrogen gas. The latter possibility appears to be in agreement with the previous reported results⁽⁷²⁾ which showed that hydrogen only adsorbed on γ -alumina in minute amounts. The model, N3, could also be obtained from the mechanistic Scheme D by assuming the decomposition of alkoxide, step (5.26), and the desorption of acetone, step (5.24), to be rate-controlling. Again, expressing b_2 in terms of the adsorption and desorption constants for this mechanism gives $b_2 = K_{30} = 0$. This implies that 2-propanol was not adsorbed, which is contrary to the experimental evidence. Also, acetone was not observed on the catalyst surface under reaction temperatures by infrared analysis. Since acetone is formed, it is presumed that the surface concentration is so small that desorption of acetone cannot be rate-controlling. This ruled out the possibility that model N3 was obtained from the mechanistic Scheme D. Thus N3 should be regarded as obtained only from Scheme B with both steps (5.22) and (5.26) to be rate-controlling. Comparing model N5 to N8 it can be seen that if b_3 of N5 is zero then N5 is reducible to N8. By fitting the existing 24

data points, to model N5, it was found that $b_3 = -0.001 \pm 0.0016$ (95% confidence interval) and this implies that b_3 indeed is insignificant. Therefore, if N8 represents the data best, the kinetic model for dehydrogenation could be derived from Scheme D with the surface reaction step being rate-controlling.

The posterior probabilities of N3 and N8 were computed and were found to be 0.82 and 0.18, respectively. Although N3 showed a better fit than N8, its superiority is not conclusive. To discriminate further between these two rival models, the region of feasible experimentation was examined using the expected entropy change criterion⁽⁹⁸⁾. However, the scope of conditions available for predicting expected entropy changes was greatly restricted due to the inability of the IR analysis to detect hydrogen partial pressure. Theoretically, introducing excess hydrogen into the reaction system was desirable for model discrimination, but due to the inability of the IR to detect H_2 , it was decided to adjust the weight of the catalyst pellet to give desired dehydrogenation conversions. At such conditions, one obtains a hydrogen partial pressure which will give a maximum entropy change but without adding hydrogen gas into the feed stream. The partial pressure of hydrogen can thus be varied by adjusting the fractional conversion of the reactant and the partial pressure of hydrogen can still be assumed to be equal to the partial pressure of acetone, which can be accurately measured, because no side reactions were detected.

The selected values of entropy change at various partial

pressures of 2-propanol and hydrogen are shown in Table 5-10. Accordingly, the data point at $P_A \approx 20$ cm Hg and $P_{H_2} \approx 0.4$ was chosen by reducing the catalyst weight to 0.0586 gm from the 0.2747 gm used in the previous experiments. The new data point taken at the maximum expected entropy change yielded $(-r_A) = 0.07259$, $P_A = 19.972$ cm Hg, and $P_{H_2} = P_K = 0.397$ cm Hg. This data point together with the previous 24 data points provided enough information to rule out model N8. In fact the posterior probability for N8 was practically zero and that for N3 was unity. The results of the calculation are summarized as follows:

N3

Parameters $b_1 = 0.0045$ $b_2 = -0.00012$ $b_3 = 0.00734$ $b_4 = 1.16624$

95% limits $\pm 1.787 \times 10^{-5}$ ± 0.0043 ± 0.000124 ± 0.00887

Variance of fit (σ^2) = 1.479×10^{-9}

Posterior probability = 1

N8

Parameters $b_1 = 0.004$ $b_2 = 0.954$ $b_3 = 0.0038$

95% limits $\pm 6 \times 10^{-5}$ ± 0.034 ± 0.0003

Variance of fit (σ^2) = 3×10^{-8}

Posterior probability = 4.44×10^{-17}

The proposed models other than N3 and N8 were again fitted with the 25 data points. The results again revealed that these models were inadequate. Thus, the successful model involved the dual dissimilar-sites mechanism (Scheme B) with adsorption of 2-propanol and decomposition of alkoxide jointly rate-controlling.

Table 5-10
Expected Entropy Change at Various Partial Pressure of
2-Propanol (A) and Hydrogen (H₂) for Dehydrogenation Reaction

P_A , cm Hg	P_{H_2} , cm Hg	Expected Entropy Change - R
5	0.5	2×10^{-6}
5	1.0	0.0005
5	2.0	0.0006
10	0.66	1.02×10^{-6}
10	0.67	1.36×10^{-7}
10	1.00	0.001
20	0.4	0.0196
20	0.5	0.0190
20	0.6	0.0160
20	1.0	6.0×10^{-7}
30	0.3	0.016
30	0.5	0.02
30	0.7	0.02
30	0.8	0.018
30	1.0	0.0056

5.3.9 Activation Energy for the Dehydrogenation of 2-Propanol

The most successful model, N3, obtained from the isothermal data at 343.2°C, is rewritten below according to Arrhenius expression:

$$(-r_A) = \frac{b_{1,0} \exp\left(-\frac{E_1}{RT}\right) P_A / \sqrt{P_{H_2}}}{1 + b_{3,0} \exp\left(-\frac{E_3}{RT}\right) \frac{P_A}{\sqrt{P_{H_2}}} + b_{4,0} \exp\left(-\frac{E_4}{RT}\right) \sqrt{P_{H_2}}} \quad (5.31)$$

In order to estimate $b_{1,0}$ and E_1 , low conversion data at various temperatures were obtained and are shown in Table 5-11. The low value of P_A together with the small value (0.00734) of b_3 at 343.2°C ensured that $b_{3,0} \exp(-E_3/RT) P_A / \sqrt{P_{H_2}}$ in equation 5.31 is much smaller than unity. In this way equation 5.31 may be reduced to 5.32,

$$(-r_A) = \frac{b_{1,0} \exp\left(-\frac{E_1}{RT}\right) P_A / \sqrt{P_{H_2}}}{1 + b_{4,0} \exp\left(-\frac{E_4}{RT}\right) \sqrt{P_{H_2}}} \quad (5.32)$$

Fitting the experimental data with the above equation, it was found that the parameter estimation using Singh's method did not converge. It has been reported that similar difficulty may be due to the inherent functional form of the model under investigation⁽¹²¹⁾. A particular model leading to such difficulty was

$$(-r_A) = \frac{1 + b_1 P_A}{b_2 + b_3 P_A} \quad (5.33)$$

Table 5-11
Data for Estimation of the Activation Energy
of the Dehydrogenation Reaction

Catalyst weight = 0.2853 gm

Feed rate - 0.04088 g-mole of 2-propanol per hour*

Run No.	Reaction Temperature, °K	Reaction rate ($\times 10^3$)	P_A , cm Hg	P_{H_2} , cm Hg
44	556	2.961	3.810	0.085
45	567	4.110	3.783	0.112
46	577	5.462	3.750	0.147
47	585	6.780	3.709	0.186
48	593	8.331	3.669	0.226
49	599	9.659	3.633	0.262
50	607	11.700	3.577	0.318

*N₂ flow rate = 0.378 g-mole/hr

The form of equation (5.32) is similar to that of (5.33) and this is the reason for its lack of convergence. However, the Arrhenius plot, by assuming $b_{4,0} \exp(-E_4/RT) = b_4 = 1.166$, shows a linear relationship with uniform distributed errors (Figure 5-15). Therefore E_4 would be expected to be a small value and b_4 to be temperature insensitive. The apparent activation energy, E_1 , is estimated to be 30.3 k cal/g-mole from the slope in Figure 5-15. Again Singh's method for parameter estimation was applied. The constants, b_3 and b_4 , which are functions of the equilibrium constants for each elementary step, are now assumed to be temperature insensitive for the range of temperatures studied, with the values, $b_3 = 0.00734$ and $b_4 = 1.166$, as obtained from the isothermal data. The data of Runs 44 to 50 in Table 5-11 together with the first 16 isothermal runs (Table 5-8) were correlated for equation (5.31). The following results were obtained:

Parameters	$b_{1,0} = 2.148 \times 10^8$	$E_1 = 30,090$
95% limits	$\pm 4.66 \times 10^7$	± 257
Variance of fit	$= 2.34 \times 10^{-9}$	

An apparent activation energy of 30 k cal/g-mole is obtained which is in agreement with the Arrhenius plot and which is much higher than that of dehydration (14.6 k-cal/g-mole). It is thus expected that the dehydration reaction will be predominant on the γ -alumina surface at lower temperatures. Since aluminum ions, which are responsible for the dehydrogenation reaction, are believed to be abundant on pure γ -alumina, the dehydrogenation of 2-propanol on γ -alumina is possible

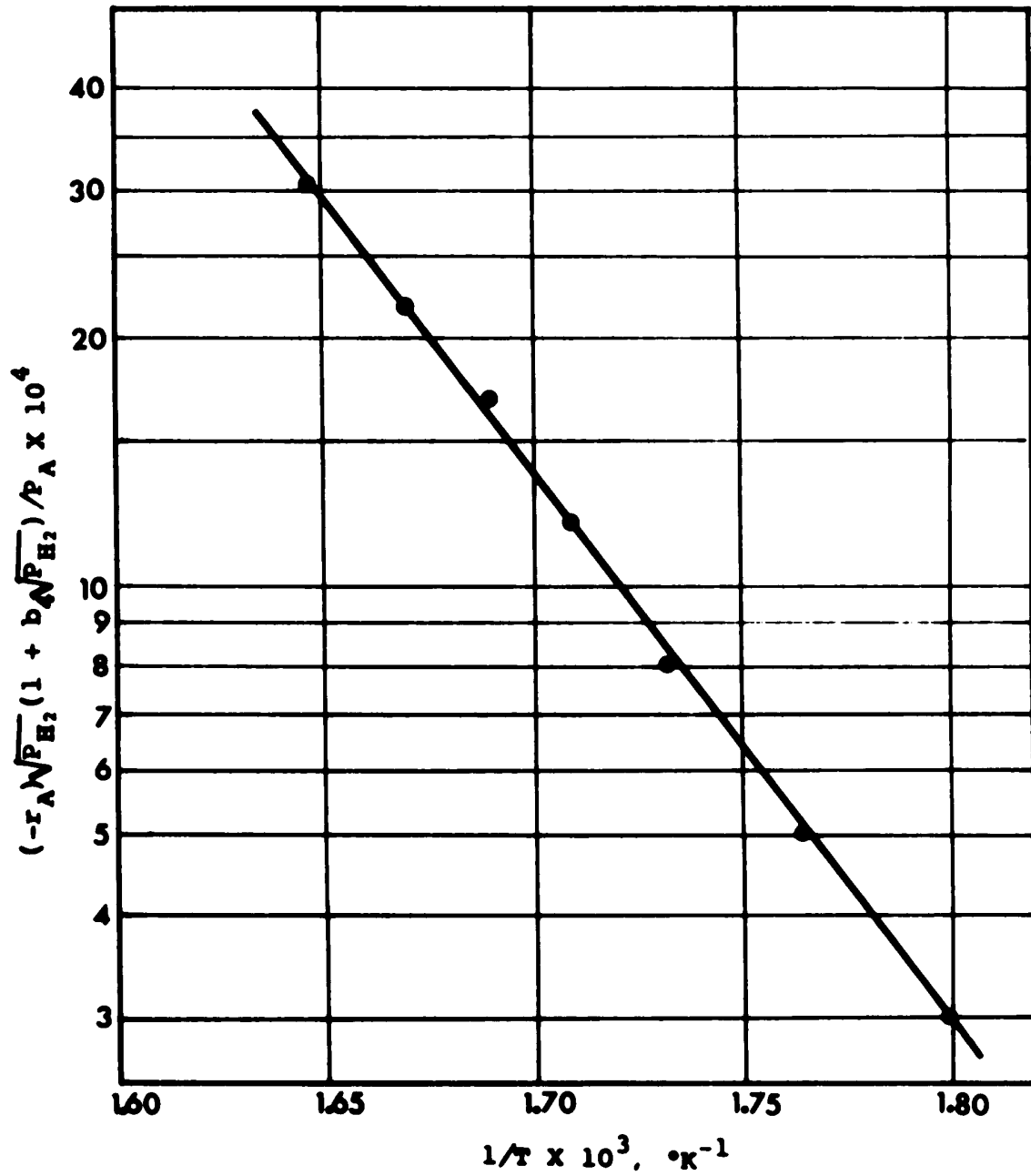


Figure 5-15. Temperature Dependency of the Rate of Dehydrogenation of 2-Propanol.

for temperatures above 500°C⁽⁹⁴⁾. However side reactions, such as the thermal decomposition of 2-propanol, become significant at high temperatures⁽²⁾ so that little information can be obtained for the study of simultaneous dehydration and dehydrogenation of alcohols on pure γ -alumina.

CHAPTER VI

CONCLUSIONS**6.1 Adsorption of Secondary Alcohols on γ -Alumina and NaOH-doped γ -Alumina**

Secondary alcohols are primarily dehydrated by hydrogen bonding to surface hydroxyl groups on γ -alumina at high temperatures. At lower temperatures, an alkoxide surface species also appeared and reacted at higher temperatures to form a surface carboxylate structure, which was stable up to 300°C. Contrary to other reports^(6,79) the alkoxide did not lead to the formation of detectable amounts of ether.

Doping of γ -alumina with sodium hydroxide reduced the number of surface hydroxyl groups at 3785 and 3680 cm^{-1} , thus leading to a reduction in the hydrogen-bonded surface species formed from secondary alcohols. The amounts of the surface Lewis sites were found to be unaffected by increasing the catalyst NaOH content. Consequently, the surface alkoxide species, which were obtained by adsorption of the alcohol on Lewis acid sites, were found to be identical for all of the catalyst samples investigated. An adsorbed ketone-like intermediate was observed analogous to the adsorbed secondary alcohol for the catalyst containing more than 1% of NaOH. With further heating to 300°C the ketone-like intermediate formed a stable carboxylate surface structure accompanied by the release of methane from secondary alcohols, 2-propanol and 2-butanol.

6.2 Catalytic Properties of γ -Alumina Towards Decomposition of Secondary Alcohols

The Bronsted-type acidity exhibited by γ -alumina surfaces is related to the hydroxyl bands appearing at 3785, 3720, and 3680 cm^{-1} . Roughly 10 to 15% of the Bronsted-acid sites are stronger acidic sites than the remaining 85 to 90% sites. The Lewis-type acidity behavior is related to incompletely coordinated aluminum ions. The 3720 cm^{-1} hydroxyl groups and the Lewis-acid sites appear to be less accessible than the 3785 and 3680 cm^{-1} hydroxyl bands to doping agents such as NaOH or to chemical reactants. The 3785 cm^{-1} hydroxyl groups are more catalytically active and acidic than the 3680 cm^{-1} hydroxyl groups, contrary to the model of the surface of γ -alumina developed by Peri.

The structures, = Al-O-Na, seem to be formed when alumina is doped with NaOH. The number of aluminum ion sites remains unaffected by increased NaOH content but their accessibility increases, hence the catalyst selectivity may be continuously modified from dehydration alone, to dehydration plus dehydrogenation, to dehydrogenation alone by proper doping procedures.

The selectivity of various catalysts towards simultaneous dehydration and dehydrogenation reactions could be related to the number and accessibility of Bronsted-acid and Lewis-acid sites on the surface. It also appears that the catalytic activity of the weak Bronsted-acid sites and the Lewis-acid sites do not differ substantially, but the Bronsted-acid sites (hydroxyl groups) are more accessible than the Lewis-acid sites (aluminum ions) because of their greater

proximity to the exterior surface planes.

The mechanisms for dehydration and dehydrogenation of 3-pentanol on pure γ -alumina or NaOH-doped γ -aluminas involve hydrogen bonding of the alcohol to the Bronsted-acid sites (via the oxygen in the alcohol) or formation of a surface alkoxide species with the Lewis-acid sites, respectively. NaOH-doping reduces the number of Bronsted-acid sites thus suppressing the dehydrating activity of alumina.

6.3 Kinetics of Dehydration and Dehydrogenation of 2-Propanol on γ -Alumina Catalysts

The recirculation reaction system for the study of simultaneous kinetics and mechanism of 2-propanol decomposition using infrared spectroscopy was found to be versatile, simple and accurate. Since mass transfer limitations for the pressed catalysts were shown to be negligible, the pressed wafers were suitable for the kinetic studies.

On the basis of the surface spectra obtained under the reaction conditions, together with the results from the adsorption studies, the dehydration and dehydrogenation of 2-propanol appear to involve two types of active sites for each reaction: surface hydroxyl and surface oxide for dehydration, and surface aluminum ion and surface oxide for dehydrogenation. The mechanism proposed from the adsorption studies for the decomposition of 2-propanol on pure γ -alumina and on 8% NaOH-doped γ -alumina are in agreement with the results from the kinetic data obtained. The kinetic data were correlated for the

proposed mechanisms by a Bayesian approach to model discrimination.

The reaction rate expressions that fit the data best are $(-r_A) =$

$b_1 P_A / (1 + b_2 P_A)(1 + b_3 P_W)$ for the dehydration reaction and $(-r_A) =$

$b_1 P_A / \sqrt{P_{H_2}} (1 + b_2 P_A / \sqrt{P_{H_2}} + b_3 / \sqrt{P_{H_2}})$ for the dehydrogenation reaction.

The apparent activation energies for the dehydration and dehydrogenation reactions are 14.6 and 30.1 k cal/g mole, respectively.

CHAPTER VII

RECOMMENDATIONS

(1) The design of the infrared cells in the present study was restricted by the width of the sample compartment of the infrared spectrophotometer (11 cm). In order to determine low concentration components accurately, a long infrared cell may be required. This can be achieved by a combination of three mirrors, similar to those used in commercially available multi-path gas cells, as shown in Figure 7-1. The cells should be enclosed in an isolated system which has been purged with dry nitrogen gas. This will prevent the spectral interference due to atmospheric water vapor and carbon dioxide.

(2) Figure 7-2 illustrates a proposed scheme whereby the flexibility and reliability of a high-quality infrared spectrophotometer can be used as an "infrared analyzer". The experimental parameters, such as temperature or reactant flow-rate, are under direct digital control during either a planned sequence or computer-determined sequence of experimental conditions. The IR spectrophotometer monitors a particular band continuously via the computer interface or alternatively, it is instructed by the computer to commence a scan over a pre-set range. The latter scan may be repeated as often as desired under computer program control. Both qualitative and quantitative analyses are feasible with such a scheme.

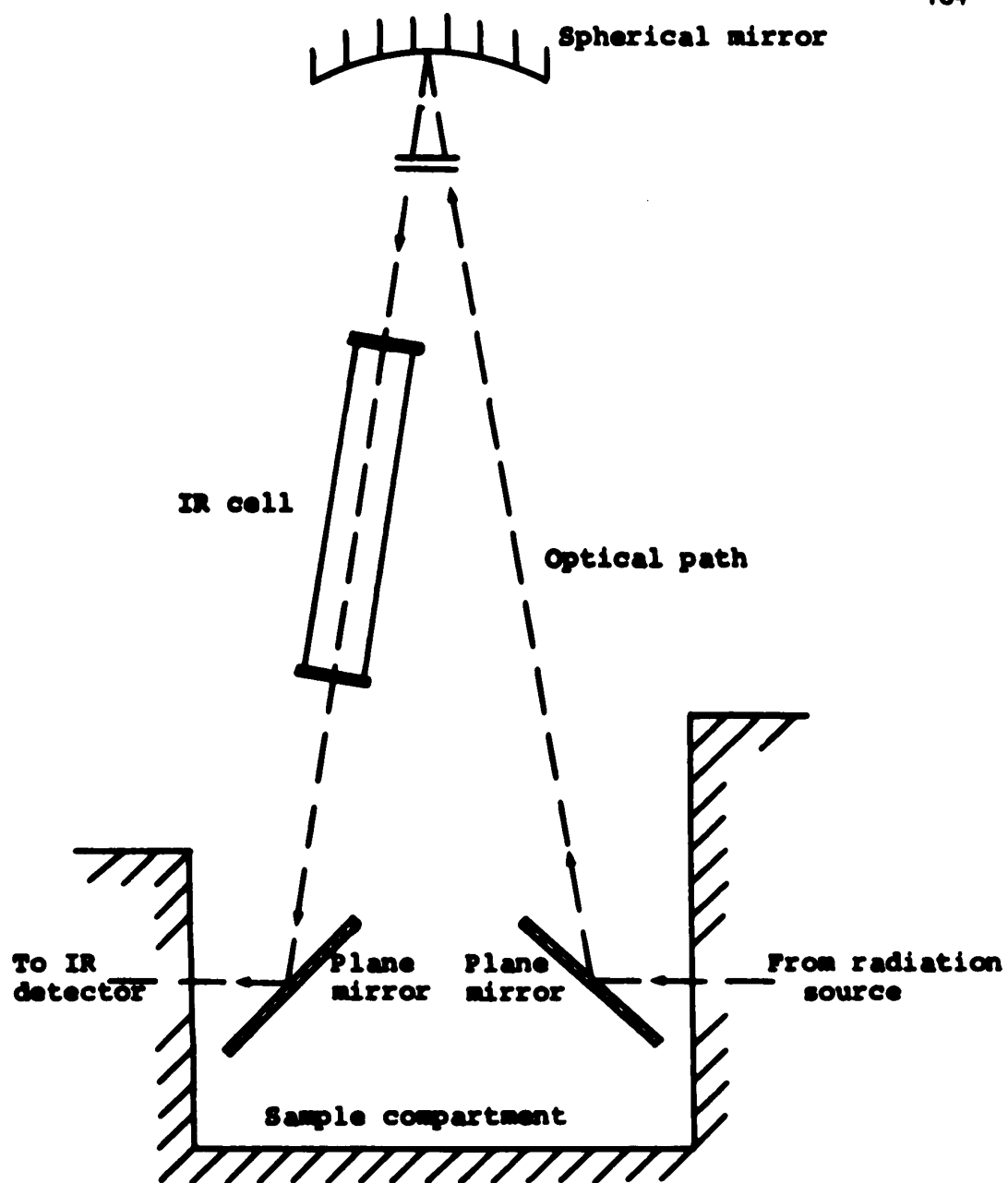


Figure 7-1. Schematic Diagram for the Use of Long IR Cell in Kinetic Studies.

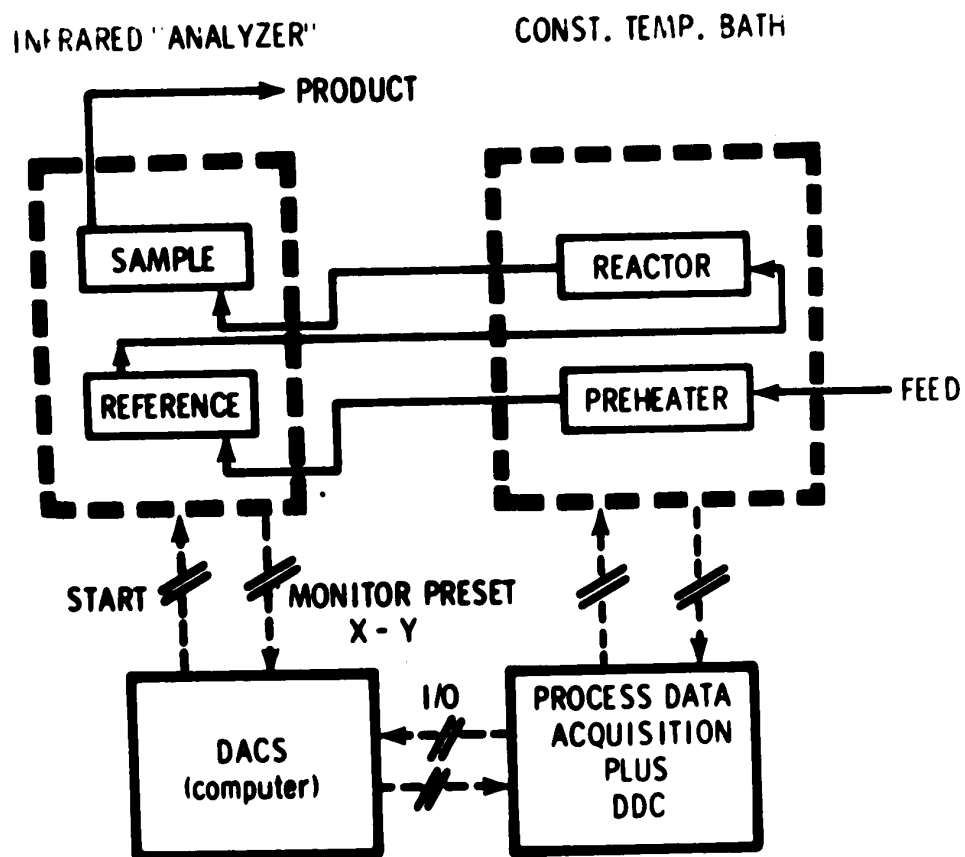


Figure 7-2. Online Monitoring and Control of Chemical Reaction/Kinetics Studies.

(3) Simultaneous dehydration and dehydrogenation reactions were observed for the catalysts containing one to eight per cent NaOH. It is further recommended that additional experiments need to be performed on these catalysts in order to determine the effects of NaOH content in γ -alumina on the decomposition of alcohols. By assuming the same mechanisms obtained from dehydration and dehydrogenation studies, the rate expressions for simultaneous dehydration and dehydrogenation of 2-propanol on NaOH-doped γ -alumina can be derived. They are given as follows:

(1) Generalized mechanism for dehydration reaction:



(2) Generalized mechanism for dehydrogenation reaction:





where l_1 , l_2 and l_3 are surface hydroxyl, surface oxide and surface aluminum ion, respectively.

(a) The rate expression for the dehydration reaction is derived by assuming that the surface reaction, step (3), is rate-controlling. Then

$$r_1 = r_3 = r_4 = 0$$

$$\text{rate of dehydration} = r_2 = k_2 C_{Al_1} C_{l_2}$$

A further assumption is that the total number of sites of type 2, L_2 , is constant and $L_1 = \text{constant} = L_{1,0} f(\text{Na})$, where $L_{1,0}$ is number of OH groups on pure γ -alumina and $f(\text{Na})$ is some function of NaOH content which can be determined experimentally. Thus

$$\begin{aligned} L_1 &= L_{1,0} f(\text{Na}) = Cl_1 + C_{Al_1} + C_{Pl_1} \\ &= Cl_1 \left(1 + K_1 P_A + \frac{P_P}{K_3} \right) \end{aligned}$$

$$L_2 = C_{L_2} + C_{WL_2} + C_{HL_2} = C_{L_2} \left(1 + \frac{P_W}{K_4} + \frac{\sqrt{P_{H_2}}}{\sqrt{K_8}} \right)$$

and

$$r_2 = k_2 C_{AL_1} C_{L_2} = k_2 P_A C_{L_1} C_{L_2}$$

$$= \frac{k_2 L_{1,0} L_2 f(\text{Na}) P_A}{\left(1 + K_1 P_A + \frac{P_P}{K_3} \right) \left(1 + \frac{P_W}{K_4} + \frac{\sqrt{P_{H_2}}}{\sqrt{K_8}} \right)}$$

Let the coefficient of $P_P \rightarrow 0$, then the rate of dehydration of 2-propanol on NaOH-doped γ -alumina can be expressed as

$$r_2 = \frac{b_1 f(\text{Na}) P_A}{(1 + b_2 P_A) (1 + b_3 P_W + b_4 \sqrt{P_{H_2}})}$$

(b) The rate expression for the dehydrogenation reaction can be derived in a way similar to that for the dehydration. By assuming that the adsorption of 2-propanol (step (5)) and the surface reaction (step (7)), are both rate-controlling, the rate of dehydrogenation can be written as:

$$\text{rate of dehydrogenation} = \frac{b_5 P_A}{(1 + b_3 P_W + b_4 \sqrt{P_{H_2}}) (\sqrt{P_{H_2}} + b_6 P_A + b_7 P_A \sqrt{P_{H_2}}) + b_8}$$

Thus the rate of 2-propanol conversion is the sum of the rate of dehydration and rate of dehydrogenation:

$$-r_A = \frac{b_1 P_A f(\text{Na})}{(1 + b_3 P_H + b_4 \sqrt{P_{H_2}})(1 + b_2 P_A)} +$$

$$\frac{b_5 P_A}{(1 + b_3 P_H + b_4 \sqrt{P_{H_2}})(\sqrt{P_{H_2}} + b_6 P_A + b_7 P_A \sqrt{P_{H_2}}) + b_8}$$

BIBLIOGRAPHY

1. Blyholder, G., in "Experimental Methods in Catalytic Research" edited by Anderson, R.B., Academic Press (1968).
2. Chan, A.Y., M.Sc. Thesis, Univ. of Alberta, Edmonton, Canada (1969).
3. McGregor, D., Ph.D. Thesis, Univ. of Alberta, Edmonton, Canada (1971).
4. Dent, A.L. and Kokes, R.J., J. Phys. Chem., 73, 3781 (1969).
5. Ueno, A., Onishi, T. and Tamaru, K., Trans. Farad. Soc., 66, 756 (1970).
6. Soma, Y., Onishi, T. and Tamaru, K., Trans. Farad. Soc., 65, 2215 (1969).
7. Noto, Y., Fukuda, K., Onishi, T. and Tamaru, K., Trans. Farad. Soc., 63, 3081 (1967).
8. Fukuda, K., Noto, Y., Onishi, T. and Tamaru, K., Trans. Farad. Soc., 63, 3072 (1967).
9. Baddour, R.F., Modell, M. and Heusser, U.K., J. Phys. Chem., 72, 3621 (1968).
10. Goldsmith, R.L., Ph.D. Thesis, M.I.T., Mass., U.S.A. (1966).
11. Operating Manual, Perkin-Elmer 621 Infrared Spectrophotometer, Perkin-Elmer Co., Conneticut, U.S.A.
12. Vasudeva, K., Ph.D. Thesis, Univ. of Alberta, Edmonton, Canada (1965).

13. Notari, B., *Chim. Ind.*, 51, 1200 (1969).
14. Knozinger, H., and Kohne, R., *J. Catalysis*, 3, 559 (1964).
15. Knozinger, H., and Kohne, R., *J. Catalysis*, 5, 264 (1966).
16. deMourgues, L., Peyron, F., Trambouze, Y. and Prettre, M.
J. Catalysis, 7, 117 (1967).
17. Esam, I., Balandir, A. and Rudenko, A., *Kinet. Kat.*, 9, 1101
(1968).
18. Pines, H. and Manassen, J., *Adv. Catalysis*, 16, 49 (1966).
19. Wanke, S.E., M.Sc. Thesis, Univ. of Alberta, Edmonton, Canada
(1966).
20. Imai, T., M.Sc. Thesis, Univ. of Alberta, Edmonton, Canada (1967).
21. Winfield, M.E., in "Catalysis", edited by Emmett, P.H., Reinhold,
New York, 7, 93 (1960).
22. Verwey, E., *Z. Krist.*, 91, 65 (1935).
23. Lippens, B. and deBoer, J., *Acta Crystallogr.*, 17, 1312 (1964).
24. Saalfeld, H., and Mehrotra, B., *Ber. dt. Keram. Ges.*, 42, 161
(1965).
25. Lippens, B.C., "Structure and Texture of Aluminas", Ph.D. Thesis,
Delft University of Technology, The Netherlands. (1961).
26. Pines, H. and Haag, W.O., *J. Amer. Chem. Soc.*, 82, 2471 (1960).
27. Dabrowski, J.E., Ph.D. Thesis, Yale University, Connecticut (1969).
28. deBoer, J.H., et al, *J. Catalysis*, 1, 1 (1962).
29. Wanke, S.E., private communication.
30. Moliere, K., Rathje, W. and Stranski, I., *Disc. Farad. Soc.*, 5,
21 (1949).
31. Dabrowski, J., Butt, J. and Bliss, H., *J. Catalysis*, 18, 297
(1970).

32. deBoer, J., Fortuin, J., Lippens, B. and Meys, W., *J. Catalysis*, 2, 1(1963).
33. Lippens, B. and Steggerda, J., in "Physical and Chemical Aspects of Adsorbents and Catalysts" Edited Linsen, B.G., Academic Press (1970).
34. Bhasin, M., Curran, C. and John, G., *J. Phys. Chem.*, 74, 3973 (1970).
35. Peri, J.B., *J. Phys. Chem.*, 69, 211 (1965).
36. Peri, J.B., *Actes Congr. Intern. Catalysis, 2e., Paris*, 1, 1333 (1960).
37. Parry, E.P., *J. Catalysis*, 2, 371 (1963).
38. Knozinger, H. and Spannheimer, H., *Ber. Bunsenges Phys. Chem.*, 70, 575 (1966).
39. Bandiera, J. and Naccache, C., *Bull. Soc. Chim. France*, 2637 (1969).
40. Koberstein, E., *Ber. Bunsenges. Phys. Chem.*, 64, 906 (1960).
41. Peri, J.B. and Hannan, R.B., *J. Phys. Chem.*, 64, 1526 (1960).
42. Peri, J.B., *J. Phys. Chem.*, 69, 220 (1965).
43. Van Tongelen, M., *J. Catalysis*, 5, 535 (1966).
44. Little, L.H., "Infrared Spectra of Adsorbed Species", Academic Press Inc., (London) Ltd., (1966).
45. Kagel, R.O., *J. Phys. Chem.*, 71, 844 (1967).
46. Cornelius, E.B. et al, *J. Phys. Chem.*, 59, 809 (1955).
47. Hindin, J.G. and Meller, S.W., *Advan. Catalysis*, 9, 79 (1957).
48. Deo, A.V. and Dalla Lana, I.G., *J. Phys. Chem.*, 73, 716 (1969).

49. Ross, R. and Bennett, D., *J. Catalysis*, 8, 289 (1967).
50. Knozinger, H., Röss, E. and Buhl, H., *Naturwissenschaften*, 54, 516 (1967).
51. Greenler, R.G., *J. Chem. Phys.*, 37, 2094 (1962).
52. Knozinger, H., Buhl, H. and Röss, E., *J. Catalysis*, 12, 121 (1968).
53. Treibmann, D. and Simon, A., *Ber. Bunsenges. Phys. Chem.*, 70, 562 (1966).
54. Babushkin, A. and Uvarov, A., *Doklady Akad. Nauk. SSSR*, 110, 581 (1956).
55. Arai, H., et al., *J. Catalysis*, 9, 146 (1967).
56. Boreškov, G.K., et al, *Doklady Akad. Nauk. SSSR*, 156, 901 (1964).
57. Bremer, H., et al., *Z. Chem.*, 10, 161 (1970).
58. Fink, P., *Rev. Roum. Chim.* 14, 811 (1969).
59. Dalla Lana, I.G. and Chan, A.Y., paper presented at the 3rd Symposium on Catalysis, Edmonton, Canada (1969).
60. Geschke, D. and Pfeifer, H., *Z. Phys. Chem.*, 232, 127 (1966).
61. Krylov, O.V., *Zh. Fiz. Khim.*, 39, 2656 (1965).
62. Jain, J.R. and Pillai, C.N., *J. Catalysis*, 9, 322 (1967).
63. Knozinger, H., *Angew. Chem. Internat. Edit.* 7, 791 (1968).
64. Corso, V., *Compt. Rend.*, 259, 1413 (1964).
65. Knozinger, H. and Buhl, H., *Z. Naturforsch*, 246, 290 (1969).
66. Lusky, H., Thesis, TH Merseburg, Germany, (1969).
67. Knozinger, H., *Z. Phys. Chem. (Frankfurt)*, 48, 151 (1966).
68. Knozinger, H. and Röss, E., *Z. Phys. Chem. (Frankfurt)*, 59, 49 (1968).

69. Spannheimer, H. and Knozinger, H., Ber. Bunsenges. Phys. Chem., 70, 570 (1966).
70. Hair, M.L., "Infrared Spectroscopy in Surface Chemistry", Marcel Dekker, Inc., New York, (1967).
71. Terenin, A., Filimonov, W. and Bystrov, D., Z. Elektrochem, 62, 180 (1958).
72. Rubinshtein, A.M. et al, Doklady Akad. Nauk SSSR, 167, 1308 (1966).
73. Duken, H., Fink, P. and Pilz, E., Chem. Technol., 18, 490 (1966).
74. Pines, H. and Haag, W., J. Amer. Chem. Soc., 83, 2847 (1961).
75. Figueras Roca, F., DeMourges, L. and Trambouze, Y., J. Catalysis, 14, 107 (1969).
76. Knozinger, H. and Stolz, H., Ber. Bunsenges Phys. Chem., 74, 161 (1970).
77. Misono, M., Saito, Y. and Yoneda, Y., Proc. III Intern. Congr. Catalysis, Amsterdam, P408, North-Holland Publ. Company, Amsterdam, (1964).
78. Topchieva, K., Yun-Pin, K. and Smirnova, J., Advan. Catalysis, 9, 799 (1957).
79. Heiba, E. and Landis, P., J. Catalysis, 3, 471 (1964).
80. deBoer, J. and Visseren, W., Catalysis Reviews, 5, 55 (1971).
81. Rericha, R. and Kochloefl, K., Collect. Czech. Chem. Commun., 34, 206 (1969).
82. Brey, W.S. Jr. and Krieger, K., J. Amer. Chem. Soc., 71, 3637 (1949).

83. Dowden, D.A., J. Chem. Soc., 242 (1950).
84. Yakerson, Y., Lafer, L. and Rubinshtein, A., Doklady Akad. Nauk SSSR, 174, 111 (1967).
85. Knozinger, H. and Scheglila, A., J. Catalysis, 17, 252 (1970).
86. Kittrell, J.R. and Mezaki, R., Ind. Eng. Chem., 59, 28 (1967).
87. Carra, S., Santangelo, S. and Fusi, A., Chem. Ind. (Milano), 48, 229 (1966).
88. Solomon, H.J., Bliss, H. and Butt, J.B., Ind. Eng. Chem. (Fundamentals), 6, 325 (1967).
89. Mezaki, R. and Butt, J.B., Ind. Eng. Chem. (Fundamentals), 7, 120 (1968).
90. Kasaoka, S. et al, Kogyo Kagaku Zasshi, 68, 49 (1965).
91. Dohse, H. and Kalberer, W.Z., Z. Phys. Chem., B5, 131 (1924).
92. Kuriacose, J.C., Daniel, C. and Balakrishnan, N., Indian J. Chem., 7, 367 (1969).
93. Piśman, I., Kaśyanov, V. and Dalin, M., Kinet. Katal., 6, 741 (1965).
94. Maatman, R.W. and Vande Griend, L.J., J. Catalysis, 20, 238 (1971).
95. Bard, Y. and Lapidus, L., Catalysis Reviews, 2, 67 (1968).
96. Kittrell, J.R., Advan. Chem. Eng., 8, 97 (1970).
97. Kulback, S., Information Theory and Statistics, John Wiley, (1959).
98. Singh, H., M.Sc. Thesis, Univ. of Alberta, Edmonton, Canada (1971).

99. Deo, A.V., Dalla Lana, I.G. and Habgood, H.W., *J. Catalysis*, 21, 270 (1971).
100. Brunauer, H., Emmett, P.H. and Teller, E., *J. Am. Chem. Soc.*, 60, 309 (1938).
101. Gregg, S. and Sing, K., "Adsorption, Surface Area and Porosity", Academic Press, 1967, Chapter 3.
102. Rao, C.N.R., "Chemical Applications of Infrared Spectroscopy", Academic Press, 1963, Chapter 11.
103. Friedel, R.A. and Queiser, J.A., *Anal. Chem.*, 29, 1362 (1957).
104. Bertsch, L. and Habgood, H.W., *J. Phys. Chem.*, 67, 1621 (1963).
105. Peri, J.B., *J. Phys. Chem.*, 69, 211 (1965).
106. DeRossett, A., Finstrom, C. and Adams, C., *J. Catalysis*, 1, 235 (1962).
107. Carberry, J.J., *Catalysis Reviews*, 3, 62 (1970).
108. Satterfield, C.N., "Mass Transfer in Heterogeneous Catalysis" MIT Press, Massachusetts, 1970, P. 142.
109. Johnson, W.C., Ph.D. Thesis, University of Wisconsin, Madison, Wisconsin (1960).
110. Bradshaw, R.W. and Davidson, B., *Chem. Eng. Sci.*, 24, 1519 (1969).
111. Thaller, L.H. and Thodos, G., *A.I.Ch.E. Journal*, 6, 369 (1960).
112. Levenspiel, O., "Chemical Reaction Engineering", John Wiley, New York, 1962, Chapter 14.
113. Hougen, O.A. and Watson, K.M., *Ind. Eng. Chem.*, 35, 529 (1943).

114. Boudart, M., "Kinetics of Chemical Process", Prentice-Hall, 1968, P. 104.
115. Bischoff, K.B. and Froment, G.F., Ind. Eng. Chem., Fundamentals, 1, 195 (1962).
116. Kolboe, S., Ind. Eng. Chem. Fundamentals, 6, 169 (1967).
117. Kolboe, S., J. Catalysis, 13, 193 (1969).
118. Mezaki, R. and Watson, C.C., Ind. Eng. Chem., Process Design and Develop. 5, 62 (1966).
119. Kittrell, J.R., Ph.D. Thesis, University of Wisconsin, Madison, Wisconsin (1966).
120. Weller, S.W. and Montagna, A.A., J. Catalysis, 21, 303 (1971).
121. Kittrell, J.R., Hunter, W.G. and Watson, C.C., A.I.Ch.E.J. 12, 5 (1966).
122. Savitzky, A. and Golay, J.E., Anal. Chem., 36, 1627 (1964).
123. Savitzky, A., Paper #4 presented at the 8th European Congress on Molecular Spectroscopy, Copenhagen, Denmark, August (1965).
124. Instruction Manual for Model 8RLS Encoder Readout/Computer Interface, The Perkin-Elmer Corporation (1967).
125. McManus, T., "Systems Programming Considerations for On-line IR Operation", DACS, Chem. Eng. Dept., Univ. of Alta. (1969).
126. Savitzky, A. and Crisler, R.A., "FORTRAN routines", Perkin-Elmer Corporation, Connecticut.
127. Eischens, R.P. and Pliskin, W.A., Actes Congr. Intern. Catalyse, Paris (1960).
128. Marquardt, D.W., J. Soc. Ind. Appl. Math., 11, 431 (1963).
129. Stull, D. et al, "The Chemical Thermodynamics of Organic Compounds", John Wiley, 1969.

LIST OF NOMENCLATURE

The nomenclature in use throughout this thesis is given in the following list. Symbols and constants are also defined where they first occur. Special symbols which are defined and used in the Appendix are not included here.

English Letter Symbols

A	Alcohol
A_λ	Absorbance at wavelength λ
a	Arbitrary constant
\underline{a}_k	Vector of unknown parameters corresponding to the k^{th} model
B_i	Total number of active sites which can be occupied by i^{th} component
b_i	Arbitrary constant of i^{th}
C	Concentration (g-mole/l)
\underline{C}_j	Variance covariance matrix of the parameters in a kinetic model
D	Effective diffusivity
E	Activation energy
E_n	Entropy as defined in equation (2.32)
E_0	Apparent activation energy (K cal/g-mole)
E_T	True activation energy (K cal/g-mole)
ϵ_i	Error term in the i^{th} kinetic model

F, F_{A0}	Molal flow rate of the reactant (g-mole/hr)
H_i	Enthalpy change for adsorption of component i
I_λ	Intensity of the transmitted beam
$I_{0\lambda}$	Intensity of the incident beam
K	Ketone
K_i	Equilibrium constant for the reaction step i , or adsorption constant for i^{th} species
k_i	Reaction rate constant for the reaction step i
L_i	Total number of active sites of type i on the catalyst surface
$1/L$	External surface area-to-volume ratio for the catalyst wafer
l	Length of the IR cell
l_i	Surface active sites of type i
M_i	Assigned model number i for the dehydration reaction
N_i	Assigned model number i for the dehydrogenation reaction
n	Total number of data point obtained
P	Propylene
P_i	Probability that the i^{th} model form is correct, or partial pressure of i^{th} component
p_i	Partial pressure of i^{th} component in the product mixture
p_0	Partial pressure of reactant in the feed
p_{ir}	Partial pressure of i^{th} component measured in the reference cell
R	Ideal gas law constant
$-R$	Expected entropy change

r, r_A	Rate of reaction; g-mole of reactant converted per hour per gm of catalyst
r_1	Rate of reaction for the reaction step 1
r_0	Initial rate of reaction
\hat{S}_k^2	Minimum sum of errors squared; equals $\min. \sum_{i=1}^n (Y_{\text{observed},i} - Y_{\text{calcd},i})^2$
T	Absolute temperature ($^{\circ}\text{K}$)
W	Water
w	Weight of catalyst (gm)
X_j	Design matrix for j^{th} kinetic model
X_{L_1}	Surface alkoxide species
x	Independent variable
x_A	Fraction of reactant converted in to product
y	Dependent variable

Greek Letter Symbols

ϵ	Extinction coefficient; equals $1/C \log (I_0/I)$
σ^2	Error of variance of a single measurement
σ_j^2	The unbiased estimate of error variance
ϕ_1	Proposed i^{th} kinetic model
ϕ_L	Thiele diffusion modulus

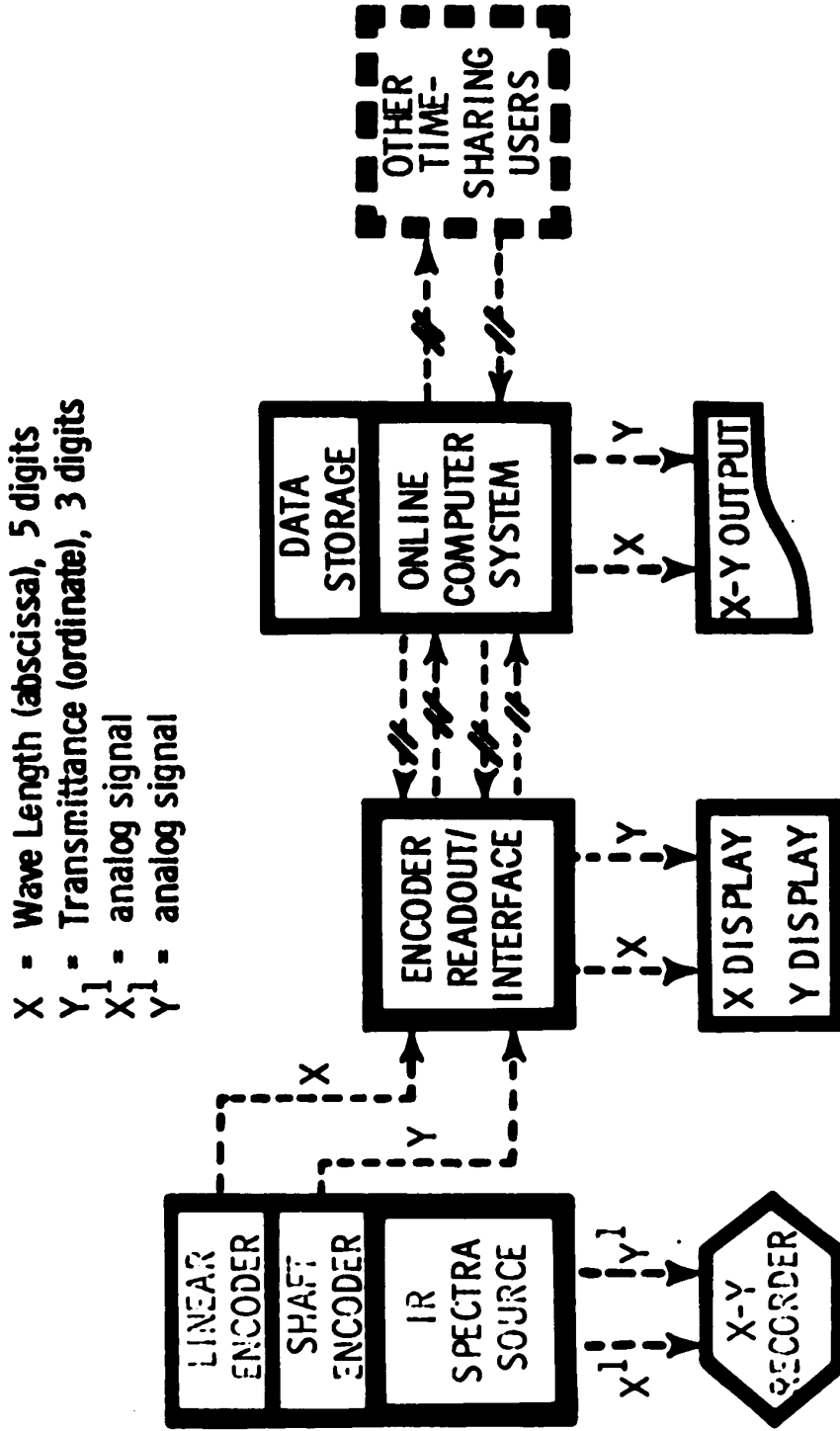
APPENDIX

A. ON-LINE OPERATION OF A PE621 - IBM 1800 SYSTEM

Analytical instruments, such as infrared spectrophotometers equipped with digital encoders, can generate a great deal more data, and of higher precision, than is normally available with conventional instruments. This additional data and precision is easily handled by a real-time digital computer, such as an IBM 1800, and sophisticated data processing methods, including signal filtering and averaging, can be used in generating quantitative descriptions of spectral bands which characterize molecular species. Moreover the manner of processing each set of data is left for the user to decide after data acquisition; this gives a wide range of flexibility. Several references in which such concepts are developed are already available^(122,123).

A block diagram of the infrared spectrophotometer interfaced to the computer is shown in Figure A-1. The multi-application capability of the system is also indicated but emphasis is placed upon the participating role of the IR unit. The diagram shows the flow of data originating as the signals, Y' and X', through to their presentation in several forms of digitized output, Y and X.

The advantages of this type of computerized application arise from the elimination of conventional input-output control systems, greater quantity, and often superior quality of data taken in the same scan time, and benefits accruing from rapid, detailed processing of the data. The following section will describe in de-



X - Wave Length (abscissa), 5 digits
 Y - Transmittance (ordinate), 3 digits
 X^1 - analog signal
 Y^1 - analog signal

Figure A-1. Block Diagram of IR-Computer System.

tail the three major equipment items comprising the PE621 - IBM 1800 system, and their methods of communicating information or instructions.

A-1 System Components

A-1.1 PE621 Infrared Spectrophotometer

This instrument and its capabilities are well known and so, detailed comments on its design are unnecessary in this thesis. The conventional output signals are percent transmittance (Y' = source signal, Y = digitized signal) and wave-length (X' = source signal, X = digitized signal). The PE621 was purchased with Perkin-Elmer X' and Y' encoders installed. The two encoders are one-brush absolute position types and their shaft positions are tracked continuously by flip-flop registers⁽¹²⁴⁾. Freedom from gearing, backlash and possibly servo errors, particularly those inherent in systems taking data from the recorder servo unit, are eliminated through the use of encoders. The Y signal in three digits is obtained from the comb servosystem. The X signal, resolved to a tenth of a wave-number, is obtained from a 100-count encoder mounted to the wave-length shaft (monochromator). An up-down counter (three digits) in the interface unit counts the number of revolutions of the 100-count encoder (two digits), thereby giving a total wave number of five digits. Since subsequent transmission of the encoded signals to the computer is in BCD code, this system permits the monitoring of $Y-X$ signals with high resolution, the resolution being limited only by that of the encoders.

A-1.2 Encoder Readout-Computer Interface

The Perkin-Elmer Model 8RLS encoder readout-computer interface includes an operating mode for direct transmission of $Y-X$ data

to a digital computer. The signals are received continuously from the IR in encoder switching code and are then translated to BCD and stored in an encoder register. The BCD data may be decimalized for visual Nixie display or alternatively, transmitted to a data-logging device such as an external paper tape punch coupler. The data in the encoder register is strobed into a buffer storage register which freezes the information. A translator converts the buffer register output into 8-4-2-1 BCD output in positive logic (logical one = +8 volts, zero = - 12 volts) and transmits it to a rear panel connector for direct hookup to the IBM 1800 computer.

The encoder readout has a maximum capacity of 32 bits (eight decimal digits) and can accept up to 300 bits/sec (roughly, ten Y-X points per second). The data encoding rate is operated asynchronously with the computer since synchronized real-time monitoring of data points is not desirable with the hardware-controlled operation of the spectrophotometer. The wave number interval which determines the data sampling rate is specified by operator selection of multiples of the minimum increment (0.1 cm^{-1}) available for the X-axis. The sampling rate is generated by a data trigger which strobes the signals at the specified intervals of X from the encoder register into the buffer register for parallel transmission of all bits in the 8-digit data word to the computer. Each time that a Y-X point has been transmitted from the encoder register to the buffer register, and thus to the computer, the encoder register is left in a "reset" position. The computer acknowledges receipt of the data point by sending a voltage

pulse to the interface unit (one pair of wire needed), which returns the encoder register to "set" position. If a second point should be strobed into the buffer register without the preceding computer acknowledgement, the "reset" position indicates loss of data and initiates an electronic contact operation alarm.

In the kinetics studies, the IR spectrophotometer monitors a particular frequency as a function of time via the encoder read-out - computer interface. Since the data trigger is not activated without varying the wave length, λ , a pulse generator was installed to transmit data from the encoder register to the buffer register. The sampling rate is controlled by the rate of pulse generated. The other functions are identical to the normal operation mode.

The computer and IR-interface are separated by about 125 ft. of the communication cable (two 18-pair 22-gauge individually shielded twisted-pair cables). The cables are totally shielded as well and are run through conduits for mechanical protection, providing rather excessive shielding protection. The BCD signal, the start-up communication, and the computer acknowledgement pulse require 34 pairs leaving two pairs in reserve. It is interesting to note that the essentially noise-free 32 pairs of cable could be replaced by at most two pairs if the analog signals, $Y-X$, were to be transmitted. Noise pick-up in transmitted $Y-X$ signals is more likely and could reduce the data accuracy considerably.

The direct generation of digital values and the transmission of the digital BCD signals should be essentially noise-free. The

quality of data input to the computer therefore is directly dependent on the accuracy of the encoder readout and the basic IR components.

A-1.3 IBM 1800 System

The hardware configuration most pertinent to the on-line operation of the IR unit is shown in Figure A-2. The equipment designated by the boxes with slightly thicker margins has been involved in the current studies. Access to such an extensive facility with its large core and disk storage facilities, full range of conventional input-output peripheral hardware, substantial computing power, and supporting system analysts greatly simplified the task of developing a powerful and convenient-to-use system.

The system was initially operating with an IR data acquisition program permanently resident in core when the IBM 1800 was operated under Time-Sharing Executive (TSX) System. After the computer was converted to operate under Multi-Programming Executive (MPX) System in 1970, the IR data acquisition program was stored on disk and alternated with the Department's Gas Chromatograph Monitoring Program in core load area three. The program responds to interrupts generated by the interface unit and reads in 32 bits of data. The 32 BCD input data bits are converted to binary integer numbers and stored into two 16-bit words of a core buffer. When the 320-word core buffer is filled, it is transferred to one sector of disk storage. In view that this is a time-shared operation, the disk could be busy completing a disk operation for another program. Thus provision had to be made for queuing time and disk-seek operations as well as for the actual

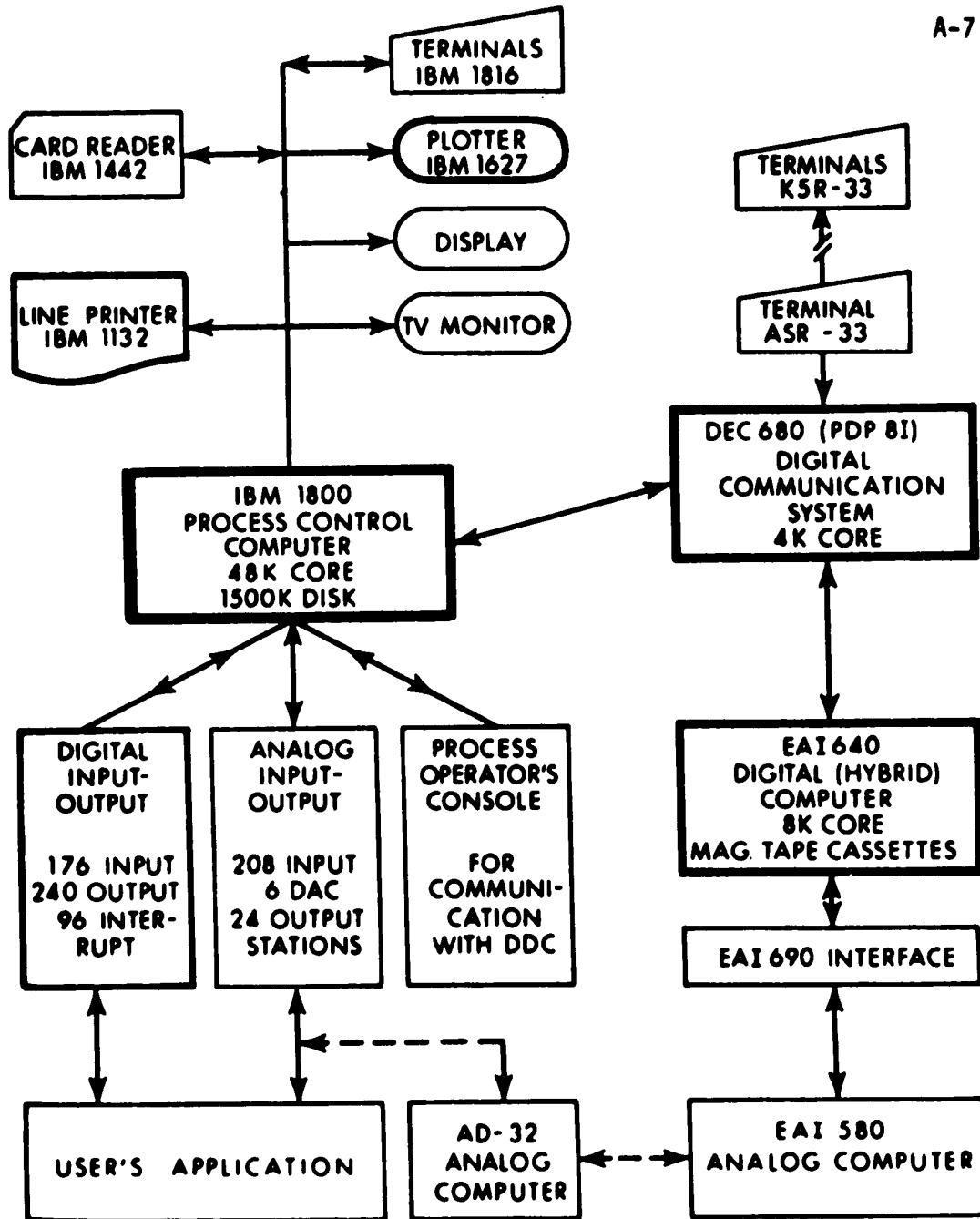


Figure A-2. IBM 1800 Data Acquisition and Control System.

10 ms. of write time. Four possible methods⁽¹²⁵⁾ of insuring a disk write time compatible with the IR data acquisition program limitations are dedication of a disk, dual internal buffering, look ahead method, and secondary overflow buffering. Only the last method makes efficient use of both core and disk. Since minimized core requirements were a design specification for the IR data acquisition program, it was decided to use the secondary overflow buffering technique.

The provision of a secondary overflow buffer would allow the IR routine to accept a limited number of data samples while the main buffer is being written to disk. When the main buffer is freed, data stored temporarily in the secondary buffer would be transferred into the main buffer. For the maximum data rate (100 ms. sampling interval), a 40-word secondary buffer would allow 2 seconds for disk write operations. The size of the auxiliary buffer can be changed by an equate card at system generation time.

The disk data files were stored in a form accessible by FORTRAN coded programs so that the users could write their own data processing programs. Since the five-digit wave number could be as large as 40,000 and since the largest number that can be represented by the 16-bit data word of the IBM 1800 is 32,767 it was necessary to use either a two word integer or a special data code. To conserve core, it was initially decided to store the four least significant digits of the wave number in a one word integer format with the associated transmittance in the adjacent word. Each time that the fifth (highest order) digit changes, it is recorded by putting a special entry in the

file with a transmittance of "-1" (a physical impossibility) and a wave number equal to the fifth digit. The users' program can then access the file and handle it as one-word integers, or convert it to two-word integers or floating-point numbers. Negative values for percent transmittance are also used to "flag" special codes to indicate run termination or alarm conditions. They are shown in Table A-1.

A-2 Operation of the System

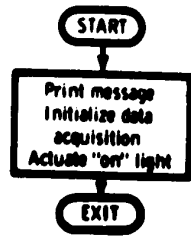
The flow diagrams in Figures A-3 to A-5 describe in simplified terms the role of the computer during the startup, operation and shutdown of program-controlled data acquisition. The IR operator in the remote laboratory actuates a "request to computer" electronic signal when an IR scan is to be performed.

In the "start" procedure, upon assuming the "ready" state, the computer informs its operator via print message that it has initialized data acquisition and also informs the IR operator of its "ready" state. The latter action is accomplished via a light on the panel of the interface unit. It then returns to its time-sharing service role until the IR operator, at his convenience, starts the hardware-controlled IR scan.

When reading data, the computer files all of the raw data before any data processing is commenced. When the IR operator signals by turning the on-line switch to the "off" position that the scan has been completed, the computer again advises its operator that the job

Table A-1
The Usage of the Special Indicators in Data File

Transmittance	Wave Number	Explanation
-2	Undefined	This record indicates the end of valid data for the most recent run and that the run was terminated normally by either the operator or the preset range switch of the IR spectrophotometer.
-3	Undefined	This record indicates the end of valid data for the most recent run and that the run was terminated due to either an external or internal data over flow.



Flow Diagram of Program Controlled Data Acquisition

Figure A-3. Start Procedure.

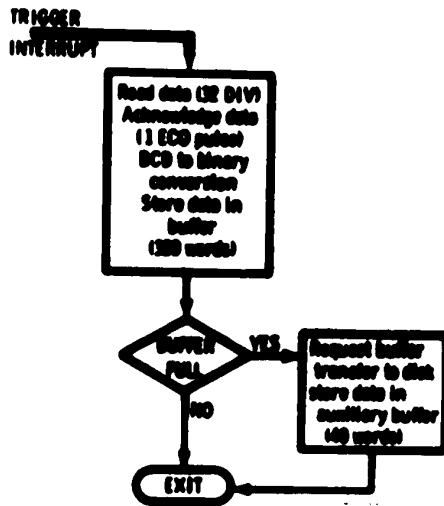


Figure A-4. Data Acquisition.

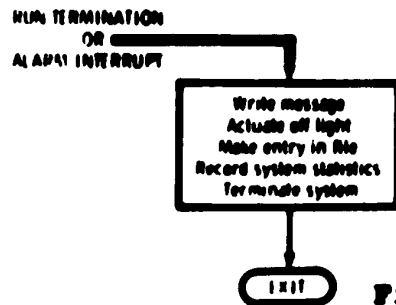
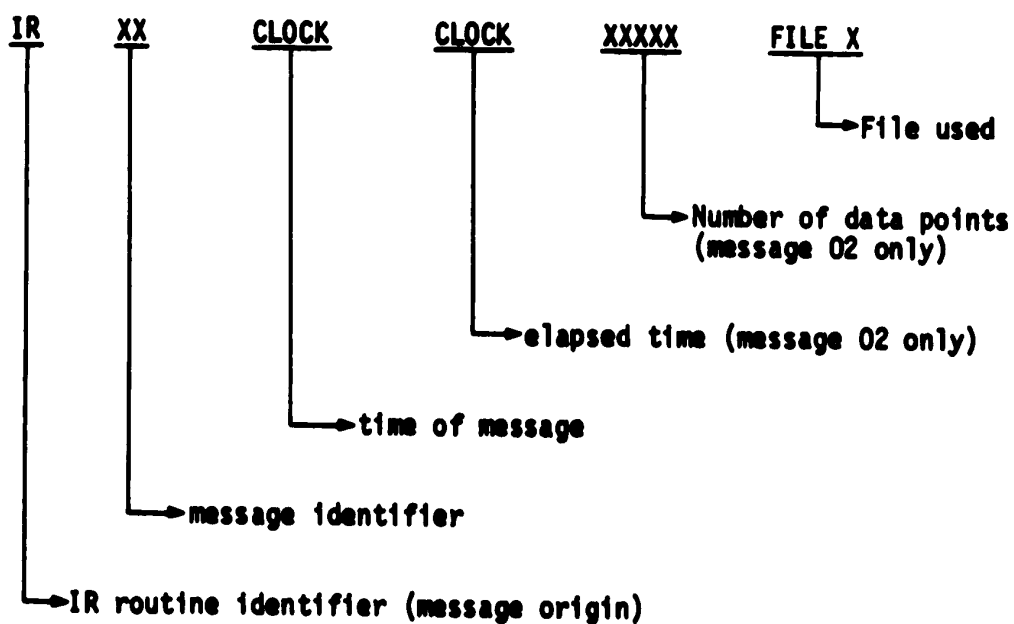


Figure A-5. Stop Procedure.

has been completed and it then summarizes the system statistics.

In the above procedures, all logging and error messages issued by the IR routine are typed on the log typewriter in a standard format for reasons of simplicity and core economy. The message format is:



The messages are further identified by color, with normal logging messages being typed in black and error messages typed in red. The present system messages are defined as follows:

<u>Message Identifier</u>	<u>Explanation</u>
01	Log-on message (indicates that the IR system was initialized for a data acquisition run)
02	Log-off message (indicates that data acquisition was terminated normally)
03	Internal data overflow (indicates that data acquisition was terminated because of the failure of a disk write operation to be completed before the maximum allowable number of overflow samples were accumulated)
04	External data overflow (indicates that data acquisition was terminated due to a signal from the IR spectrophotometer signifying that a data sample was not acknowledged by the system before the next sample was ready)
05	Data file overflow (indicates that data acquisition was terminated due to the fact that the maximum allowable number of samples, as specified by the size of the defined file, were accumulated)

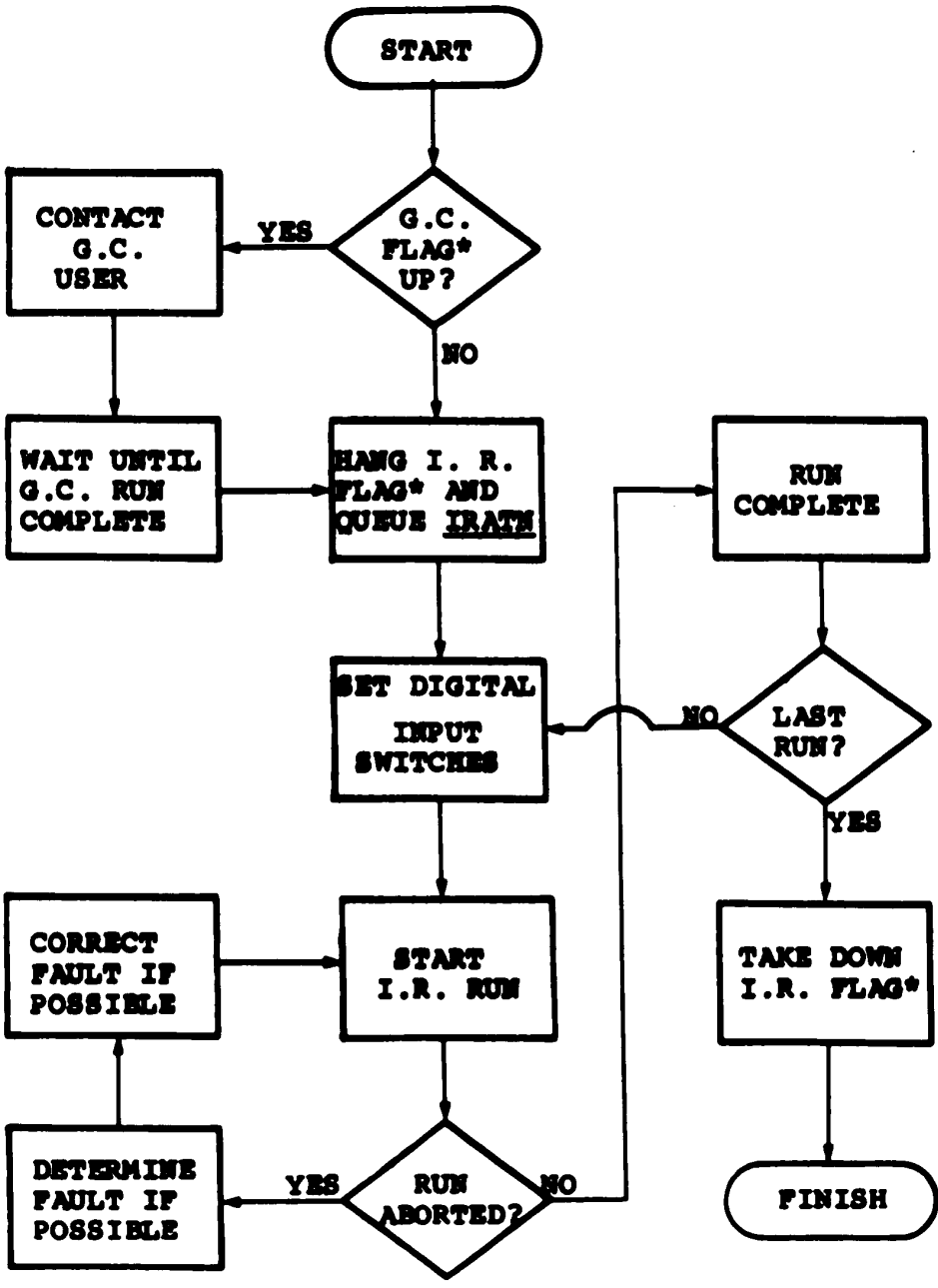
On the initiation of a run, the IR program reads the last four positions of the "Special Digital Input Switches" to determine at what wave number to start collecting data and what file to put the data into. The significance of these four switches is as follows:

<u>Digit Switch</u>			<u>Data Acquisition to Start at Wave Number</u>
<u>13</u>	<u>14</u>	<u>15</u>	
OFF	OFF	OFF	09999 or less
OFF	OFF	ON	19999 or less
OFF	ON	OFF	29999 or less
OFF	ON	ON	39999 or less
ON	OFF	OFF	49999 or less
	<u>12</u>		
	OFF		Data stored in file "IRDT0"
	ON		Data stored in file "IRDT1"

Since October, 1970, the IBM 1800 computer was converted from the TSX operating system to the MPX operating system. The IR data acquisition program was thus revised according to the requirements of the MPX System. However, the system role remains much the same. Figure A-6 shows the details of the operational procedures for the present data acquisition system.

A-3 Data Processing

The treatment of infrared spectroscopic data which has been



*STATUS BOARD FLAG

Figure A-6. IR On-line Data Acquisition Procedures (MPX System).

obtained with the system described herein involves processing up to 38,000 Y-X points if the full range of 3800 cm^{-1} is scanned. These points would occupy 76,000 words of memory, or more if several complete spectral scans were to be retained. Only with access to a time sharing computer system, with relatively large disk storage and rapid computing capability, can the experimenter obtain reduction of such large amounts of data in a speedy manner.

Data processing routines such as data filtering, peak picking and other numerical methods can be used on the data file, and where advantageous, the benefits from varying the computational parameters can be exploited. The raw data and/or the resulting smoothed data can be stored on disk cartridges or punched cards, printed on the line printer or typewriters, or displayed using the digital plotter or the oscilloscope.

For the sake of efficiency, for both the user and the computer, the development of adequate data reduction programming must involve a careful evaluation of the user's needs. Smoothing of the data is advantageous in research applications such as this study if spectral characteristics may be ambiguously interpreted because of high random-noise levels in the percent transmittance or Y data, i.e., random error superimposed upon the significant output signal. If the signal-to-noise ratio is very high, routine smoothing of data may be wasteful through unnecessary use of computational time in a time-sharing system. If selection of peaks, i.e., the significant spectral bands which characterize the sample molecule, is required, then some

level of data smoothing may be advantageous so that those changes in slope which define significant peaks can be more readily detected. A considerable amount of work on such problems has already been reported by Savitzky⁽¹²⁷⁾. Much of this thinking and programming⁽¹²⁶⁾ has been incorporated into the data reduction methods employed in this work. The methods involve least squares fitting and assume that the error is associated with the Y signal (three significant digits) and not with the X signal (five significant digits).

Figure A-7 presents a simplified data-reduction flow diagram which relates the major steps involved in the data smoothing and peak-picking routines. The data acquisition involves multiple-user, on-line operation and so, the data reduction and output functions are not commenced until the scan is completed. Although not shown in Figure A-7, the data points are read from the disk file, sector by sector. They are subjected to least-squares smoothing and a slope calculation except where the transmittance reads 3% or less. The slope is calculated at each point using a quadratic function fitted to the smoothed data. When the sign of the slope inverts, defining passage across an absorption band, a 15-point cubic equation is used to determine the ordinate and abscissa at the peak minimum. The raw data is completely treated, the smoothed data replaces it in the disk file. At present, if a plot of the raw data is required, this output must proceed the smoothing since the latter is destructive to the original memory file. Upon completion of these steps, the Y-X plotter programs calculate appropriate scales and automatically plot the function. The evaluation of the effect of computational parameters

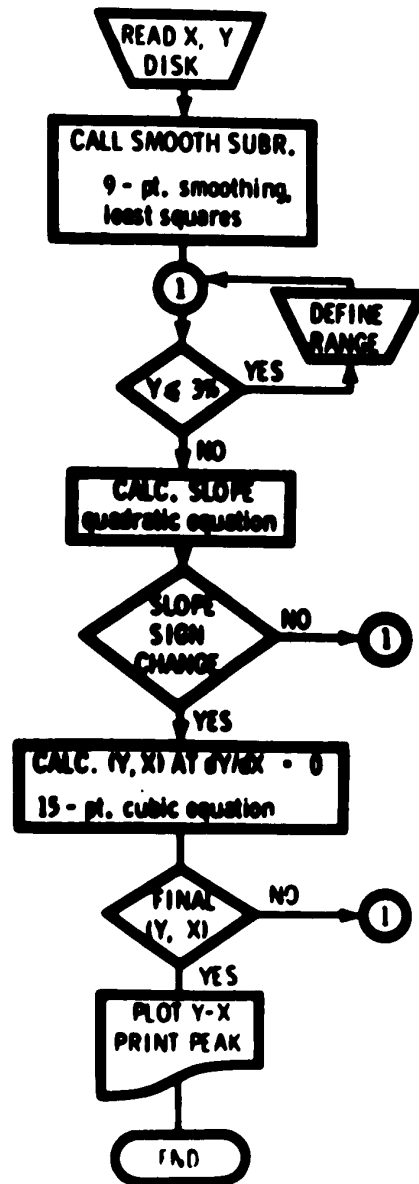


Figure A-7. Data Reduction Flow Diagram.

upon smoothing and peak-picking, e.g., different levels of filtering, was usually done by off-line processing.

Figure A-8 illustrates a comparison on an expanded scale between some raw and smoothed data for a polystyrene film in an ATR cell. The figure was actually plotted by programmed control, in the manner shown, to conform to a preset 18-inch ordinate scale. This range of the X-axis was chosen because of the relatively high noise level visible on the PE621 drum recorder chart, a line of thickness roughly 1% transmittance. The four curves on Figure A-8 show the raw data, taken at highest sampling rate of every 0.1 cm^{-1} interval, and the influence of smoothing these raw data. Some differences in data filtering are indicated from using all of the data, half or one-quarter of the data.

In the smoothing procedure, it would be expected that the nine-point filter band (or "smoothing gate") is effective in suppressing random noise if the width of the gate is considerably larger than the period of the noise frequency to be removed. The application of smoothing to the complete file of data sample involved a 0.9 cm^{-1} gate width (as shown by the second plot of Figure A-8); this did not prove to be effective. Since the wider spacing of the data points produced by using every Nth point in the file generates a wider effective band with the nine-point filter, the smoothing became more noticeable as can be seen on plots 3 and 4. Because less data is employed when the gate is increased, the quality or significance of the resulting plot could also be reduced. Replication of a run, and averaging to eliminate

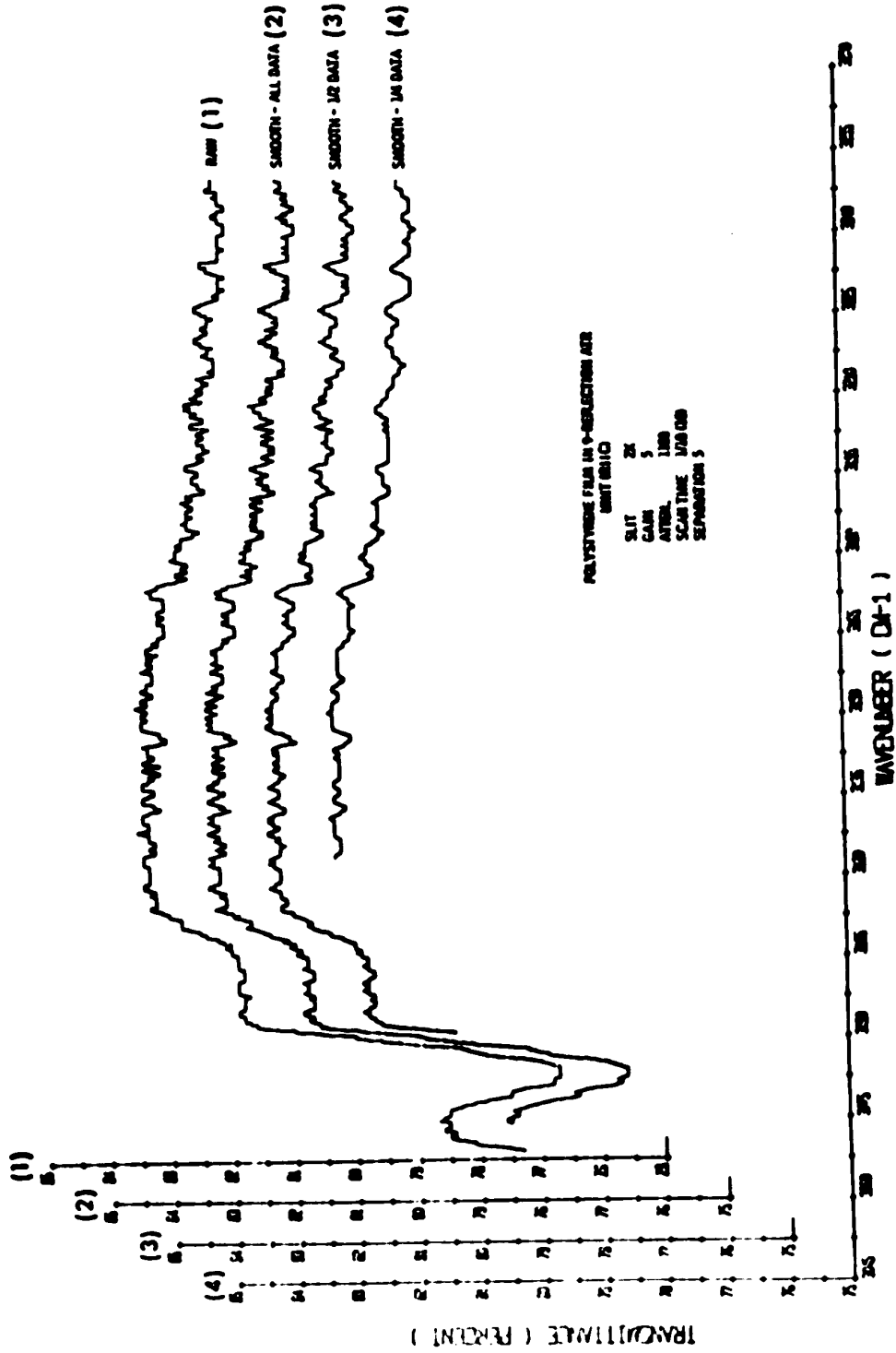


Figure A-8. Comparison between Raw and Smoothed Data.

random noise, is essential to establish the best smoothed function which could be used as a criterion of smoothing effectiveness.

An alternative explanation, originating with Savitzky⁽¹²²⁾, relates the lack of smoothing which resulted from use of all of the data to the difference in magnitudes of time constants between that of the signal-generating instrument and that associated with the span of smoothing-gate. Until the time constant of the latter exceeds that of the instrument, it would be unrealistic to expect beneficial smoothing. This may be the case for the ATR signal until the time constant associated with a 1.8 cm^{-1} gate span was attained. This span was obtained with the nine-point gate using each second Y-X point.

A.4 Research Applications

The research programs, which utilized on-line capabilities, have presented two types of data interpretation problems. The first involves a comparison of infrared spectra of catalyst surface "before and after" the adsorption experiments to determine the spectra of adsorbed species. The second problem involves obtaining kinetic data from monitoring the characteristic peak intensities of the reactant and product. Both of these studies have benefitted from computerized treatment of data: the former, by more sensitive diagnostic analysis resulting from increased numbers of data points and by elimination of tedious point-by-point visual measurements, and the latter by replacement of manual calculations with computer operations thus permitting a direct output of kinetic data when the calibration functions were stored in the disk files. This feature enables the operator in attendance to change experiments or conditions quickly when non-routine unanticipated results are encountered.

A-4.1 Measurement of Differential Spectra on a Single Catalyst

Figure A-9 illustrates some of the spectral characteristics which are encountered during infrared studies of adsorbed molecules and surface reactions on solid catalytic substances using the Eischens technique⁽¹²⁷⁾. By plotting the difference in percent transmittance between the two spectra at the same frequency, taken before and after the experiment and noting also the mid-points for all peaks, the extensive data are reduced to that which appears to be significant.

Often, the full spectral range spanning 3800 cm^{-1} must be studied for the "before" as well as the "after" experiments so that the significant differences between the two sets of spectra can be plotted. The differences between the two sets of spectra may be plotted in the form of the "delta-plot" shown in Figure A-9. This being a tedious but simple task, it is ideally suited for computer processing, especially when smoothing is advantageous. The delta-plot shows only the differences in transmittance at each frequency and thus classifies the changes according to whether they are positive or negative peaks. Positive peaks imply an increase in an existing band or the appearance of a new band, except when a frequency shift occurs. The negative peaks indicate either disappearance or a decrease in transmittance for an existing band. The use of the delta-plot together with a list of mid-peak frequencies for both before and after spectral scans, all provided by computer output, would present savings in calculation time and an improved reliability in the results.

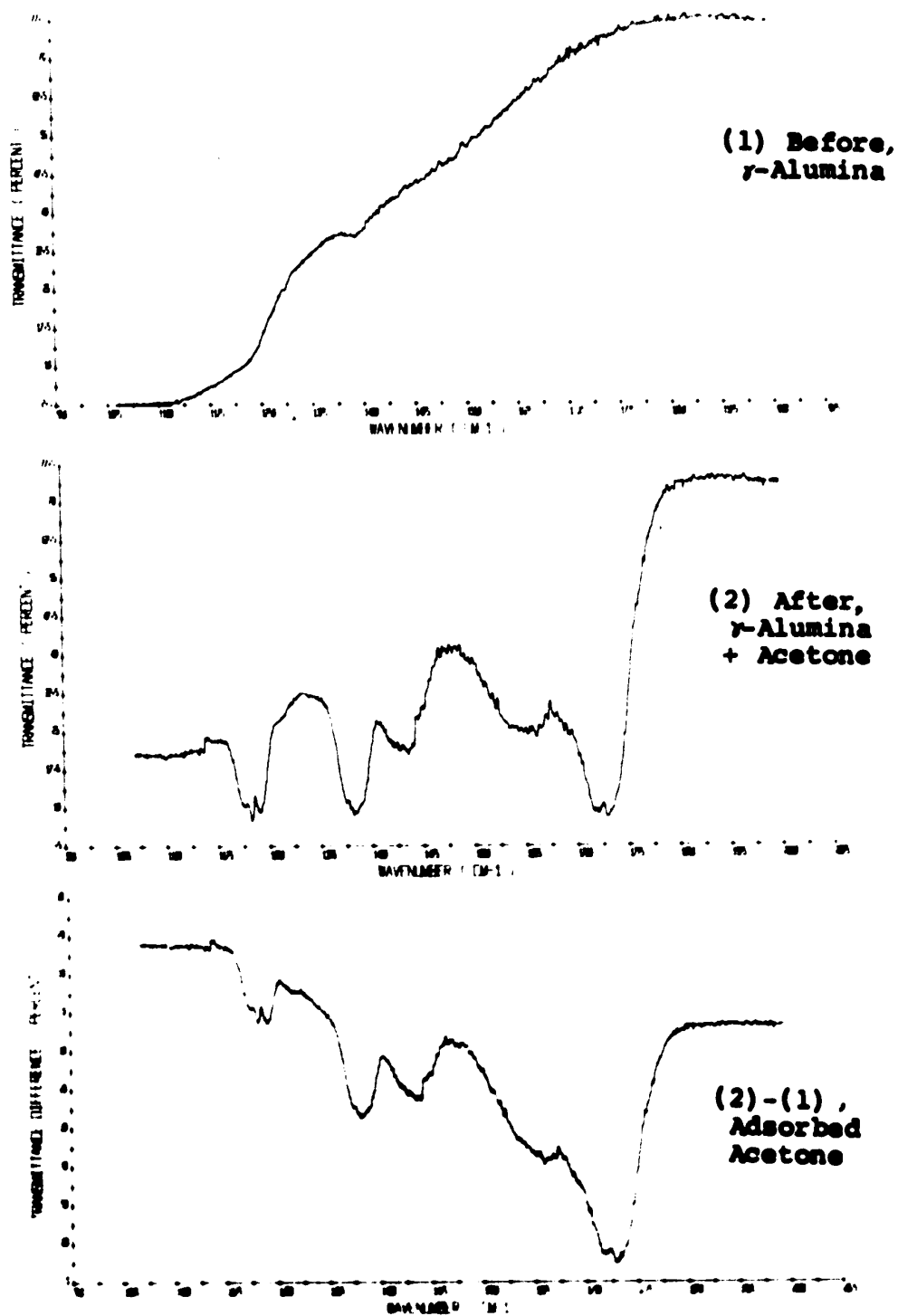


Figure A-9. Comparison of IR Spectra "Before and After" the Experiment.

A-4.2 Infrared Monitoring of a Reaction System

In this case the IR spectrophotometer monitors a particular band continuously via the encoder readout-computer interface. Since large amounts of data were generated, it was able to determine the reaction steady state by fitting the data with a least squares equation over several periods of time and observed the change of slope of the concentration curve. Both qualitative and quantitative analyses are feasible with such a scheme. The computer programs used for the data processing are listed as follows:

1. IRIST: Remove special indicators in data file and smooth the raw data
2. PCNTR: Determine peak centre by 15-point cubic equation
3. PKFND: Calculate slope by 7-point quadratic equation
4. DETRN: Determine if transmittance < 3%, define range for peak picking routines
5. BKGRD: Remove special indicators in data file, store data in data file of either IRDT1 or IRDT0 for plotting programs.
6. IRPLT: Plot data from file IRDT0 or IRDT1
7. DELTA: Compute the difference in transmittance for the data between IRDT0 and IRDT1, plot the resulted data
8. KINET: Obtain kinetic data by following the procedures described in Section 4.2.3.

C MAINLINE IRIST

C MAINLINE IRIST

C MAIN LINE OF IR PROGRAM

C SHORTEN RECORD WHEN WAVENUMBER PASSES MULTIPLE OF
C 1000.0 CMS1

C SETS CONDITIONS FOR FIRST AND LAST RECORDS

C

```

DIMENSION DAT(80) ,WAVE(80) ,KDATA(210),IWAV(210),
INDATA(210),LDATA(210),LWAV(210),PP(10),BAT(80)
2,MWAV(25),MDATA(25)

```

COMMON IIL,JJWAV,CONST

```

DEFINE FILE 1(15,320,U,KI),2(30,320,U,IK),3
1(30,320,U,KO)

```

KN=0

CALL TSTOP

IY=1

MEND=0

IN=1

IP=1

IQ=1

DO 695 JK=1,15

READ(1,JK)(IWAV(LQ),KDATA(LQ),LQ=1,160)

DO 667 JJ=1,160

LL=160

ITER=0

3 THIS INDICATES WITH END OF DATA OR A MULTIPLE OF

C 1000.0 CMS1

C

```

IF(KDATA(JJ)+1) 668,669,667
668 IF(JJ-1)745,745,670
670 LL=JJ-1
ITER=1
GO TO 798
669 CONST=FLOAT(IWAV(JJ))*1000.0
WRITE(6,671) IWAV(JJ)
671 FORMAT(1H1,21H#WAVENUMBER HAS PASSED,15,10H000.0 CM=1)
DO 672 LJ=JJ,160
KDATA(LJ)=KDATA(LJ+1)
IWAV(LJ)=IWAV(LJ+1)
672 CONTINUE
LL=LL-1
GO TO 798
667 CONTINUE

```

C MAINLINE IR1ST ... (CONT'D)

C THIS IS AN INSERTION
C STORE UNSMOOTHED DATA IN FILE FOR PLOTTING PROGRAM
C

```

798 DO 799 LM=1,LL
      DAT(IN)=FLOAT(KDATA(LM))
      WAVE(IN)=(FLOAT(IWAV(LM))) +CONST *10.0
      IF(IN=80)788,791,791
791 WRITE(2'IP) (DAT(IU),WAVE(IU),IU=1,80)
      IP=IP+1
      IN=0
788 IF(ITER) 775,775,789
789 IF(LM=LL)775,601,601
601 DAT(IN+1)=-1.0
      WAVE(IN+1)=FLOAT(IP*80+IN)
      KN=IN+1
      GO TO 796
775 IN=IN+1
799 CONTINUE
      GO TO 123
796 WRITE(2'IP) (DAT(JN),WAVE(JN),JN=1,KN)
123 IF (JK-1)674,674,673
674 LL=139

```

C SMOOTHING LOOP IS INTRODUCED
C DEFINE CONTROL CONSTANTS

```

673 IQP=LL+20
      IQQ=LL+16
      IF(JK-1) 675,675,676
675 IBA=-1
      IBB=5
      IBD=1
      IBE=1
      DO 12 IW=1,4
12  NDATA(IW)=KDATA(IW)
      GO TO 677
676 IBA=11
      IBB=17
677 LA=LL
      IF(JK-1)625,625,626
625 IBG=20
      GO TO 627
626 IBG=IBD-1
627 DO 624 K=1,IBG
      LDATA(K)=MDATA(K)
      LWAV(K)=MWAV(K)
624 CONTINUE
      IF(JK-1) 681,681,679
681 LA=LL+20

```

C MAINLINE IRIST ... (CONT'D)

```

679 DO 678 IXZ=1,LA
    KK=IBD+IXZ-1
    LDATA(KK)=KDATA(IXZ)
678 LWAV(KK)=IWAV(IXZ)

C INITIALIAE SMOOTHING

DO 10 KZ=2,9
    JZ=KZ+IBA
10 PP(KZ)=FLOAT(LDATA(JZ))
    IF(JK-1) 664,664,665
664 IBC=LL+16
    GO TO 867
665 IBC=LL+IBD-5
867 CONTINUE

C MAIN SOOTHING LOOP

DO 200 IA=IBB,IBC
    JA=IA+4
    DO 11 KY=1,8
        KA=KY+1
11 PP(KY)=PP(KA)
        PP(9)=FLOAT(LDATA(JA))
        SUM1=59.0*PP(5)/231.0
        SUM2=54.0*(PP(4)+PP(6))/231.0
        SUM3=39.0*(PP(3)+PP(7))/231.0
        SUM4=14.0*(PP(2)+PP(8))/231.0
        SUM5=21.0*(PP(1)+PP(9))/231.0
        SUM=SUM1+SUM2+SUM3+SUM4-SUM5
        NDATA(IA)=IFIX(SUM)
200 CONTINUE
    CALL DETRN(NDATA,LWAV,LL,JK,I,IT,MEND)
    DO 202 IL=IBE,IBC
        BAT(IY)=FLOAT(NDATA(IL))
        BAVE(IY)=FLOAT(LWAV(IL)) +CONST *10.0
        IF(IY=80) 740,741,741
741 WRITE(3'IQ) (BAT(IZ),BAVE(IZ),IZ=1,80)
        IQ=IQ+1
        IY=0
740 IF(ITER=1) 743,742,742
742 BAT(IY+1)=-1.0
        BAVE(IY+1)=FLOAT(IQ*80+IY)
        IXX=IY+1
        WRITE(3'IQ) (BAT(K),BAVE(K),K=1,IXX)
        GO TO 745
743 IY=IY+1
202 CONTINUE

C PREVIOUS RECORD IS TACKED TO BEGINNING OF NEXT RECORD

```

C MAINLINE IRIST ... (CONT'D)

```
IF (IBD-20) 684,685,686
684  IAQ=LL+1
     IBE=17
     GO TO 687
685  IAQ=LL
     IBE=IBD-5
     GO TO 687
686  IAQ=LL+1
     IBE=IBD-4
687  IBC=IBC+4
     DO 680 IAA=IAQ,IBC
     IW=IAA-LL
     NDATA(IW)=NDATA(IAA)
     MDATA(IW)=LDATA(IAA)
680  MWAV(IW)=LWAV(IAA)
     IBD=21
695  CONTINUE
745  CALL EXIT
     END
```


C SUBROUTINE PCNTR

```

C SUBROUTINE PCNTR
C SUBROUTINE PCNTR(KIDAT,MWAV,ICL,ICK)

C COMPUTATION OF PRECISE SPECTROSCOPIC PEAK POSITION
C AND INTENSITY USING A CUBIC FIT TO THE CENTRAL 15 PTS
C OF THE 'ARRAY' KIDAT HE WAVE NUMBER POSITION OF THE
C PEAK MUST BE WITHIN THE GATE AND INTENSITY IS THE
C LOWER ROOT
C EQUATION IS  $Y=A30+A32*SQ+A33*CUB$ 
C COEFFICIENTS ARE DETERMINED BY ORTHOGONAL POLYNOMIALS
C INPUT
C KIDAT--THE ARRAY OF 15 PTS IN WHICH SLOPE CHANGED
C FROM NEGATIVE TO POSITIVE
C MWAV--WAVE NUMBER POSITION OF THESE PTS
C ICL-- BEGININGS OF ARRAY
C ICK-- END OF ARRAY

DIMENSION KIDAT(25),MWAV(25),DNS(25),P(7),PM(7),
1DWAY(25)
COMMON IIL,JJWAV,CONST
DO 411 NI=1,15
ND=NI
DNS(NI)=FLOAT(KIDAT(ND))
411 DWAV(NI)=FLOAT(MWAV(ND))
DO 412 NJ=1,7
NIP=16-NJ
P(NJ)=DNS(NJ)+DNS(NIP)
412 PM(NJ)=DNS(NJ)-DNS(NIP)
A30=-78.*P(1)-13.*P(2)+42.*P(3)+87.*P(4)+122.*P(5)
1+147.*P(6) +162.*P(7)+167.*DNS(8)
A30=A30/1105.
A31=12922.*PM(1)-4121.*PM(2)-14150.*PM(3)-18334.*PM(4)
*-17842.*
1 PM(5)-13843.*PM(6)-7506.*PM(7)
A31=A31/334152.
A32=91.*P(1)+52.*P(2)+19.*P(3)-8.*P(4)-29.*P(5)-44.
1*P(6) -53.*P(7)-56.*DNS(8)
A32=A32/12376.
A33=-91.*PM(1)-13.*PM(2)+35.*PM(3)+58.*PM(4)+61.*PM(5)
1+49.*PM(6)+27.*PM(7)
A33=A33/47736.
IF(ABS(A33)-0.000001)530,530,420
530 X=-A31/(2.0*A32)
Y=A30+X*(A31+X*A32)
SWAV=(DWAY(8)+X)/10.+ CONST
Y=Y/10.
WRITE (6,520) Y,SWAV
520 FORMAT (1H0,5X,14HQUADRATIC PEAK,3X,14HTRANSMITTANCE =,
1F10.3,3X, 5HPRCNT,5X,13HWAVE NUMBER =,F10.3,3X,4HCL-1)
GO TO 499

```

C SUBROUTINE PCNTR ... (CONT'D)

```

420 DENOM = 3. *A33
    DISC=A32*A32-A31*DENOM
    IF (DISC)421,422,423
421 RAD=SQRT(-DISC)
    REAL=-A32/DENOM
    ROOT=RAD/DENOM
    DWAV(8)=DWAV(8)/10.+CONST
    WRITE(6,502)REAL,ROOT,DWAV(8)
502 FORMAT (1H0,5X,19HCOMPLEX SOLUTION ,
122HWAVENUMBER=REAL PART ,
2F10.3,3X,16HIMAGINARY PART =,F10.3,10HPOSITION =,
3F10.3,3X,4HCM-1)
    GO TO 499
422 X=-A32/DENOM
    Y=A30+X*(A31+X*(A32+X*A33))
    SWAV=(DWAV(8)+X)/10.0+CONST
    Y=Y/10.
    WRITE (6,521) Y,SWAV
521 FORMAT (1H0,16HONE ROOT PEAK ,14HTRANSMITANCE =,
1F10.3,3X,
15HPRCNT,5X,12HWAVENUMBER =,F10.3,3X,4HCM-1)
    GO TO 499
423 RAD=SQRT(DISC)
    XM1=(-A32+RAD)/DENOM
    XM2=(-A32-RAD)/DENOM
    ORD1=A30+XM1*(A31+XM1*(A32+XM1*A33))
    ORD2=A30+XM2*(A31+XM2*(A32+XM2*A33))
    IF(ABS(XM1)-7.0)424,425,425
425 IF(ABS(XM2)-7.0)426,427,427
427 SWAV=DWAV(8)/10.0+CONST
    Y=ORD1/10.0
    WRITE (6,428) Y,SWAV
428 FORMAT (1H0,5X,36HSOLUTION IS OUTSIDE THE ARRAY CENTE
1,12HR OF ARRAY=,14HTRANSMITANCE =,F10.3,3X,5HPRCNT
2,5X,12HWAVENUMBER =,F10.3,
23X,4HCM-1)
    GO TO 499
426 SWAV=(XM2+DWAV(8))/10.0+CONST
    Y=ORD2/10.
432 WRITE (6,429) Y,SWAV
429 FORMAT(1H0,5X,17HBEST SOLUTION - ,
114HTRANSMITANCE =,F10.3,3X,
15HPRCNT,5X,12HWAVENUMBER =,F10.3,3X,4HCM-1)
    GO TO 499
424 IF(ABS(XM2)-7.0)430,431,431
431 SWAV=(XM1+DWAV(8))/10.0+CONST
    Y=ORD1/10.
    GO TO 432
430 IF (ORD1-ORD2) 426,426,431
499 CONTINUE

```

C SUBROUTINE PCNTR ... (CONT'D)
RETURN
END

C SUBROUTINE PKFND

```

C SUBROUTINE PKFND
SUBROUTINE PKFND(NDATA,LWAV,LL,JK,I,IT,LEND)
DIMENSION NDATA(210),LWAV(210),KIDAT(25),MWAV(25)
COMMON IIL,JJWAV,CONST

C DEFINE LIMITS OF PK FIND ROUTINE

ILK=0
JU=0
IF(LEND) 333,333,334
333 INF=I+6
GO TO 335
334 INF=I-9
335 IFI=IT-7

C CHECK WHETHER TRANSMITTANCE IS LESS THAN 3.0(

DO 260 IB=INF,IFI
IF(JK=6) 1,2,3
3 IF(JK=7) 1,2,4
4 IF(JK=8) 1,2,1
2 JU=1
IF(LWAV(IB)-7057)5,5,1
5 CALL TSTRT
GO TO 6
1 CALL TSTOP
6 CONTINUE
IF(NDATA(IB)-30)206,207,205
206 IF(NDATA(IB-1)-30)260,260,208
208 TWAV=FLOAT(LWAV(IB))/10.+CONST
WRITE (6,211) TWAV
211 FORMAT(1H0,5X,36HTRANSMITTANCE IS LESS THAN 3 PERCENT,
116H AT WAVENUMBER= ,F12.3)
GO TO 260
207 IF(NDATA(IB-1)-30)260,260,208
205 IF(NDATA(IB-1)-30)209,209,210
209 TWAV=FLOAT(LWAV(IB))/10.+CONST
WRITE(6,212)TWAV
212 FORMAT(1H0,5X,52HTRANSMITTANCE IS MORE THAN 3 PERCENT
* AT WAVENUMBE
1R= ,F12.3)
GO TO 260
210 IF(NDATA(IB)-800)440,440,442
442 ISUMT=0
DO 443 J=1,6
IBJ=IB+J
IBK=IB-J
ISUM=J*(NDATA(IEK)-NDATA(IEJ))
ISUMT=ISUMT+ISUM
443 CONTINUE

```

C SUBROUTINE PKFND ... (CONT'D)

```

      GO TO 444
440  ISUMT=0
      DO 441 J=1,4
         IBJ=IB+J
         IBK=IB-J
         ISUM=J*(NDATA(IBK)-NDATA(IBJ))
         ISUMT=ISUMT+ISUM
441  CONTINUE
444  IF(JK-1) 445,445,214
445  IF(IB-INF) 250,250,214
214  CONTINUE
      IF(ISUMT)216,218,250
216  IF(IASU)250,220,219
218  JJWAV=LWAV(IB)
      GO TO 250
219  ICL=IB-7
      ICK=IB+7
224  DO 221 IKL=ICK,ICK
         ILK=ILK+1
         MWAV(ILK)=LWAV(IKL)
221  KIDAT(ILK)=NDATA(IKL)
      ILK=0
      CALL PCNTR(KIDAT,MWAV,ICK,ICK)
      GO TO 250
220  IF(JJWAV-LWAV(IB)-15)222,223,223
222  ICL=IB-12
      ICK=IB+2
      GO TO 224
223  XWAV=(FLOAT(JJWAV))/20.0
      YWAV=(FLOAT(LWAV(IB)))/20.0
      ZWAV=XWAV+YWAV+CONST
      WRITE (6,225) ZWAV,NDATA(IB)
225  FORMAT(1H0,5X,32HFLAT PEAK-SLOPE CONSTANT LONGER ,
           127HTHAN1.5CMS1 AVER WAVE NO. =,
           2F10.3,3X,14HTRANSMITTANCE =,16.11H/10 PERCENT)
250  IASU=ISUMT
260  CONTINUE
      CALL TSTOP
      RETURN
      END

```

C SUBROUTINE DETRN

```

C SUBROUTINE DETRN
SUBROUTINE DETRN(NDATA,LWAV,LL,JK,I,IT,MEND)

C THIS SUBROUTINE DETERMINES WHETHER PEAKING FINDING
C ROUT SHOULD BE
C CALLED. THE CONDITION TRIGGERING THE CALLING OF PKFIND
C IS THAT THE
C DATA POINTS MUST BE 0.1 WAVENUMBERS APART.

DIMENSION NDATA(210),LWAV(210)
COMMON IIL,JJWAV,CONST
IF(MEND) 505,505,506
505 LEND=0
GO TO 507
506 LEND=1
MEND=0
507 I=0
IT=0
ILO=LL+16
IF(JK-1) 681,681,682
681 IF(LWAV(2)-LWAV(1)-1) 683,683,684
683 I=1
684 DO 685 IB=2,ILO
IF(LWAV(IB+1)-LWAV(IB)-1) 686,686,687
686 IF(LWAV(IB)-LWAV(IB-1)-1) 685,685,689
689 I=IB
GO TO 685
687 IF(LWAV(IB)-LWAV(IB-1)-1) 690,690,685
690 IT=IB-1
IF(IT-I-20) 945,945,946
946 CALL PKFND(NDATA,LWAV,LL,JK,I,IT,LEND)
GO TO 685
945 I=C
IT=0
685 CONTINUE
GO TO 688
682 IF(LWAV(17)-LWAV(16)-1)691,691,692
691 I=17
692 DO 693 IB=17,ILO
IF(LWAV(IB+1)-LWAV(IB)-1) 694,694,940
694 IF(LWAV(IB)-LWAV(IB-1)-1) 693,693,941
941 I=IB
GO TO 693
940 IF(LWAV(IB)-LWAV(IB-1)-1) 942,942,693
942 IT=IB-1
IF(IT-I-20) 943,943,944
944 CALL PKFND(NDATA,LWAV,LL,JK,I,IT,LEND)
GO TO 693
943 I=0
IT=0

```

C SUBROUTINE DETRN ... (CONT'D)

```
693 CONTINUE
688 IF(I) 947,947,948
948 IF(IT)949,949,947
949 IT=ILO
      MEND = 1
      CALL PKFND(NDATA,LWAV,LL,JK,I,IT,LEND)
947 RETURN
      END
```

```

      C      MAINLINE BKGRD

C      MAINLINE BKGRD

C      SHORTEN RECORD WHEN WAVENUMBER PASSES MULTIPLE
C      OF 1000.0 CM$1
C      SETS CONDITIONS FOR FIRST AND LAST RECORDS
C

      DIMENSION DAT(80) ,WAVE(80) ,KDATA(210),IWAV(210)
      DEFINE FILE 1(45,320,U,KI),3(26,320,U,IK)
      KN=0
      IY=1
      MEND=0
      IN=1
      IP=1
      IQ=1
      DO 695 JK=1,13
      READ(1'JK)(IWAV(LQ),KDATA(LQ),LQ=1,160)
      IF(JK-1)10,10,11
10     CONST=FLOAT(IWAV(1)) *1000.
11     CONTINUE
      DO 667 JJ=1,160
      LL=160
      ITER=0

C      THIS INDICATES WITH END OF DATA OR A MULTIPLE
C      OF 1000.0 CM$1
C

      IF(KDATA(JJ)+1) 668,669,667
668   IF(JJ-1)745,745,670
670   LL=JJ-1
      ITER=1
      GO TO 798
669   CONST=FLOAT(IWAV(JJ))*1000.0
      WRITE(6,671) IWAV(JJ)
671   FORMAT(1H1,21HWAVENUMBER HAS PASSED,15,10H000.0 CM-1)
      DO 672 LJ=JJ,159
      KDATA(LJ)=KDATA(LJ+1)
      IWAV(LJ)=IWAV(LJ+1)+10*IFIX(CONST)
672   CONTINUE
      LL=LL-1
      GO TO 798
667   IWAV(JJ) = IWAV(JJ)+10*IFIX(CONST)

C      THIS IS AN INSERTION
C      STORE UNSMOOTHED DATA IN FILE FOR PLOTTING PROGRAM
C

798   DC 799 LM=1,LL
      DAT(I')=FLOAT(KDATA(LM))

```


C MAINLINE BKGRD ... (CONT'D)

```
WAVE(IN)=FLOAT(IWAV(LM))
IF(IN=80)788,791,791
791 WRITE(3'IP) (DAT(IU),WAVE(IU),IU=1,80)
    IP=IP+1
    IN=0
788 IF(ITER) 775,775,789
789 IF(LM=LL)775,601,601
601 KN=IN+1
    DAT(KN)=-2.0
    WAVE(KN)=FLOAT(IP*80+IN)
    GO TO 796
775 IN=IN+1
799 CONTINUE
695 CONTINUE
796 WRITE(3'IP) (DAT(JN),WAVE(JN),JN=1,KN)
    WRITE(6,655) IP
655 FORMAT(1X,'END OF DATA..IP=',I4)
745 CALL EXIT
END
```

```

      C      MAINLINE IRPLT

C      MAINLINE IRPLT

C      PLOTTING IR SPECTRUM FROM FILES NO. 2 AND 3

      DEFINE FILE 2(30,320,U,M), 3(30,320,U,M)
      DIMENSION WMNMX(2), TMNMX(2)
      DIMENSION DAT(80), WAV(83)
      DIMENSION BX(9), BY(9)
      DATA BX / 4*0.0,1.2,0.20,3*0.0 /
      DATA BY / 2*0.0,1.5708,0.0,0.9,0.10,0.0,-1.5708,0.0 /

C      DETERMINE MINIMUM AND MAXIMUM VALUE FOR WAVENUMBER AND
C      TRANSMITTANCE
C

      WMNMX(1) = 99999.0
      WMNMX(2) = -99999.0
      TMNMX(1) = 9999.0
      TMNMX(2) = -9999.0
      DO 20 I=2,3
      DO 20 J=1,30
      READ (I,J) (DAT(K), WAV(K), K=1,80)
      DO 20 K = 1,80
      IF (DAT(K)) 21,5,5
5 IF (WAV(K) - WMNMX(1)) 6,7,7
6 WMNMX(1) = WAV(K)
7 IF (WAV(K) - WMNMX(2)) 9,9,8
8 WMNMX(2) = WAV(K)
9 IF (DAT(K) - TMNMX(1)) 10,11,11
10 TMNMX(1) = DAT(K)
11 IF (DAT(K) - TMNMX(2)) 20,20,12
12 TMNMX(2) = DAT(K)
20 CONTINUE
21 DO 25 K=1,2
      WMNMX(K) = WMNMX(K)/10.0
25 TMNMX(K) = TMNMX(K)/10.0

C      PLOT GRAPHS FROM FILES 2 AND 3
C

      DO 200 I=2,3

C      SELECT ORIGIN AND SCALE FOR THE GRAPH FOR BOTH AXES
C

      CALL COSGR (WMNMX,2,XMIN,XMAX,15,XSCFA)
      CALL COSGR (TMNMX,2,YMIN,YMAX,10,YSCFA)

C      SET THE SCALE AND DRAW THE GRIDS
C

```

C MAINLINE IRPLT ... (CONT'D)

CALL SCALF (1.0,1.0,-0.5,-1.5)
 CALL FGRID (0,0,0,0,0,0.6,30)
 CALL FGRID (1,0,0,0,0,0.45,20)

C LABEL BOTH AXES
 C

CALL FCHAR (-0.70,2.35,0.17,0.25,1.5708)
 WRITE (7,30)
 30 FORMAT ('TRANSMITTANCE (PERCENT)')
 CALL FCHAR (7.3,-0.72,0.17,0.25,0.0)
 WRITE (7,40)
 40 FORMAT ('WAVENUMBER (CM-1)')
 CALL FPLOTT (0,0,0,0,0)

C ANNOTATE BOTH AXES
 C

CALL SCALF (1.2/XSCFA,0.9/YSCFA,XMIN,YMIN)
 BX(1) = XMIN
 BX(2) = YMIN
 BX(4) = XMAX - XMIN
 BX(5) = XSCFA
 BX(9) = XMIN
 CALL ANOTS (BX,0.08,0.17,1.2/XSCFA,0.9/YSCFA)
 BY(1) = XMIN
 BY(2) = YMIN
 BY(4) = YMAX - YMIN
 BY(5) = YSCFA
 BY(9) = YMIN
 CALL ANOTS (BY,0.08,0.17,1.2/XSCFA,0.9/YSCFA)

C PLOT THE GRAPH
 C

ICNTL = -2
 DO 100 J=1,30
 READ (I,J) (DAT(K),WAV(K), K=1,80)
 DO 100 K = 1,80
 IF (DAT(K))150,50,50
 50 X = (WAV(K)/10.0)
 Y = (DAT(K)/10.0)
 CALL FPLOTT (ICNTL,X,Y)
 100 ICNTL = 0
 150 CALL FPLOTT (1,XMAX+2.5/(1.2/XSCFA),YMIN-2.0/
 1(0.9/YSCFA))
 200 CONTINUE
 CALL EXIT
 END

C MAINLINE DELTA

```

C MAINLINE DELTA
  DIMENSION DAT2(80),WAV2(80),DAT3(80),WAV3(80)
  DIMENSION DEL23(80)
  DIMENSION WMNMX(2), DMNMX(2)
  DIMENSION BX(9), BY(9)
  DEFINE FILE 2(45,320,U,IK),3(30,320,U,IL)
1,4(30,320,U,IO)
  EQUIVALENCE (DEL23(1),DAT3(1))
  DATA BX / 4*0.0,1.2,0.20,3*0.0 /
  DATA BY / 2*0.0,1.5708,0.0,0.9,0.10,0.0,-1.5708,0.0 /

C CALCULATE THE DIFFERENCE B/W FILES 2 AND 3 AND STORE
C IN FILE 4
C CALCULATE MINIMUM AND MAXIMUM FOR BOTH VARIABLES
C OF FILE 4 SIMULTANEOUSLY

  WMNMX(1)=99999.0
  WMNMX(2)=-99999.0
  DMNMX(1)=9999.0
  DMNMX(2)=-9999.0
  DO 20 I=1,70
  READ(2'I')(DAT3(J),WAV3(J),J=1,80)
  READ(3'I')(DAT2(J),WAV2(J),J=1,80)
  DO 15 J=1,80
  IF (DAT2(J)) 21,5,5
5 IF (WAV2(J)-WAV3(J))99,6,99
6 DEL23(J)=DAT2(J)-DAT3(J)
  IF(WAV2(J)-WMNMX(1))7,8,8
7 WMNMX(1)=WAV2(J)
8 IF (WAV2(J)-WMNMX(2))10,10,9
9 WMNMX(2)=WAV2(J)
10 IF(DEL23(J)-DMNMX(1))11,12,12
11 DMNMX(1)=DEL23(J)
12 IF(DEL23(J)-DMNMX(2))15,13,13
13 DMNMX(2)=DEL23(J)
15 CONTINUE
  WRITE(4'I')(DEL23(J),WAV2(J),J=1,80)
20 CONTINUE
  GO TO 24
21 DEL23(J) = 99999.0
  WRITE(4'I')(DEL23(K),WAV2(K),K=1,J)
24 DO 25 I=1,2
  WMNMX(I)=WMNMX(I)/10.0
25 DMNMX(I)=DMNMX(I)/10.0
  CALL COSGR (WMNMX,2,XMIN,XMAX,15,XSCFA)
  CALL COSGR (DMNMX,2,YMIN,YMAX,10,YSCFA)
  CALL SCALF ( 1.0,1.0,-0.5,-1.5)
  CALL FGRID (0,0,0,0,0,0.6,30)
  CALL FGRID (1,0,0,0,0,0.45,20)
  CALL FCHAR (-0.70,1.50,0.17,0.25,1.5708)

```

C MAINLINE DELTA ... (CONT'D)

```

WRITE (7,30)
30 FORMAT('TRANSMITTANCE DIFFERENCE ( PERCENT )')
CALL FCHAR (7.3,-0.72,0.17,0.25,0.0)
WRITE (7,40)
40 FORMAT ('WAVENUMBER ( CM-1 )')
CALL FPLOT (0,0,0,0.0)
CALL SCALF (1.2/XSCFA,0.9/YSCFA,XMIN,YMIN)
BX(1) = XMIN
BX(2) = YMIN
BX(4) = XMAX - XMIN
BX(5) = XSCFA
BX(9) = XMIN
CALL ANOTS (BX,0.08,0.17,1.2/XSCFA,0.9/YSCFA)
BY(1) = XMIN
BY(2) = YMIN
BY(4) = YMAX - YMIN
BY(5) = YSCFA
BY(9) = YMIN
CALL ANOTS (BY,0.08,0.17,1.2/XSCFA,0.9/YSCFA)
ICNTL = -2
DO 100 J=1,70
READ (4,J)(DEL23(K),WAV2(K),K=1,80)
DO 100 K = 1,80
IF (DEL23(K) = 9999.0) 50,150,150
50 X = (WAV2(K)/10.0)
Y=(DEL23(K)/10.0)
CALL FPLOT (ICNTL,X,Y)
100 ICNTL = 0
150 CALL FPLOT (1,XMAX+2.5/(1.2/XSCFA),YMIN-2.0/
1(0.9/YSCFA))
CALL EXIT
99 WRITE (6,999) WAV2(J), WAV3(J)
999 FORMAT (10X,'WAVENUMBER SYNC. ERROR = ',2(2X,F9.1))
GO TO 21
END

```

C MAINLINE KINET

C MAINLINE KINET

C THIS PROGRAM COMPUT PERCENT CONVERSION OF ALCOHOL
 C ALSO THE PARTIAL PRESSURE OF EACH COMPONENT IN THE
 C PRODUCT MIXTURE AND THE REACTION RATE.

C INPUT DATA REQUIRED--FEED RATE AND CATALYST WEIGHT

C W---WEIGHT OF THE CATALYST, GM
 C FAO---FEED RATE,G-MOLE/HK.

```

DIMENSION IWAVE(160),IDATA(160)
DEFINE FILE 1(45,320,U,KO)
II=0
J=0
RTAL=0.
400 J=J+1
READ(1,J)(IWAVE(K),IDATA(K),K=1,160)
IF(J-1)3,3,1
3 N=2
GO TO 4
1 N=1
4 DO 2 IR=N,160
IF(IDATA(IR)-1)7,7,5
5 RTAL=RTAL+FLOAT(IDATA(IR))
II=II+1
GO TO 2
7 WRITE(6,102)IWAVE(IR),IDATA(IR),II
102 FORMAT(1X,'WAVE NO.=',I4,'TRANS.=',I4,'AT POINT',I6
*,'INCORRECT')
IF(II-2000)401,401,6
401 II=II+1
2 CONTINUE
GO TO 400
6 RI=RTAL/II
R2=(RI/10.0)+6.0*(RI-30.)/70.
R=(RI/10.0)+6.0*(R2-30.)/70.
ABS=(ALOG(0.81)-ALOG(R/100.0))/2.3025
WRITE(6,100)R,II
100 FORMAT(1X,'AVG. PERCENT TRANS.=',F10.2,3X,'TOTAL
* POINT=',I5,/)
WRITE(6,101)ABS
101 FORMAT(1X,'ABSORBANCE=',F15.6)
READ(5,10)FAO,w
10 FORMAT(2F15.6)
PO=0.09518+92.94480*FAC

C COMPUT PA FROM CALIBRATION FUNCTION
PCAL=(-0.0027+ABS)/0.15966

```

C MAINLINE KINET ... (CONT'D)

```
C CORRECT FOR TEMP=170 C.  
PAR=PCAL*(273.+170.)/(273.+29.)  
CONV=(1.-(PAR/PO))/(1.+(PAR*0.09518*FAO)/PO**2)  
PCONV=100.*CONV  
WRITE(6,103) PCONV  
103 FORMAT(1X,'PERCENT CONVERSION=',F10.4)  
RATE=CONV*FAO/W  
WRITE(6,104)RATE  
104 FORMAT(/,1X,'REACTION RATE=',F15.6)  
PA=PAR*(PO+(0.09518*FAO*CONV))/PO**2  
PW=PG-PA  
WRITE(6,105)PA,PW  
105 FORMAT(/,1X,'PA=',F10.3,5X,'PW=PP=',F10.3)  
CALL EXIT  
END
```

B. COMPUTER PROGRAMS FOR MODEL DISCRIMINATION

The appendix contains the programs used in this thesis.
The notation used in the following programs is described here.

A	Dispersion matrix $\underline{X}^t \underline{X}$
AO	Prior estimate of the dispersion matrix
B	Least squares estimate of the parameters (vector)
C	Variance-covariance matrix
D	Determinant, normalizing matrix
DSNM	A function subprogram to set up the design matrix
ER	Errors vector
FUCN	A function subprogram to compute the model predictions
INX	Mesh size in the design of experiments
IT	Reference index for the competing models
L,L1,L2	Expected likelihoods
LAM	A parameter in Marquardt's algorithm
M	Number of parameters in the given model
MUO	Prior estimate of the parameters (vector)
N	Number of data points
NM	Total number of competing models
PA,PW	Independent variables
R	Negative of the expected entropy change
SS	Minimum sum of errors squared

SETUP A function subprogram to specify the prior parameter distribution for the given model

VAR Error variance

Y Vector of observations

YH Expected value of the prediction from the entire methamodel

- * SAMPLE OUTPUT USING THE PROGRAMS OF APPENDIX B.
- * DEHYDRATION MODEL M3, SPECIFIED HERE BY LM=2.
LM=2
- * SPECIFY THE PARAMETER PRIOR VARIANCE-COVARIANCE
MATRIX AND THE STARTING VALUE FOR THE PARAMETERS.
A0=3 3p0
B=.1 .01 .1
- * MARQUARDT'S(1963) ALGORITHM IS USED TO COMPUTE THE
LEAST SQUARE ESTIMATE OF PARAMETERS AND VARIANCE-
COVARIANCE MATRIX IS COMPUTED AS DESCRIBED IN
CHAPTER TWO. PROGRAM 'HST' IS USED TO OBTAIN
THE MODEL LIKELIHOOD. CALL 'MGT' TO PERFORM THE
ABOVE CALCULATIONS. A SAMPLE OUTPUT IS:

```

MGT
0.0798712325  0.01163917306  0.1354432714  PARAMETER VALUES AT
0.08485636293  0.01001486825  0.1888224163  VARIOUS ITERATIONS
0.09233897556  0.008185821263  0.2382591273  OF MARQUARDT'S ALG-
0.09519688775  0.007873153225  0.2560221165  ORITHM.
0.09543472473  0.007855672149  0.2574704119

PARAMETERS : 0.09543515955  0.007855869105  0.2574720037
95 PCNT LMT: 0.007987637281  0.001980287403  0.04827574289

VARIANCE : 4.125640078E-5  STD DEV: 0.00642311457
VAR-COVAR:
  1.595058733E-5  -2.857511393E-6  9.130670633E-5
 -2.857511393E-6  9.803845500E-7  -2.152669197E-5
  9.130670633E-5  -2.152669197E-5  5.826368378E-4

MODEL LIKLIHD: 3.436255498E17

```

PROGRAM 'INV'

THIS PROGRAM COMPUTES THE INVERSE OF A NON-SINGULAR MATRIX BY GAUSS-JORDAN PIVOTING.

```

      VINV(I)
V Z←INV M;I;J;K;P
[1]  +3×1(2=pp:1)A= /p:1
[2]  +0,p!←'NO INVERSE FOUND'
[3]  M←Q(1 0 +pM)p(,QM),J+1<P+1T+1+p:1
[4]  M[K,1;]←M[1,K+K1 /K←M[1I;1];]
[5]  P+1ΦP,0pP[K,1]←P[1,K]
[6]  M[;1+pJ]←~J
[7]  +2×11E-30>|M[1;1]|+| /|,M
[8]  M+1Φ1Φ[1] M-(J×M[;1])×M[1;]+M[1;]+M[1;1]
[9]  +4×10=J+1-1
[10] Z←M[ΔP]
      V

```

PROGRAM 'DET'

'DET' OBTAINS THE DETERMINANT OF A SQUARE MATRIX BY CHIO'S METHOD.

```

      VDET(I)
V D←DET A;N:A
[1]  H←pA[1;]
[2]  I←0
[3]  D←1
[4]  +LAD×1H=1
[5]  LAL:I+I+1
[6]  D←D×A[I;I]
[7]  A[I;]←A[I;]+A[I;I]
[8]  L←I
[9]  LAD:L+L+1
[10] A[;L]←A[;L]-A[I;L]×A[I;I]
[11] +LAD×1L<N
[12] +LAL×1I<N-1
[13] LAB:D←D×A[N;N]
      V

```

PROGRAM 'UST'

THIS PROGRAM COMPUTES THE EXPECTED LIKELIHOODS FROM THE SUFFICIENT STATISTICS OF THE DATA WHEN IMPROPER UNIFORM PRIORS ARE USED.

```

VHST[1]V
V HST;M;N
[1] A+PB
[2] N+PXL[1]
[3] L+((2*OVAR)*(-H+2))*(0.5*(H+2))*(*(-SS+(2*VAR)))
V

```

PROGRAM 'USS'

'USS' COMPUTES THE EXPECTED LIKELIHOOD OF A GIVEN MODEL FROM THE SUFFICIENT STATISTICS OF THE DATA AS DEVELOPED IN CHAPTER 2 OF THIS THESIS. U1 USES THE POSTERIOR DISTRIBUTION AND U2 USES THE PRIOR DISTRIBUTION OF THE PARAMETERS.

```

VUSS[1]V
V USS;AE;AA;AB;AC;L11;AD;DD;N
[1] A+PXL[1]
[2] DD+DET(A0+A)
[3] L11+((2*OVAR)*(-H+2))*(*(-SS+(2*VAR)))
[4] AA+(A0+.XIU0)+A+.XB
[5] AB+(A0+.XIU0)+2*A+.XB
[6] AD+((QB)+.XA+.XB)+(QAA)+.X(IHV A0+A)+.XAA
[7] L1+(*-0.5*(AD-(QB)+.XA+.XB)+(IHV A0+2*A)+.XAA)*L11
[8] L1+(L11*(DET(A0+A*2))*0.5)*DD*0.5
[9] AF+((Q7)+.XA+.XB)-(QAA)+.X(IHV A0+A)+.XAA
[10] AC+(AF+((QIU0)+.XA0+.XIU0))
[11] L2+L11*((DET A0)*0.5)*(*-0.5*AC)+(DD*0.5)
V

```

* PROGRAM 'MGT'
 * THIS PROGRAM IS BASED ON MARQUARDT'S (128)
 * ALGORITHM FOR PARAMETER ESTIMATION FROM A
 * NON-LINEAR MODEL.

```

      V MGT[ ] V
    V MGT
  [1] LAM+0.01
  [2] IT+0
  [3] I+(1/M)*. = 1/M
  [4] LBB:→10
  [5] PHI←FUCN LM
  [6] X←DSUM LM
  [7] G+(QX)+.*(Y-PHI)
  [8] SS+(Q(Y-PHI))+.*(Y-PHI)
  [9] A+((QX)+.*X)+A0
  [10] AA+A
  [11] D+I
  [12] IL+0
  [13] LAS:IL+IL+1
  [14] D[IL;IL]←A[IL;IL]*-0.5
  [15] →LAS*1IL<M
  [16] A+D+.*A+.*D
  [17] D1+(D+.*(INV(A+LAM*I))+.*D)+.*G
  [18] D2+(D+.*(INV(A+(LAM+NU)*I))+.*D)+.*G
  [19] B1+B+D1
  [20] B2+B+D2
  [21] BB+B
  [22] B+B1
  [23] PHI1←FUCN LM
  [24] B+B2
  [25] PHI2←FUCN LM
  [26] IT+IT+1
  [27] S1+(Q(Y-PHI1))+.*(Y-PHI1)
  [28] S2+(Q(Y-PHI2))+.*(Y-PHI2)
  [29] →THRE*1((1/(BB-B1))<0.0001)
  [30] B+B1
  [31] B
  [32] →TWO*1S1>SS
  [33] →LBB
  [34] ONE:LAM←LAM+NU
  [35] →LBB
  [36] TWO:LAM←LAM*NU
  [37] →LBB
  [38] THRE:→FOUR*1SS<S1
  [39] X←DSUM LM
  [40] VAR←S1+M
  [41] CONTINUED ON NEXT PAGE
  
```

```

[41] A+((QX)+.X)+A0
[42] C+VAR*(INV A)
[43] →FIVE
[44] FOUR:B+BB
[45] VAR+SS+N
[46] C+VAR*(INV AA)
[47] FIVE:'PARAMETERS : ';B
[48] 'VARIANCE : ';VAR
[49] 'VAR-COVAR: ';C

```

```

*          PROGRAM 'EXPD1'

```

```

* 'EXPD1' COMPUTES THE EXPECTED CHANGE IN
* ENTROPY FOR A HYPOTHETICAL EXPERIMENT.

```

```

      VEXPD1[ ]V
V EXPD1;M;N;IT;I;NM
[1] N+1
[2] VARV←YHV+2ρ0
[3] I+0
[4] NM+2
[5] INX+2
[6] VAR+10*-3
[7] PA+PW+2
[8] LAB:I+I+1
[9] →LAT×\PW>40
[10] →LAS×\PA>50
[11] IT+0
[12] LAC:IT+IT+1
[13] A0←SETUP IT
[14] YHV[IT]←B FUCH IT
[15] PHI←YHV[IT]
[16] X←B DSNM IT
[17] VARV[IT]←X+.×(INV(A0))+.×(QX)×VAR
[18] →LAC×\IT<NM
[19] YH←+/PO×YHV
[20] VARR←(+/(VARV×PO))+VAR
[21] VTT←(●(VARR+(VARV+VAR)))
[22] R←0.5×((+/(PO×(VTT+(((YHV-YH)×2)+VARR))))))
[23] R;' PA,PW = ';PA;' ';PW
[24] PA←PA+INX
[25] →LAB
[26] LAS:P!←PW+INX
[27] PA←0.2
[28] →LAB
[29] LAT:→10
V

```

* PROGRAM 'FUCN'
 * THIS PROGRAM STORES THE FUNCTIONAL FORMS
 * FOR THE VARIOUS DEHYDRATION MODELS.

```

      VFUCN[ ]V
V PHI←B FUCN LM;LM;B
[1] →TWO×\LM=2
[2] →THRE×\LM=3
[3] →FOUR×\LM=4
[4] →FIVE×\LM=5
[5] →SIX×\LM=6
[6] ONE:PHI←B[1]×PA+((1+(B[2]×PA)+(B[3]×PW)))
[7] →TEN
[8] TWO:PHI←B[1]×PA+(((1+(B[2]×PA))×(1+B[3]×PW)))
[9] →TEN
[10] THRE:PHI←B[1]×PA+(1+(B[2]×PA))
[11] →TEN
[12] FOUR:PHI←B[1]×PA+((1+(B[2]×PW)+(B[3]×PA))*2)
[13] →TEN
[14] FIVE:PHI←B[1]×(*-B[2]+(1.987×T/P))×PA+((1+(B[3]×PW))*2)
[15] →TEN
[16] SIX:PHI←B[1]×PA+(((1+B[2]×PA)+B[3]×PP)×(1+B[4]×PW))
[17] →TEN
[18] TEN:→10
V
  
```

PROGRAM 'LWV'

THIS PROGRAM GENERATES THE MODEL PREDICTIONS

FOR THE DEHYDRATION OF 2-PROPANOL.

```
      FUCH(I)J
V PHI←3 FUCH LM=2
  → TWO*LM=2
  → THREE*LM=3
  → FOUR*LM=4
  → FIVE*LM=5
  → SIX*LM=6
  → SEVEN*LM=7
  ONE:PHI←B[1]*PA+((PH2*0.5)+(B[2]*PA)+B[3]*PH2)
  → LM
  TWO:PHI←B[1]*(PA+PH2*0.5)+((1+B[2])*PH2*0.5)*(1+B[3]*PA+PH2*0.5)
  → LM
  THREE:PHI←B[1]*(PA+PH2*0.5)+((1+B[2])*PH2*0.5)*(1+B[3]*PA+PH2*0.5)
  → LM
  FOUR:PHI←B[1]*PA+((PH2*0.5)+(B[2]*PA)+B[3]*PH2)
  → LM
  FIVE:PHI←B[1]*(PA+PH2*0.5)+((1+(B[2]*PH2*0.5)+(B[3]*PA+PH2*0.5)+(B[4]*PA))
  → LM
  SIX:PHI←B[1]*PA+((B[4]*PA+PH2*0.5)+(1+B[2])*PA+PH2*0.5)*(1+B[3]*PH2*0.5)
  → LM
  SEVEN:PHI←B[1]*(PA+PH2*0.5)+((1+B[2])*PH2*0.5)+((1+B[3]*PA)+B[4]*PH2*0.5)
  → LM
  → 10
```


* PROGRAM 'DSHM'
 * DSHM COMPUTES THE DESIGN MATRIX X FOR THE
 * VARIOUS DEHYDRATION MODELS.

```

VDSHM(L) V
V K←B DSHM LM;LM;B
[ 1 ] X←( N )•. = N
[ 2 ] →TWO×\LM=2
[ 3 ] →THREE×\LM=3
[ 4 ] →FOUR×\LM=4
[ 5 ] →FIVE×\LM=5
[ 6 ] →SIX×\LM=6
[ 7 ] ONE: X[ ; 1 ]←PHI+B[ 1 ]
[ 8 ] X[ ; 2 ]←-PHI×PA+(1+(PA×B[ 2 ])+(PW×B[ 3 ]))
[ 9 ] X[ ; 3 ]←X[ ; 2 ]×PW+PA
[10 ] →TEH
[11 ] TWO: X[ ; 1 ]←PHI+B[ 1 ]
[12 ] X[ ; 2 ]←-PHI×PA+(1+B[ 2 ]×PA)
[13 ] X[ ; 3 ]←-PHI×PW+(1+B[ 3 ]×PW)
[14 ] →TEH
[15 ] THREE: X[ ; 1 ]←PHI+B[ 1 ]
[16 ] X[ ; 2 ]←-PHI×PA+(1+(B[ 2 ]×PA))
[17 ] →TEH
[18 ] FOUR: X[ ; 1 ]←PHI+B[ 1 ]
[19 ] DNM←1+(B[ 2 ]×PW)+(B[ 3 ]×PA)
[20 ] X[ ; 2 ]←-2×PHI×PW+DNM
[21 ] X[ ; 3 ]←-2×PHI×PA+DNM
[22 ] →TEH
[23 ] FIVE: X[ ; 1 ]←PHI+B[ 1 ]
[24 ] X[ ; 2 ]←-PHI+(1.987×TMP)
[25 ] X[ ; 3 ]←-2×PHI×PW+(1+(B[ 3 ]×PW))
[26 ] →TEH
[27 ] SIX: X[ ; 1 ]←PHI+B[ 1 ]
[28 ] DNM←((1+(B[ 2 ]×PA)+B[ 3 ]×PP)×(1+B[ 4 ]×PW))
[29 ] X[ ; 2 ]←-PHI×PA×(1+B[ 4 ]×PW)+DNM
[30 ] X[ ; 3 ]←-PHI×PP×(1+B[ 4 ]×PW)+DNM
[31 ] X[ ; 4 ]←-PHI×PW×(1+(B[ 2 ]×PA)+B[ 3 ]×PP)+DNM
[32 ] →TEH
[33 ] TEM: →10
  
```

* PROGRAM 'DSNM'
 * 'DSNM' COMPUTES THE DESIGN MATRIX FOR THE
 * DEHYDROGENATION MODELING.

```

VDSNM(I)IV
  V X←B DSNM LM;LM;B;DMM
[ 1] X←(NH)°. = VM
[ 2] →TWO×\LM=2
[ 3] →THREE×\LM=3
[ 4] →FOUR×\LM=4
[ 5] →FIVE×\LM=5
[ 6] →SIX×\LM=6
[ 7] →SEVEN×\LM=7
[ 8] ONE: X[ ;1]←PHI+B[1]
[ 9] DMM←(PH2*0.5)+(B[2]*PA)+(B[3]*PH2)
[10] X[ ;2]←-PHI*PA+DMM
[11] X[ ;3]←-PHI*PH2+DMM
[12] →TEH
[13] TWO: X[ ;1]←PHI+B[1]
[14] X[ ;2]←-PHI*(PH2*0.5)+(1+B[2]*PH2*0.5)
[15] X[ ;3]←-PHI*(PA+PH2*0.5)+(1+B[3]*PA+PH2*0.5)
[16] →TEH
[17] THREE: X[ ;1]←PHI+B[1]
[18] X[ ;2]←-PHI*(PH2*0.5)+(1+B[2]*PH2*0.5)
[19] X[ ;3]←-PHI*(PA+PH2*0.5)+(1+B[3]*PA+PH2*0.5)
[20] →TEH
[21] FOUR: X[ ;1]←PHI+B[1]
[22] DMM←(PH2*0.5)+(B[2]*PA)+(B[3]*PH2)
[23] X[ ;2]←-PHI*PA+DMM
[24] X[ ;3]←-PHI*PH2+DMM
[25] →TEH
[26] FIVE: X[ ;1]←PHI+B[1]
[27] DMM←1+(B[2]*PH2*0.5)+(B[3]*PA+PH2*0.5)+(B[4]*PA)
[28] X[ ;2]←-PHI*(PH2*0.5)+DMM
[29] X[ ;3]←-PHI*(PA+PH2*0.5)+DMM
[30] X[ ;4]←-PHI*PA+DMM
[31] →TEH
[32] SIX: X[ ;1]←PHI+B[1]
[33] DMM←((1+B[2]*PA+PH2*0.5)*(1+B[3]*PH2*0.5)+(B[4]*PA+PH2*0.5)
[34] X[ ;2]←-PHI*(PA+PH2*0.5)*(1+B[3]*PH2*0.5)+DMM
[35] X[ ;3]←-PHI*(PH2*0.5)*(1+B[2]*PA+PH2*0.5)+DMM
[36] X[ ;4]←-PHI*(PA+PH2*0.5)+DMM
[37] →TEH
[38] SEVEN: X[ ;1]←PHI+B[1]
[39] DMM←B[1]*(PA+PH2*0.5)+PHI
[40] X[ ;2]←-PHI*(PH2*0.5)*(1+(B[3]*PA)+(B[4]*PA+PH2*0.5))+DMM
[41] X[ ;3]←-PHI*PA*(1+B[2]*PH2*0.5)+DMM
[42] X[ ;4]←-PHI*(PA+PH2*0.5)*(1+B[2]*PH2*0.5)+DMM
[43] →TEH
[44] →TEH
[45] →TEH
  
```

C. CALIBRATION OF LIQUID SYRINGE FEEDER

The Sage syringe pump was used to inject liquid feed into the reaction system. The syringe feeder was calibrated by feeding freshly distilled water at room temperature of 24°C. The water was collected in a 25 ml pycnometer after it has passed through a syringe needle which is just big enough to fit in the capillary plug. To prevent the loss of water due to evaporation, the pycnometer was cooled in an ice-water bath. The duration of each run was one hour. The amount of water was obtained by weighing the water at 24°C. Each piston speed was calibrated four times in such a way that the whole range of the piston travel (about 12 cm) was covered. The results showed that the speed was reproducible within $\pm 0.1\%$ with respect to the position of the syringe piston. The average values of the four runs for each speed is used to obtain calibration curves. For the speed range of $1/1000 X$, six data points (average values) were collected and of $1/100 X$ five were obtained. These two sets of data were fitted by the least squares method and the results are shown in Tables C-1 and C-2 for each speed range. The computer programs, LEAST, of the least squares method are also listed below.

TABLE C-1. CALIBRATION OF THE SYRINGE FEEDER BY
LEAST SQUARES METHOD (LOW SPEED RANGE)

X = OF (1/1000X) ON THE CONTROL DIAL OF THE FEEDER
Y = FEED RATE- CC PER HOUR AT 24 DEG.

THE COEFFICIENTS OF THE POLYNOMIAL, $Y=A_0+A_1*X+A_2*X**2$,

A0 = -0.00690
A1 = 0.05274
A2 = -0.00000

REGENERATED DATA

X MEASURED	Y OBSERVED	Y CALCULATED	PCT ERROR
10.0000	0.5211	0.5197	0.2554
20.0000	1.0433	1.0449	0.1564
30.0000	1.5666	1.5685	0.1264
40.0000	2.0935	2.0907	0.1329
60.0000	3.1300	3.1304	0.0120
80.0000	4.1640	4.1641	0.0029

VARIANCE = 0.000003

STANDARD DEVIATION = 0.001803

MAXIMUM PCT ERROR = 0.255461

NO3 NOT CONTROL STMT

// END 23 JUL 71 21.47.14

TABLE C-2. CALIBRATION OF THE SYRINGE FEEDER BY
LEAST SQUARES METHOD (HIGH SPEED RANGE)

X = OF (1/100X) ON THE CONTROL DIAL OF THE FEEDER
Y = FEED RATE - CC PER HOUR AT 24 DEG.

THE COEFFICIENTS OF THE POLYNOMIAL: $Y = A_0 + A_1 * X$

A0 = -0.03847
A1 = 0.52202

REGENERATED DATA

X MEASURED	Y OBSERVED	Y CALCULATED	PCT ERROR
10.000	5.211	5.181	0.561
20.000	10.439	10.402	0.360
30.000	15.575	15.622	0.304
40.000	20.765	20.842	0.372
60.000	37.341	31.283	0.184

VARIANCE = 0.003467

STANDARD DEVIATION = 0.058884

MAXIMUM PCT ERROR = 0.561762

C MAINLINE LEAST

C MAINLINE LEAST

```

C *****
C *
C *          MAINLINE LEAST
C *
C * THIS PROGRAM WAS WRITTEN FOR FITTING A MAXIMUM OF
C * 50 DATA POINTS TO POWER SERIES TYPE POLYNOMIALS OF
C * ANY ORDER UP TO A MAXIMUM OF FOURTH DEGREE.
C *   INPUT DATA
C *   NCASE  - NUMBER OF SETS OF DATA
C *   NCOPY  - NUMBER OF COPIES OF OUTPUT DESIRED
C *   N      - NUMBER OF DATA POINTS
C *   M      - DEGREE OF POLYNOMIAL
C *   NTL    - NUMBER OF CARDS FOR TITLE
C *   NPAGE  - PAGE NUMBER OF OUTPUT
C *   NPLT   - DATA REGENERATION FLAG
C *             ...0-REGENERATE GIVEN DATA ONLY
C *             ...1-REGENERATE GIVEN DATA PLUS 20
C *             INTERMEDIATE POINTS
C *   DES(K) - ALPHANUMERIC DESCRIPTION OF THE TITLE
C *   XNAME  - ALPHANUMERIC DESCRIPTION OF X
C *   YNAME  - ALPHANUMERIC DESCRIPTION OF Y
C *   X(I)   - INDEPENDENT VARIABLE
C *   Y(I)   - DEPENDENT VARIABLE
C *
C *****

```

```

DIMENSION X(50),Y(50),A(50,5),P(20,20),V(20),Z(20),
1DES(10,15),SNAM(5),XNAME(100),YNAME(100)
DATA SNAM/'A0 ','A1 ','A2 ','A3 ','A4 '/
READ(5,1) NCASE,NCOPY
DO 9 NC=1,NCASE
READ(5,1) N,M,NTL,NPAGE,NPLT
1 FORMAT(5I5)
DO 11 NT=1,NTL
11 READ(5,12) (DES(NT,K),K=1,15)
12 FORMAT(15A4)
READ (5,20) (XNAME(I),I=1,15)
20 FORMAT (15A4)
READ (5,21) (YNAME(J),J=1,15)
21 FORMAT (15A4)
13 FORMAT(10X,15A4/)
MM=M+1
DO 2 I=1,N
2 READ(5,3) X(I),Y(I)
3 FORMAT(2F10.5)
DO 4 I=1,N
DO 4 J=1,MM
4 A(I,J)=X(I)**(J-1)

```

C MAINLINE LEAST ... (CONT'D)

```

DO 5 I=1,MM
DO 5 J=1,MM
P(I,J)=0.
DO 5 K=1,N
5 P(I,J)=P(I,J)+A(K,I)*A(K,J)
DO 6 I=1,MM
V(I)=0.
DO 6 J=1,N
6 V(I)=V(I)+Y(J)*A(J,I)
CALL GAUSS(P,V,MM,Z)
DO 16 ICOP=1,NCOPY
WRITE(6,10) NPAGE
10 FORMAT('1',///,66X,'A-',I2,/)
DO 17 I=1,NTL
17 WRITE(6,13)(DES(I,K),K=1,15)
WRITE(6,30)(XNAME(I),I=1,15)
30 FORMAT(///,12X,15A4)
WRITE(6,31)(YNAME(J),J=1,15)
31 FORMAT(12X,15A4)
WRITE(6,8)
8 FORMAT(///,10X,'THE COEFFICIENTS OF THE POLYNOMIAL '
1,'AREA'//)
DO 15 I=1,MM
15 WRITE(6,7) SNAM(I),Z(I)
7 FORMAT(15X,A4,F11.5/)
16 CALL REGEN(X,Y,Z,MM,N)
IF(NPLT) 9,9,14
14 CALL POLYT(X,Z,N,MM)
9 CONTINUE
CALL EXIT
END

```

C SUBROUTINE POLYT

```

C SUBROUTINE POLYT
C *****
C * SUBROUTINE POLYT *
C * * * * *
C * POLYT SUPPLIES REGENERATED DATA AT POINTS INTER- *
C * MEDIATE TO THE GIVEN DATA. *
C * * * * *
C *****

SUBROUTINE POLYT(X,Z,N,MM)
DIMENSION X(50),Z(20)
WRITE(6,1)
1 FORMAT(///,32X,'PLOT TEST DATA'//25X'X CALCULATED',4X
1,'Y CALCULATED'//)
XMAX=0.
XMIN=99999.
DO 2 I=1,N
IF(XMAX-X(I)) 3,3,4
3 XMAX=X(I)
4 IF(X(I)-XMIN) 5,5,2
5 XMIN=X(I)
2 CONTINUE
DELX=(XMAX-XMIN)/20.
XY=XMIN
DO 6 I=1,20
CAL=0.
DO15 J=1,MM
15 CAL=CAL+Z(J)*XY**(J-1)
WRITE(6,7) XY,CAL
7 FORMAT(24X,2(F10.3,5X))
6 XY=XY+DELX
RETURN
END

```


C SUBROUTINE REGEN

```

C SUBROUTINE REGEN
C *****
C *
C * SUBROUTINE REGEN *
C *
C * THIS SUBROUTINE REGENERATES THE GIVEN DATA AND *
C * CALCULATES THE VARIANCE AND STANDARD DEVIATION OF *
C * THE FIT. *
C *
C *****
SUBROUTINE REGEN(X,Y,Z,MM,N)
DIMENSION X(50),Y(50),Z(20)
WRITE(6,1)
1 FORMAT(///,29X,'REGENERATED DATA'//10X,'X MEASURED',5X
1,'Y OBSERVED',5X,'Y CALCULATED',3X,'PCT ERROR',/)
VAR=0.
HI=0.
DO 2 I=1,N
CAL=0.
DO 3 J=1,MM
3 CAL=CAL+Z(J)*X(I)**(J-1)
CAT=ABS(Y(I)-CAL)
PCE=CAT/Y(I)*100.
VAR=VAR+CAT**2
IF(HI-PCE)4,4,2
4 HI=PCE
2 WRITE(6,5) X(I),Y(I),CAL,PCE
5 FORMAT( 9X,4(F10.3,5X)/)
VAR=VAR/(N-1)
DEV=VAR**0.5
WRITE(6,6) VAR,DEV,HI
6 FORMAT(//,10X'VARIANCE =',F10.6//10X,
1'STANDARD DEVIATION =',F10.6//10X,
2'MAXIMUM PCT ERROR =',F10.6)
RETURN
END

```

C SUBROUTINE GAUSS

C SUBROUTINE GAUSS

```

C *****
C *
C *          SUBROUTINE GAUSS
C *
C * THE FUNCTION OF THIS SUBROUTINE IS TO SOLVE THE
C * SET OF EQUATIONS A*X=B USING GAUSSIAN ELIMINATION
C * AND BACK SUBSTITUTION ROTATING ABOUT THE ELEMENT
C * OF MAXIMUM MODULUS.
C *
C *****

```

```

SUBROUTINE GAUSS (A,R,N,X)
DIMENSION A(20,20),R(20),X(20)
M=N-1
DO 11 J=1,M
  S=0.
  DO 12 I=J,N
    U=ABS(A(I,J))
    IF(U-S) 12,12,112
112 S=U
    L=I
  12 CONTINUE
    IF(L-J) 119,19,119
119 DO 14 I=J,N
    S=A(L,I)
    A(L,I)=A(J,I)
  14 A(J,I)=S
    S=R(L)
    R(L)=R(J)
    R(J)=S
  19 IF(ABS(A(J,J))-1.E-30) 115,115,15
115 WRITE(6,3)
    GO TO 500
  15 MM=J+1
    DO 11 I=MM,N
    IF(ABS(A(I,J))-1.E-30) 11,111,111
111 S=A(J,J)/A(I,J)
    A(I,J)=0.0
    DO 16 K=MM,N
  16 A(I,K)=A(J,K)-S*A(I,K)
    R(I)=R(J)-S*R(I)
  11 CONTINUE
    DO 17 K=1,N
    I=N+1-K
    S=0.0
    IF(I-N) 117,17,117
117 MM=I+1
    DO 18 J=MM,N

```

C SUBROUTINE GAUSS ...(CONT'D)

```
18 S=S+A(I,J)*X(J)
17 X(I)=(R(I)-S)/A(I,I)
500 RETURN
3  FORMAT (1H , 'MATRIX SINGULAR')
END
```

D. PORE DIFFUSION LIMITATIONS

The method of estimating the effectiveness factor, η (the ratio of the actual rate to the rate which would be observed in the absence of diffusion limitations), for kinetic expressions such as Hougen-Watson type of rate equations, as reported by Satterfield⁽¹⁰⁸⁾, was employed to determine whether concentration gradients existed within the alumina catalyst wafer. The following parameter values are required:

$$D_A = 9700 \cdot \gamma_e \cdot (T/M)^{1/2} \quad (D.1)$$

$$\phi_L = \frac{L^2}{D_A} (-r_A)/C_A \quad (D.2)$$

$$K = [K_A - D_A \sum_i (K_i v_i / D_i)] / w \quad (D.3)$$

and

$$w = 1 + \sum_i K_i (P_i + (P_A v_i D_A / D_i)) \quad (D.4)$$

The terms within the expression for D_A , ϕ_L , K and w are defined as follows:

D_A = effective diffusivity of reactant based on Knudsen diffusion within the pores

γ_e = pore radius, cm

- T = absolute temperature, °K
 M = molecular weight
 ϕ_L = Thiele diffusion modulus
 $-r_A$ = the observed reaction rate, g-mole/sec. cc of catalyst
 L = ratio of the catalyst volume to outside surface area through which reactant has access, cm
 K, w = parameters used to evaluate η
 i = subscript for species other than reactant A
 ν = stoichiometric coefficient
 C_A = concentration of the reactant, g-mole/cc

The rate of 2-propanol dehydration is determined as discussed in Section 5.3.6. The effectiveness factor was calculated using the highest $-r_A/C_A$ value obtained in this work at 252.7°C ($-r_A = 0.03947$ g-mole/hr-g-catalyst, $P_A = 0.479$ cm Hg, and $P_W = 0.570$ cm Hg; see Table 5-4) which would give the most severe, if any, diffusion limitation.

From Section 3.2, the γ_e was measured to be $84A^0$ and from Table 5-4 $-r_A$ is taken to be

$$0.03947 \times 0.138 / (0.012 \times \frac{\pi}{4} \times (2.54)^2 \times 3600) \frac{\text{g-mole}}{\text{sec-cc catalyst}}$$

where the thickness of the wafer is about 0.012 cm, weight of the catalyst is 0.138 gm and diameter of the wafer is 2.54 cm. Using ideal gas law, the external concentration of 2-propanol at 252.7°C is

$C_A = 0.479 / (76 \times 82.06 \times 523.7)$ g-mole/cc. The ratio of catalyst volume to outside surface area, L , was about 0.006 cm. Thus, from equations (D.1) and (D.2), we get

$$D_A = 7.1596 \times 10^{-3} \text{ and } \phi_L = 0.21 \quad (\text{D.5})$$

The best form of rate equation for the dehydration was found to be

$$(-r_A) = \frac{kP_A}{(1 + K_A P_A + K_W P_W + K_A K_W P_A P_W)} \quad (\text{D.6})$$

The diffusivity is approximately inversely proportional to the square root of molecule weight by equation (D.1). Thus $D_A/D_W = \sqrt{18/60}$.

From Equations (D.3) and (D.4), by assuming adsorption constants of 2-propanol, K_A , to be 0.007856 (b_2 in M3) and of water, K_W , to be 0.25747 (b_3 in M3), we have

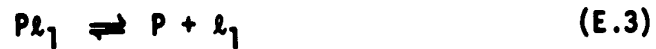
$$w = 1.03 \text{ and } K = -3.6$$

Hence $KP_A = -0.0227$. Using Figure 4-2 of Satterfield⁽¹⁰⁸⁾, the above parameters ϕ_L and KP_A give an effectiveness factor for this reaction system of virtually unity. Since the $-r_A/C_A$ ratios employed in other experimental runs were always lower than the value used in the calculation, pore diffusion can thus be neglected.

In case of dehydrogenation, the effectiveness factor calculated using the same criterion as that of dehydration was also found to be unity. Therefore, only chemical reactions are considered to be the rate-controlling steps.

E. SAMPLE DERIVATIONS OF RATE EQUATIONS

E.1 Dehydration, (dual dissimilar-site mechanism)



where notations are identical to that given in Section 5.3.6. Assume surface reaction (E.2) to be rate-controlling, then $-r_A = r_2 = k_2 C_{Al_1} C_{l_2}$ where the subscripts refer to the reaction step numbers in the above reaction scheme. The other reaction steps are assumed to be in equilibrium thus $r_1 = r_3 = r_4 = 0$ or expressing in equilibrium constants

$$K_1 = C_{Al_1} / P_A C_{l_1}, \quad K_3 = P_P C_{l_1} / C_{Pl_1} \quad \text{and} \quad K_4 = P_W C_{l_2} / C_{Wl_2}$$

Now, total number of active sites, L_1 and L_2 , are assumed to be constant at L_1 and L_2 , respectively, then

$$L_1 = C_{\ell_1} + C_{A\ell_1} + C_{P\ell_1} = C_{\ell_1}(1 + K_1 P_A + P_P/K_3)$$

$$L_2 = C_{\ell_2} + C_{W\ell_2} = C_{\ell_2}(1 + P_W/K_4)$$

The rate expression can now be written as

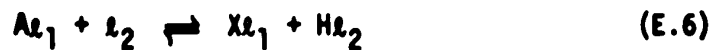
$$-r_A = kK_1 P_A C_{\ell_1} C_{\ell_2} = \frac{k_2 K_1 L_1 L_2 P_A}{(1 + K_1 P_A + \frac{P_P}{K_3})(1 + \frac{P_W}{K_4})}$$

By assuming $K_3 \rightarrow \infty$, as discussed in Section 5.3.6, the above equation reduces to

$$-r_A = kK_1 L_1 L_2 P_A / (1 + P_W/K_4)(1 + K_1 P_A)$$

which is the form of M3 in Table 5-3.

E.2 Dehydrogenation, dual dissimilar-sites mechanism (Scheme B)





again the notations are identical to that given in Section 5.3.8.

(1) Assume both adsorption of A, step (E.5), and surface reaction step (E.7) to be rate-controlling, then

$$-r_A = r_5 = r_7 \text{ or, } -r_A = k_5 P_A C_{\ell_1} - k_{-5} C_{A\ell_1} = k_7 C_{X\ell_1} C_{\ell_2} \quad (\text{E.10})$$

For steps other than E.5 and E.7, they are assumed to be in equilibrium, i.e. $r_6 = r_8 = r_9 = 0$ or by definition of the equilibrium constant

$$K_L = \frac{C_{X\ell_1} C_{H\ell_2}}{C_{A\ell_1} C_{\ell_2}}, \quad K_8 = \frac{P_{H_2} C_{\ell_2}^2}{C_{H\ell_2}} \text{ and } K_9 = \frac{P_K C_{\ell_1}}{C_{K\ell_1}}$$

On rearrangement, we get

$$C_{K\ell_1} = P_K C_{\ell_1} / K_9 \quad (\text{E.11})$$

$$C_{H\ell_1} = \sqrt{P_{H_2} - C_{\ell_2}} / K_8 \quad (\text{E.12})$$

$$C_{X\ell_1} = K_6 \sqrt{K_8} C_{A\ell_1} / \sqrt{P_{H_2}} \quad (\text{E.13})$$

From equation (E.10),

$$C_{A\ell_1} = \frac{k_5}{k_{-5}} P_A C_{\ell_1} - \frac{k_7}{k_{-5}} C_{X\ell_1} C_{\ell_2} \quad (\text{E.14})$$

Combining equations (E.11) to (E.14), we have

$$C_{Al_1} = k_5 P_A C_{l_1} / k_{-5} \left(1 + \frac{k_7}{k_{-5}} C_{l_2} \frac{K_6 \sqrt{K_8}}{\sqrt{P_{H_2}}} \right)$$

and

$$C_{Xl_1} = K_6 \sqrt{K_8} P_A C_{l_1} / k_{-5} \sqrt{P_{H_2}} \left(1 + \frac{k_7}{k_{-5}} C_{l_2} \frac{K_6 \sqrt{K_8}}{\sqrt{P_{H_2}}} \right)$$

Again, total number of active sites for each type, l_1 and l_2 , is assumed to be constant, thus

$$L_1 = C_{l_1} + C_{Al_1} + C_{Xl_1} + C_{Kl_1}$$

$$L_2 = C_{l_2} + C_{Hl_2}$$

Substitute expressions of C_{Al_1} , C_{Xl_1} , C_{Kl_1} and C_{Hl_2} into the above two equations, then

$$L_1 = C_{l_1} \left[1 + \frac{P_K}{K_9} + \frac{k_5 P_A \left(1 + \sqrt{\frac{P_{H_2}}{K_8}} \right)}{k_{-5} \left(1 + \sqrt{\frac{P_{H_2}}{K_8}} + \frac{k_7 L_2 K_6 \sqrt{K_8}}{\sqrt{P_{H_2}}} \right)} \right. \\ \left. + \frac{K_6 \sqrt{K_8} k_5 P_A \left(1 + \sqrt{\frac{P_{H_2}}{K_8}} \right)}{k_{-5} \sqrt{P_{H_2}} \left(1 + \sqrt{\frac{P_{H_2}}{K_8}} + \frac{k_7 L_2 K_6 \sqrt{K_8}}{\sqrt{P_{H_2}}} \right)} \right]$$

$$L_2 = C_{l_2} \left(1 + \sqrt{\frac{P_{H_2}}{K_8}} \right)$$

Substitute L_1 and L_2 into the rate expression (E.10), one gets

$$-r_A = k_{12} C_{x_{l_1}} C_{l_2} = \frac{k_7 K_6 \sqrt{K_8} k_5 P_A C_{l_1} C_{l_2}}{k_{-5} \sqrt{P_{H_2}} \left(1 + \frac{k_7}{k_{-5}} C_{l_2} \frac{K_6 \sqrt{K_8}}{\sqrt{P_{H_2}}} \right)}$$

or

$$-r_A = \frac{k_7 K_6 \sqrt{K_8} k_5 P_A L_1 L_2}{k_{-5} \left(1 + \frac{P_A}{K_9} \right) \left(1 + \sqrt{\frac{P_{H_2}}{K_8}} + \frac{k_7 L_2 K_6 \sqrt{K_8}}{\sqrt{P_{H_2}}} \right) \sqrt{P_{H_2}} + \left(1 + \sqrt{\frac{P_{H_2}}{K_8}} \right) (k_5 P_A \sqrt{P_{H_2}} + K_6 \sqrt{K_8} k_7 P_A)}$$

Since acetone has no effect on the reaction rate and since it was not observed on catalyst surface, it is assumed that $K_9 \rightarrow \infty$. By incorporating this assumption into the above rate expression, we get

$$-r_A = \frac{k_7 K_6 \sqrt{K_8} k_5 P_A L_1 L_2}{\sqrt{P_{H_2}} \left(1 + \sqrt{\frac{P_{H_2}}{K_8}} \right) \left(1 + K_5 P_A + \frac{K_5 K_6 \sqrt{K_8} P_A}{\sqrt{P_{H_2}}} \right) + \frac{k_7 L_2 K_6 \sqrt{K_8}}{k_{-5}}}$$

Combining all the constants the rate equation is in the form of equation (E.15) which is N3 in Table 5-7.

$$-r_A = \frac{b_1 P_A}{\sqrt{P_{H_2}}} \left(1 + b_2 P_A + b_3 \frac{P_A}{\sqrt{P_{H_2}}} + b_4 \sqrt{P_{H_2}} \right) \quad (E.15)$$

(ii) Again assume both reaction steps E.7 and E.8 to be rate controlling, then

$$(-r_A) = r_7 = r_8 = k_7 C_{Xl_1} C_{l_2} = k_8 C_{Hl_2}^2 - k_{-8} P_{H_2} C_{l_2}^2$$

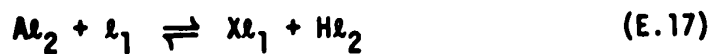
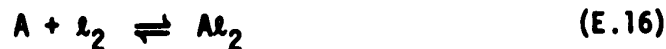
and, $C_{Al_1} = K_5 P_A C_{l_1}$ and $C_{Xl_1} = K_6 C_{Al_1} C_{l_2} / C_{Hl_2}$

Substitute expressions of C_{Al_1} and C_{Xl_1} into the rate expression, we have

$$k_8 C_{Hl_2}^3 - k_{-8} P_{H_2} C_{l_2}^2 C_{Hl_2} = k_7 K_6 K_5 P_A C_{l_1} C_{l_2}^2$$

From the above equation, it can be seen that the expression for C_{Hl_2} is not a simple function.

E.3 Dehydrogenation, dual dissimilar-sites mechanism (Scheme C)



the notations are also identical to that given in Section E.2. Assume both adsorption of A (step E.16) and surface reaction (step E.7) to be rate-controlling, then $(-r_A) = r_{16} = r_7$

$$\text{or} \quad (-r_A) = k_7 C_{Xl_1} C_{l_2} = k_{10} P_A C_{l_2} - k_{-16} C_{Al_2} \quad (\text{E.18})$$

$$\text{and } r_{17} = r_8 = r_9 = 0.$$

In terms of equilibrium constants for steps E.17, E.8, and E.9, one gets

$$C_{Kl_1} = \frac{P_K C_{l_1}}{K_9}; \quad C_{Hl_2} = \frac{\sqrt{P_{H_2}} \cdot C_{l_2}}{\sqrt{K_8}} \quad \text{and} \quad C_{Xl_1} = \frac{K_{17} C_{Al_2} C_{l_1}}{C_{Hl_2}}$$

From equation E.18,

$$C_{Xl_1} = \frac{k_{16} P_A C_{l_2} - k_{-16} C_{Al_2}}{k_7 C_{l_2}} \quad (\text{E.20})$$

Solve for C_{Xl_1} and C_{Al_2} from equations (E.19) and (E.20), we have

$$C_{Al_2} = \frac{k_{16} P_A C_{l_2} \sqrt{P_{H_2}}}{k_{-16} \sqrt{P_{H_2}} + \sqrt{K_8} K_{17} k_7 C_{l_1}}$$

and

$$C_{Xl_1} = \frac{K_{17} k_{16} P_A C_{l_1}}{\frac{k_{-16}}{\sqrt{K_8}} \sqrt{P_{H_2}} + K_{17} k_7 C_{l_1}}$$

Assume L_1 and L_2 are constants as in the previous section,

$$\begin{aligned}
 L_1 &= C_{\ell_1} + C_{X\ell_1} + C_{K\ell_1} \\
 &= C_{\ell_1} + \frac{K_{17}k_{16}P_A C_{\ell_1}}{\frac{k_{-16}}{\sqrt{K_8}} \sqrt{P_{H_2}} + K_{17}k_7 C_{\ell_1}} + \frac{P_A C_{\ell_1}}{K_5} \quad (E.21)
 \end{aligned}$$

$$\begin{aligned}
 L_2 &= C_{\ell_2} + C_{A\ell_2} + C_{H\ell_2} \\
 &= C_{\ell_2} + \frac{k_{16} P_A \sqrt{P_{H_2}} C_{\ell_2}}{k_{-16} \sqrt{P_{H_2}} + \sqrt{K_8} K_{17} k_7 C_{\ell_1}} + \frac{\sqrt{P_{H_2}} C_{\ell_1}}{\sqrt{K_8}} \quad (E.22)
 \end{aligned}$$

It can be seen from equations E.21 and E.22 that C_{ℓ_1} and C_{ℓ_2} can not be solved to give simple expressions.

F. THERMODYNAMIC ANALYSIS OF THE DEHYDRATION
AND DEHYDROGENATION OF 2-PROPANOL

In planning chemical research, it is customary first to make a thermodynamic analysis of the system in order to determine the feasibility of the reaction. However, once the Gibbs energy change, ΔG , is established for a reaction, its feasibility may readily be calculated in terms of the equilibrium constant, K , by the following equation:

$$\Delta G = - RT \ln K . \quad (F.1)$$

The ΔG value for the reaction can be computed from equation (F.2).

$$\Delta G = \Sigma[G_f \text{ (products)}] - \Sigma[G_f \text{ (reactants)}] \quad (F.2)$$

where G_f is the standard Gibbs energy of formation.

For the dehydration of 2-propanol at 252.7°C, G_f (2-propanol), G_f (propylene) and G_f (water) are - 22.55, - 4.33 and - 52.04 K cal/g-mole, respectively. These values were obtained by interpolating the data given in Reference (129). The ΔG value for the dehydration reaction is thus calculated to be - 33.82 K cal/g-mole, according to equation (F.2). The equilibrium constant, computed from equation (F.1), is $e^{32.36}$ or, in terms of partial pressure:

$$K = e^{32.36} = \frac{P_P P_W}{P_A} = \frac{P_{A0} x^2}{1-x} \quad (F.3)$$

It is clear from the above expression that the equilibrium conversion, x , is essentially unity when p_{A0} is less than one atm.

Again in the case of the dehydrogenation reaction at 343.2°C, G_f (2-propanol) and G_f (acetone) are - 14.40 and - 18.72 K cal/g-mole, respectively. At the highest p_{A0} , 52 cm Hg, used in this investigation, an equilibrium conversion of 0.98 is obtained by solving equation (F.4) for x .

$$\frac{K}{P_{A0}} = \frac{34.124}{(52/76)} = \frac{x^2}{1-x} \quad (F.4)$$

From these results it appears that the assumption that both dehydration and dehydrogenation reaction are irreversible reactions is reasonable.

G. LIST OF IR BANDS ON THE ADSORPTION
OF 2-PROPANOL ON γ -ALUMINA

	<u>Frequency, cm^{-1}</u>	<u>Intensity*</u>	<u>Assignment</u>
Isopropoxide ⁽⁵³⁾ :	1130	st	$\nu_{\text{C-O}}$
	1170	st	$\nu_{\text{as}} \text{C}_3$
	1340	w	$\delta_{\text{C-H}}$
	1380	st	$\delta_{\text{s}} \text{CH}_3$
	1460	m	$\delta_{\text{as}} \text{CH}_3$
	2870	w	$\nu_{\text{s}} \text{CH}_3$
	2960	st	$\nu_{\text{as}} \text{CH}_3$
Carboxylate ⁽⁵³⁾ :	1380	w	$\delta_{\text{s}} \text{CH}_3$
	1470	st	$\nu_{\text{s}} \text{COO}^-$
	1575	st	$\nu_{\text{as}} \text{COO}^-$
	2960	w	$\nu_{\text{as}} \text{CH}_3$
Hydrogen-bonded 2-propanol:	1170	st	$\nu_{\text{as}} \text{C}_3$
	1373	st	$\delta_{\text{s}} \text{CH}_3$
	1465	st	$\delta_{\text{as}} \text{CH}_3$
	2870	st	$\nu_{\text{s}} \text{CH}_3$
	2930	m	$\nu_{\text{s}} \text{C-H}$
	2960	st	$\nu_{\text{as}} \text{CH}_3$
	3550	st, b	$\nu_{\text{O---H}}$

*Abbreviations: st = strong
m = medium
w = weak
b = broad